Science Research Council

RHEL / R 215

Rutherford Laboratory Report

THE WORK OF THE RUTHERFORD LABORATORY 1970

Hobbs the Printers Ltd
Second Avenue, Millbrook, Southampton

Science Research Council

THE WORK OF THE RUTHERFORD LABORATORY IN 1970

Edited by

J R Smith and F M Telling

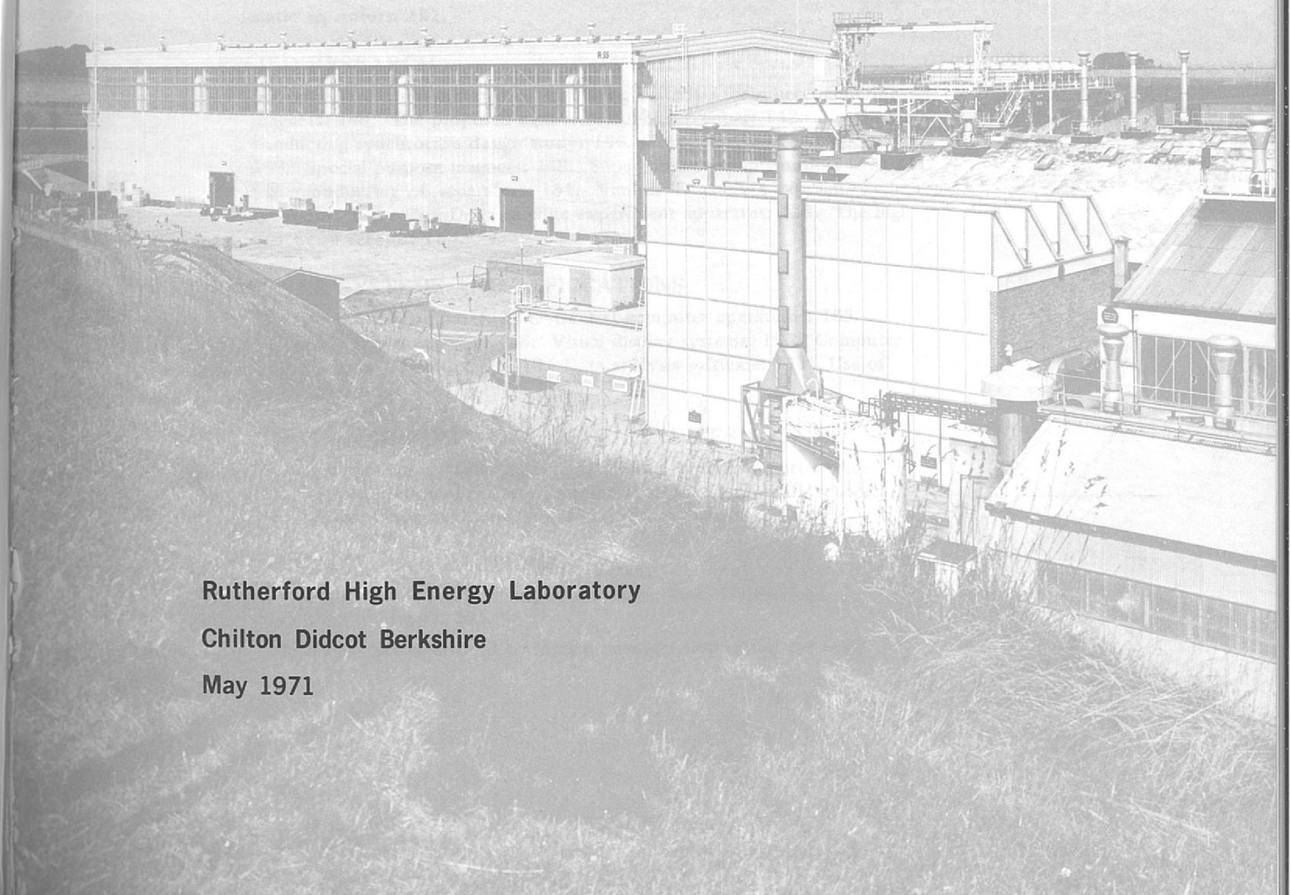

Rutherford High Energy Laboratory
Chilton Didcot Berkshire
May 1971

Contents

Director's Foreword

The year under review has been a successful one for the Laboratory scientifically. Our high energy physics research programme has continued at a level similar to that achieved in 1969. Ways are still being found of increasing the intensity of the circulating proton beam in Nimrod; an intensity of over 3×10^{12} protons per pulse, accelerated to full energy, has been achieved. The total number of protons accelerated during the year also showed an improvement as did the overall operational efficiency.

The trend towards increased use of the CERN accelerators has also continued. Two counter experiments were completed there during 1970; a new one was started, several are being designed and plans are well advanced for making use of two major new devices about to come into operation there, namely the Intersecting Storage Rings and the Omega spectrometer.

Experiments continue to demand increased computing power, but as plans to replace our IBM 360/75 central computer with the larger IBM 360/195 have now been approved we shall be able to cope with the anticipated growth in computing for a number of years.

Towards the end of 1970 we were all greatly heartened by the Government's decision to support the 300 GeV project at CERN. British participation will mean economies in the Rutherford Laboratory, but the future viability of high energy physics in Europe is now assured and it is to be expected that our programme will become even more closely linked with that of CERN. A particular example of this is the work being done in the Laboratory on Superconducting Synchrotron magnets in conjunction with laboratories in Germany and France. A potential application of this work is the up-grading of the energy of this new CERN accelerator. The prospects are promising.

G. H. Stafford

Rutherford Laboratory
Internal Organisation

HIGH ENERGY PHYSICS DIVISION

Experiments in fundamental particle physics using electronic and visual (bubble chamber and spark chamber) techniques, in collaboration with University groups, at Nimrod and CERN. Nuclear Electronics. Photographic Services.

DIVISION HEAD & DEPUTY DIRECTOR: G. MANNING
DEPUTY DIVISION HEAD: J. J. THRESHER

NIMROD DIVISION

Operation and development of Nimrod. Experimental area management. Design and installation of beam-lines. Superconducting beam-line elements. Liquid hydrogen targets. Bubble chamber operations and development.

DIVISION HEAD: D. A. GRAY
DEPUTY DIVISION HEAD: G. N. VENN

APPLIED PHYSICS DIVISION

Superconducting magnet studies. High Field Bubble Chamber project. Polarized targets. Radio-biological studies and radiation protection. High Flux Beam Reactor design study.

DIVISION HEAD: L. C. W. HOBBIS
ACTING DIVISION HEAD: D. B. THOMAS

COMPUTING & AUTOMATION DIVISION

Operation and development of the Central Computer System. On-line applications including hardware and software for bubble and spark chamber film analysis. Theoretical High Energy Physics.

DIVISION HEAD: W. WALKINSHAW

ENGINEERING DIVISION

Design and manufacture of nuclear physics apparatus and applied research equipment. Engineering Science. Mechanical, Electrical and Building services. Chemical Technology. Safety services.

DIVISION HEAD & CHIEF ENGINEER: P. BOWLES

ADMINISTRATION DIVISION

Personnel, Finance and Accounts, Stores, Library, Transport, General and Specialised Administrative Support.

DIVISION HEAD & LABORATORY SECRETARY: J. M. VALENTINE

View of the hydrogen target, particle detectors and spectrometer magnet used in Experiment 8.

HIGH ENERGY PHYSICS

High Energy Physics

The year 1970 saw a continuing high level of utilisation of Nimrod, and an increase in the involvement of the Rutherford High Energy Laboratory (RHEL) supported groups at CERN. The universities and institutions whose researches are supported by the facilities of the Rutherford Laboratory are listed in Table 1.

At Nimrod several new records have been established. The total number of accelerated protons was some 20% higher than in any previous year and the highest ever circulating beam intensity was achieved, being in excess of 3×10^{12} protons per pulse. The original design figure for Nimrod was 1×10^{12}. Extraction efficiencies have been higher than ever before; in the X3 beamline the use of a new 'thin septum' extraction magnet, in conjunction with 'header quadrupoles', led to ~40% extraction, and an actual extracted beam down X3 of $1{\cdot}2 \times 10^{12}$ protons per pulse. The successes of the Nimrod operations group have had a direct impact on the ease with which the high energy physics programme could be carried out. For example, the large available Nimrod beam intensity has enabled the ever increasing demands by counter groups to be met with minimal delay to individual experiments.

Experiments at Nimrod

During the year, five counter experiments and four bubble chamber experiments were brought to completion. These experiments are all reported in this issue. The first stage in the development of the new experimental hall (Hall 3) reached fruition with two experiments taking data (Experiments 8 & 16). Both are of considerable interest; the first (Experiment 8) studies K^+p interactions and will give information on possible Z* states (baryon resonances with positive strangeness) which are forbidden in the simplest quark model; the second experiment will test for the existence of a charge asymmetry in the eta decay ($\eta^\circ \to \pi^+\pi^-\pi^\circ$). A precise experiment by a Columbia group, with 36,000 events, showed an asymmetry which is taken to imply an important symmetry failure in the electromagnetic interaction. The early running of the RHEL experiment has already produced about twice the number of events of the Columbia experiment, so that a significant preliminary result should be obtained before the full data taking is completed. Plans to expand the use of Experimental Hall 3 were completed in early 1970, and installation of the new equipment was started during a six week summer shutdown of the X3 extracted beam. The phase II plans are shown in figure 1. The extracted proton beam will pass through the first target in which interactions produce secondary π's and K's for the two existing beamlines (π8 and K15), and will be refocused on to the new target at the second target station. This target will supply two new beamlines, one of which will be a high momentum pion beam (π9) which will be installed in the spring of 1971. When phase II is completed, four out of the nine counter teams using Nimrod will run their experiments simultaneously using the same extracted protons, thus adding further to the operational efficiency of the Nimrod experimental programme.

Table 1

Institutions Participating in the High Energy Physics Programme

Counter Experiments	Bubble Chamber Experiments
AERE, Harwell	University of Birmingham
University of Bergen, Norway	University of Brussels, Belgium
University of Birmingham	University of Cambridge
University of Bristol	CEN, Saclay
University of Cambridge	CERN, Geneva
University of Glasgow	College de France
Imperial College, London	Ecole Polytechnique, France
University College, London	University of Durham
University of Liverpool	University of Edinburgh
University of Oxford	University of Glasgow
Queen Mary College, London	Imperial College, London
Rutherford High Energy Laboratory	University of Liverpool
University of Southampton	University of Oxford
University of Sussex	Rutherford High Energy Laboratory
University of Warwick	University of Strasbourg, France
Westfield College, London	Tufts University, USA
	University College, London
	Westfield College, London

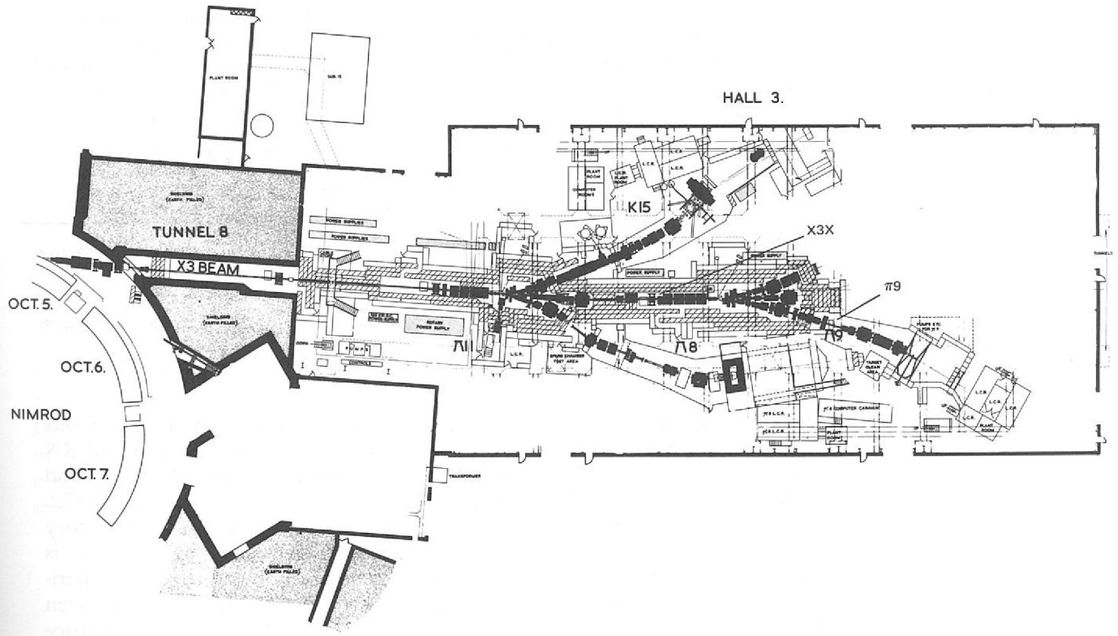

Figure 1. Beam lines in Experimental Hall 3 in January 1971.
The Phase II extension of beam-lines consists of X3X (continuation of the external proton beam X3 to a second target station), beam-line π9 together with provision for two other beam-lines, one in the forward direction.
(This figure is also available in pullout form at the end of the Report).

In the other Experimental Halls (1 and 2) two important long-standing elastic scattering experiments have come to an end and have vacated their beamlines. These are:

1. The large scale πp scattering experiment using a polarized target (Experiment 4) of the RHEL/Oxford/Warwick group, which made polarization measurements at 68 momentum points, over the momentum range 0·6 GeV/c to 2·7 GeV/c. Data from this experiment is already partially analysed, and the accurate polarization measurements will prove invaluable in improving the phase shift analysis over this momentum region. The magnets used in this beamline (K14A) were needed for the Experimental Hall 3 expansion; their removal has eased congestion in Experimental Hall 1.
2. The K^- and K^+p scattering experiment (Experiment 2) of the UCL/RHEL group which used a highly automated wire spark chamber system with core read-out, connected to an on-line computer. This experiment produced an extensive amount of elastic scattering data over 32 momentum points for K^-p scattering, and 28 momentum points for K^+p scattering. Analysis is now well advanced and the preliminary data has been fed into a phase shift analysis. A nuclear structure experiment (Experiment 32) has now moved into this beamline (K8 modified to π10 in Experimental Hall 2) and data taking will commence in early 1971.

Composition of Teams using Nimrod in 1970

	Physicists		Research Students		Support Staff*	
	Electronic Techniques	Bubble Chambers	Electronic Techniques	Bubble Chambers	Electronic Techniques	Bubble Chambers
Visitors**	58	33	30	20	12	-
Resident RL staff †	30	9	-	-	22	13
TOTAL	88	42	30	20	34	13

* Includes only technical assistance directly concerned with experiments and does not include engineering support.

** Staff from Universities and other groups.

† These numbers include 31 fixed term Research Associates and 5 staff members with joint University appointments.

Experiments at CERN

A clearly developing trend is the increasing interest in using CERN shown by our counter teams. Two experiments have recently been completed at CERN (Experiments 7 and 14), two more will run in 1971 (Experiments 10 and 18) and two further experiments are being proposed and could start taking data in 1972. By the end of 1972 all nine counter teams supported by the Rutherford Laboratory are likely to have participated in experiments at CERN. This development is illustrated in Table 2 where links with CERN experiments, or proposed experiments, are listed. In one or two cases the planning is still tentative. As can be seen all the counter teams supported financially and technically by the Laboratory appear in the table, which spans a period of about four years; some groups appear more than once. It is interesting to note that many groups are amalgamating to carry out experiments at CERN and in some cases are collaborating with CERN or other European groups.

In Table 2 we can see how the various CERN commitments are developing. The first, and earliest, of the listed experiments (Experiment 14) $K^{\pm}\to\pi^{\pm}\pi^{\circ}\gamma$ completed

Table 2

COUNTER GROUPS USING CERN

Group	Experiment	Present State	Year of Data Taking
RHEL(C)/Oxford / Liverpool/Warwick	$K^{\pm}\to\pi^{\pm}\pi^{\circ}\gamma$ } (No. 14) $K^{\pm}\to\pi^{\pm}\pi^{\circ}\pi^{\circ}$ }	Analysis	1969
RHEL(B)/Cambridge	$\pi^{\pm}$p at 300 MeV/c (No. 7)	Analysis	1970
QMC/RHEL/Liverpool/ DNPL	$\bar{p}$p interactions (No. 10)	Mounting Apparatus	1971
UCL/RHELS(B)/Bristol/ Liverpool/Scandinavian Universities	ISR experiment (No. 18)	Preparing Apparatus	1971
Oxford/CERN	π and K scattering with polarized target	Data taking/ Tentative	1971
RHEL(A)/Westfield/ Birmingham	Boson studies on Omega Magnet	Design	1972
Imperial College/ Southampton/ETH	Ξ studies in Omega	Tentative	1972/3
RHEL (C)	$K^-p\to\bar{K}^{\circ}n$ polarization	Tentative	1972/3
Birmingham/RHEL/ CERN	Kp and πp large angle scattering	Tentative	1972

data taking in autumn 1969 and the team has returned to the UK. Data analysis has been going on throughout 1970 using the Rutherford Laboratory's IBM 360/75 computer and preliminary results are given in this report. The next experiment (Experiment 7) was a detailed study of the first discovered π^-p resonance, the $\Delta(1238)$.

This experiment completed running at the CERN synchro-cyclotron in the summer of 1970, and since that time data analysis has continued at both Cambridge and the Rutherford Laboratory. Results have already been obtained (see figures 22 and 23) and it is clear that the precision is considerably better than in all previous studies of the Δ particles. As a result it has been possible to determine the masses of the Δ's to a substantially better accuracy than before, and to obtain a value for the electromagnetic mass splitting, for which predictions exist in SU(3) theory.

The group carrying out the $\bar{p}p$ experiment moved to CERN in the autumn of 1970. Their experimental equipment has been designed and manufactured at the Daresbury Laboratory and the Rutherford Laboratory and is shown schematically in figure 2. The large wire chambers use core read-out and are on-line to a computer. Installation will be completed by spring 1971 and data taking should start in the summer.

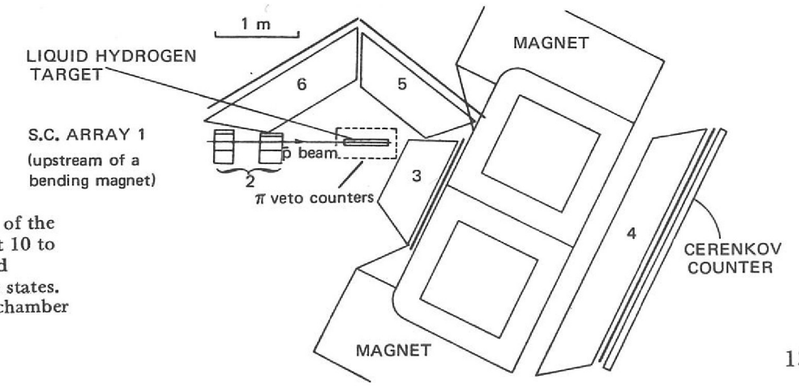

Figure 2. Schematic diagram of the apparatus used in Experiment 10 to study $\bar{p}p$ elastic scattering and annihilation into two particle states. Numbered blocks are spark chamber arrays.

Figure 3(b). Photograph taken during the construction of the large array of magnetised steel and spark chambers to be used in Experiment 18.

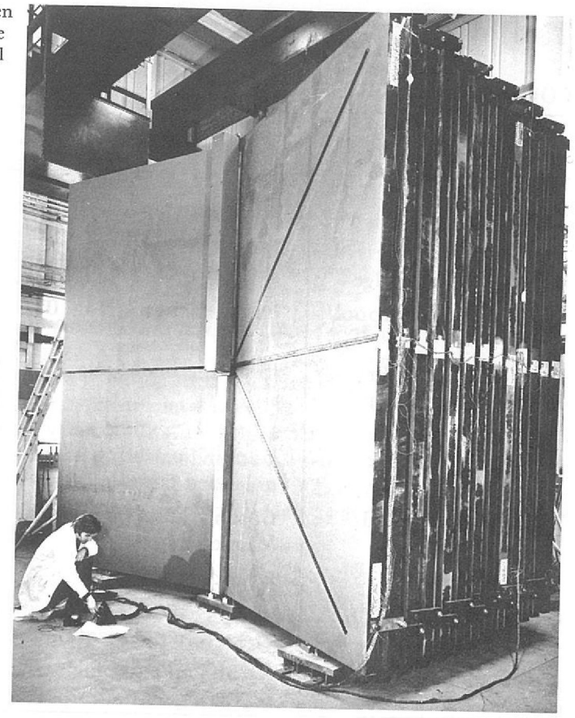

Figure 3(a). A scale model of the apparatus to be used in Experiment 18 to study production of particles at large angles to the colliding beams of the CERN Intersecting Storage Rings.

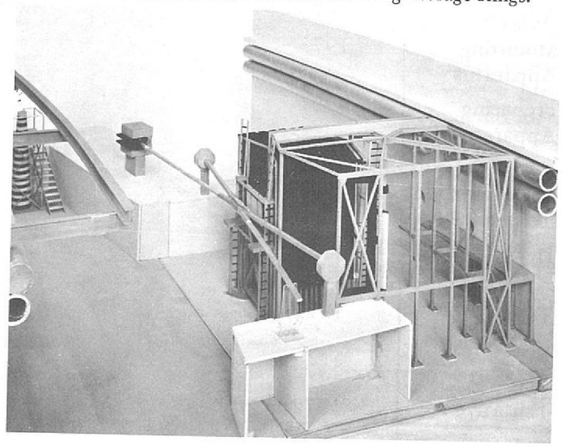

Experiments at the Intersecting Storage Rings

The construction and development programme of the Intersecting Storage Rings (ISR) at CERN is on schedule and two 15 GeV beams have already been made to interact. Experimental work is due to start in April 1971. As discussed in detail in the 1969 Annual Report, the ISR is a circular machine in which two beams of protons travelling around in opposite directions are brought into head-on collision in each of 8 intersection zones. Such a collision of two 28 GeV protons has 56 GeV of kinetic energy completely available for the production of new heavy particles. The same 'available' energy could be achieved with a conventional machine (single proton beam hitting a stationary proton target) only by going up to a beam energy of about 1500 GeV. Although the interaction probability for the colliding beams is low, the ISR will give us a glimpse of 1500 GeV physics which has hitherto been available only through cosmic ray work. The Rutherford Laboratory supported experiment at the ISR (Experiment 18) is intended primarily to search for the 'intermediate boson' (the 'messenger' particle of weak interactions) by looking for μ mesons produced around the ISR at large angles. This experiment will, in addition, study particle production at wide angles. A model of the planned apparatus is shown in figure 3a; the spark chambers are of the optical type and have dimensions up to 4 m x 2 m. The total spark chamber arrays contain 22 of the large chambers between plates of magnetized steel (figure 3b) and will weigh 300 tons.

The next experiment listed involves π and K elastic scattering studies with a polarized target. This is a CERN experiment which members of the Oxford Group have recently joined. It is hoped to continue the collaboration with further experiments.

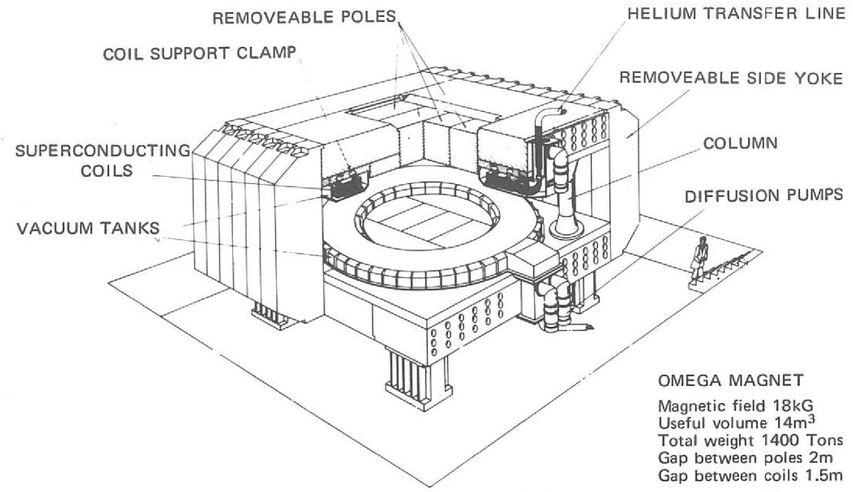

Figure 4. A scale drawing of the magnet to be used in the Omega project at CERN (Photograph by courtesy of CERN).

The Omega Magnet Project (ref. 173)

Another CERN project which is coming close to fruition, and which is causing a great deal of interest, is the Omega magnet project. This is a large volume superconducting magnet producing a field of 18 kG over a volume 3 m in diameter by 2 m in height (figure 4) which will be filled by optical spark chambers. This system is built with the aim of dealing with multi-particle final states, and will have almost 4π collecting solid angle. It is believed that it will compete very strongly with the bubble chamber for multi-particle studies. The very low material density in the spark chambers (70 m radiation length) and long track length (up to 3 m) will enable very good momentum accuracy to be obtained ($\Delta p/p \sim \pm 0{\cdot}25\%$) making it superior to present day bubble chambers, and on a par with advanced design bubble chambers (e.g. the BEBC project) in momentum and mass accuracy. It will have the advantage of being a triggered device, capable of operating with high beam fluxes ($\sim 2 \times 10^5$/burst).

For these reasons the project is gathering a large following, and some twelve experiments have been submitted for the first 2 to 3 years of running. It is interesting to note that approximately half the support comes from counter physicists and half from bubble chamber physicists.

A collaboration consisting of counter physicists from Birmingham University, Westfield College and Rutherford Laboratory with bubble chamber physicists from Birmingham University is proposing to use a 'slow neutron trigger' with Omega for the study of meson states in the mass range 1·4 to 2·2 GeV/c^2. Groups from Glasgow University and Liverpool University are planning to participate in an experiment with a 'slow proton trigger' which will yield complementary data.

Strong Interaction Experiments

The strong interaction experiments listed in Table 3 have as a common theme the search for new resonant states and the determination of their quantum numbers (spin, parity, isotopic spin, strangeness etc). The purpose in establishing a 'periodic table' of the particles is of course to recognise some pattern in their properties. SU(3), Quark theory, and Regge theory predict that certain patterns in mass and quantum numbers should exist, and to a large extent these patterns appear to be seen experimentally. One of the present main spheres of elementary particle physics research is to establish the properties of the large number of baryons and mesons, in order to test more carefully the truth of the theories. Should it turn out that the Quark theory is correct, and that quarks exist physically, then elementary particle physics would move one stage further, to the physics of the three quarks and their anti-quarks.

Table 3

Strong Interaction Experiments using Electronic Techniques

Number	Experiment	Beam Line	Status of Expt (at Dec. 1970)
1	$K^{\pm}p$ Differential Cross-Sections in the Momentum Range 0·45 – 0·90 GeV/c	K12	Analysis
2	$K^{\pm}p$ Differential Cross-Sections in the Momentum Range 0·9 – 2·2 GeV/c (K^-) and 1·6 – 2·4 GeV/c (K^+)	K8	Analysis
3	Neutral States produced in K^-p Elastic Scattering	K10S	Analysis
4	Polarization Effects in π^+p Elastic Scattering	K14A	Analysis
5	Wide Angle Elastic pp Scattering	P71	Analysis
6	An Investigation of Narrow Width Mesons produced in π^-p Interactions	π7	Analysis
7	Low Energy Pion-Nucleon Interactions	CERN	Analysis
8	K^+p Differential Cross-Sections in the Momentum Range 1 – 2 GeV/c	K15	Data Taking
9	$K^{\pm}n$ Elastic and K^+ Charge Exchange Differential Cross-Sections	K12A	Setting up
10	$\bar{p}p$ Elastic Scattering and two-body Annihilation	CERN	In preparation

These resonant searches can be classified into two experimental types:

(a) the 'formation' experiments in which bombarding and target particles (e.g. π^-p) coalesce to form the new particle or 'resonance' (e.g. Δ), the bombarding energy being just right for the total available energy to equal the mass of the new particle. The new particle soon decays either back to the original particles (π^-p, elastic scattering) or to the original particle 'types' with charges interchanged (π^0n, charge exchange) or to different particles (e.g. Σ^-K^+, inelastic scattering).

(b) the 'production' experiments in which the new particle is produced in conjunction with one or several other particles e.g.

$$\pi^-p \rightarrow n\,X^0 \quad \hookrightarrow \pi^+\pi^-\pi^0$$

The mass of X^0 can be determined in this case from two body kinematics, being the missing mass to the 'other particle' (n). Alternatively the mass of X^0 can be determined from the total mass energy going to the decay particles ($\pi^+\pi^-\pi^0$).

It is interesting to note that out of some 30 elementary particle physics experiments discussed in this year's report, no fewer than 13 are formation experiments involving π^+p, π^-p, K^+p and K^-p scattering. The π^+p and π^-p scattering forms baryons of strangeness zero and isotopic spin $\frac{3}{2}$ and $\frac{1}{2}$; these are called Δ particles and N* particles, respectively. K^-p scattering can form baryons of strangeness -1 and isotopic spin 0 or 1, which are called Λ*'s and Σ*'s. The K^+p scattering would form baryons of strangeness +1 (called Z*'s), which should not exist in the simplest Quark theory.

Nimrod is one of the best machines for producing high fluxes of π mesons in a momentum region which is very rich in N* and Δ states (see Table 4). As a result physicists working at Nimrod have put a lot of effort into π^+p and π^-p scattering experiments and have contributed an important part of the world data from these studies.

Table 4

Pion-Nucleon Resonances in the Nimrod Energy Range

Mass	Pion Momentum	$N^*(I=\frac{1}{2})$	$\Delta(I=\frac{3}{2})$
MeV/c^2	MeV/c	J^P	J^P
1236	304		$\frac{3}{2}^+$
1470	660	$\frac{1}{2}^+$	
1520	740	$\frac{3}{2}^-$	
1535	760	$\frac{1}{2}^-$	
1650	960		$\frac{1}{2}^-$
1670	1000	$\frac{5}{2}^-$	
1670	1000		$\frac{3}{2}^-$
1688	1030	$\frac{5}{2}^+$	
1700	1050	$\frac{1}{2}^-$	
1780	1200	$\frac{1}{2}^+$	
1860	1360	$\frac{3}{2}^+$	
1890	1420		$\frac{5}{2}^+$
1910	1460		$\frac{1}{2}^+$
1950	1540		$\frac{7}{2}^+$
1990	1630	$\frac{7}{2}^+$	
2040	1730	$\frac{3}{2}^-$	
2190	2070	$\frac{7}{2}^-$	
2420	2640		$\frac{11}{2}^+$
2650	3260	?	
2850	3850		?

It is of interest to look at the impact of Rutherford Laboratory work in this field. A list of all the π^-p experiments performed up to the present time at Rutherford Laboratory is given in Table 5a. The type of interaction process is listed in the fifth column; in the majority are those described as $\pi^{\pm}p \rightarrow \pi^{\pm}p$, i.e. simple elastic scattering experiments; there are two cases of experiments which are described as 'inelastic' or 'quasi-elastic' processes, and there are two cases of charge exchange scattering ($\pi^-p \rightarrow \pi^\circ n$).

In the field of 'formation' studies the first experiments are always simple total cross-section measurements. In these the loss of beam particles in passing through a hydrogen target is measured as a function of beam energy. The principle is that whenever the beam energy goes through a value where the particles (πp) coalesce into some new N* or Δ a 'resonance' will occur and the cross-section will show a peak. Such behaviour is seen in the graphs of π^+p and π^-p total cross-sections shown in figure 5. Peaks which imply resonances are visible at energies of 1920 MeV in the π^+p case and 1512 MeV and 1688 MeV in the π^-p case. At the time when Nimrod became operational (August, 1963) these, with the $\Delta(1238)$, were the only known Δ or N* baryons, and many of the early experiments at Nimrod were designed to investigate their properties.

Table 5a

Experiments on πN scattering carried out in the 7 years of operation of Nimrod

Beam	Measurement*	Reaction	Momentum (GeV/c)	Team
π1	$\frac{\partial\sigma}{\partial\Omega}$	$\pi^{\pm}p \rightarrow \pi^{\pm}p$	0·88 to 1·58	RHEL
	P_o	$\pi^-p \rightarrow \pi^-p$		
π2	$\frac{\partial\sigma}{\partial\Omega}$	$\pi^{\pm}p \rightarrow \pi^{\pm}p$	1·72 to 2·8	UCL/Westfield
π3	$\frac{\partial\sigma}{\partial\Omega}$	$\pi^-p \rightarrow \pi^\circ n$	1·7 to 2·5	Oxford
K6	σ_{TOT}	$\pi^{\pm}N$	0·5 to 2·65	Cambridge/B'ham/RHEL
K7	P_o	$\pi^-p \rightarrow \pi^-p$	0·64 to 2·09	RHEL
K7′	P_o	$\pi^-p \rightarrow \Sigma^-K^+$	1·13	AERE/QMC/RHEL
K14	P_o	$\pi^+p \rightarrow \Sigma^+K^+$	1·11	Westfield/RHEL
π5	$\frac{\partial\sigma}{\partial\Omega}$	$\pi^-p \rightarrow \pi^-p$	1·5 to 3·5	Bristol/RHEL
K1 + HBC	inelastic processes	$\pi^{\pm}p$	0·6 to 1·2	Imperial/Westfield/ Oxfo Saclay
K14A	P_o	$\pi^+p \rightarrow \pi^+p$	0·62 to 2·69	RHEL/Oxford
K9 + HBC	inelastic processes	π^+p	1·1 to 1·9	Westfield/Imperial Colleg
K15	$\frac{\partial\sigma}{\partial\Omega}$	$\pi^+p \rightarrow \pi^+p$	0·6 to 2·0	Bristol/RHEL
π9	P_o	$\pi^-p \rightarrow \pi^\circ n$	0·6 to 3·0	RHEL/Glasgow
K8	$\frac{\partial\sigma}{\partial\Omega}$	$\pi^{\pm}p \rightarrow \pi^{\pm}p$	1·0 to 1·4	UCL/RHEL

* $\frac{\partial\sigma}{\partial\Omega}$: measurement of angular distributions

P_o : measurement of polarization effects using a polarized target

σ_{TOT}: measurement of total cross-section

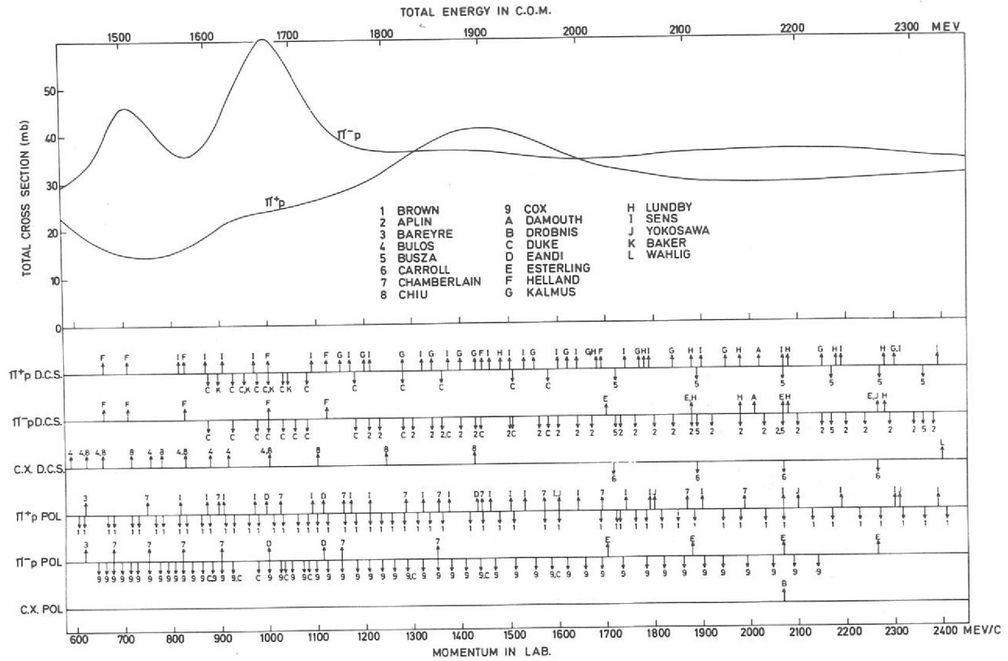

Figure 5. Summary of the world data on πp elastic scattering measurements in the range 600 to 2400 MeV/c. The arrows below the line indicate measurements made at RHEL; arrows above the line indicate measurements at all other laboratories.

In these experiments angular distributions and polarization effects were measured, which then allowed the very powerful phase shift analysis method to be applied to the unravelling of particle states of different spin. It very quickly became clear from the results of these early experiments that the broad peaks in the total cross-section graphs contained several resonances superimposed on each other. In particular the 1688 MeV peak in the π^-p cross-section was found to be dominated by two resonances, and in fact a total of four resonances were finally shown to exist in this small region. With this work came the realisation that in the πN system there existed a very large number of resonance states (this also implies via SU(3) theory that an equally large number of strange baryons Ξ*, Λ*, Σ* should exist). As is shown in the table this work has progressed vigorously at RHEL with polarization and differential scattering experiments of increasing accuracy and increasing numbers of momentum settings being performed. A typical angular distribution curve is shown in figure 6; some typical polarization measurements are shown in figure 15. Referring back to figure 5, the arrows below the line show momentum points at which measurements have been made at RHEL, and those above the line represent measurements at all other laboratories; RHEL is seen to have produced approximately one half of the world's data.

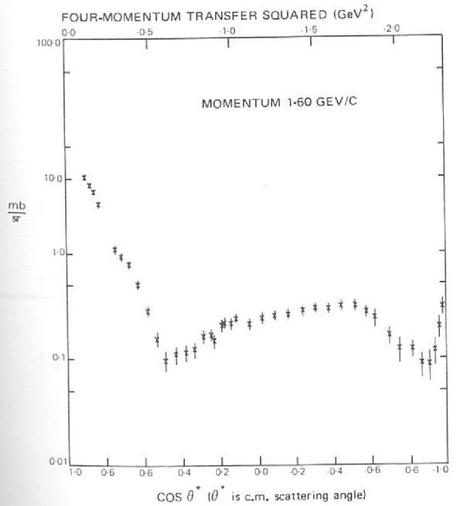

Figure 6. π^-p Differential cross-section measurements made at 1·60 GeV/c from Aplin et al (Experiment No. 1, 1969 Annual Report).

Various detailed phase shift analyses have been made on this vast bulk of data and the results show that at least 20 πN resonances exist in the mass region up to 2·85 GeV/c^2. The first total cross-section experiments showed little more than the tip of the iceberg. Many of the resonances are highly inelastic (i.e. they tend to decay to other channels rather than back to πp) and hence studies of inelastic scattering are essential if this rather complex situation is to be fully understood. It is invaluable to have the momentum points as closely spaced as possible, so that the phase shift analysis can be continued smoothly through the whole momentum scale.

A similar situation exists with respect to the baryons with strangeness -1 which have to be studied through K^-p and K^-n interactions. Table 5b and figure 7 summarises the Rutherford Laboratory contribution to this field.

Table 5b

Experiments on $\bar{K}N$ interactions in the momentum range up to 2·5 GeV/c

Reference on figure 7	Experiment No. in this report	Measurement$^\phi$	Reaction	Momentum (GeV/c)	Team
A	(Beam K6)	σ_{TOT}	K^-p and K^-n	0·59 to 2·66	B'ham/Cambridge/RHEL
B	1	$\frac{d\sigma}{d\Omega}$	$K^-p \to K^-p$	0·62 to 0·94	Birmingham/RHEL
C	2	$\frac{d\sigma}{d\Omega}$	$K^-p \to K^-p$	1·12 to 1·40 and 1·75 to 2·45	University College/RHEL
D	19	$\frac{d\sigma}{d\Omega}$	$K^-p \to K^-p$	1·25 to 1·85	CRSS*
E	20‡	$\frac{d\sigma}{d\Omega}$	$K^-p \to K^-p$	0·96 to 1·36	RHEL
F	25	$\frac{d\sigma}{d\Omega}$	$K^-n \to K^-n$	1·04 to 1·70	Glasgow/Imperial College
G	(Beam K7)	$\bar{P}\frac{d\sigma}{d\Omega}$	$K^-p \to K^-p$	1·085 to 1·370	Oxford/RHEL
D	19	$\frac{d\sigma}{d\Omega}$, $\bar{P}\frac{d\sigma}{d\Omega}$	$K^-p \to \Lambda\pi^\circ$	1·25 to 1·85	CRSS*
F	25	$\frac{d\sigma}{d\Omega}$, $\bar{P}\frac{d\sigma}{d\Omega}$	$K^-n \to \Lambda\pi^-$	1·04 to 1·70	BEGI†
H	3	$\frac{d\sigma}{d\Omega}$, $\bar{P}\frac{d\sigma}{d\Omega}$	$K^-p \to \Lambda\pi^\circ$	0·685 to 0·990	Oxford
E	20‡	$\frac{d\sigma}{d\Omega}$, $\bar{P}\frac{d\sigma}{d\Omega}$	$K^-p \to \Lambda\pi^\circ$	0·96 to 1·36	RHEL
H	3	$\frac{d\sigma}{d\Omega}$, $\bar{P}\frac{d\sigma}{d\Omega}$	$K^-p \to \Sigma^\circ\pi^\circ$	0·685 to 0·990	Oxford
D	19	$\frac{d\sigma}{d\Omega}$, $\bar{P}\frac{d\sigma}{d\Omega}$	$K^-p \to \Sigma^\pm\pi^\mp$	1·25 to 1·85	CRSS*
E	20‡	$\frac{d\sigma}{d\Omega}$, $\bar{P}\frac{d\sigma}{d\Omega}$	$K^-p \to \Sigma^\pm\pi^\mp$	0·96 to 1·36	RHEL
D	19	$\frac{d\sigma}{d\Omega}$, $\bar{P}\frac{d\sigma}{d\Omega}$	$K^-p \to \Lambda\omega$, $\to Y^*\pi$, $\to K^*N$	1·25 to 1·85	CRSS*
E	20‡	$\frac{d\sigma}{d\Omega}$, $\bar{P}\frac{d\sigma}{d\Omega}$	$K^-p \to \Lambda\omega$, $\to Y^*\pi$, $\to K^*N$	0·96 to 1·36	RHEL
F	25	$\frac{d\sigma}{d\Omega}$, $\bar{P}\frac{d\sigma}{d\Omega}$	$K^-n \to Y^*\pi$	1·04 to 1·70	BEGI†

*CRSS : Collaboration of College de France, Rutherford Lab., Saclay, Strasbourg.
†BEGI : Collaboration of Birmingham, Edinburgh, Glasgow, Imperial College.
‡Film for this experiment obtained from CERN 2 m bubble chamber.
ϕ σ_{TOT} : measurement of total cross-section.
$\frac{d\sigma}{d\Omega}$: measurement of differential cross-section.
$\bar{P}\frac{d\sigma}{d\Omega}$: measurement of polarization x $\frac{d\sigma}{d\Omega}$

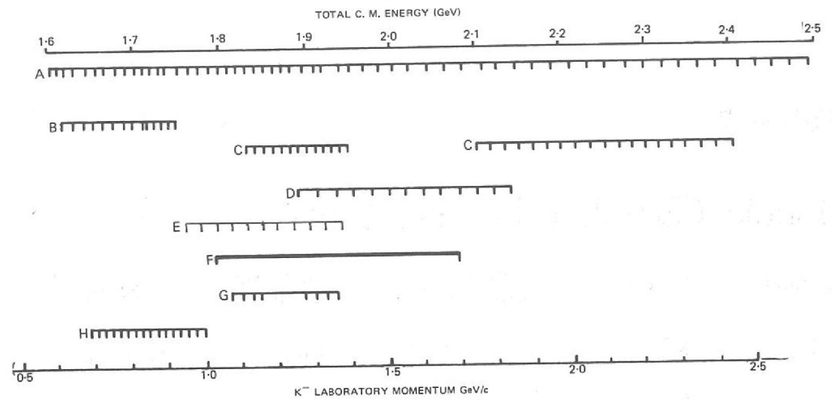

Fig. 7. Summary of Rutherford Laboratory measurements on the $\bar{K}N$ interaction. The vertical marks indicate the momentum points at which measurements have been made. The experiments with unbroken horizontal bars had a continuous effective momentum coverage.

Weak Interaction Experiments

Approximately one quarter of the experiments discussed in this year's report relate to the weak and electromagnetic interactions. A central feature for most of the experiments has been the search for small violations to the normal, and quite well understood, weak and electromagnetic interactions. Most of these experiments are in an analysis or data taking stage, and should produce intermediate or final results during 1971.

Table 6

Weak and Electromagnetic Interaction Experiments using Electronic Techniques

Number	Experiment	Beam Line	Status of Expt. (at Dec. 1970)
11	A Measurement of the Electron Asymmetry Parameter of the Polarized Σ^-	π4	Analysis
12	Test of the $\Delta I = \frac{1}{2}$ Rule in the Decay $\Sigma^+ \to p\pi^\circ$	K14	Analysis
13	Test of the $\Delta S = \Delta Q$ Rule for K° Leptonic Decays	K13	Analysis
14	Study of the Decay Modes $K^\pm \to \pi^\pm\pi^\circ\gamma$ and $K^\pm \to \pi^\pm\pi^\circ\pi^\circ$	CERN	Analysis
15	Bremsstrahlung Anomalies	K13B	Analysis
16	Search for Charge Asymmetry in η Decay	π8	Data Taking
17	A Search for the C-violating Decay $\eta \to \pi^\circ e^+e^-$	π8	Setting up
18	ISR Search for the Intermediate Boson	CERN	In Preparation

Table 7

Bubble Chamber Experiments

Number	Reaction	Momentum Range (GeV/c)	No. of Pictures x 10^6	Status
19	K^-p	1·25 to 1·85	1·65	Analysis
20	K^-p	0·96 to 1·36	0·43 at CERN	Analysis
21	$\bar{p}p$	1·23 to 1·43	0·1 at CERN	Analysis
22	K^-p	14·25	0·35 at CERN	Analysis and data taking
23	π^+d	4·0	0·42 at CERN	Analysis and data taking
24	π^+p	0·8 to 1·7	0·62	Analysis
25	K^-d	1·45 and 1·65	0·71	Analysis
26	K^+p K^+d	2·1 to 2·9 2·2, 2·45, 2·7	0·21 0·92	Analysis Analysis
27	np	1·0 to 7·5	0·11	Analysis
28	np	1·0 to 3·5	0·09	Analysis
29	K^- in heavy liquid	2·2	0·68	Analysis
30	Anomalies in electromagnetic processes		0·31	Analysis
31	Development of Neon-hydrogen track sensitive target facility for 1·5 m hydrogen chamber.			

1·5 m Bubble Chamber Programme

The programme for the 1·5 m hydrogen bubble chamber has been concerned largely with the development of the track sensitive target facility, whilst the CERN 2 m chamber provided the bulk of conventional film for analysis. Nevertheless the 1·5 m chamber has produced over a million conventional pictures for four experiments during 1970, about half being taken with the chamber filled with hydrogen and half with the chamber filled with deuterium. This is to be compared with the British groups use of CERN which yielded 1·86 million pictures. The chamber has therefore contributed more than one third of the film for analysis in the UK during the year in addition to its major development programme.

Bubble Chamber Experiments

The conventional high energy physics programme saw the completion of the Imperial College/Westfield College K^+p and K^+d experiment (Experiment 26). A total of 920,000 pictures of K^+d interactions and 210,000 pictures of K^+p interactions have been taken to study the K^+N interaction in the centre of momentum energy range 2270 to 2540 MeV. The preliminary results show no evidence for the formation of exotic resonances. The Cambridge group observed anomalous behaviour of the electron bremsstrahlung and pair production processes in a test exposure made in 1969 and this has been followed up by an experiment in hydrogen using positrons and electrons at 1 GeV/c (Experiment 30). A total of 310,000 pictures were taken and analysis is in progress. The Cambridge group also received 90,000 pictures taken with a neutron beam for the analysis of inelastic np channels (Experiment 28). Finally an exposure of 133,000 pictures went to the Imperial College/Westfield collaboration for a further study of the π^+p interaction in the range 0·8 to 1·25 GeV/c (Experiment 24).

Two attempts were made during 1970 to operate the track sensitive target facility. It had been hoped that this system would be productive for high energy physics during 1970; however difficulties with chamber filling and operation occurred which have necessitated some development work. Experiments were performed to test filling procedures, and a procedure developed to give $\lesssim\frac{1}{2}\%$ variation in the stopping power of the mixture with height in the chamber. An understanding of the reasons for target failure in the June/July runs has led to a major overhaul of the chamber top-plate seals and a slight modification of the target design to include a cooling loop. This allows direct control of the temperature of the liquid inside the target.

During the past year partial wave analyses have been completed on the two body final states of the K^-p survey experiment (Experiment 19). New results include a measured width of 300 MeV for the $\Lambda^*(2100)$ and a large elasticity of 0·15 for the $\Sigma^*(1915)$ from analysis of the elastic channel. Other possible resonances require confirmation from further experiments. This experiment has been extended to lower energies with new film taken in the CERN 2 m hydrogen bubble chamber (Experiment 20).

The 14 GeV/c K^-p experiment has produced a measurement of the K^-p elastic total and differential cross-section (Experiment 22) with greatly improved accuracy over previous counter experiments in this region. This experiment will acquire more pictures in 1971. The new 4 GeV/c π^+d experiment (Experiment 23) received the first half of its requested pictures ($0{\cdot}8 \times 10^6$) from the CERN 2 m chamber.

The Bubble Chamber Film Analysis Facilities

The film analysis facilities at RHEL have been considerably improved in the past year. The film is scanned for interactions which are classified according to topology and then measured either manually or automatically with high precision. The large quantity of film involved and the need for high statistics makes automatic measurement, giving both speed and precision, imperative. The principle source of data is the HPD flying spot digitiser preceded by scanning and a fast manual rough digitiser stage.

The main effort during 1970 has been concentrated on improving the throughput of the combined rough digitiser – HPD system. This year has seen the installation of 6 new rough digitisers to provide guidance measurements for the HPD bringing the total to 12 digitisers at present in operation. All 12 are connected to the IBM 1130 computer which collects and checks the measurements from all machines. The 1130 programs allow for on-line scanning and calibration of the digitisers. The average event measuring rate has increased by over 50% since the system went on-line. A necessary accompaniment to this increased sophistication has been regular scheduled maintenance of the equipment.

A semi-automatic method of handling scanning information has been introduced which is designed to handle of the order of 20,000 events per week with the minimum of operator intervention. A parallel program has been developed to provide scanning efficiencies as a function of scanner, event topology, scan-table, etc, in a quickly accessible form. This allows a constant check to be maintained on the performance of the whole scanning system.

The HPD programming chain has seen continued improvements to increase the overall efficiency; in particular, a reduction in computer CPU time of the order of 20% has been achieved for the CERN filter program HAZE. Ionisation measurements from the HPD system are in routine use as an aid to the kinematic fitting. A light pen 'patch-up' system is used in production to increase the HAZE pass rate for events from approximately 70% to 85% for a single pass.

The throughput of the film analysis laboratory as determined from the number of events passing successfully through the HAZE program is given for the year in figure 8. The total number of events measured in the calendar year 1970 exceeds 200,000.

Two film plane manual digitisers have also been installed during the year and have proved of great value for the measurement of events which present the HPD with some difficulty. The machines have also been in demand for spark chamber film analysis.

The events measured in 1970 have been distributed between three experiments ranging from the 0·96 to 1·36 GeV/c K^- survey up to the 14·3 GeV/c $\bar{K}p$ experiment; the latter being the highest energy K^- experiment so far attempted by any group. These experiments are described in the subsequent sections of this report.

Figure 8. Monthly output of the Rutherford Laboratory Bubble Chamber Film Analysis System in 1970.

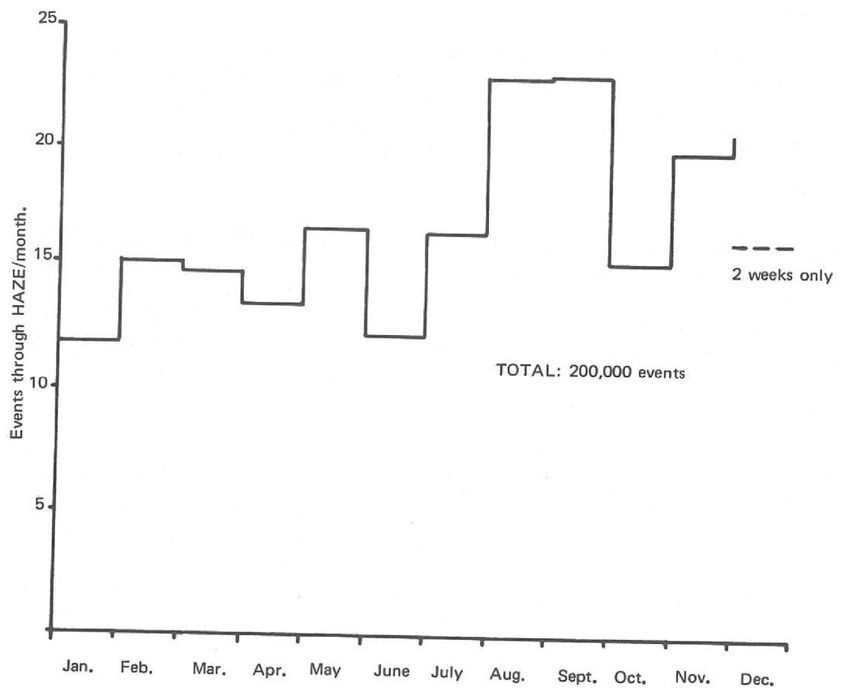

Table 8

Nuclear Structure Experiments

Number	Experiment	Accelerator	Status
32	Total Reaction Cross-Sections for Pions on Nuclei	π10 beam Nimrod	Setting up
33	A Search for Superheavy Elements	CERN Proton Synchrotron	Data taking
34	Neutron-Proton Bremsstrahlung	AERE 110 inch Synchro-Cyclotron	Data taking/ Analysis
35	Medium Energy Nucleon Reaction Studies	Tandem Van de Graaf and AERE Variable Energy Cyclotron	Data taking/ Analysis

With the closure of the 50 MeV Proton Linear Accelerator (PLA), mentioned in the 1969 Annual Report, the Rutherford Laboratory ceased to have a machine specifically designed for studies in nuclear structure physics. However, the Laboratory continues to take an active interest in this field through the resident Nuclear Physics Group. The activities of this group now mainly lie in the use of high energy particle beams, from accelerators such as Nimrod, for studies of the structure and properties of atomic nuclei. Two such experiments are described below. One of these uses high energy pion beams from Nimrod in a measurement of total reaction cross-sections to gain further information about the density distribution of neutrons in nuclei. The other experiment uses targets irradiated in 24 GeV proton beams from the CERN Proton Synchrotron in an attempt to produce, by secondary reactions in the targets themselves, the very heavy nuclei which it has recently been suggested should exist in the region around Z = 114.

The Laboratory also actively supports some of the university groups using the accelerators available at AERE, in particular, those groups which previously used the PLA for nuclear physics research. Two members of the resident group have collaborated with a combined AERE/Queen Mary College, London, group to use high energy neutron beams from the 140 MeV Synchro-Cyclotron for studies of elastic and inelastic neutron – proton scattering. Active support has also been given to a combined team based on the Kings College, London, group who have carried out a variety of experiments concerned with nuclear reactions and scattering at medium energies on the Tandem Van de Graaf and Variable Energy Cyclotron at AERE. Groups from the universities of Birmingham and Manchester have also used the Laboratory's computing facilities to complete the analysis of experiments originally carried out using the PLA.

Publications associated with the various experiments, described in the following pages, are indicated by marginal reference numbers linked to the List of Publications at the end of the Report.

Experiment 1

UNIVERSITY OF BIRMINGHAM
RUTHERFORD LABORATORY

$K^{\pm}p$ Differential Cross Sections in the Momentum Range 0·45 to 0·90 GeV/c (ref. 4, 103, 104, 126, 136)

The purpose of these experiments on K^-p and K^+p elastic scattering is to improve the accuracy of the data in a region where many Y* resonances have been found, or are suspected, and to clarify the question of possible structure in the K^+p cross-section which might have a bearing on the existence of the controversial Z* resonances.

Data taking has been completed for these two experiments. The detection system used included sonic spark chambers to measure the differential scattering cross-sections for K^+p scattering at 13 momenta between 430 and 930 MeV/c, and for K^-p scattering at 14 momenta between 600 and 930 MeV/c. Analysis of these data has proceeded during 1970 in parallel with the setting up of a related experiment (Experiment 9) to measure $K^{\pm}n$ scattering over the same momentum range.

Two arrangements were used, and angular distributions from one of these, the correlation mode, at centre of momentum angles in the range $-0{\cdot}7 \leqslant \cos\theta^* \leqslant 0{\cdot}7$, have been extracted from the data. These results improve on the statistics of previous data in the same momentum region by factors of between 4 and 20. There remain some corrections, affecting primarily the absolute values of the results which are still being studied. Typical distributions are shown in figure 9.

The analysis of the data for forward and backward angles has involved a careful study of systematic effects in the spark chambers which affect the accuracy of momentum fitting. Good momentum resolution is essential to separate elastic events as well as possible from the high background of kaon decays. Figure 10 shows a typical momentum distribution and illustrates the way in which this separation is achieved.

The data at low momenta are of sufficient statistical quality to determine unambiguously the sign of the K^+p Coulomb interference which was poorly measured in previous experiments. Preliminary results at one momentum (476 MeV/c) indicate a positive sign. This information will help to reduce the number of possible phase shift solutions.

Figure 10. Momentum distribution of tracked particles through the spectrometer magnet of Experiment 1. The momentum of the incident K beam was ~800 MeV/c and the selected particles have angles of about 7° to the incident beam in the laboratory reference frame.

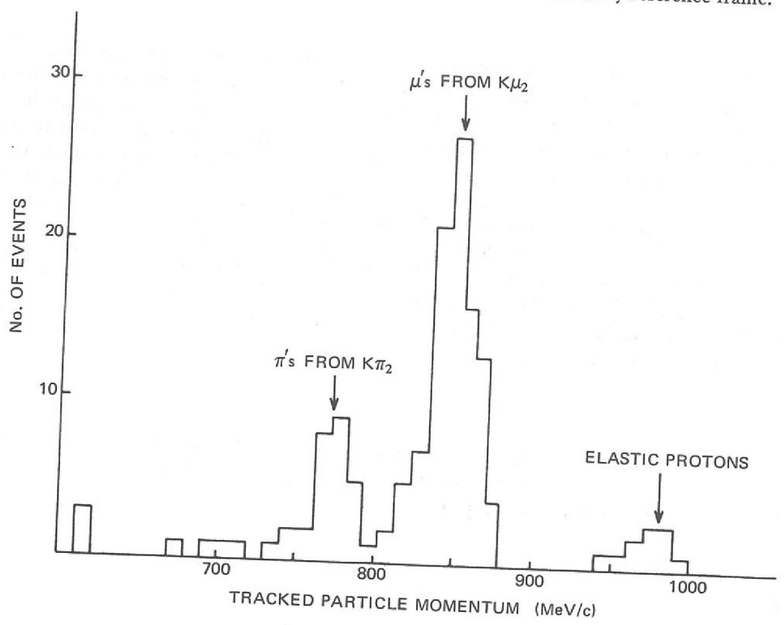

Figure 9. Typical angular distributions for K^-p elastic scattering from Experiment 1, with correlation geometry. The statistical quality considerably exceeds earlier experiments. Absolute normalisation is being finalised.

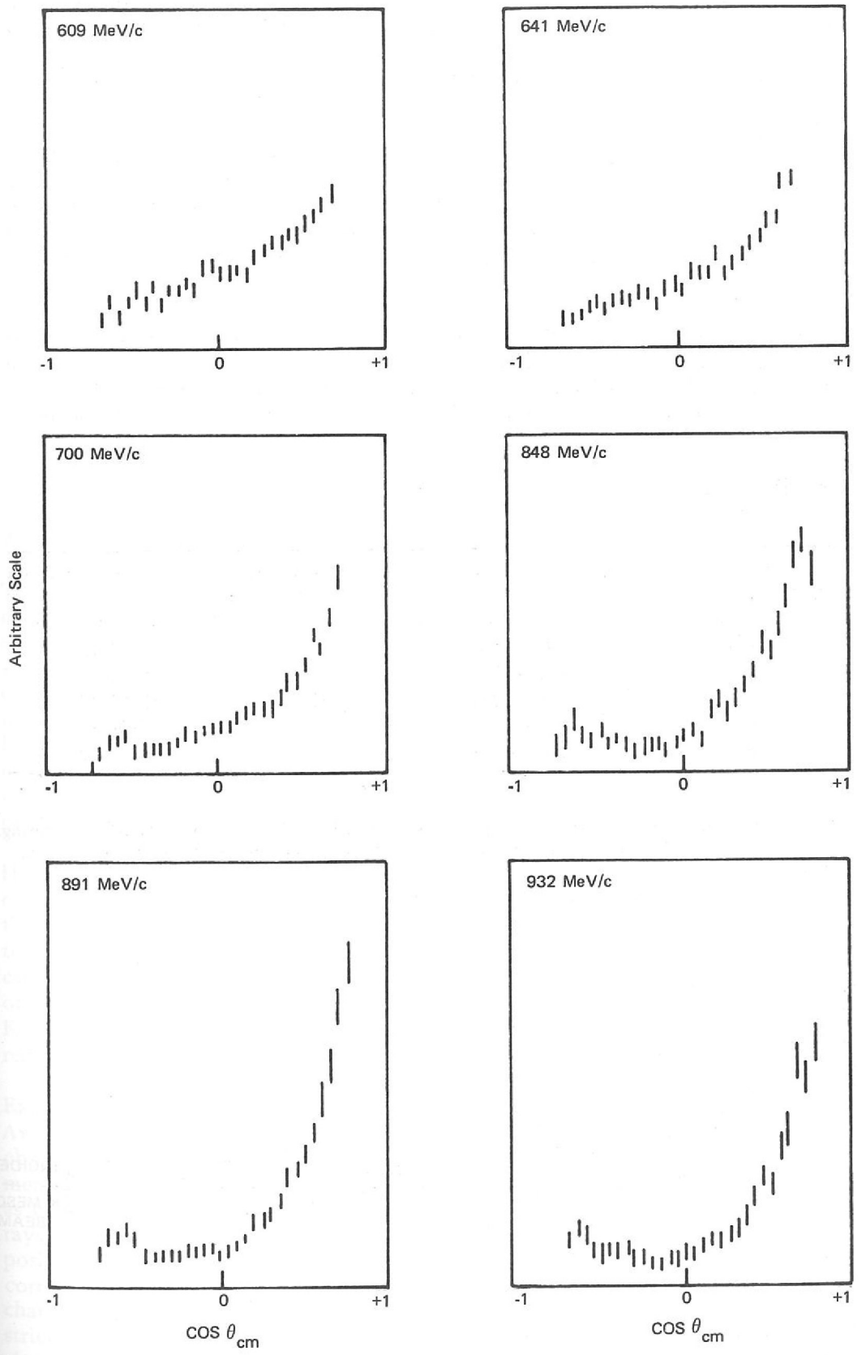

Experiment 2

UNIVERSITY COLLEGE, LONDON
RUTHERFORD LABORATORY

$K^{\pm}p$ Differential Cross-Sections in the Momentum Range 0·9 to 2·2 GeV/c (K^-) and 1·6 to 2·4 GeV/c (K^+)

The aim of this particular group of experiments is the measurement of the differential cross-sections of K^+p and K^-p elastic scattering over a wide range of momenta to provide data to assist in the classification of some of the hyperon resonances and search for effects due to possible 'exotic' Z^* resonances. The range of measurements made is shown in table 9. A substantial amount of πp data was obtained as a useful by-product.

The experimental arrangement is shown in figure 11. Incident particle directions were determined by two counter hodoscopes (H1 and H2) and particles scattered from a 15 cm liquid hydrogen target were detected by core read-out wire spark chambers (S1 to S8) on-line to a PDP-8 computer. Data acquisition was completed in May 1970 and the analysis has reached an advanced stage. Table 9 summarises the experiments and gives the number of elastic events obtained from the raw data.

A phase shift analysis was performed on the K^+p preliminary data together with existing data and four solutions were found (figure 12). The solutions are characterised by partial wave amplitudes which become increasingly absorptive with increasing momentum and no solution gives any evidence of a Z_1^* resonance.

Table 9

Process	Momentum GeV/c	No. of Momenta	No. of Elastic Events
π^+p	1·715	1	60,000
π^+p	1·0 to 1·4	14	100,000
π^-p	1·0 to 1·4	14	100,000
K^+p	1·4 to 2·3	28	150,000
K^-p	1·0 to 1·4	13	60,000
K^-p	1·7 to 2·4	19	80,000

Figure 11. Schematic diagram of the apparatus used in Experiment 2 to study $K^{\pm}p$ scattering. C1 to C5 are scintillation counters, V1 to V5 are veto counters and S1 to S8 are wire spark chambers.

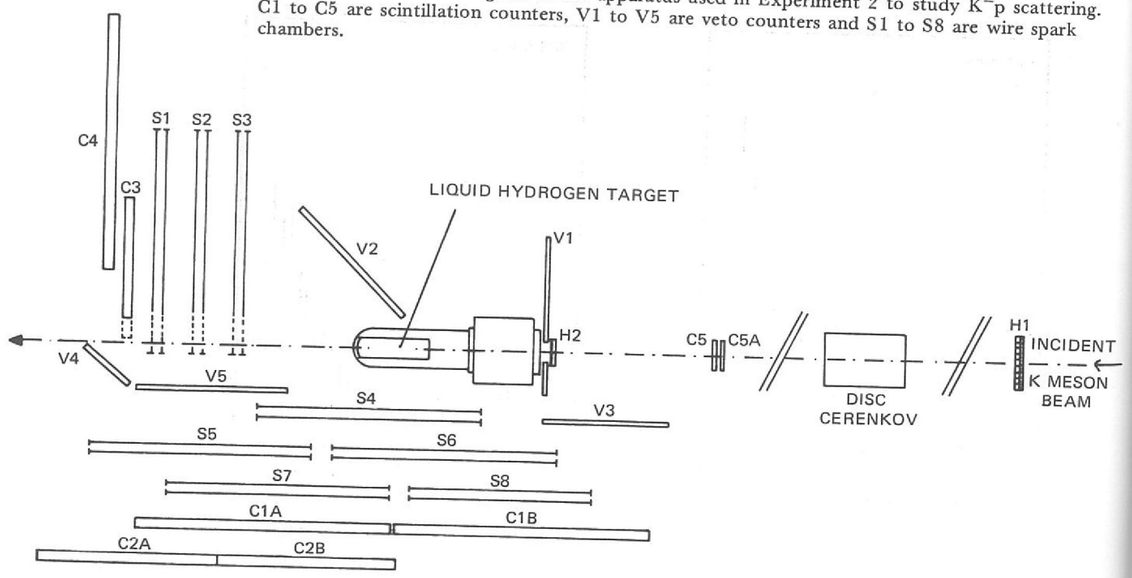

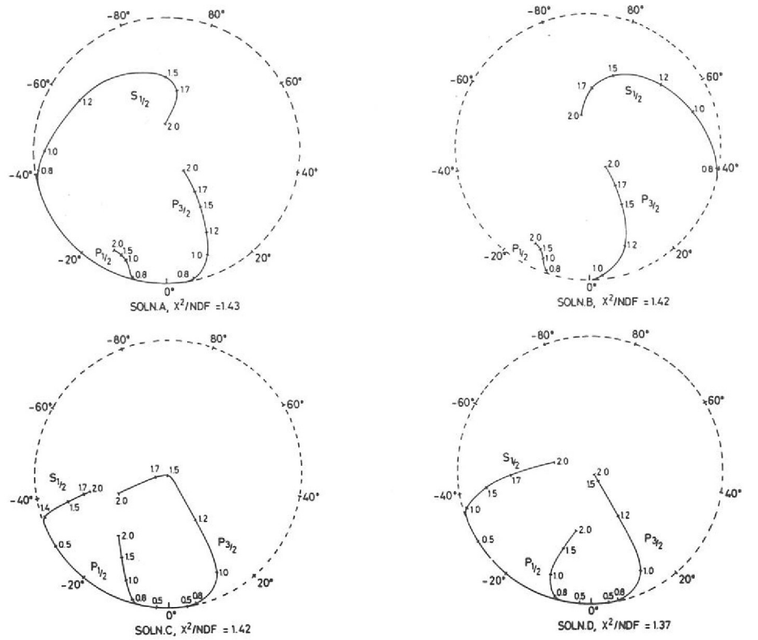

Figure 12. Four solutions found from phase shift analysis of the K^+p preliminary data from Experiment 2 together with existing data.

Experiment 3

UNIVERSITY OF OXFORD

Neutral States Produced in K^-p Elastic Scattering

The properties and quantum numbers of unstable particles (loosely called resonances) are of considerable interest in the study of the systematics of the strong interactions. If it is experimentally possible, these resonances are best studied in 'formation' experiments wherein a target particle and a missile particle collide and coalesce to form a new particle or resonance, which then has quantum numbers that are the sum of those of the initial particles. The new particle is short lived and soon decays either back to the two original particles or to some other combination of particles. The total energy available in the collision corresponds to the mass of the particle formed. By working at a series of beam energies it is possible to form a range of new particles.

Hyperon resonances can decay into $\bar{K}N$, as well as other channels such as $\Lambda\pi$ and can thus be studied by careful analysis of K^-p formation experiments, as a function of the incident K^- momentum. A partial wave analysis, which projects out the behaviour of amplitudes with specific angular momentum quantum numbers is essential. Such analysis is simplified by looking at processes in which the number of accessible isotopic spin quantum states is restricted. Two such channels are $K^-p \to \Lambda\pi^\circ$ and $K^-p \to \Sigma^\circ\pi^\circ$ where the isotopic spin is restricted to I = 1 and I = 0 respectively. This experiment concentrates on these two interactions.

Experimentally, the unambiguous separation of these states, and others like $\Lambda\pi^\circ\pi^\circ$, depends on high gamma ray detection efficiency, for it is essential to observe all the gamma rays from the decay of the neutral pions. In this experiment the high efficiency is achieved by surrounding the liquid hydrogen target as completely as possible with steel plate spark chambers. In these the gamma rays have an individual probability of 98% of converting into a visible electron-positron shower. A scintillation counter system rejects those events which do not correspond to an 'all neutral' final state, from which a later Λ decay produces charged particles. These charged particles are also detected, both in magnetostrictive wire spark chambers which lie between the hydrogen target and the gamma chambers, and in the gamma chambers themselves.

Selection of events is initially made by scanning and then by kinematic fitting. A total of $\sim$ 3,500 $\Lambda\pi^\circ$ events and $\sim$ 1,600 $\Sigma^\circ\pi^\circ$ events is expected when analysis is complete.

Data was taken at 16 momentum values between 685 MeV/c and 990 MeV/c, and some data has been analysed to obtain preliminary $\Lambda\pi^\circ$ and $\Sigma^\circ\pi^\circ$ angular distributions for momenta between 685 MeV/c and 800 MeV/c.

A partial wave analysis has been carried out on this data combining our new data with that of the CERN Heidelberg Saclay collaboration (CHS) in the same region. Figure 13 shows the solution for the $\Sigma^\circ\pi^\circ$ channel. The lighter lines on the amplitude diagrams are the energy independent solution of CHS, shown for the full range 440 to 1200 MeV/c, and the heavy lines are our combined solution for the range 680 to 800 MeV/c. The overall fit is reasonable, χ^2 of 100 on 87 points, though our data requires larger couplings for the $\Lambda(1670)S_{01}$ and $\Lambda(1750)P_{01}$ states, while the D_{03} state remains unchanged.

Figure 13. Solution for the $\bar{K}N \to \Sigma^\circ\pi^\circ$ channel obtained from a partial wave analysis of the data from Experiment 3 combined with data from the CERN/Heidelberg/Saclay collaboration.

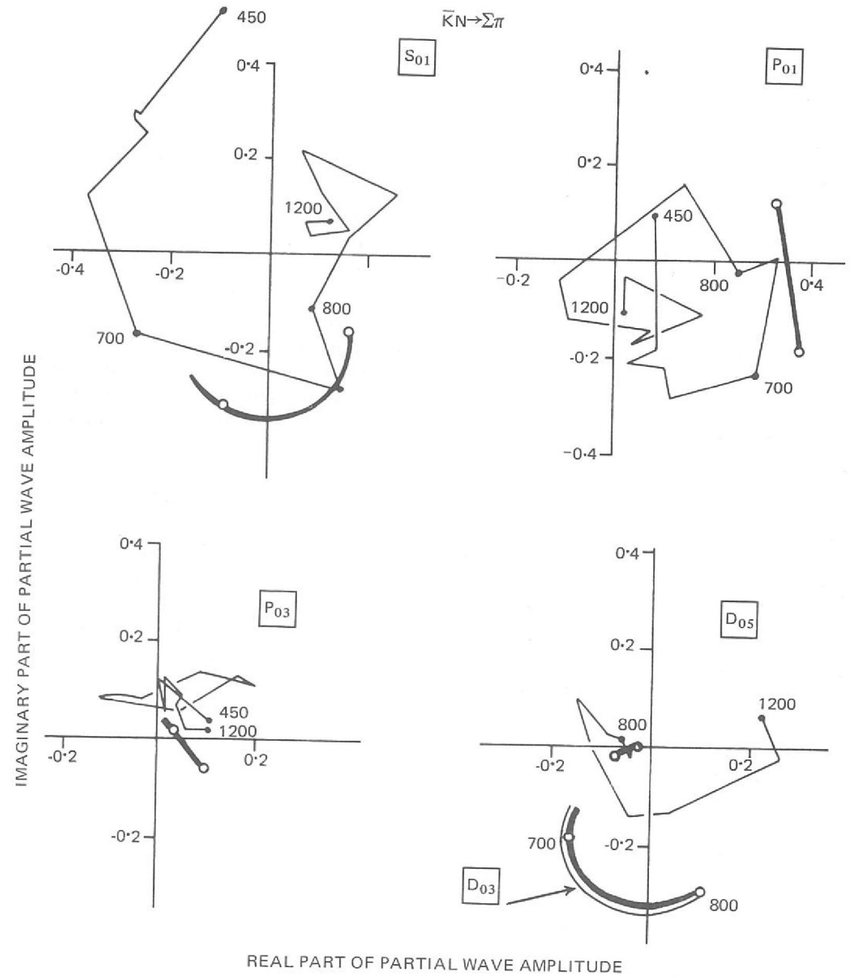

Experiment 4

UNIVERSITY OF OXFORD
RUTHERFORD LABORATORY

Polarization Effects in π^+p Elastic Scattering (ref. 101)

In this experiment the asymmetry in the elastic scattering of pions by polarized protons has been measured as a function of the centre of momentum angle at 68 lab. momenta between 600 and 2700 MeV/c. A large number of pion-nucleon resonances are known to be produced in this momentum range and others have been suggested by current theoretical models. One of the objects of the experiment was to provide new data to incorporate into an analysis in terms of partial wave amplitudes or phase shifts; from the behaviour of these phase shifts as a function of the momentum of the incident pion it is possible to obtain information on the properties of any resonant states which may be formed in the scattering process.

The experimental arrangement is shown in figure 14. The target consisted of an assembly of Lanthanum Magnesium Nitrate crystals, in which the free protons in the water of crystallisation were polarized by means of the 'solid effect'. The polarization, which reached values in excess of 70% during the experiment, was continuously monitored by a nuclear magnetic resonance system to an accuracy of ±4%. The target contained approximately 16 times as many bound protons as free protons and these were not polarized.

Scattered particles were detected in hodoscopes which consisted of vertical and horizontal scintillation counters. They defined the scattering angles to within ±3° over most of the angular range, so enabling elastic events to be distinguished from the large number of background events produced, in particular, by the bound protons in the target material.

Water and perspex Cerenkov counters were used to separate pions from protons in the region where they were not clearly distinguishable by kinematics; a gas Cerenkov counter was used to reject the high background of inelastic pions which contaminated the forward scattered protons. Information from the counters was recorded on magnetic tape by a DDP 516 computer, which was also used for diagnostic purposes.

Figure 14. Schematic diagram of the apparatus used in Experiment 4 to study π^+ scattering on polarized protons.

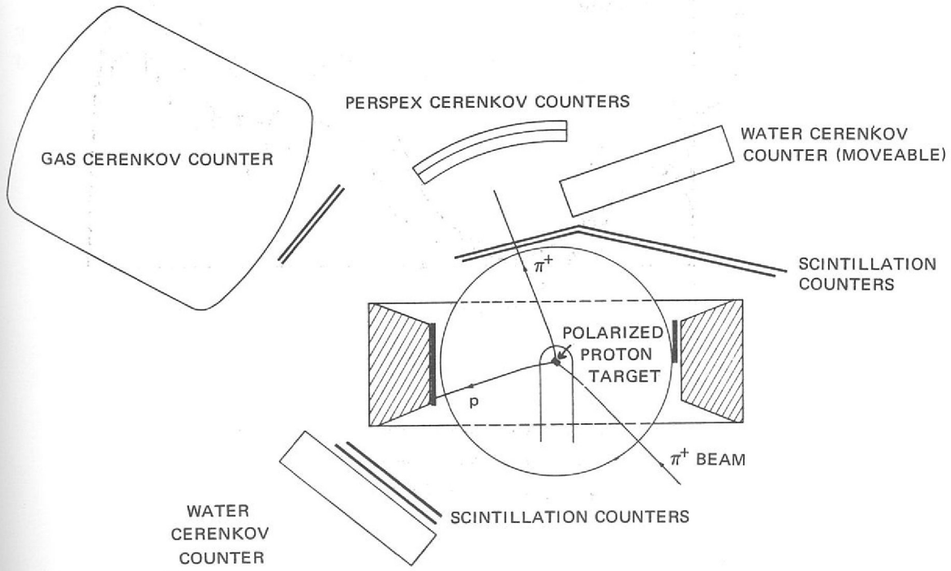

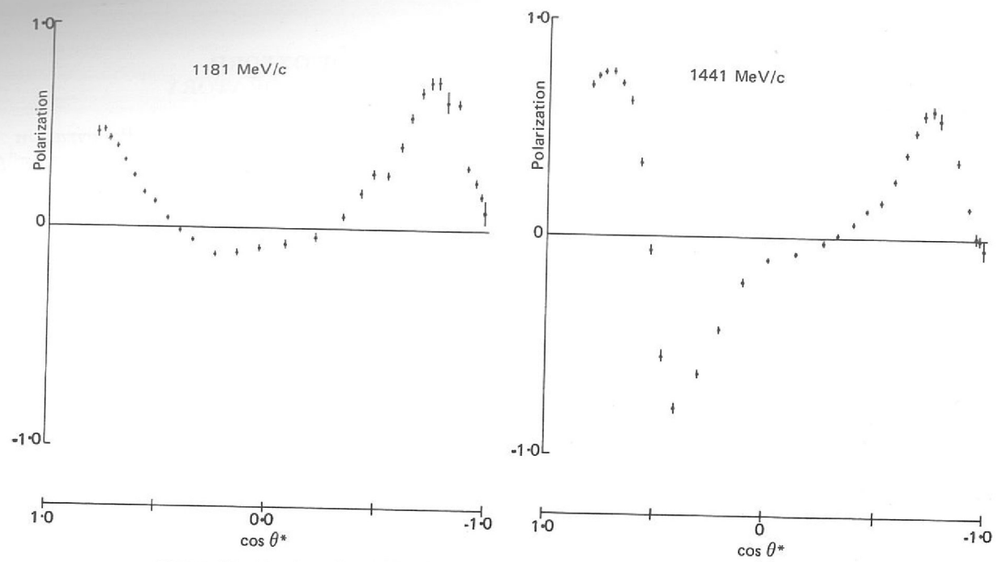

Figure 15. Results of polarization measurements at two momenta from Experiment 4. θ^* is the centre of momentum scattering angle.

The experiment was completed in November 1970. A substantial fraction of the data has undergone preliminary analysis, and the results at two momenta are shown in figure 15. Some of the data have been compared with the results of various phase shift analyses. A typical example is shown in figure 16. A search for new and better solutions will be made when the final analysis of the data is complete. However, it is already clear that the polarization is a very sensitive function of the phase shifts in this momentum region and that the results of this experiment should substantially reduce the range of values that they can assume.

Figure 16. Polarization data at 975 MeV/c from Experiment 4 compared with some phase shift predictions.

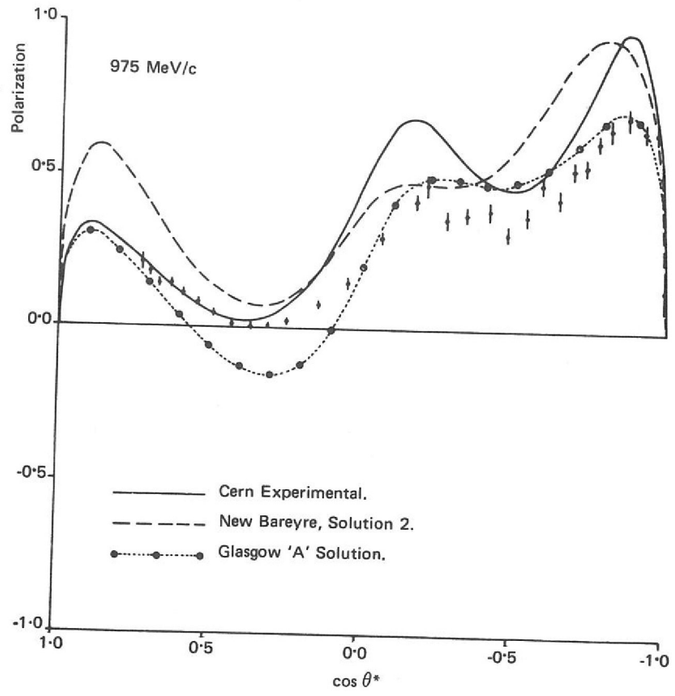

QUEEN MARY COLLEGE, LONDON.
UNIVERSITY OF BERGEN
AERE, HARWELL
RUTHERFORD LABORATORY

Experiment 5

Wide Angle Elastic pp Scattering

This experiment is a measurement of differential cross-sections for proton-proton elastic scattering at lab. momenta in the range 1·3 to 3·6 GeV/c and at large cm angles (40° to 90°). Previous experiments have shown a sudden change of slope in the angular distributions when the data is presented graphically in the form log ($d\sigma/dt$) against t. It was therefore decided to make detailed studies with high statistics using a scattered proton beam from Nimrod. Figure 17 shows a schematic diagram of the apparatus used. Protons in the P71 beam line were identified using a DISC Cerenkov counter and were elastically scattered in a 10 cm long liquid hydrogen target. Two arrays of scintillation counters detected the presence of the two outgoing protons. The electronics were set up so that only certain combinations of left and right counters gave a trigger. This lowered contamination by unwanted background processes, since many of these had the wrong angular correlation.

Three arrays of core read-out wire spark chambers recorded the trajectories of the interacting particles. An on-line PDP8 computer wrote the spark co-ordinates on to 7-track magnetic tape and also performed a series of histogramming tasks aimed at monitoring the performance of the apparatus.

Data was taken at 14 momenta and 1·25 million triggers were written on to tapes. A single program package scanned the data tapes, fitted vectors to the spark co-ordinates and wrote the parameters of possible elastic scatters on to a summary tape. A second program package scanned the summary tapes applying cuts to the candidates and calculating cross-sections from those found to be elastic events. These raw cross-sections were then corrected for any background still contained in the sample, and also for inefficiencies in spark chamber performance.

Figure 18 shows a plot of the differential cross-section versus centre of momentum angle for beam momenta of 1·7 and 3·0 GeV/c. A few corrections remain to be made but these are unlikely to exceed 5%. All the cross-sections are smoothly falling and flatten at 90° as required by particle identity. No trace of the structure seen at higher momenta in plots of $d\sigma/dt$ versus $-t$ is present.

There is some evidence for structure in the 90° cross-section (figure 19) which can be seen by plotting $d\sigma/dt$ versus $-t$ 90° data only.

Figure 17. Schematic diagram of the apparatus used in Experiment 5 to study pp elastic scattering at large angles.

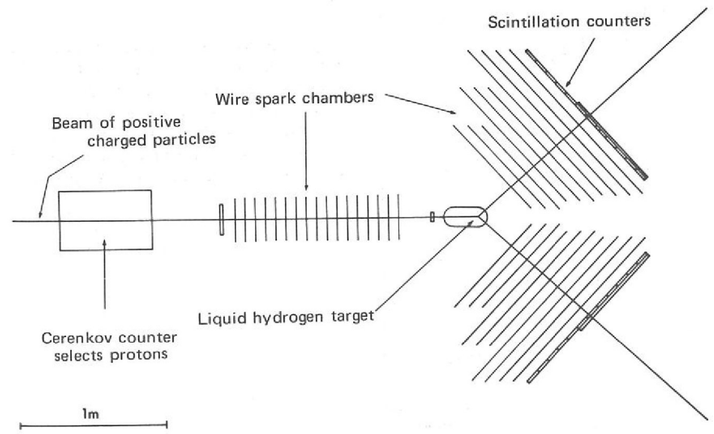

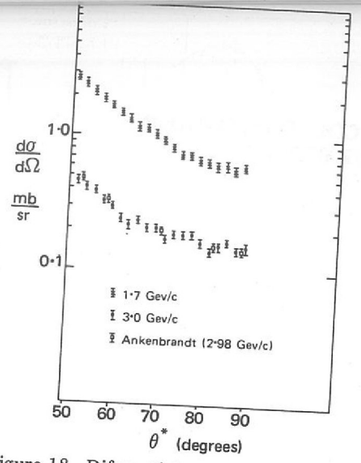

Figure 18. Diferential cross-sections for pp elastic scattering versus centre of momentum angle. The points at 1·7 and 3·0 GeV/c are from Experiment 5.

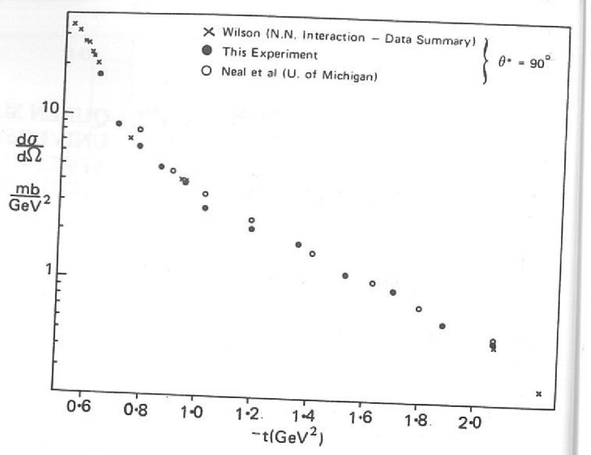

Figure 19. pp differential cross-sections at 90° centre of momentum angle versus −t (four-momentum transfer squared) (Experiment 5).

Experiment 6

IMPERIAL COLLEGE, LONDON
UNIVERSITY OF SOUTHAMPTON

An Investigation of Narrow Width Mesons Produced in π^-p Interactions (ref. 138)

This is a 'missing mass' type of experiment, in which the yield of neutrons and protons from π^-p interactions is studied as a function of the incident pion momentum. When the direction and momentum of the outgoing nucleon are known, the mass of the recoiling system (the 'missing mass') can be directly calculated, using kinematical constraints of energy and momentum conservation. The intention in this experiment is to search for, and study, narrow mesons in the mass range 500 to 2000 MeV/c².

The equipment consists essentially of a precisely controlled and variable momentum pion beam, a hydrogen target, six neutron counters near the forward direction and, surrounding the target, an arrangement of counters differentially sensitive to both charged particles and photons. Such an all-counter system permits very high data rates, compared with experiments incorporating spark chambers, but relatively little rejection of spurious events is possible once the data has been recorded.

One of the problems in all missing mass experiments is the background signal which has to be subtracted. Analysis procedures have been devised to enable this to be done reliably. As an example, the yield as a function of missing mass to the proton in $\pi^+\pi^-\pi^-$p final states is shown in figure 20a together with the estimated background. Figure 20b shows the substracted signal, with clear evidence for A_2 production.

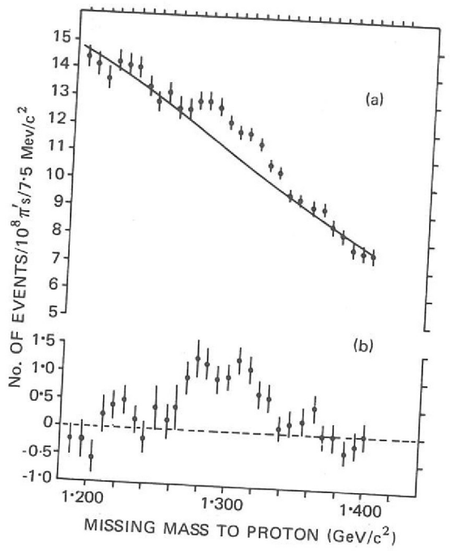

Figure 20(a) The yield as a function of missing mass to the proton in π^-p→$\pi^+\pi^-\pi^-$p events (Experiment 6). The solid line shows the deduced background.
(b) The remaining signal after the deduced background has been subtracted showing clear evidence for A_2 production.

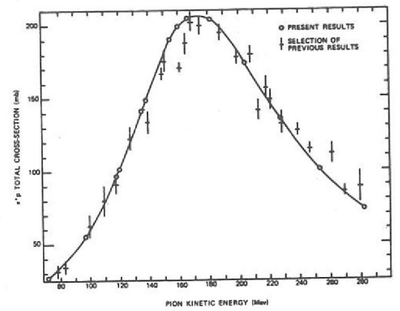

Figure 21. π^+p total cross-sections from Experiment 7 with a selection of previous results.

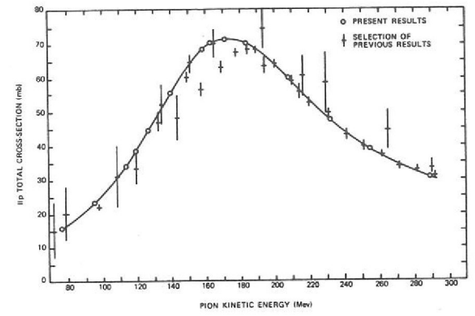

Figure 22. π^-p total cross-sections from Experiment 7 with a selection of previous results.

Experiment 7

UNIVERSITY OF CAMBRIDGE
RUTHERFORD LABORATORY

Low Energy Pion-Nucleon Interactions (ref. 13, 17, 70, 127)

A knowledge of πN interactions in the region around the first Δ resonance is fundamental to a general study of meson-nucleon physics at higher energies. The available data were sparse and relatively inaccurate, such as to warrant a comprehensive series of measurements of total cross-sections (at the ½% level of accuracy) and angular distributions (at the 1% level of accuracy) over the energy region 80 to 300 MeV.

The experiment, carried out at the CERN Synchro-Cyclotron, completed data-taking during the summer of 1970. The total cross-sections were measured by the conventional transmission counter technique, and the charge exchange total cross-section by surrounding a liquid hydrogen target with a box of scintillators. The elastic scattering angular distributions were measured by the correlation method in the angular range where both the proton and the pion emerged from the target and otherwise by an analysis with a spectrometer magnet and sonic spark chambers, of the scattered pion only.

The results so far published include the π^+p and π^-p total cross-sections, shown in figures 21 and 22 and the π^-p → π°n total charge exchange cross-section given in figure 23.

The P_{33} phase-shift has been evaluated separately for both π^+p and π^-p states. By removing the 'inner Coulomb' effects (neglected in previous analyses) parameters have been obtained for the Δ resonance in both the neutral and doubly charged states. The mean mass is 1231·7 MeV/c², with a $\Delta^\circ - \Delta^{++}$ mass difference of ≃2·9 MeV/c². The same elastic width of 113 MeV/c² is observed in both states, indicating the isospin invariance of the pion-nucleon coupling constant.

The P_{13} phase-shift shown in figure 24 has been calculated from the π^-p total cross-section and the π^-p → π°n total cross-section.

The analysis of the angular distribution data taken in the correlation mode has been completed, while that using the spectrometer magnet and sonic spark chambers is still in progress.

Figure 23. π^-p total charge exchange cross-section from Experiment 7 with a selection of previous results.

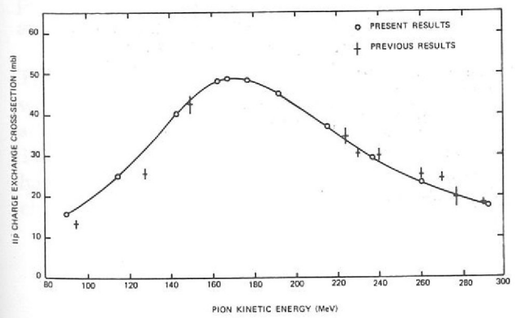

Figure 24. The P_{13} phase shift calculated from the π^-p total cross-sections and the π^-p→π°n total cross-sections measured in Experiment 7.

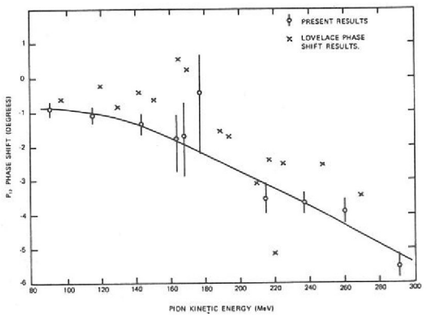

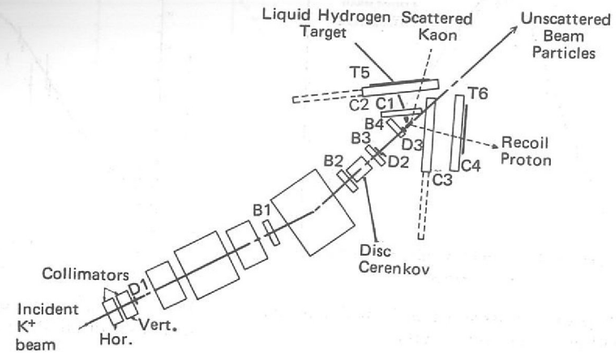

Figure 25. Schematic diagram of the apparatus used in the correlation mode of Experiment 8 to study K^+p scattering. D1 to D3 are scintillation counters and T5 and T6 are arrays of similar counters. B1 to B4 and C1 to C4 are sonic spark chambers.

Experiment 8

UNIVERSITY OF BRISTOL
RUTHERFORD LABORATORY

K^+p Differential Cross-Sections in the Range 0·9 to 2·0 GeV/c

The scattering by nucleons of positive kaons differs from that of other mesons in that resonant states are produced either very weakly, or not at all! This fact agrees well with the quark model; the composite states (π^+p), (π^-p) or (K^-p) have quantum numbers which could be made up by combining just three quarks (qqq) whereas the state (K^+p) cannot be obtained from three quarks, but would require a five quark combination $(qqqq\bar{q})$. In the simplest quark model it is postulated that these more complex states either do not exist or are produced relatively weakly. These facts have made K^+p scattering of especial interest, first to confirm whether there is in fact a small amount of resonance-like behaviour, and second to study other mechanisms of scattering in a situation where they are not dominated by resonance scattering.

The purpose of this experiment is to measure differential cross-sections for K^+p elastic scattering which, with polarization measurements from other experiments, provide a basis for a detailed phase-shift analysis of the K^+p interactions.

The Nimrod extracted proton beam X3 strikes a 10 cm copper target to produce a secondary beam of positive kaons with a momentum which can be varied from 900 to 2000 MeV/c. This passes through two stages of electrostatic separation to remove unwanted pions and protons. The kaon beam is focused on a 30 cm liquid hydrogen target after passing through a series of beam defining counters (D_1, D_2 and D_3, see figure 25) and a DISC differential Cerenkov counter which gives positive identification of kaons. There are also four acoustic spark chambers (B_1, B_2, B_3 and B_4 in figure 25) which are situated in the beam in front of the target. Of these the combination B_1 B_2 B_3 serves to determine the momentum of the beam particle from the angle of bend in the magnet M205 while the combination B_3 B_4 gives the angle at which the kaon enters the target.

Figure 26. Schematic diagram of the apparatus used in the spectrometer mode of Experiment 8. D1 to D3 are scintillation counters, and T1 to T4 arrays of similar counters. B1 to B4 and S1 to S6 are sonic spark chambers.

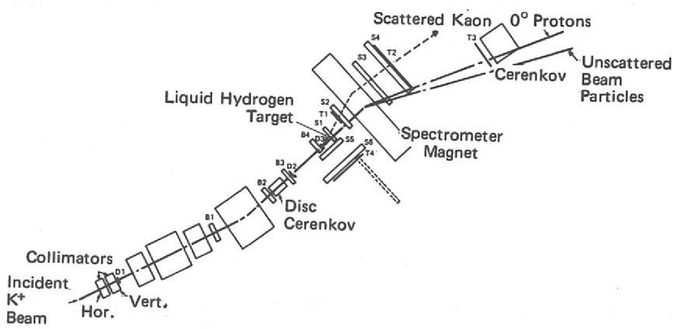

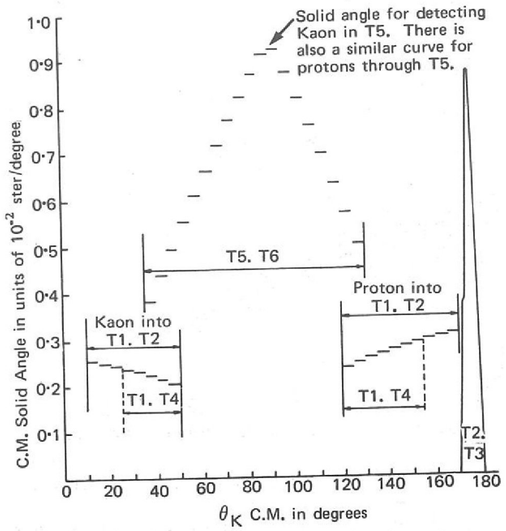

Figure 27. The solid angle for particle detection obtained with different trigger conditions for a K^+ beam momentum of 1 GeV/c (Experiment 8).

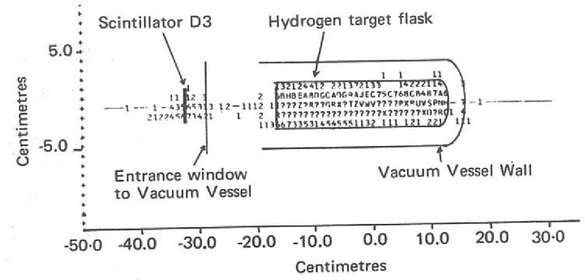

Figure 28. Scatter plot showing the distribution of scattering vertices in the region of the hydrogen target. The number of times vertices occur at the various points are indicated by incrementing through 1 to 9 then A to Z while symbol ? indicates greater than 35. (Experiment 8).

The elastic scattering events are detected in two alternative sets of acoustic spark chambers, each with its appropriate trigger counters which provide the signal to fire the spark chambers. Figure 25 shows the correlation system which identifies elastic K^+p scattering by observing the angles with respect to the incident kaon of both the scattered kaon and recoil proton; this covers a range of laboratory angles from 17° to 80°, the trigger condition being one particle through the trigger counter array T5 in coincidence with one through T6 (i.e. T5 + T6).

Figure 26 shows the 'spectrometer' mode which covers those angles where one particle may not have sufficient energy to escape from the target. The identification of elastic events is obtained by measuring the scattering angle and momentum of one particle. The spark chambers S_1 and S_2 give the scattering angle, while S_3 and S_4 give the momentum from the bend in the magnet M505/M506.

The spectrometer system covers a range of scattering angles from 3° to 25° in the laboratory reference frame; for the upper part of this range, the recoil particle has sufficient energy to be detected in the chambers S_5 and S_6. This provides some data which may be analysed either as 'spectrometer' or 'correlation' mode, giving a valuable check on the analysis. The trigger combinations for the above are T1 + T2 or T1 + T4. A third combination of trigger arrays, T2 + T3, examines the case of scattering near 180° which gives a recoil proton near 0° with momentum considerably higher than that of the incident kaon. The large threshold Cerenkov counter behind the array T3 serves to reduce the trigger rate from the decay of unscattered beam kaons. The solid angle for particle detection in the different trigger conditions is shown in figure 27.

Digital information of the positions of tracks in the spark chambers is fed, along with readings of scalers and trigger counter registers, into the core of an on-line Ferranti Argus 400 computer, which stores details of up to ten scattering events per Nimrod burst, checking the first and copying all on to magnetic tape for further analysis on the IBM 360 computer.

The apparatus has now been set up and tests with a pion beam have been made which will give π^+p differential cross-sections having value in their own right. In addition some K^+p data has been taken at momenta of 1615, 1465, 1300 and 1170 MeV/c. A total of 130,000 events (including about 48,000 elastic scatters) have been recorded in the correlation mode and 300,000 events including 10,000 elastic scatters in the spectrometer mode.

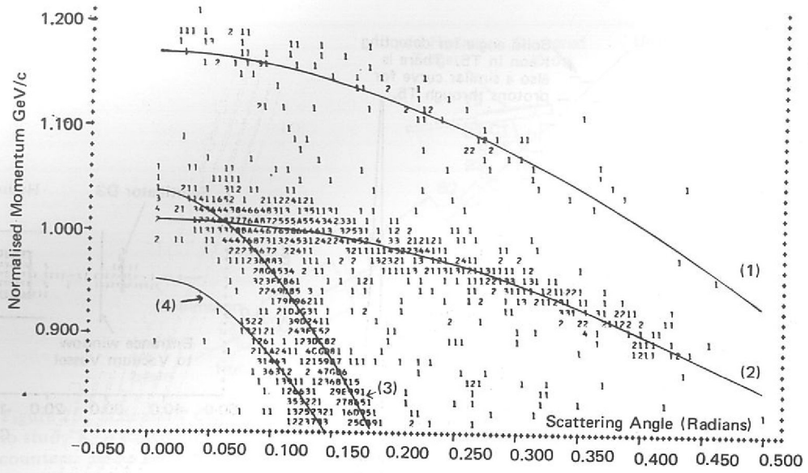

Figure 29. Scatter plot of particle momentum against angle of emission for K^+p scattering at 1·45 GeV/c. (Experiment 8).
The solid lines on the plot are kinematical predictions:—(1) Recoil protons from elastic scatters. (2) Elastically scattered kaons. (3) Muons from the decay $K^+ \rightarrow \mu^+\nu$. (4) pions from the decay $K^+ \rightarrow \pi^+\pi^\circ$.

Preliminary analysis shows good separation of elastic events. In the correlation mode the background is completely negligible because of the tight limits which can be imposed. The accuracy of reconstruction of events is illustrated by figure 28, which shows the distribution of scattering vertices in the region of the target. In the spectrometer mode, a plot of particle momentum against angle of emission (figure 29) shows satisfactory discrimination of elastic events from the background of $K^+ \rightarrow \mu^+\nu$ and $K^+ \rightarrow \pi^+\pi^\circ$ decays.

The recoil protons from events near 180° are particularly well distinguished, and it is expected that good backward points will be a valuable feature of the final results. Analysis is proceeding.

Experiment 9

UNIVERSITY OF BIRMINGHAM
RUTHERFORD LABORATORY

$K^\pm n$ Elastic and K^+ Charge Exchange Differential Cross-Sections

This experiment, which complements Experiment 1, is a measurement of K^+n elastic and charge exchange scattering and K^-n elastic scattering over the momentum range 0·45 to 0·95 GeV/c using a liquid deuterium target and sonic spark chambers. The K^+n scattering, when combined with K^+p which is a pure isotopic spin state with I = 1, allows the I = 0 state of the K-nucleon system to be studied. There is great interest in the structure in this system centred at 0·75 GeV/c, as observed in measurements of K^+p and K^+d total cross-sections made by a group at this Laboratory and more recently by an Arizona group working at Berkeley, which could be an exotic Z* resonance. The K^-n data, on the other hand, will add to our knowledge of Y* resonances and has the advantage of being a pure I = 1 state. Relatively little is known about the details of the angular distributions for any of these processes at the present time and this experiment will provide about 10^4 events for each channel at each of the momenta studied in Experiment 1.

Figure 30 shows a sketch of the apparatus which relies on identifying a K-meson by its decay in flight between chambers C3 and C4. Protons from the charge exchange process are recognised by their longer time of flight to T4 counters as well as their non-decay. Extensive tests of the equipment were carried out prior to the December shutdown and in the last few days some test data were obtained, following the first filling of the deuterium target in the beamline, with most of the apparatus working. If these data prove to be satisfactory data taking will start early in 1971.

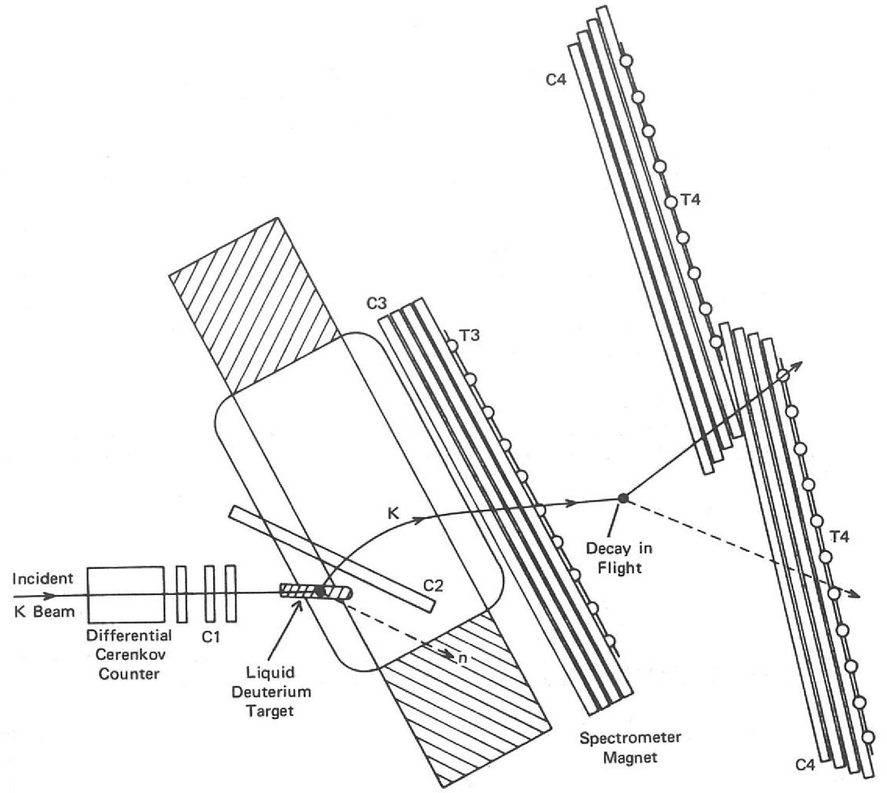

Figure 30. Schematic diagram of the apparatus used in Experiment 9 to study $K^\pm n$ scattering. C1 to C4 are sonic spark chambers and T3 and T4 are counter hodoscopes. There are veto counters (not shown) around the target and in the residual beam.

Experiment 10

QUEEN MARY COLLEGE, LONDON.
UNIVERSITY OF LIVERPOOL
DARESBURY LABORATORY
RUTHERFORD LABORATORY

Antiproton-Proton Elastic Scattering and Two Body Annihilation

Some meson resonances have masses greater than two nucleons and hence may decay into a proton-antiproton pair as well as into other mesons. It is possible therefore to study such heavy mesons by means of a 'formation' experiment in which stationary protons in a hydrogen target are bombarded by an antiproton beam. The beam momentum is chosen so that the invariant mass of the $\bar{p}p$ system equals the mass of the meson being studied. By varying the beam momentum in a number of steps a range of masses can be studied. In this experiment it is proposed to run at momenta from about 0·7 to 2·0 GeV/c so that mesons having masses from about 2·0 to 2·4 GeV/c^2 would be studied. The apparatus is designed to investigate the reactions

$$\bar{p} + p \rightarrow \bar{p} + p$$
$$\bar{p} + p \rightarrow \pi^- + \pi^+$$
$$\bar{p} + p \rightarrow K^- + K^+$$

which correspond to heavy mesons decaying into $\bar{p}\,p$, $\pi^-\pi^+$ or K^-K^+ by means of the strong interaction which was also responsible for their formation. By measuring the differential cross-sections of these reactions information about the angular momentum quantum numbers of heavy mesons and the coupling strengths to the $\pi^-\pi^+$ or K^-K^+ states can be obtained.

This experiment is being conducted at the CERN Proton Synchrotron since an accelerator having a higher energy than Nimrod is required to produce a sufficient flux of antiprotons. A new beamline has been designed which will increase the number of antiprotons in the required energy range over that previously available, and this will be set up at the beginning of 1971. Counters and wire spark chambers with ferrite core read-out will be used to detect the positions of the incoming and outgoing particles, and the momentum of one outgoing particle will be determined by passing it through a large spectrometer magnet. The spark co-ordinates and information from the counters and other components of the experiment will be read into a PDP 9/L computer, which will provide an on-line monitor of the experiment and also record data from each scattering event on to magnetic tape for subsequent full analysis by a large computer.

Most members of the experimental group moved to CERN during the Autumn of 1970. It is expected that the setting up and running of the experiment will occupy the whole of 1971 and that the group will return to the UK in 1972 to analyse the data.

Experiment 11

QUEEN MARY COLLEGE, LONDON.
RUTHERFORD LABORATORY

A Measurement of the Electron Asymmetry Parameter in the Decay of Polarized Σ^- (ref. 130)

The sigma minus decay:

$$\Sigma^- \rightarrow n + e^- + \bar{\nu}$$

is a weak interaction, and is classified to be of the semi-leptonic type. That is, it involves two leptons and two hadrons (strongly interacting particles). The presence of the strong interactions is known to produce important corrections to the otherwise simple and rather well understood weak interaction processes. The sigma beta decay, in common with neutron beta decay, cascade beta decay, and many other semi-leptonic processes has the interesting feature that the strong interaction will upset only two out of the four particles involved in the basic weak interaction. The process is described by an interaction Hamiltonion:

$$H = J_W^{\text{Hadrons}} \times J_W^{\text{Leptons}}$$

i.e. a product of two 'currents', J_W^{Leptons} is a weak interaction 'current' involving the two leptons, similarly J_W^{Hadrons} acts between the two hadrons and is therefore perturbed by the strong interaction.

N. Cabbibo has invented a most interesting theory in which the currents J_W^{Hadrons} for all possible Hadron pairs are algebraically related by way of SU(3) theory. This means in practice that the behaviour of all semi-leptonic processes can be interrelated through SU(3) algebra and its Clebsch-Gordon coefficients. Thus if the physical behaviour of a few processes is known, it is possible to make predictions about many other processes. One of the key tests of the Cabibbo theory is to study the asymmetry in the Σ^- beta decay. The prediction, using data from other leptonic processes, is that a weak interaction admixture of the form V + 0·3A will apply, in dramatic contradiction to simpler theories which give the standard V–A form for the weak interaction process, where V refers to vector interaction and A refers to axial-vector interaction.

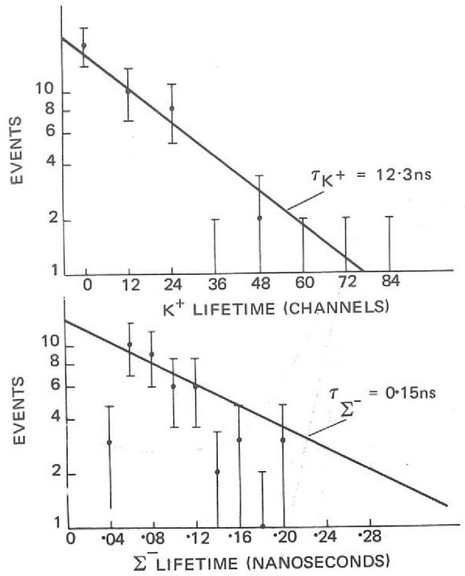

Figure 31. K^+ and Σ^- lifetime spectra determined in the Σ β-decay experiment (Experiment 11).

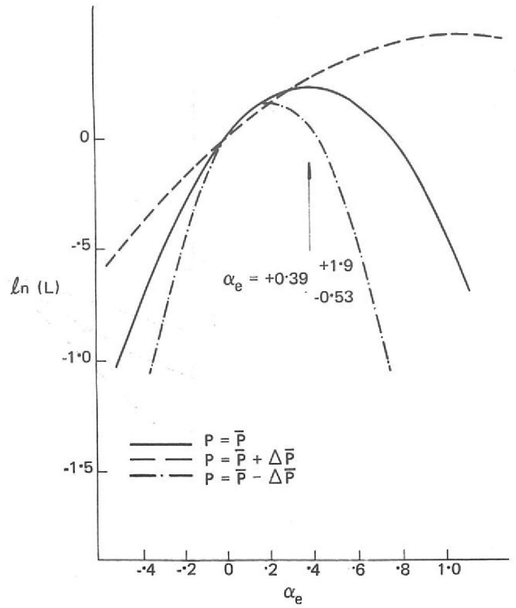

Figure 32. The logarithm of the likelihood function plotted against the electron asymmetry parameter α_e. (Experiment 11).

The experiment has now been completed. The experimental method has been described in earlier Annual Reports. Some normal Σ^- decay data were recorded and analysed to provide a check of the method and apparatus. 857 normal decay events were analysed. The K^+ and Σ^- lifetime spectra are shown in figure 31. Fits to these spectra, which are shown in table 10, give lifetimes in agreement with previously measured values and indicate that no background is present.

Table 10

	K^+		Σ^-	
	Lifetime nano-seconds	Background Events per 6 nano-seconds	Lifetime nano-seconds	Background Events per 0·05 nano-seconds
Normal Decay	13·7 ± 0·7	-1·3±1·2	0·15 ± ·01	-0·6±1·5
Beta Decay	14·2 ± 4·4	0·7±0·7	0·12 ± ·10	0·3±3·0
World Value	12·35 ± 0·04	—	0·149 ± ·003	—

The same method of analysis was used for the Σ^- beta decay data, except that each event was visually scanned to remove background, e.g. electron-positron pairs from the Dalitz decay of π^0's, which are not significant in the normal decay data. 43 Σ^- beta decay events were found. The logarithm of the likelihood function is shown plotted against the electron asymmetry parameter, α_e, in figure 32.

Three Σ^- polarization spectra were used viz. $P(\theta) = \bar{P}(\theta) - \Delta P(\theta)$, $P(\theta) = \bar{P}(\theta)$ and $P(\theta) = \bar{P}(\theta) + \Delta P(\theta)$ where $\bar{P}(\theta)$ is the measured Σ^- polarization distribution so that the statistical error on the Σ^- polarization ($\Delta P(\theta)$) is folded in. We find:

$$\alpha_e = 0{\cdot}39^{+1{\cdot}9}_{-0{\cdot}53}$$

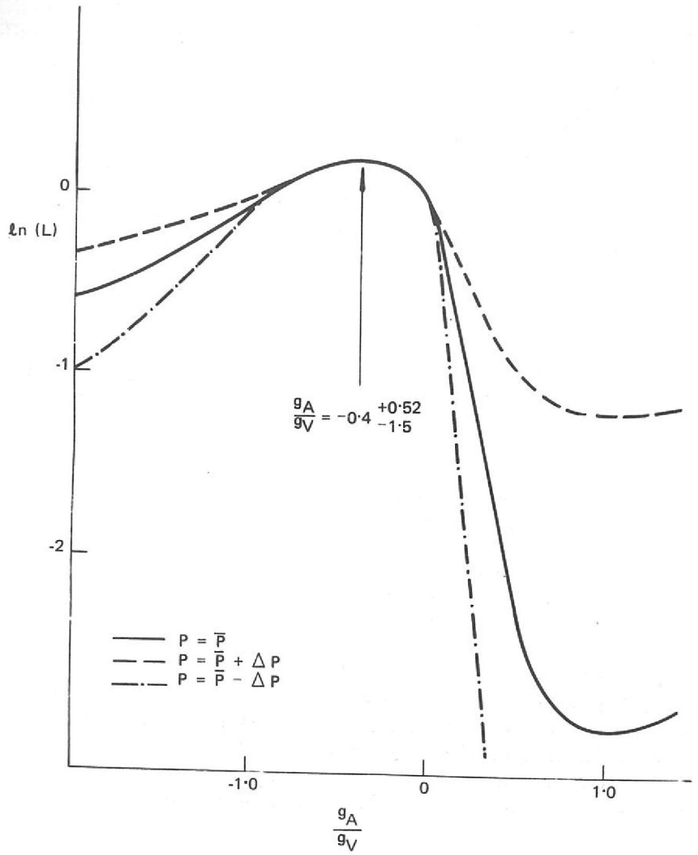

Figure 33. The logarithm of the likelihood function plotted against g_A/g_V (Experiment 11).

Figure 33 shows the logarithm of the likelihood function plotted against g_A/g_V, the coefficient of A in the weak interaction admixture, which is calculated from the asymmetry again for each of the three Σ^- polarization spectra. The ratio was found to be:

$$g_A/g_V = -0{\cdot}4^{+0{\cdot}52}_{-1{\cdot}5}$$

that is the interaction is within the errors quoted, V - 0·4 A.

In Cabibbo theory the $|\Delta S| = 0$ and $|\Delta S| = 1$ weak currents are in the same SU(3) octet so that $|\Delta S| = 0$ and $|\Delta S| = 1$ decays should be fitted by the same parameter values.

From the parameters obtained by using all data other than that on g_A/g_V, one obtains a prediction for this quantity of +0·33. Although this disagrees with our result the discrepancy is less than two standard deviations. There are two other measurements of the sign and magnitude of g_A/g_V, which are of comparable accuracy to our own. Combining the three results one obtains two solutions of comparable probability, $g_A/g_V = \pm 0{\cdot}25$ with an error of $\pm 0{\cdot}11$. Thus, in spite of three measurements, the sign of this quantity is unresolved at the present time.

Experiment 12

WESTFIELD COLLEGE, LONDON
RUTHERFORD LABORATORY

Test of the $\Delta I = \frac{1}{2}$ Rule in the Decay $\Sigma^+ \to p\pi^\circ$

The general theory of weak interactions allows non-leptonic strangeness changing transitions with a change in isotopic spin $\Delta I = \frac{1}{2}, \frac{3}{2}$ or $\frac{5}{2}$. A good experimental rule appears to be that in such transitions $\Delta I = \frac{1}{2}$ dominates. Small contributions of $\Delta I \geqslant \frac{3}{2}$ transitions are allowed by the experimental data. A sensitive test for violation of the empirical $\Delta I = \frac{1}{2}$ rule is a measurement of the so-called γ parameter in the decay $\Sigma^+ \to p\pi^\circ$.

A separated beam of π^+ mesons at 1·11 GeV/c incident upon a liquid hydrogen target was used to produce polarized sigmas by the reaction $\pi^+p \to \Sigma^+K^+$. Thin foil spark chambers measured the direction of the K^+ and the decay proton from $\Sigma^+ \to p\pi^\circ$, and the polarization and range of the proton were measured in a 60 gap aluminium spark chamber. The image of the spark chamber tracks were digitised on-line using a vidicon system.

The decay angular distribution is given by:

$$I = 1 + \alpha \underline{P}_\Sigma \cdot \underline{q}$$

where $\underline{q}$ is a unit vector along the momentum of the decay proton and $\underline{P}_\Sigma$ is the polarization of the Σ^+ in the production reaction.

Figure 34. The distribution of $-\alpha P$ plotted against the centre of momentum production angle. The data from Experiment 12 is compared with existing bubble chamber data at the same momentum and the predicted polarization from phase shift solutions of all the ΣK production data up to 1170 MeV/c.

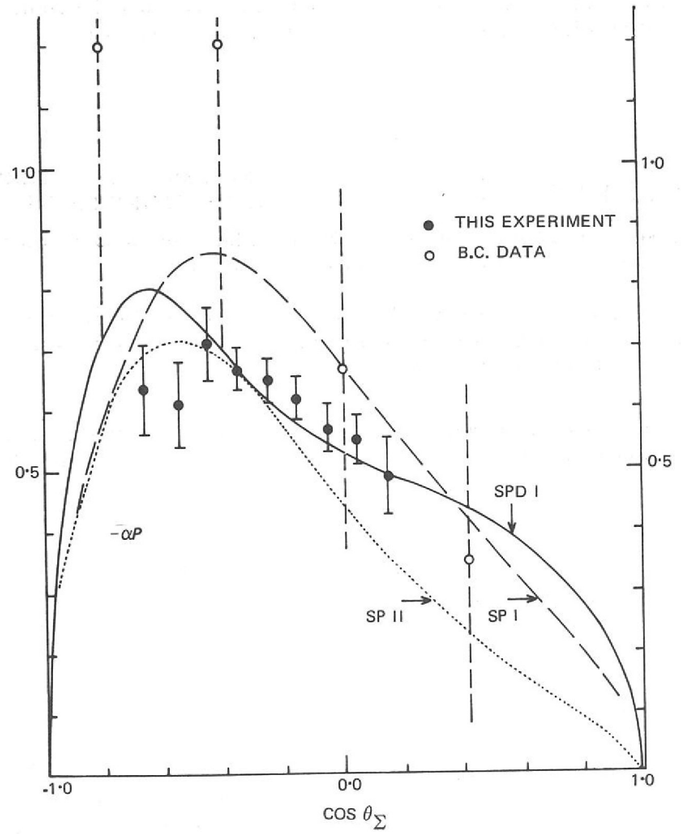

In figure 34 the distribution of $-\alpha P$ is plotted against the centre of momentum production angle. The present data is compared with the existing bubble chamber data at this momentum and with the predicted polarization from phase shift solutions of all the ΣK production data up to 1170 MeV/c by another Nimrod group. (Experiment 2, Annual Report 1968). Since α is close to $-1{\cdot}0$, the experiment selects the SPD I solution in preference to the solutions SP I and SP II. The S and P wave solutions (SP.....) were found in an energy dependent search between threshold and 1130 MeV/c. The SP and D wave solution (SPD I) was found by fitting all the previous data from threshold to 1170 MeV/c.

The presence of $\Delta I \geqslant \frac{3}{2}$ and of time reversal violating contributions to the decay $\Sigma^+ \to p\pi^\circ$ can be inferred from the decay parameters α, β and γ obtained by measuring the decay proton polarization in the aluminium plate spark chamber. Since $\alpha^2 + \beta^2 + \gamma^2 = 1$ it is convenient to parameterize the decays in terms of α and the angle ϕ defined by

$$\beta = (1 - \alpha^2)^{\frac{1}{2}} \sin \phi$$

$$\gamma = (1 - \alpha^2)^{\frac{1}{2}} \cos \phi$$

Several thousand scatters have been identified and these data are being investigated for systematic effects. A subset of 1,400 events in a restricted range of production angles has been analysed by the maximum likelihood method, yielding:

$$\alpha = -0{\cdot}95 \pm 0{\cdot}05, \phi = -6^\circ \pm 45^\circ$$

When the complete sample of data is analysed an overall fit to all the charged sigma decays will be made. The present indications are that the contributions from $\Delta I \geqslant \frac{3}{2}$ transitions and time reversal violations are indeed small.

Experiment 13

UNIVERSITY OF CAMBRIDGE
RUTHERFORD LABORATORY

Test of the $\Delta S = \Delta Q$ Rule for K° Leptonic Decays

The present theory of weak interactions has been built up assuming several basic selection rules. Amongst these, two fundamental ones are:

a) CP Conservation (This assumes that the forces governing the weak decays are unchanged if one simultaneously changes particles into antiparticles and reflects the co-ordinate systems in a mirror).

b) $\Delta S = \Delta Q$ rule (The rule permits weak decays for which the change in strangeness of the strongly interacting particles (ΔS) is equal to the corresponding change in charge (ΔQ)).

The theory has enjoyed considerable success; violation of the two selection rules outlined above is not easily fitted into the theory. In the last few years experimental proof of CP non-conservation has been obtained for K° decay and, while no conclusive evidence exists for violation of the $\Delta S = \Delta Q$ rule, experiments on $K^\circ \to \pi e \nu$ decay give an indication of such effects.

This experiment aims at obtaining a large sample of $K^\circ \to \pi e \nu$ decays resulting from the decay of a pure K° state produced in the reaction $\pi^- + p \to \Lambda + K^\circ$. By studying the time distribution of the decaying K° mesons into positive and negative electrons, the amplitudes for the 'forbidden' processes $K^\circ \to \pi^+ e^- \bar{\nu}$, $\bar{K}^\circ \to \pi^- e^+ \nu$, for which $\Delta S = -\Delta Q$, are compared with the 'allowed' processes $K^\circ \to \pi^- e^+ \nu$, $\bar{K}^\circ \to \pi^+ e^- \bar{\nu}$.

The amplitude ratio is defined as:

$$x = \frac{\text{Amplitude for } \Delta S = -\Delta Q \text{ processes (forbidden)}}{\text{Amplitude for } \Delta S = \Delta Q \text{ processes (allowed)}}$$

CP conservation in the decays is checked by measuring the imaginary part of the amplitude ratio which should be zero if CP is a good symmetry for the decays.

The data analysis of the experiment is now at an advanced state. Of the 421,000 spark chamber events recorded on film, 137,000 have been completely analysed (scanned, measured, kinematically fitted and physicist scanned) giving a preliminary sample of 1,800 useful $K \to \pi e \nu$ events. Of the remaining pictures one half have been scanned and measured.

The final number of events expected (before kinematical cuts) is 5,400, half of which are carbon induced events. The expected statistical error on the amplitude ratio, x, is 3% for both the real and imaginary parts.

12,000 of an estimated total of 31,400 events recorded with a $K^\circ \to \pi^+\pi^-$ trigger have been measured on CYCLOPS and rough digitised using DMAC tables and two different interactive graphics systems.

The $K^\circ \to \pi^+\pi^-$ events will be used to check the Monte Carlo program. This program is used in the crucial task of estimating the detection efficiency of the experimental apparatus as a function of K° proper time. The number of events already rough digitised is sufficient for this purpose.

Studies on the preliminary data indicate that backgrounds in the $K^\circ \to \pi e \nu$ event sample due to $K^\circ \to \pi^+\pi^-$, and $K^\circ \to \pi^\circ e^+ e^- \gamma$ decays are at an acceptably low level. A preliminary value for the amplitude ratio, x, will be published as soon as all systematic effects have been evaluated.

UNIVERSITY OF GLASGOW
UNIVERSITY OF LIVERPOOL
UNIVERSITY OF OXFORD
UNIVERSITY OF WARWICK
RUTHERFORD LABORATORY

Experiment 14

The aims of this experiment are:

A Study of the Decay Modes $K^\pm \to \pi^\pm\pi^\circ\gamma$ and $K^\pm \to \pi^\pm\pi^\circ\pi^\circ$ (ref. 92, 102)

(i) To measure the charge asymmetry in the rates for $K^\pm \to \pi^\pm\pi^\circ\gamma$ in order to test for C non-invariance in electromagnetic interactions and CP non-invariance in the weak interaction, and also to measure for this mode the electric and magnetic dipole structure amplitudes and the interference between the electric dipole amplitude and the inner bremsstrahlung.

(ii) To measure the charge asymmetry in the rates for $K^\pm \to \pi^\pm\pi^\circ\pi^\circ$ (τ' decay) in order to test for $I = \frac{5}{2}, \frac{7}{2}$ CP non-invariant terms in the non-leptonic weak interaction.

The experiment was carried out in a 5 GeV/c unseparated kaon beam at the CERN PS. A differential gas Cerenkov counter identified the kaons in the beam, and a system of counter hodoscopes and wire spark chambers at B_1, B_2 and B_3 defined their momenta and directions. The layout of the experiment is shown in figure 35. The vector momentum of the charged pion, produced when a kaon decayed into either of the two desired final states, was measured by 12 sonic spark chambers at S_1 and S_2 in conjunction with a large spectrometer magnet. As shown in figure 35, six of these chambers were placed within the gap of the spectrometer magnet.

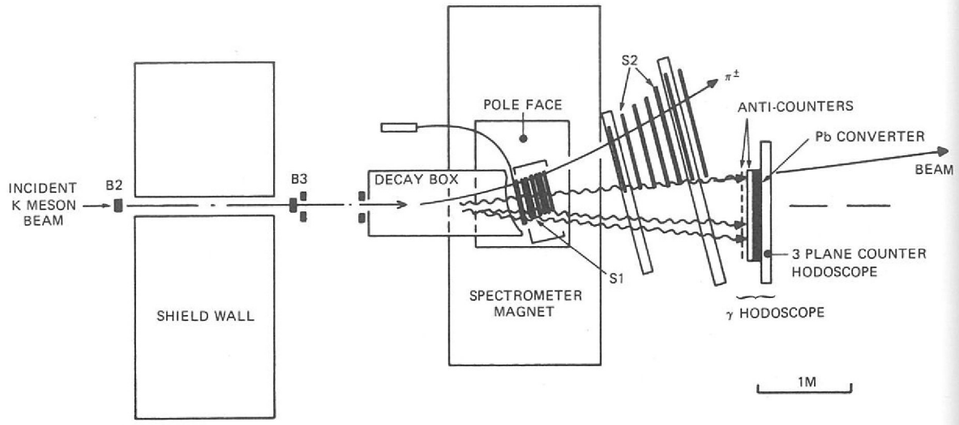

Figure 35. Schematic diagram of the apparatus used in Experiment 14 to study $K^{\pm}\to\pi^{\pm}\pi^{\circ}\gamma$ and $K^{\pm}\to\pi^{\pm}\pi^{\circ}\pi^{\circ}$.

The final state γ-rays (including those from the decay of the neutral pions) were detected by a 1 metre square counter hodoscope. This enabled the outgoing directions of the γ-rays to be defined to within $\pm 0{\cdot}5^{\circ}$ in the laboratory system.

Information from the counters and spark chambers was fed into a DDP 516 computer for preliminary analysis and also recorded on magnetic tape for detailed analysis. Data collection was completed in September 1969 and the results are now being analysed at the Rutherford Laboratory using the IBM 360/75.

About 30% of the data has been analysed for τ' events and about 220,000 such events have been found. The asymmetry parameter is defined by

$$A_{\tau'} = \frac{(N^{+} - N^{-})}{\frac{1}{2}(N^{+} + N^{-})}$$

where $N^{\pm}$ are the numbers of $K^{\pm}$ decaying by the τ' mode normalised to the number of $K^{\pm}\to\pi^{\pm}\pi^{\circ}$ decays. The distribution of values of $A_{\tau'}$ for 49 independent samples of data is shown in figure 36. The values follow a Gaussian distribution, with a mean of $-0{\cdot}0009 \pm 0{\cdot}0055$. This result is consistent with zero.

These events have also been used to determine the asymmetry of the slope parameter a in the τ' decay matrix element $M \propto (1+aY)$ where $Y=(2T_3-Q)/Q$, T_3 is the kinetic energy of the charged pion and Q is the energy release in the decay. A value of

$$a_{\tau'} = (a^{+}_{\tau'} - a^{-}_{\tau'})/\tfrac{1}{2}(a^{+}_{\tau'} + a^{-}_{\tau'}) = +0{\cdot}009 \pm 0{\cdot}008$$ has been obtained.

About 800 events of the type $K^{\pm}\to\pi^{\pm}\pi^{\circ}\gamma$ have been found. This represents about 25% of the total amount of data for this decay mode. For the asymmetry in this decay mode a value of $A_{\pi\pi\gamma} = -0{\cdot}11 \pm 0{\cdot}10$ has been obtained.

The conclusion to be drawn from the data analysed so far is that there is no significant evidence for a violation of CP invariance in either decay mode.

Figure 36. The distribution of $A_{\tau'}$, the assymetry parameter for the decays $K^{\pm}\to\pi^{\pm}\pi^{\circ}\pi^{\circ}$, for 49 independent samples of data from Experiment 14.

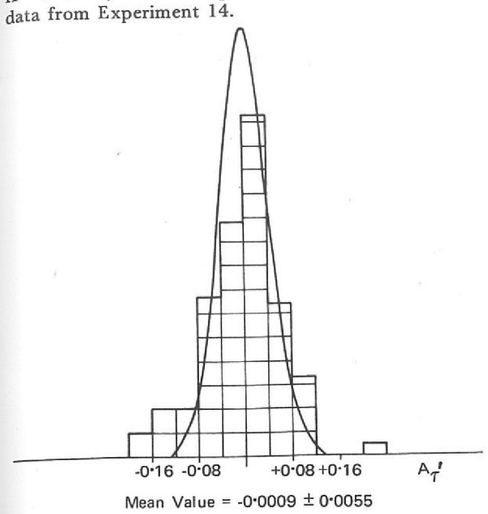

Figure 37. Efficiency of the gas Cerenkov counter as a function of gas pressure, (Experiment 15).

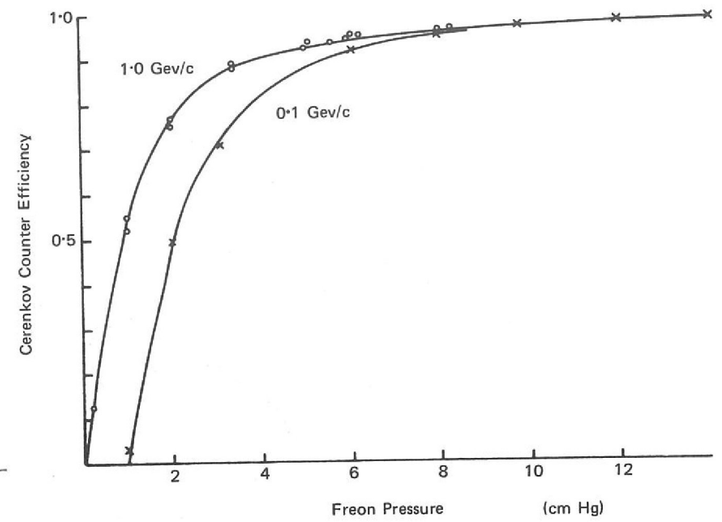

Experiment 15

UNIVERSITY OF CAMBRIDGE
RUTHERFORD LABORATORY

Investigation of Bremsstrahlung Anomalies

When a light charged particle passes close to an atomic nucleus it is accelerated by the electric force between the two and as a result of this acceleration it is deflected from its original path and looses some of its energy in the form of a γ-ray (bremsstrahlung - braking radiation). The distribution of fractional energy losses in such processes can be calculated accurately using quantum electrodynamic theory. Such calculations indicate a smoothly decreasing probability as the radiated energy increases. Some recent bubble chamber results (described in the 1969 Annual Report) have indicated that a supposedly pure electron beam did not behave in this predicted way or, alternatively, that some previously undiscovered light particle existed in the electron beam.

The present experiment consisted of two parts. In the first a very sensitive gas Cerenkov counter was used to analyse the velocities, and hence the masses, of the particles in a beam of fixed momentum. In such an investigation the counting rate of the Cerenkov counter is recorded as the pressure of the gas inside it is increased. Such a curve is shown in figure 37. Any new particle heavier than the electron would show as a sharp step in the counting rate on the otherwise flat portion of the curve; a particle lighter than the electron would be detected below the electron threshold. No such effects were observed. Departures from the pressure curves for electrons are plotted in figure 38, from which it is concluded that there is no evidence for any new particle with a mass below 45 MeV/c^2.

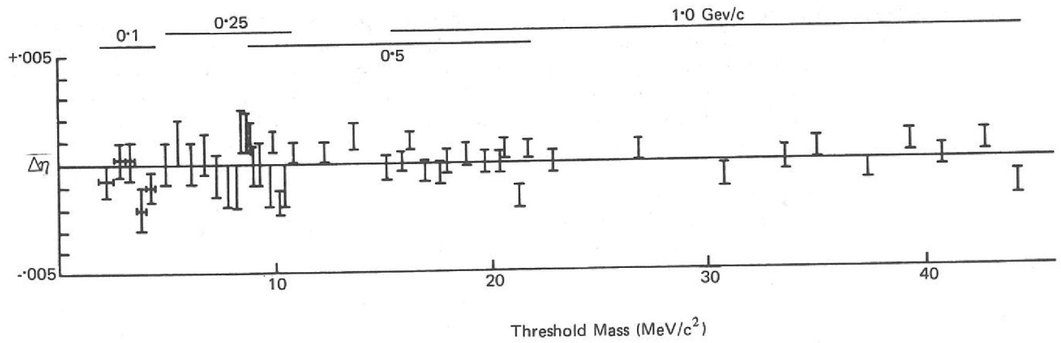

Figure 38. Measured departures from the expected gas Cerenkov counter pressure curves for electrons plotted against the threshold mass of the hypothetical particle. Horizontal lines at top of figure indicate mass regions covered by given electron beam momentum.

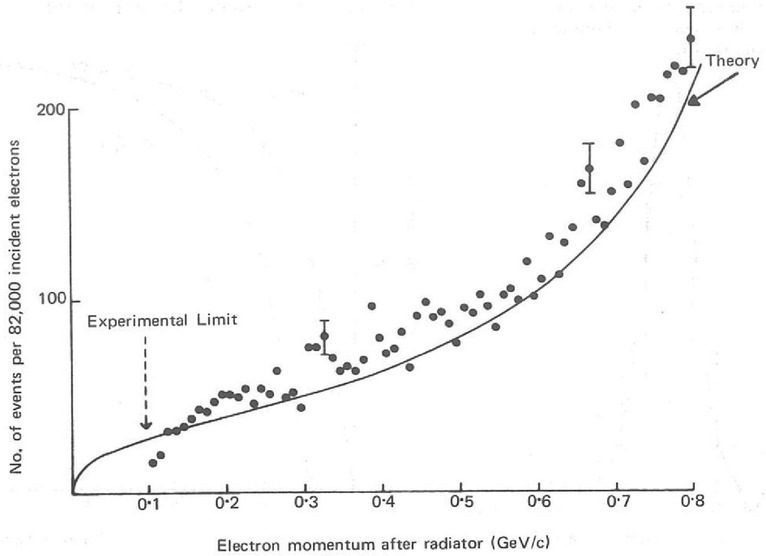

Figure 39. Electron momentum spectrum after passing through 0·91 radiation lengths of carbon. The solid line is a theoretical curve, normalised to incident electron flux and not to the experimental points.

The second part of the investigation consisted of measurements of the momenta of individual electrons both before and after they had passed through one of a variety of radiators (carbon, copper, etc). The ratio of the two can be compared with the predictions of the bremsstrahlung theory. The measurements were made using sonic spark chambers in two magnetic spectrometers working on-line to a DDP 516 computer. A preliminary analysis of each event was made within 20 milliseconds of its occurrence and up-to-date histograms produced for display. Records for approximately 200,000 events were also written on magnetic tape for subsequent detailed analysis. The number of electrons incident on the radiators during the course of the experiment was about 500,000. No effect comparable to that reported in the bubble chamber experiment has been found; see figure 39.

Final results are not yet available but it already appears that no breakdown of quantum electrodynamics, or evidence for a new light particle will be found in this experiment.

WESTFIELD COLLEGE, LONDON
UNIVERSITY OF SUSSEX
RUTHERFORD LABORATORY

Experiment 16

Search for Charge Asymmetry in Eta Decay

An important insight into the interaction processes that occur in elementary particle physics can be gained by applying and studying certain symmetry principles. One asks whether the laws of physics remain unchanged when, for example, a set of interacting particles are replaced by the equivalent set of anti-particles (the operation C), or time is made to run backwards (the operation T), or the world is viewed as reflected in a mirror (the parity operation P). The surprising result of experiments testing these symmetry rules is that for the weak interaction the operations C, P, or CP each produce a new physical situation with different physical behaviour. As a result of these findings our understanding of the weak interaction has changed considerably.

There are now indications that the electromagnetic interaction may also lack symmetry under the particle – antiparticle interchange operation C. If this result were confirmed, it would have a fundamental impact on our model of the electromagnetic interaction, which is thought to be very well understood and symmetric under C.

This experiment tests C symmetry in the electromagnetic interaction by looking at the decay of the eta meson:

$$\eta \rightarrow \pi^+ \pi^- \pi^\circ$$

The π^+ and π^- are particle and antiparticle, and C symmetry requires that nature should treat them both with equal respect. Thus if:

$N^+ = N(E^+ > E^-)$ i.e. the number of times the π^+ is more energetic than the π^-, and

$N^- = N(E^- > E^+)$, then C symmetry implies:

$$A = \frac{N^+ - N^-}{N^+ + N^-} = 0$$

The most recently published value for this quantity is:

$$A = 1{\cdot}5\% \pm 0{\cdot}5\%$$

for a measured sample of 36,000 η decay events. This is a result with three standard deviations of significance, and clearly requires confirmation.

The $\pi 8$ group have set out to repeat this experiment and hope to obtain approximately ten times as many events. The apparatus being used is shown in figure 40. The η mesons to be studied are produced in the process $\pi^- p \rightarrow \eta n$ and are selected from unwanted background by measuring the time of flight of the neutron from the target to the ring of 60 neutron counters. An array of spark chambers surrounds the hydrogen target and the whole is situated in a large electromagnet. This allows the π^+ and π^- mesons from the η decay to be detected and have their energies measured.

Data taking started in September and to date a total of 600,000 events have been recorded on magnetic tape. This represents about 20% of the final expected total. A preliminary analysis using simple helix fitting in a uniform magnetic field to determine the decay pion momenta indicates that some 12% of the events recorded are useful η decays.

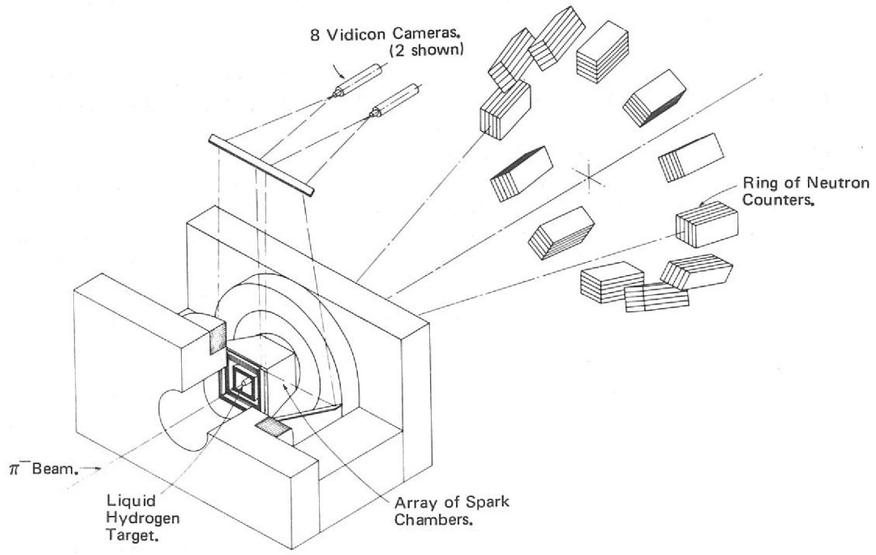

Figure 40. Schematic diagram of the apparatus used in Experiment 16 to study η decay.

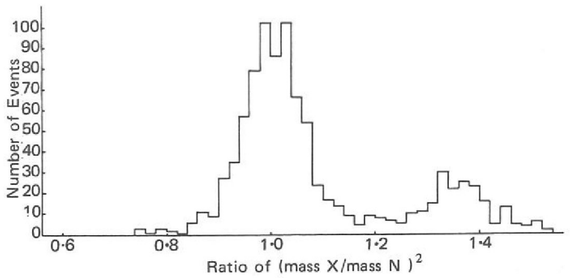

Figure 41. Plot of [(mass X)/(mass neutron)]^2 where X is the total missing neutral mass in the reaction $\pi^- p \rightarrow \pi^+ \pi^- X$. (Experiment 16).

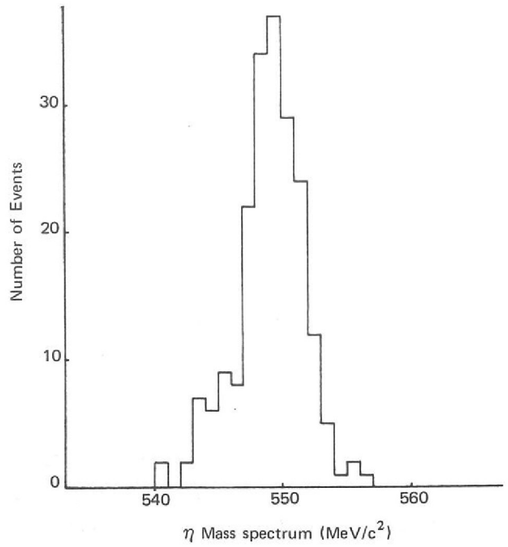

Figure 42. Mass distribution of Z for the reaction $\pi^- p \rightarrow nZ$ for events identified as etas. (Experiment 16).

Figure 41 shows the total missing neutral mass X in the reaction:

$$\pi^- p \rightarrow \pi^+ \pi^- X$$

The large peak centred at the mass of the neutron is from background events of the type:

$$\pi^- p \rightarrow \pi^+ \pi^- n$$

which is the largest source of background in the experiment. A cut requiring Mass(X) > 1·2 x Mass (neutron) removes essentially all these unwanted events and the remaining events are from η decays plus some small background.

In figure 42 the mass distribution of the η decays as selected above is shown. The full width at half height of this peak is 4·5 MeV and this is the expected width from the known experimental errors. This width is expected to decrease to 3 MeV when all available information is used. The background level from $\pi^+\pi^-\pi^\circ$ phase space is seen to be small.

Experiment 17

WESTFIELD COLLEGE, LONDON
RUTHERFORD LABORATORY

Search for the Decay $\eta \rightarrow \pi^\circ e^+ e^-$

The decay $\eta \rightarrow \pi^\circ e^+ e^-$ is essentially forbidden; unless there is a charge conjugation (C) violating component in the electromagnetic interaction this decay is immeasurably rare. The allowed rate has been estimated as being of the order of 10^{-10} of all η decays. No decays of this kind have been observed; the current experimental upper limit is 2×10^{-4} of all η decays. A reliable rate measurement of $\eta \rightarrow \pi^\circ e^+ e^-$ is of comparable interest to the charge asymmetry in $\eta \rightarrow \pi^+ \pi^- \pi^\circ$ (Experiment 16), and a direct pointer to any C violation taking place through the electromagnetic interaction.

To detect this decay mode of the η, the charge asymmetry experiment described in Experiment 16 is modified by the addition of a large, three element gas Cerenkov counter around the spark chambers. This detects the electrons or positrons from the decay, and the event is labelled accordingly. Data is taken concurrently with the asymmetry experiment.

A rate for this forbidden process comparable with the present upper limit will give about 100 $\eta \rightarrow \pi^\circ e^+ e^-$ events in the total data. In addition to these real events about 5 background events will survive the full analysis.

Experiment 18

UNIVERSITY COLLEGE, LONDON
UNIVERSITY OF BRISTOL
UNIVERSITY OF LIVERPOOL
RUTHERFORD LABORATORY

ISR Experiment to Search for the Intermediate Boson (The Muon Experiment)

The CERN intersecting storage rings (ISR) are due to begin operation during 1971. This new facility will enable two beams of 28 GeV protons to make a 'head-on collision' thus allowing the full energy of both protons to be available for the interaction. When an energetic proton hits a stationary target the major part of the energy is used in recoil of the system and only a small fraction of the primary proton energy is available in the centre of momentum for the reaction. The ISR will provide, for pp collisions, a centre of momentum energy equivalent to that obtained from a 1600 GeV conventional accelerator, i.e. it will make available a total c.m. energy of 56 GeV, and will (in principle) allow the production of, hitherto unknown, very massive particles. The major aim of this experiment is to search for the production of one such particle, the so-called intermediate boson.

Figure 43. Schematic diagram of the apparatus to be used for Experiment 18, at the CERN ISR machine.

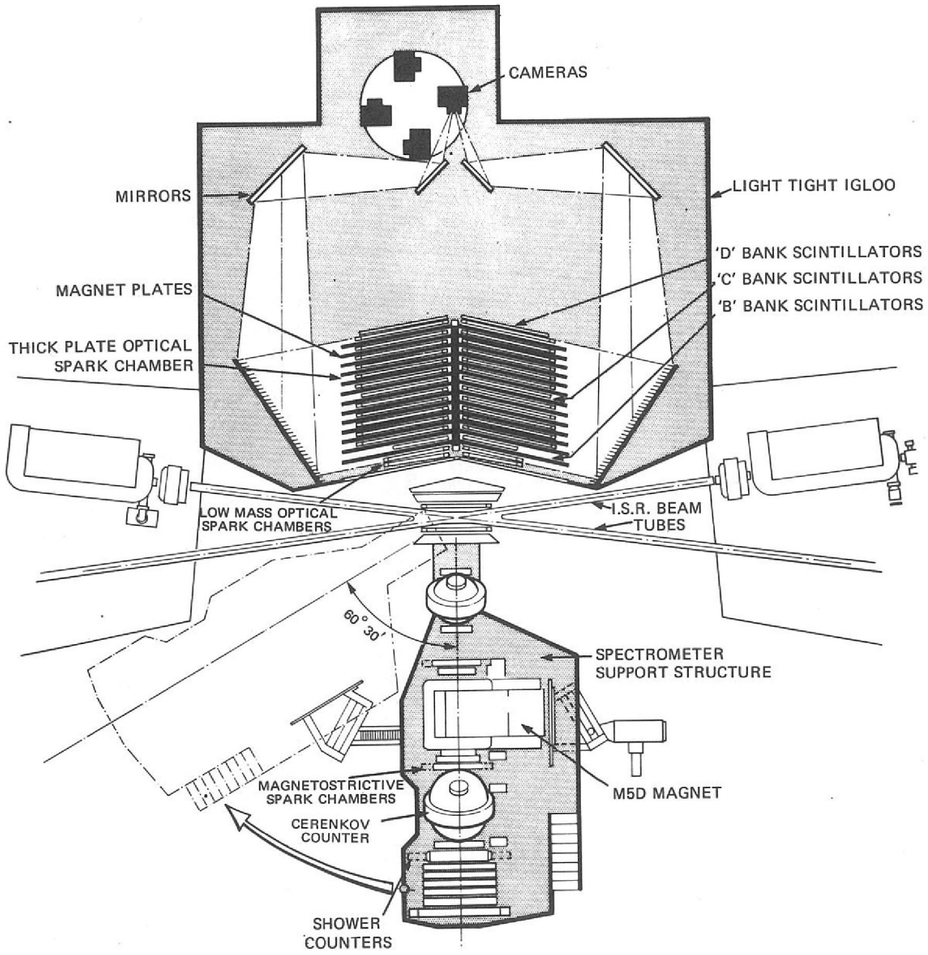

On general grounds any interaction taking place over a finite distance must have some 'messenger' that 'carries' the force between the interacting particles. For the strong interaction there are many 'messengers' (pions, kaons, baryons, etc) and for the electromagnetic interaction the 'messenger' is the photon; but for the weak interaction no particle has been discovered with the required properties. All existing experimental evidence is consistent with the weak interaction having zero range (point interaction) and thus not requiring a 'messenger', but this picture must almost certainly break down at some very short distance. Such a break down would require a large mass 'messenger' known as the 'intermediate boson'. This particle is expected to decay into leptons, e.g.

$$W^{\pm} \rightarrow \mu^{\pm} + \nu_{\mu}$$

If the W particle has a large mass the muons from the decay will have high momentum and can come at large angles from the colliding beams. The present experiment uses a large solid angle array of magnetised iron and optical spark chambers placed at 90° to the colliding beams to identify the muons and measure their momentum (see figure 43). The detector has dimensions 5m x 3m x 4½m (67m^3) and weighs ∼ 300 tons (see figures 44 and 45).

The apparatus will also be able to detect pairs of muons produced in electromagnetic interactions from virtual γ-rays and the study of the mass spectrum of these muon pairs is a secondary objective of the experiment.

Figure 44. Front view of the large array of magnetized steel plates and optical spark chambers to be used in Experiment 18. The steel plates are shown with a heavy outline; the spark chambers are shown with dotted outline. The positions of mirrors are also indicated, at 45° underneath the apparatus.

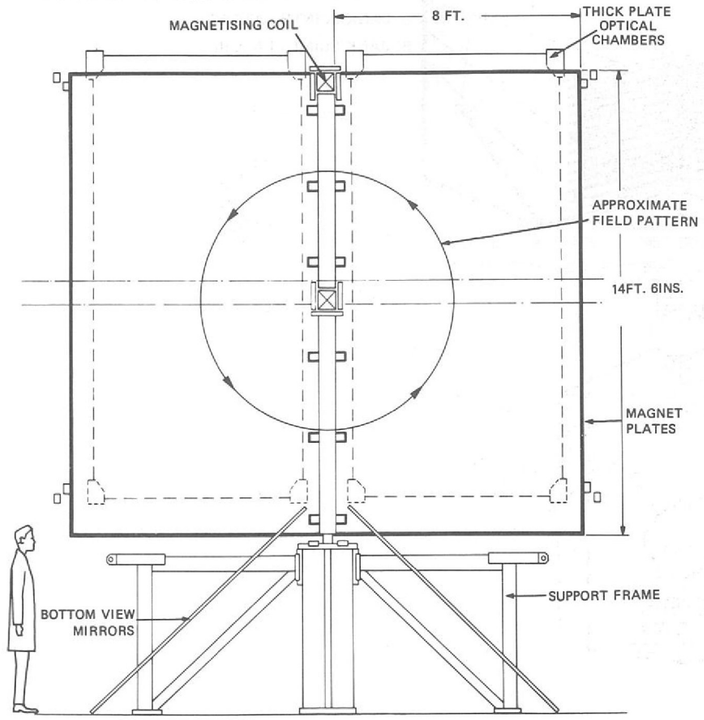

Figure 45. The photograph shows the array of figure 44 being assembled at the Rutherford Laboratory.

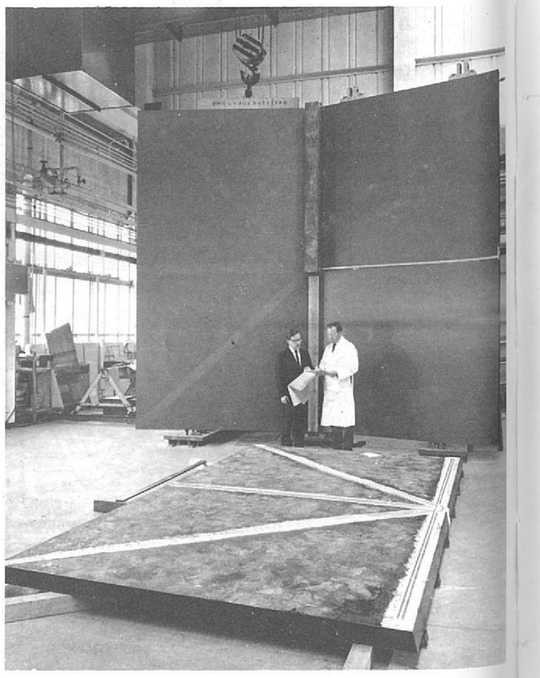

A third aim is a measurement of the yield of strongly interacting particles at large angles from the primary p-p interaction. This is of interest in its own right and is also required in the interpretation of the single muon spectrum observed in the search for the W particle. This yield study will be made using the wide angle spectrometer set on the opposite side of the intersection region, as shown in figure 43.

The major parts of both detectors are designed and construction is under way. It is planned to commence installation at the ISR in April 1971 and the experiment is expected to start in June of that year.

CEN, SACLAY.
COLLEGE DE FRANCE
UNIVERSITY OF STRASBOURG
RUTHERFORD LABORATORY

Experiment 19

Formation of Baryon Resonances with Strangeness - 1 in the Mass Range 1915 to 2170 MeV/c^2 (ref. 10, 11, 71, 86, 87, 88, 89, 99, 105, 106).

K^- mesons incident on protons combine to make composite baryonic states with particular properties of strangeness -1 and isotopic spin 0 and 1. A resonance is 'formed' when the total energy in the centre of momentum system corresponds to the mass of the resonance. Such states decay by strong interaction (in a time of the order of 10^{-24} sec) into various final states which are observable in a bubble chamber. Of particular interest, because of their simplicity, are the two body and quasi-two body final states. By studying these final states the properties of the resonances such as mass, width, spin, parity, isotopic spin and their decay amplitudes into each final state are derived.

The purpose of the experiment is primarily to make accurate measurements of cross-sections, angular distributions, polarizations and decay distributions of the final states. These data are then analysed to search for known or new resonances. Finally these resonances are examined in relation to theoretical models which attempt to explain the whole spectrum of strongly interacting particles and resonances, and whose validity rests on agreement with the increasingly accurate experimental data. Of particular success is the symmetry scheme SU(3).

In this experiment 1,650,000 pictures of K^-p interactions at 13 energies approximately equally spaced in the interval 1915 to 2170 MeV were taken at Nimrod using the CEN, Saclay, hydrogen bubble chamber. From these pictures approximately 150,000 events have been measured.

The partial wave analyses of the two body final states

$$K^-p \rightarrow \Sigma\pi \quad (1)$$
$$K^-p \rightarrow \Lambda\pi \quad (2)$$
$$K^-p \rightarrow \bar{K}N \quad (3)$$

are now complete. Results for the first two reactions have been published. Reaction (3) has two possible final states $K^-p \rightarrow K^-p$ and $K^-p \rightarrow \bar{K}^\circ n$, called elastic scattering and charge exchange respectively. The latter state is only seen when the K° decays by the K_s° mode into $\pi^+\pi^-$ in the bubble chamber. Figure 46 shows the spectrum of the missing mass squared for all events with just a K_s° decay visible. In this spectrum the $\bar{K}^\circ n$ events are clearly resolved.

The angular and polarization distributions are analysed in terms of amplitudes for partial waves of different angular momentum. In this way resonances of definite spin and parity can be isolated. The results are best displayed by the Argand diagrams of the separate partial wave amplitudes (figure 47). An amplitude which describes an anticlockwise loop with increasing energy in such a diagram may have an associated resonance.

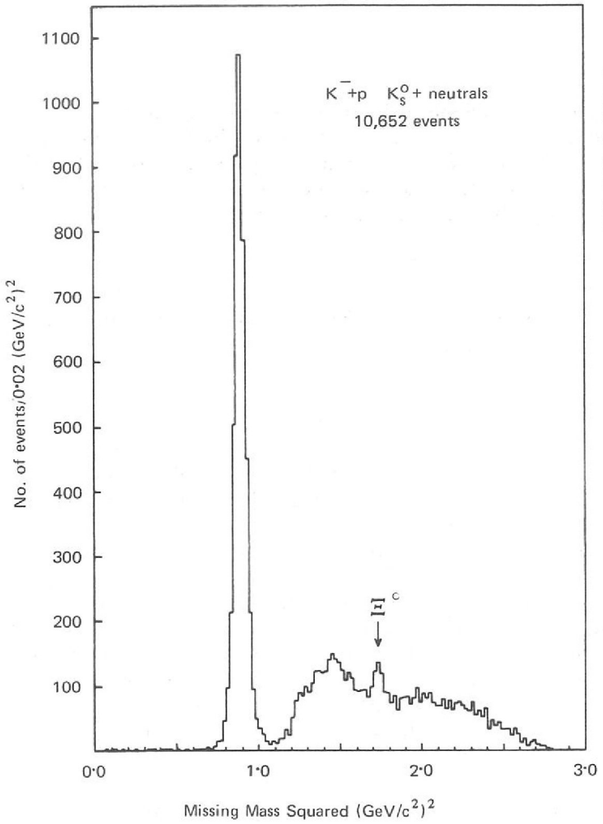

Figure 46. Spectrum of the (missing mass)^2 to the K^0_S in the reaction $K^- p \to K^0_S$ + neutrals for all energies combined. The sharp peak at 0·9 (GeV/c^2)^2 is from the reaction $K^- p \to K^0_S n$. (Experiment 19).

The three dominant resonances in this region are the F_{07} $\Lambda(2100)$, G_{17} $\Sigma(2030)$ and F_{15} $\Sigma(1915)$. The masses, widths and resonant amplitudes in each channel have been measured with the results shown in Table 11. The values are generally in good agreement between the channels except for the width of the $\Lambda(2100)$ which is nearly 3 standard deviations different between the $\Sigma\pi$ and $\bar{K}N$ channels. This problem may be resolved in the study of the other channels in this experiment. The $\Sigma(2030)$ has been placed in an SU(3) decuplet together with the $\Delta(1940)$ and the $\Sigma(1915)$ in an octet with the N(1688) and $\Lambda(1815)$.

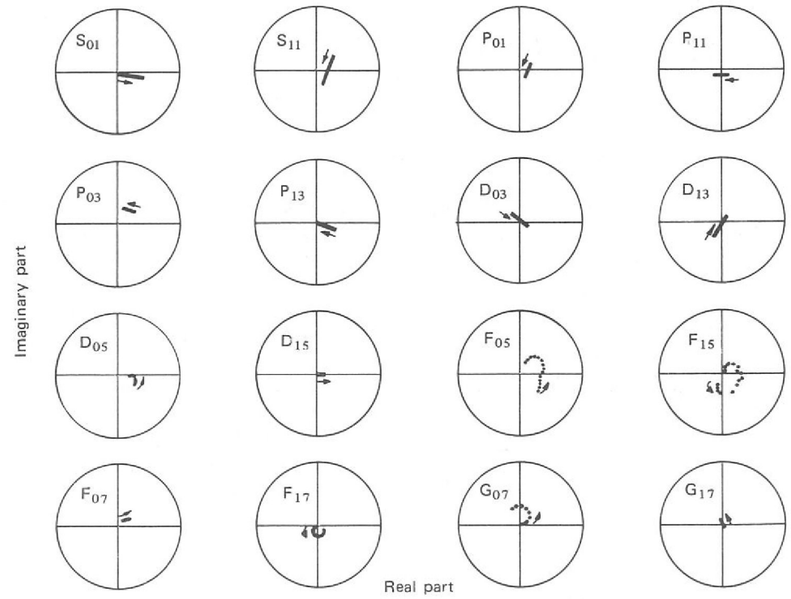

Figure 47(a). Argand diagram for partial waves in the reaction $K^- p \to \Sigma\pi$. Arrows indicate the direction of increasing energy. (Experiment 19).

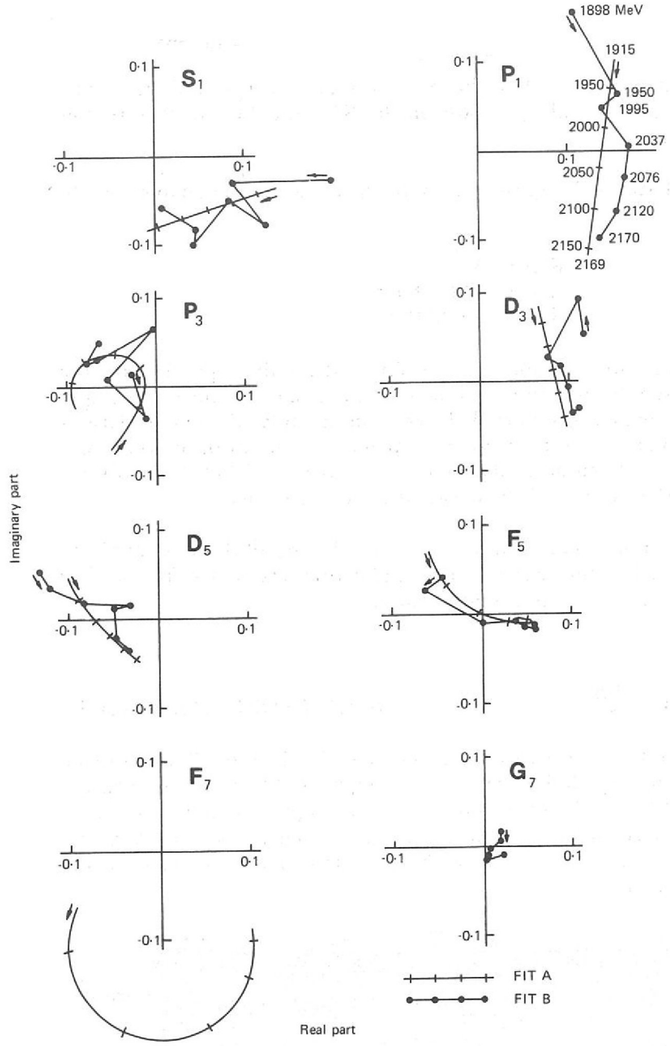

Figure 47(b). Argand diagram for partial waves in the reaction $K^- p \to \Lambda\pi^0$. Arrows indicate the direction of increasing energy. (Experiment 19).

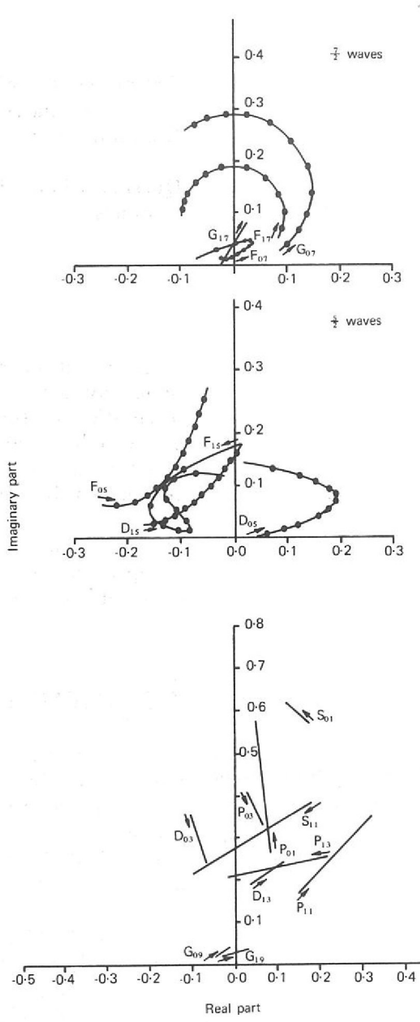

Figure 47(c) Argand diagram for partial waves in the reaction $K^- p \to \bar{K}N$. Arrows indicate the direction of increasing energy. (Experiment 19).

Table 11

Measured parameters of dominant resonances. (Experiment 19).

Resonance	Channel	E_R (MeV)	Γ (MeV)	$\sqrt{xx'}$
$\Sigma(1915)$	$K^- p \to \bar{K}N$	1910 ± 15	70 ± 15	0·15 ± 0·03
	$K^- p \to \Sigma\pi$	1900 ± 15	75 ± 20	−0·13 ± 0·03
	$K^- p \to \Lambda\pi$	1910 ± 20	60 ± 20	0·1 ± 0·02
$\Sigma(2030)$	$K^- p \to \bar{K}N$	2025 ± 15	200 ± 30	0·18 ± 0·02
	$K^- p \to \Sigma\pi$	2030 ± 10	155 ± 20	−0·10 ± 0·03
	$K^- p \to \Lambda\pi$	2030 ± 10	165^{+30}_{-15}	0·2 ± 0·02
$\Lambda(2100)$	$K^- p \to \bar{K}N$	2100 ± 15	300 ± 30	0·30 ± 0·03
	$K^- p \to \Sigma\pi$	2110 ± 30	140 ± 15	0·16 ± 0·02

Several less prominent resonances have been suggested, P_{11}, P_{13} and D_{13} states in the $\Lambda\pi$ analysis and D_{05} and F_{07} states in the $\bar{K}N$, but they all require confirmation from other data.

Quasi-two body final states. Progress is now being made on the analysis of the channels

$$\begin{aligned} K^-p &\rightarrow \Lambda\omega \\ K^-p &\rightarrow Y^*(1385)\pi \\ K^-p &\rightarrow K^*(890)N \end{aligned}$$

Angular and polarization distributions can be obtained for these processes in the same way as for the simple two body channels. The angular distribution and spin orientation of the resonance state are deduced from a study of the correlations between the decay products and the production plane. Further information is provided in the $\Lambda\omega$ channel from an analysis of the Λ decay and the study of cross correlations between this decay and the decay of the ω resonance.

The formalism for a complete partial wave analysis including all this data has been set up and analysis started on the channels. First indications are that sufficient data is available to perform an energy independent analysis.

Experiment 20

RUTHERFORD LABORATORY

Formation of Baryon Resonances with Strangeness -1 in the Mass Range 1775 to 1960 MeV/c²

Film for an extension of Experiment 19 was exposed at CERN in the 2 m hydrogen bubble chamber during April/May 1970. It comprises 11 beam momentum settings in the range 1·0 to 1·4 GeV/c and will provide approximately 4 times the statistics available in any previous experiment in this energy range. Approximately 100,000 events, about one third of the expected final total, have already been measured on the HPD.

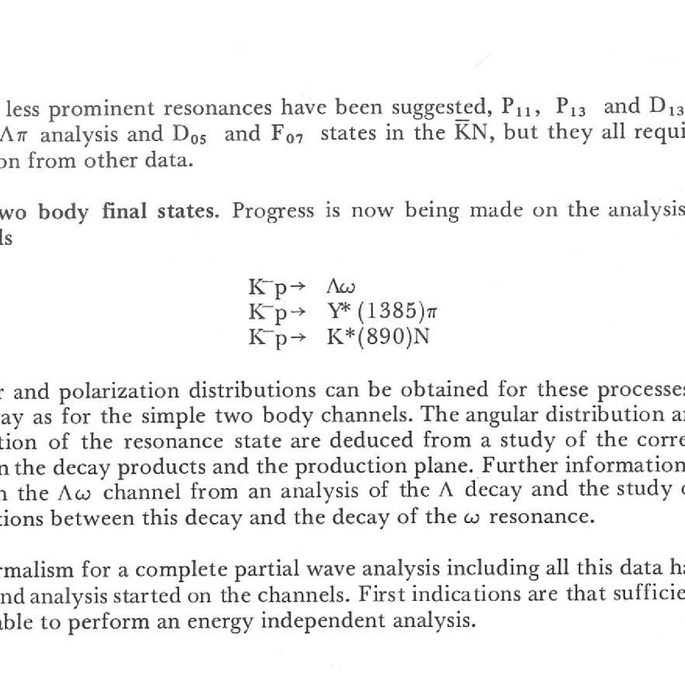

Figure 48. An example of a rare decay mode of the Σ^+ hyperon from a photograph taken in the Saclay 81 cm Bubble Chamber at Nimrod. The reaction is $K^-p \rightarrow \Sigma^+\pi^-$, followed by $\Sigma^+ \rightarrow \Lambda e^+\nu$ and $\Lambda \rightarrow p\pi^-$.

Experiment 21

UNIVERSITY OF LIVERPOOL. RUTHERFORD LABORATORY

Non-Annihilation Channels in $\bar{p}p$ Interactions near C.M. Energy 2200 MeV (ref. 90, 122)

The non-annihilation channels of the $\bar{p}p$ interactions in the C.M. energy range 2150 to 2240 MeV are being studied. This range approximately covers the width of the isospin-one structure seen in the $N\bar{N}$ total cross-section at 2190 MeV, and contains the T meson observed in the CERN missing mass spectrometer experiment. The film was taken using the CERN 2 m bubble chamber with four antiproton momentum settings centred at 1·23, 1·30, 1·36 and 1·43 GeV/c. The film was scanned for two prong events with the requirement that protons should have a projected length greater than 1 mm on the film (14 mm in the chamber). Measurements were made by the HPD and events analysed through the standard Rutherford Laboratory geometry and kinematics programs. After a remeasurement of failed events the data sample consists of 75,000 events.

The non-annihilation events were uniquely identified from kinematic and ionisation fits. The differential cross-sections at all momenta are plotted in figure 49. These distributions exhibit the well known features of $\bar{p}p$ scattering: a large forward diffraction peak, a first minimum at $t \simeq -0{\cdot}4$ GeV² and a second maximum at $t \simeq -0{\cdot}6$ GeV².

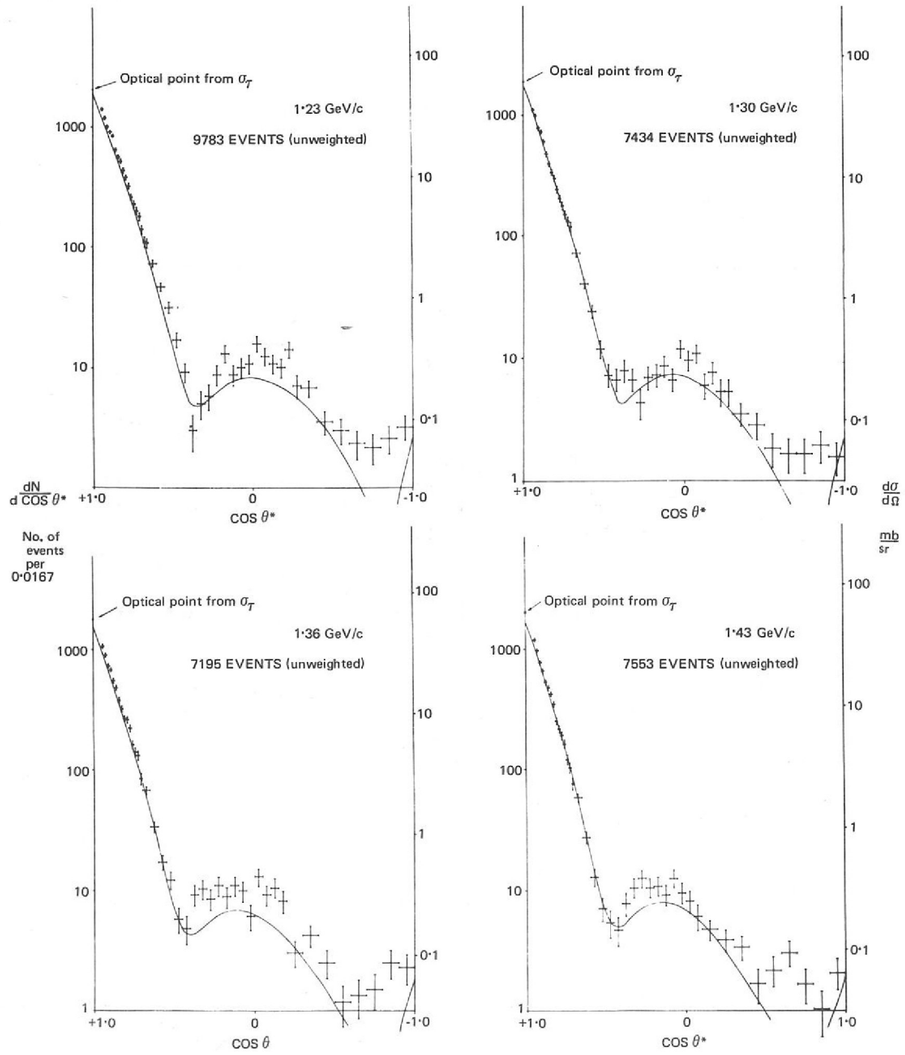

Figure 49. Differential cross-section for $\bar{p}p \rightarrow \bar{p}p$ at momenta of 1·23, 1·30, 1·36 and 1·43 GeV/c. (Experiment 21).

To obtain the total elastic scattering cross-section, the experimental differential cross-section must be extrapolated to t = 0. Since this correction is sizable (about 30%), a variety of feasible extrapolations have been used to investigate the sensitivity of the final result to the choice of functional form. The results quoted in Table 12 have been obtained by extrapolating with a Legendre Polynomial expansion fitted to the experimental centre of momentum angular distributions in the range $-1{\cdot}0 < \cos\theta < +0{\cdot}95$. All of the coefficients are increasing with energy as expected for a diffraction-like distribution exhibiting a forward peak followed by a dip at fixed t. The form $Ae^{bt + ct^2}$ also gives a good fit to the forward peak at all four momenta with $b = 13{\cdot}48 \pm 0{\cdot}33$, $c = 11{\cdot}0 \pm 1{\cdot}3$ and agrees with the Legendre expansion when extrapolated to t = 0.

The ratios of the real to imaginary part of the forward amplitude have been estimated through the optical theorem using the total cross-section data of Abrams et al.; these too are summarized in Table 12. This ratio, averaged over this rather narrow energy range, is found to be $0{\cdot}31 \pm 0{\cdot}04$ which agrees with the theoretical predictions of Soding and of Bryan and Phillips. The possibility of measuring this ratio arises through the capability of the bubble chamber technique to observe small angle scatters.

Table 12

$\bar{p}$ lab. momentum (GeV/c)	1·23	1·30	1·36	1·43
σ_{el} milli-barns	43·3 ± 1·0	41·5 ± 1·0	42·2 ± 0·9	41·8 ± 0·9
Legendre Coefficients				
A_1/A_0	2·58 ± ·06	2·62 ± ·07	2·61 ± ·06	2·65 ± ·05
A_2/A_0	3·40 ± ·09	3·53 ± ·10	3·52 ± ·08	3·63 ± ·08
A_3/A_0	3·41 ± ·11	3·68 ± ·12	3·67 ± ·10	3·91 ± ·10
A_4/A_0	2·77 ± ·11	3·18 ± ·13	3·19 ± ·11	3·54 ± ·10
A_5/A_0	1·79 ± ·11	2·29 ± ·13	2·26 ± ·11	2·73 ± ·10
A_6/A_0	0·95 ± ·11	1·39 ± ·12	1·31 ± ·10	1·80 ± ·10
A_7/A_0	0·43 ± ·10	0·76 ± ·11	0·66 ± ·10	1·05 ± ·09
A_8/A_0	0·16 ± ·08	0·35 ± ·09	0·26 ± ·08	0·59 ± ·07
A_9/A_0	0·01 ± ·07	0·14 ± ·07	0·09 ± ·07	0·32 ± ·06
A_{10}/A_0	-0·02 ± ·04	0·03 ± ·04	0·01 ± ·04	0·16 ± ·04
A_{11}/A_0	-0·02 ± ·03	0·02 ± ·03	0·01 ± ·03	0·06 ± ·03
$\frac{d\sigma\ (0)}{dt}\left(\frac{mb}{GeV^2}\right)$	626 ± 33	631 ± 31	585 ± 25	61 ± 22
$\left\|\frac{\text{Re } f(0)}{\text{Im } f(0)}\right\|^2$	0·05 ± ·05	0·09 ± ·05	0·04 ± ·05	0·17 ± ·04
$\frac{d\sigma}{d\Omega}$ (μb/sr) $(-0{\cdot}8 > \cos\theta > -1{\cdot}0)$	108 ± 18	80 ± 17	137 ± 23	71 ± 16

Single Pion Production Channels. The following single pion production reactions have also been studied:

$$\bar{p}p \to \bar{p}p\pi^\circ \quad (1)$$
$$\bar{p}p \to \bar{p}n\pi^+ \quad (2)$$
$$\bar{p}p \to \bar{n}p\pi^- \quad (3)$$

The cross-sections for these three reactions are presented in Table 13. Charge conjugation invariance requires that reactions (2) and (3) should have equal cross-sections and this is satisfied by the data.

Assuming the πN and $\pi\bar{N}$ states are predominantly isospin $\frac{3}{2}$, the following relation between the cross-sections is predicted:

$$\sigma(\bar{p}p\pi^\circ) = \sigma(\bar{n}p\pi^-) + \sigma(\bar{p}n\pi^+)$$

This is indeed found to be the case (see Table 13) within the statistical accuracy of this experiment. Using this result the single pion production cross-sections including the unobserved $\bar{n}n\pi^\circ$ final state can be calculated; these $\bar{N}N\pi$ cross-sections are listed in Table 13.

Table 13

SINGLE PION PRODUCTION CROSS-SECTIONS

Final State	Momentum (GeV/c)	Number of Events	Cross-Section (μb)
$\bar{p}p\,\pi^\circ$	1·23	239	526 ± 35
	1·30	283	739 ± 46
	1·36	383	1011 ± 54
	1·43	513	1247 ± 60
$\bar{p}n\,\pi^+$	1·23	91	200 ± 21
	1·30	107	279 ± 28
	1·36	147	388 ± 33
	1·43	241	586 ± 39
$\bar{n}p\,\pi^-$	1·23	94	207 ± 22
	1·30	136	355 ± 32
	1·36	174	459 ± 36
	1·43	266	646 ± 42
$\bar{N}N\,\pi$	1·23	-	1400 ± 70
	1·30	-	2060 ± 94
	1·36	-	2780 ± 110
	1·43	-	3720 ± 125

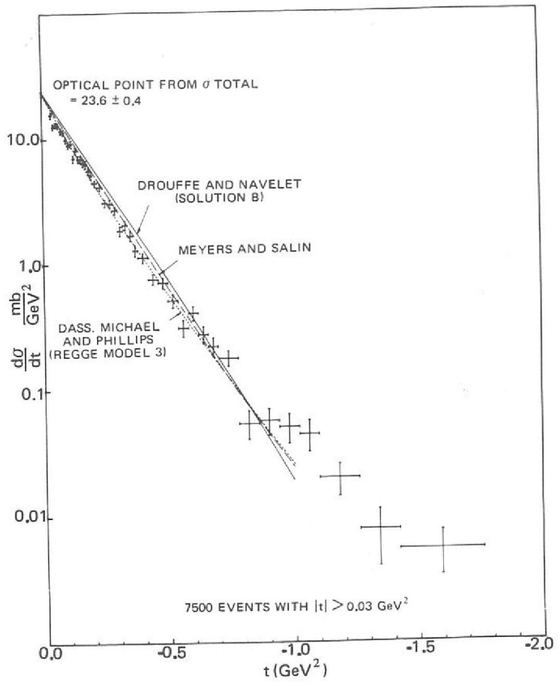

Figure 50. The differential cross-section for K^-p elastic scattering at 14·25 GeV/c. The lines shown with the experimental points are from three Regge pole models. (Experiment 22).

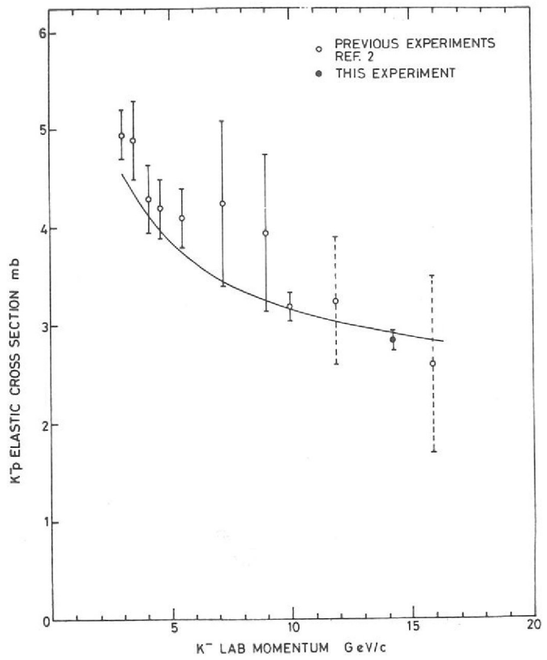

Figure 51. The integrated K^-p elastic cross-sections shown as a function of K^- laboratory momentum. (Experiment 22).

Experiment 22

CEN, SACLAY
ECOLE POLYTECHNIQUE
RUTHERFORD LABORATORY

The Study of 14 GeV/c K^-p Interactions (ref. 100)

The interactions of K^- mesons with protons at 14·25 ± 0·10 GeV/c are being studied. The aim of the experiment is exploratory since this is the highest energy K^- experiment yet attempted. Of particular interest will be the production of strange baryon and meson resonances against a relatively small 'phase space background'.

The film was obtained from CERN using the 2 m hydrogen bubble chamber in the high momentum r.f. separated beam. The first instalment of 350,000 pictures was taken in mid-1969 and measurement of the Rutherford Laboratory's share of the film is essentially complete. A further 400,000 pictures will be taken early in 1971.

First results on K^-p elastic scattering were presented at the 15th International Conference on High Energy Physics in Kiev and will be published soon. Most of these events were measured on the Rutherford Laboratory HPD measuring machine. On high momentum tracks, small residual distortions become as important as other sources of measurement error, and after extensive study, an empirical correction to the geometrical reconstruction was introduced to minimize these effects.

The elastic differential cross-section, corrected for scanning losses, is displayed in figure 50. The integrated elastic cross-section together with the results from other high energy experiments is shown in figure 51. As is readily seen, the present experiment has greatly reduced the error on this cross-section at high energy, emphasizing that the bubble chamber technique can be used efficiently for studying elastic scattering in certain cases.

Physics analysis on the many other reaction channels available in high energy K^-p interactions is now in progress.

Experiment 23

UNIVERSITY OF BIRMINGHAM
UNIVERSITY OF DURHAM
RUTHERFORD LABORATORY

The Study of 4 GeV/c π^+d Interactions

The aim of this experiment is to study the neutral boson states B° produced in the reaction $\pi^+ + d \rightarrow p + p_s + B^\circ$ where p_s is the spectator proton and p is the proton off which B° recoils. Of particular interest is the splitting of the A_2° meson, which is produced with a cross-section $\simeq 200\ \mu b$ in this reaction, and the f° meson ($\sigma \sim 100\ \mu b$).

The experiment is designed to be of high resolution and high statistics improving on similar previous experiments by a factor ∼ 4 in statistics and perhaps 2 in resolution. An exposure of 800,000 pictures, in the CERN 2 m bubble chamber filled with deuterium, has been requested. A total of 421,000 has already been taken.

The film is being scanned and measured simultaneously using the on-line scanning system recently introduced at the Rutherford Laboratory.

Experiment 24

IMPERIAL COLLEGE, LONDON
WESTFIELD COLLEGE, LONDON

π^+p Interactions in the Range 0·8-1·7 GeV/c (ref. 3,131)

This is an experiment to study the formation of baryon resonances with strangeness 0 and isotopic spin $\frac{3}{2}$, called Δ resonances.

(i) 0·9 to 1·05 GeV/c

Photographs of π^+p interactions at π^+ beam momenta of 0·895, 0·945, 0·995 and 1·040 GeV/c obtained in the Saclay 80 cm chamber at the Rutherford Laboratory have been analysed yielding approximately 55K fitted events. The differential and total elastic scattering cross-sections have been published. The results are in good agreement with previous measurements using counter techniques except at extreme backward angles where significantly lower cross-sections are obtained (figure 52).

Figure 52. The π^+p differential cross-section for backward angles at 0·945 GeV/c (from Experiment 24) compared with the counter data of Duke et al.

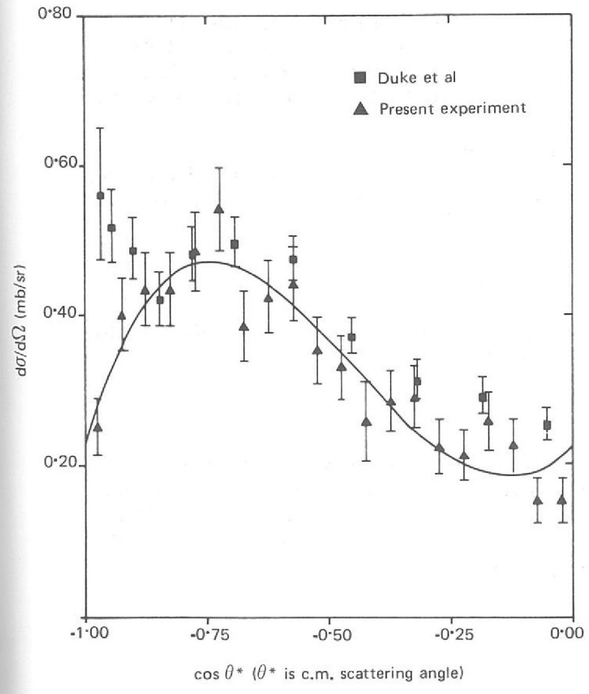

Figure 53. Isobar model fit at 0·995 GeV/c to the mass plots, the Valladas polar and azimuthal angles, Θ and Φ and the centre of momentum production angle of the proton. (Experiment 24).

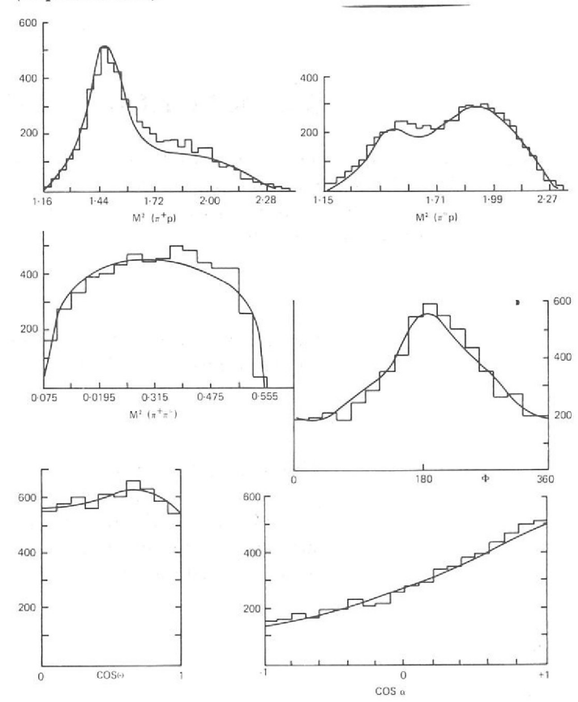

A phase shift analysis on the elastic data has been completed and was presented at the Durham Conference. The analysis shows clearly that the effect of the new data is to select strongly the CERN phase shifts rather than those of Saclay in the D_{33} and D_{35} waves where the two sets of solutions were in greatest disagreement. The only significant departure from the CERN solutions is found in an increased inelasticity of the S-wave.

The inelastic interactions at these momenta have also been fully analysed and papers are in preparation for publication. Partial cross-sections have been obtained and the single pion production is shown to be dominated by production of the $\Delta(1238)$. A detailed study of the short-comings of simple production models using the high statistics available has now been completed. A partial wave analysis of the inelastic scattering in terms of $\pi\Delta$ production has been made. It shows remarkable agreement with the incident partial wave inelasticities of the CERN phase shift solutions. Only the S-wave requires a contribution from production processes other than $\pi\Delta$. This together with the increased inelasticity required by the elastic partial wave analysis indicates the need for strong S-wave contributions from other inelastic channels such as ρN or πN^* even at these low momenta. Figure 53 shows an isobar model fit to the data at 0·995 GeV/c.

(ii) 1·1 to 1·7 GeV/c

The Cambridge film analysis group has joined Imperial College and Westfield College in the analysis of 200K pictures of π^+p interactions obtained from the 1·5 m hydrogen bubble chamber at the Rutherford Laboratory. The film at 1·1 GeV/c has been conventionally measured and that at 1·2 and 1·3 GeV/c has been measured on the Imperial College HPD.

(iii) 0·8 to 1·25 GeV/c

To complete the study at momenta around 1 GeV/c and investigate further the results reported in (i) above, 30K pictures were taken at each of four momenta 0·8, 0·85, 1·15 and 1·25 GeV/c in the 1·5 m hydrogen bubble chamber.

UNIVERSITY OF BIRMINGHAM
UNIVERSITY OF EDINBURGH
UNIVERSITY OF GLASGOW
IMPERIAL COLLEGE, LONDON

Experiment 25

K^-d Interactions at 1·45 and 1·65 GeV/c (ref. 14, 18, 134)

This experiment was performed using an electrostatically separated beam of K^- particles incident on the Saclay 80 cm bubble chamber, filled with liquid deuterium, at the Rutherford Laboratory. The main purpose of this experiment is to study the reaction

$$K^-d \rightarrow \Lambda\pi^-p \qquad (1)$$

treating the recoil proton from the deuteron as a spectator and using the Impulse Approximation to select events corresponding to

$$K^-n \rightarrow \Lambda\pi^- \qquad (2)$$

This channel is important since it selects baryon states with strangeness −1 in a pure isotopic spin state, I = 1. A partial wave analysis on this reaction has been carried out in which the parameters of the $\Sigma(2030)$ were determined; evidence supporting the existence of an $\Sigma(1915)$ F_{15}, and new evidence for a P_{13} resonance with a mass of 2080 MeV/c^2 was found.

As a by-product of this work a sample of events of type (1) where the proton could not be treated as a spectator was obtained. In this sample there is a sharp peak in the Λp effective mass distribution at the position of the Σn threshold, confirming results found in K^-d interactions from 0 to 1 GeV/c. The data is consistent with either a Λp resonance at 2130 MeV or with a threshold effect in the Σn system leading to Λp via the sequence

$$K^-d \rightarrow \Sigma^+\pi^-n,$$
$$\Sigma^+n \rightarrow \Lambda p$$

Elastic scattering, $K^-n \rightarrow K^-n$, has also been analysed in terms of partial waves. The elasticity of the $\Sigma(2030)$ was found to be 17%. Some work on other final states produced by K^-n interactions is in progress. In particular branching fractions of $\Sigma(1385)$ and $\Lambda(1520)$ are being determined and the general characteristics of Y* production processes are being studied.

CEN, SACLAY
IMPERIAL COLLEGE, LONDON
WESTFIELD COLLEGE, LONDON
} K^+p

IMPERIAL COLLEGE, LONDON
WESTFIELD COLLEGE, LONDON
} K^+d

Experiment 26

K^+N Interactions in the 2 to 3 GeV/c Region

K^+N interactions are of interest because of their relevance to the Simple Quark Model of elementary particles. So far all of the observed experimental resonance spectrum is accommodated in this model, in which baryon states are composed of three quarks. Other possible baryon states which can be constructed using a larger number of quarks are termed 'exotic'.

The search for exotic states is therefore of great importance. One particular such state is the baryon with strangeness +1 called Z*, which, in principle, can be formed in K^+N interactions. Peaks have been seen in K^+N total cross-sections and several experiments have been set up to investigate the nature of these 'bumps'.

This experiment is a survey of K^+p and K^+d interactions in the 2-3 GeV/c region. This energy was chosen because it covers the position of the third 'Cool bump' in the total cross-sections. All events from the 200,000 photographs of the K^+p interactions have been analysed. The Imperial College and Westfield College share were measured on the Imperial College HPD. This is therefore the first completed experiment using that device.

Figure 54. Legendre polynomial coefficients for the reaction $K^+p \rightarrow K^{*+}p$ as a function of the kaon laboratory momentum. (Experiment 26).

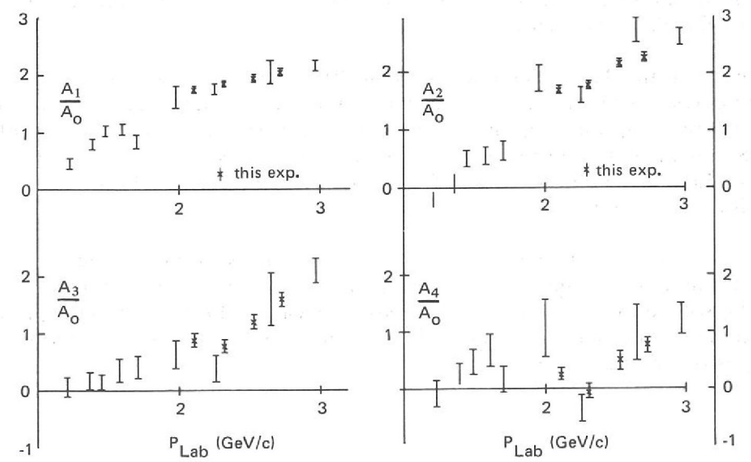

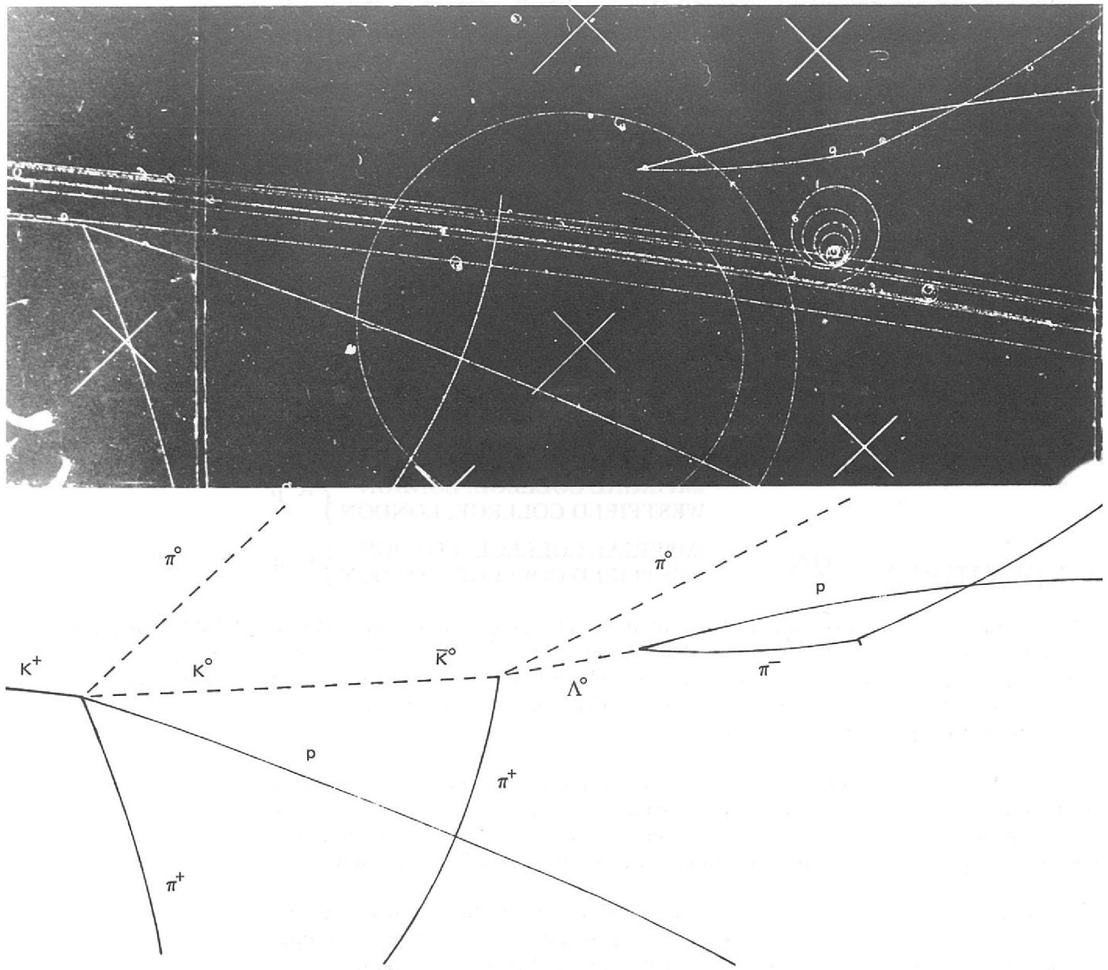

Figure 55. An event taken from K^+p film which displays the $K^\circ \rightarrow \bar{K}^\circ$ transition. (Experiment 26).

The K^+d exposure, totalling 800,000 photographs, is now complete and scanning and road-making is in progress.

Analysis of the K^+p data is continuing. There is little evidence for s-channel (baryon resonance) effects contributing to the 'Cool bump', but a survey of data through the range does appear to show some perturbations in the behaviour of the K*(890)p final state in this region. An example of this is the fluctuation of the fourth Legendre polynomial coefficient shown in figure 54. The significance of this is at present unclear.

Figure 55 shows an interesting example, found in the K^+p film, of the strangeness transformation accompanying the decay of the K°_s component of the K° meson. At the secondary interaction a Λ hyperon is created which required the presence of a negative strangeness component $\bar{K}^\circ$, although the K^+ mesons can only produce the positive strangeness K°.

Experiment 27

UNIVERSITY OF CAMBRIDGE

n-p Interactions from 1 to 7·5 GeV/c (ref. 129, 133, 137)

Neutron-Proton interactions are being studied from an exposure of 112,000 pictures in the 1·5 m hydrogen bubble chamber. A 8·3 GeV/c extracted proton beam incident on a Be target, approximately 7·8 metres from the chamber, was used to produce the neutron beam.

The final analysis of the following processes is now taking place (including data from an earlier test run of 40,000 pictures):

(a) Single and Multiple Pion Production

$$\begin{aligned} np &\rightarrow pp\pi^- \\ &\rightarrow pp\pi^+\pi^-\pi^- \\ &\rightarrow pp\pi^+\pi^+\pi^-\pi^-\pi^- \end{aligned}$$

(b) Strange Particle Production

$$\begin{aligned} np &\rightarrow \Lambda p\, K^\circ \text{ and } \Sigma^\circ p K^\circ \\ &\rightarrow \Sigma^- p\, K^+ \\ &\rightarrow \Lambda p\, K^+\pi^- \text{ and } \Sigma^\circ p\, K^+\pi^- \\ &\rightarrow \Sigma^- p\, K^\circ\pi^+ \end{aligned}$$

Experiment 28

UNIVERSITY OF CAMBRIDGE

n-p Interactions from 1 to 3·5 GeV/c

About 90,000 pictures containing on average two 3-prong events per picture were taken in the 1·5 m hydrogen bubble chamber in November 1970 using an improved design of neutron beam. The neutrons are contained within a band 2 cm wide.

It is proposed to study the following processes with high statistics:

$$\begin{aligned} np &\rightarrow pp\pi^- \\ &\rightarrow pp\pi^-\pi^\circ \\ &\rightarrow pn\pi^+\pi^- \end{aligned}$$

These account for about 75% of the 3-prong events. Approximately 40% of the observed 3-prong events are expected to be $np \rightarrow pn\pi^+\pi^-$ and higher momentum data suggest that at least one half of the events in this channel can be explained in terms of the process $np \rightarrow \Delta^-(1236)\,\Delta^{++}(1236)$, the Δ^- being associated with the neutron vertex.

The strange particle production processes

$$\begin{aligned} np &\rightarrow \Lambda p K^\circ \text{ and } \Sigma^\circ p K^\circ \\ &\rightarrow \Sigma^- p K^+ \end{aligned}$$

will also be studied chiefly with a view to observing the variation of cross-section with momentum near threshold.

Experiment 29

UNIVERSITY COLLEGE, LONDON
TUFTS UNIVERSITY, USA
UNIVERSITY OF BRUSSELS
CERN

K^- Interactions at a Momentum of 2·2 GeV/c in the 1·4 m Heavy Liquid Bubble Chamber (ref. 41)

The heavy liquid bubble chamber is particularly useful for the detection of electromagnetic processes because of its high γ-ray conversion efficiency, i.e. $\gamma \rightarrow e^+e^-$, the electron pairs being visible in the chamber; interactions involving the production of π°s can also be detected, since $\pi^\circ \rightarrow \gamma + \gamma$. By using a beam of K^- mesons, particles and resonances with strangeness -1 and -2 which under-go radiative decay can be studied.

For this experiment the chamber was filled with a propane-freon mixture with average γ-ray conversion efficiency of 55%.

The main aims are:

(i) to find the lifetime of the Ξ° by a method which uses the γ-rays from the Ξ° decay π° to fix the decay point.

(ii) to study the Λ - Λ interaction and the properties of the Ξ^- and Ξ^* resonances.

(iii) to search for X° and ϕ neutral decays and radiative Y^* decays.

One publication has now been produced from this experiment and two other pieces of work are nearing completion.

A Russian group had reported a new particle with a mass of 1327 MeV/c^2 which they had observed in the $\Lambda\gamma$ invariant mass spectrum in associated production events with a pion beam in a propane chamber. A scan on 20% of our film by three of the collaborating laboratories has shown that if such a state exists its cross-section for production by K^- collisions on nucleons at 2·2 GeV/c is much less than 100 μb.

The sample of events for our Ξ° lifetime measurement has now been scanned and measured completely. Background studies and tuning-up of the maximum likelihood programs are in progress. Three such programs have been written independently by different collaborators, and a calibration study on Ξ will be carried out as well as the Ξ° measurement.

Over 400 events with two Λ hyperons and an associated K^+ or K° have been measured. Preliminary analysis confirms earlier results that the $\Lambda\Lambda$ mass spectrum peaks strongly close to the threshold. The statistics are large enough for a decay-correlation analysis to be carried out. This will show whether an appreciable part of the low mass $\Lambda\Lambda$ spectrum is contributed by an S-wave interaction between Λ's from the same point in the nucleus.

Experiment 30

UNIVERSITY OF CAMBRIDGE

Anomalies in Electromagnetic Processes (ref. 65, 66, 125)

In a pilot experiment, using the 1·5 m hydrogen bubble chamber, anomalies were found in the distributions of the following three quantities.

(i) Pair α-Anomaly

α is defined as $(p_+ - p_-)/(p_+ + p_-)$ where p_+ and p_- are the momenta of the positive and negative tracks of the pairs which were produced by gamma rays originating in the chamber beam entry windows where incident 1 GeV/c electrons suffered energy losses.

(ii) Pair Energy Anomaly

Writing $k = p_+ + p_-$ and E_o for the incoming beam momentum an enhancement in the distribution of the ratio k/E_o was found at values around 0·83.

(iii) Bremsstrahlung Anomaly

A plot of the ratio of final to initial momentum of 1 GeV/c electrons suffering energy losses in the hydrogen bubble chamber showed an enhancement in the range 0·16 to 0·22.

About 250,000 pictures from a variety of production conditions were taken in April 1970 with a view to studying these processes with much better statistics. Analysis and measurement is still in progress.

Experiment 31

UNIVERSITY COLLEGE, LONDON
CERN
RUTHERFORD LABORATORY

Development of the Neon-Hydrogen Track Sensitive Target Facility

The track sensitive target facility combines the advantages of the hydrogen bubble chamber with those of the heavy liquid chamber. Beam particle interactions occur in a region of pure hydrogen so that the advantages of interaction with a free proton and simple production kinematics are preserved. The hydrogen is contained in a perspex bag within the main chamber which is filled with a heavy liquid mixture of neon and hydrogen. This heavy liquid is efficient for the detection of gamma rays arising from the decay of π°, η° and Σ° particles produced in the target. Operating conditions can be achieved where both the hydrogen and the neon-hydrogen mixture are simultaneously sensitive.

Work has continued during 1970 on the development of this facility in the 1·5m chamber. In collaboration with the operations group the filling problems associated with neon-hydrogen mixtures in the range 35 to 50 mole percent neon have been investigated. Using 700 MeV/c to 780 MeV/c protons which stop in the mixture and the range momentum relationship, it has been shown that the density of the mixture in the chamber agrees with that predicted from the filling technique. This has been checked by comparing the energy loss in the liquid with that in a known thickness of aluminium absorber placed in front of the chamber. Furthermore by measuring the range as a function of beam height in the chamber it has been shown that a uniform mixture with a variation of less than ±½% is obtained.

Because of the development work necessary it was not possible to take physics pictures for Proposal No. 66 during the year. This proposal was to use the heavy liquid as an electron detector to allow the study of the leptonic decays of polarized Λ hyperons produced by 1·040 GeV/c π^- interactions on hydrogen in the target. During 1970 however the CERN spark chamber group has analysed a large number of $\Lambda\beta$-decay events using a different technique so that, in view of the delay in starting physics with the target. Proposal No. 66 has been withdrawn.

It is now proposed to start the physics programme using the target in 1971 with a study of 4 GeV/c π^+p interactions to complement the 4 GeV/c π^+d experiment in progress. This proposal should yield data on the A_2 and H mesons in particular.

Experiment 32

UNIVERSITY OF BIRMINGHAM
UNIVERSITY OF SURREY
RUTHERFORD LABORATORY

Total Reaction Cross-Sections for Pions on Nuclei

This is believed to be the first experiment to be carried out on Nimrod with the object of gaining information about the properties and structure of atomic nuclei rather than the properties and interactions of elementary particles.

The experiment, which is currently in the final stages of setting up and testing of apparatus, is to measure the total reaction cross-sections for π^+ and π^- mesons on a range of nuclei at energies in the region between 0·5 and 2·0 GeV. The eventual aim of these measurements is to obtain further information about the density distribution of neutrons in nuclei, a currently controversial topic in nuclear structure physics.

In heavy nuclei both π^+ and π^- mesons are strongly absorbed in the nuclear interior. However, if for the pion – nucleon total reaction cross-sections (σ_R), the ratio:

$\frac{\sigma_R(\pi^-p)}{\sigma_R(\pi^+p)} = \frac{\sigma_R(\pi^+n)}{\sigma_R(\pi^-n)}$ is much greater than 1 then in the surface region the π^+ will be mainly absorbed by neutrons and the π^- by protons. Hence the ratio of the total reaction cross-sections for pion – nucleus interactions $R = \frac{\sigma_R(\pi^+N)}{\sigma_R(\pi^-N)}$ will be sensitive to the properties of the surface region around the 50% density point and in particular to the relative distributions of neutrons and protons. The ratio R has been measured before for 700 MeV π^+ and π^- mesons, giving R = 2·6, but the measurement was only made for lead and at one pion energy. In the present experiment these measurements will be repeated and extended to cover both a wide range of nuclei and a number of pion energies.

The experiment is being set up in a slightly modified version of the K8 beam line now designated π10. A DISC Cerenkov counter is used to distinguish between protons and π^+ mesons and a threshold Cerenkov counter used to reject electrons and muons. The latter counter will also be used to measure the pion beam momenta. The experiment itself (figure 56) consists of a 'bad-geometry' transmission measurement in which the number of particles transmitted through the target is measured as a function of the solid angle subtended by the elements of an array of scintillation counters. Problems have arisen in previous transmission counter arrays due to the detection of charged particles by Cerenkov light emitted in the plastic light-guides between the scintillators and associated photomultipliers. The present design, which is described in more detail in the instrumentation section, uses air light guides and a carefully chosen geometry which gives a detection efficiency of greater than 99·95% over the surface of the scintillator and to within 1 mm of the edge.

The scalers will be interfaced using the CAMAC system to a PDP-8 computer which will be used for on-line checking of the results. It is hoped to start data taking in the first quarter of 1971.

This experiment is also being carried out in close collaboration with the theoretical nuclear physics group at the University of Surrey who have written the computer programmes which will be required to interpret the results in terms of neutron density distributions. This group has also very fully investigated the theoretical justification for this experiment and several of the corrections which have to be applied to the simplified theory to take into account the Fermi momenta and correlations of the nucleons in the nucleus.

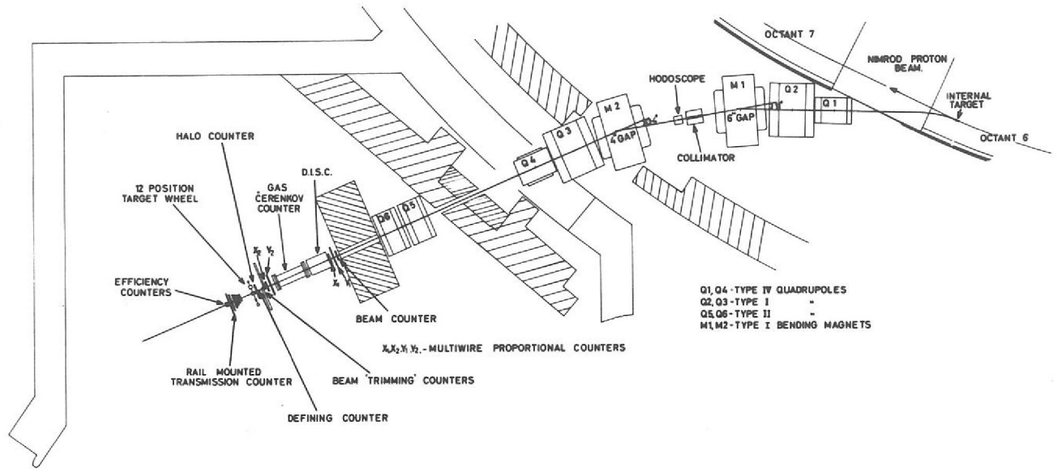

Figure 56. A schematic diagram of the π10 beam-line in Hall 2 and the apparatus used in the nuclear structure experiment on Nimrod. (Experiment 32).

Experiment 33

UNIV. RES. REACTOR, RISLEY
UNIVERSITY OF MANCHESTER
RUTHERFORD LABORATORY

A Search for Super-heavy Elements (*ref.* 82)

The possible existence of long lived super-heavy nuclei due to the formation of a closed shell of protons at Z = 114 and a closed shell of neutrons at N = 184 has recently been the topic of much theoretical speculation. For some super-heavy nuclei half-lives of as long as 10^8 years have been predicted.

Probably one of the best methods of producing these new elements, if they exist, would be to bombard a heavy element target with a beam of very heavy ions having an energy above that of the Coulomb barrier which exists between the target nuclei and the projectile. At present there are few, if any, accelerators giving directly very heavy-ion beams of sufficient energy.

In the present experiment an attempt has been made to produce super-heavy elements by using secondary reactions in targets irradiated by very high energy protons. For example when 24 GeV protons are elastically scattered from tungsten nuclei at angles greater than 45° the recoil nuclei will have energies greater than the 1·0 GeV Coulomb barrier which exists between two tungsten nuclei. Inelastic reactions may also give fast recoil nuclei. Super-heavy elements could perhaps then be produced as a result of an interaction between a recoiling nucleus and another heavy nucleus in the target.

In order to identify the super-heavy nuclei and to separate them from the other material present in the target it is necessary to rely on the predictions that elements 110, 111, 112, 113 and 114 will be the chemical homologues of Pt, Au, Hg, Tl and Pb respectively. Measurements of the alpha and spontaneous fission activity from the separated sources can then be made to try to identify the possible existence of super-heavy elements.

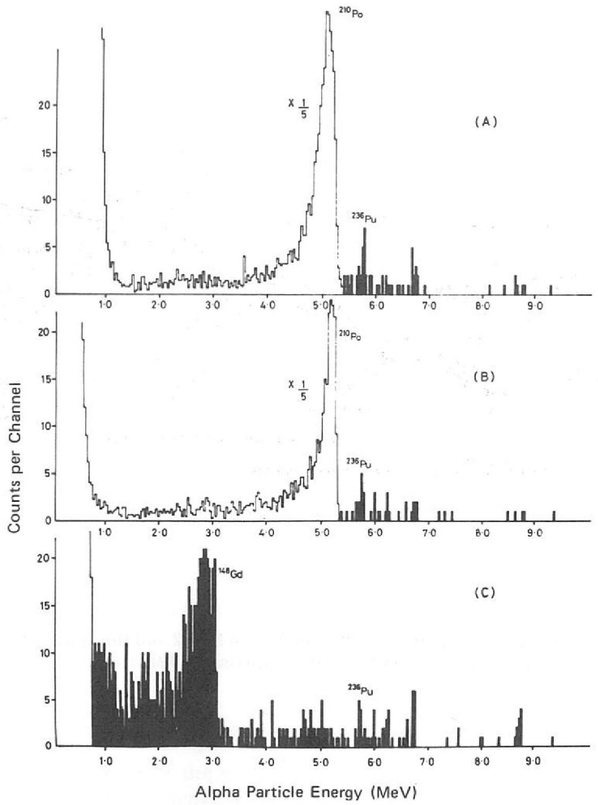

Figure 57. Alpha particle spectra measured with the Hg sources from Experiment 32. Figure (A) and (B) were obtained over periods of 406 and 236 hours respectively with the source obtained from the second tungsten target. Figure (C) was ontained over a period of 280 hours with the source from the first tungsten target.

Three cylindrical tungsten targets have been obtained after each has been irradiated by about 2×10^{18} protons of 24 GeV energy in one of the extracted beams from the CERN Proton Synchrotron. After chemical separation, measurements were then made on Pt, Au, Hg, T1 and Pb sources prepared from these targets.

The most interesting results to date have come from the Hg sources. Clear evidence for spontaneous fission activity has been obtained from the source prepared from the second tungsten target and preliminary measurements on the third target have given encouraging results. It does not seem likely that the observed activity is due to a contaminant. The first target does not seem to show any evidence for spontaneous fission – this may perhaps be due to the source thickness or to the fact that the target is considerably older than the other two.

In measurements of the alpha particle spectra from both the first and second source there is evidence for a group of alpha particles having an energy of 6·75 MeV (figure 57A, B and C). Again, although with less certainty in this case, it is believed that the observed alpha particles are unlikely to be due to any contaminant. The energy of 6·73 MeV is also in good agreement with several predictions for element 112, the homologue of Hg.

Other experiments to try to confirm the above results, and to endeavour to measure either the Z or the A of the decaying nucleus are in preparation. Measurements are also in progress on the other sources (Pt, Au, Tl and Pb) together with investigations of actinide elements which may also be produced in the tungsten targets.

Experiment 34

QUEEN MARY COLLEGE, LONDON
AERE, HARWELL
RUTHERFORD LABORATORY

Neutron-Proton Bremsstrahlung

The purpose of this experiment is to study the bremsstrahlung reaction $n+p \rightarrow n+p+\gamma$ in order to learn about the nucleon-nucleon interaction in conditions where the initial and final state energies of the two nucleons are not the same, the so-called 'off-the-energy-shell' elements of the two nucleon interaction. Calculations of the cross-section for this reaction using different parameterizations of the nucleon-nucleon interaction, which fit the elastic scattering equally well, show different predictions for the bremsstrahlung cross-section. A precise measurement of the $np\gamma$ cross-section will therefore differentiate between the various nucleon-nucleon potentials currently in use.

The plan of the experiment is shown in figure 58. A neutron beam is produced by peeling off the proton beam from the AERE 110 in synchro-cyclotron onto a beryllium target. The neutron beam is collimated and allowed to strike a liquid hydrogen target. An event is defined by coincidence between a neutron and proton arm on opposite sides of the beam at non conjugate angles, i.e. $\overline{B}(P_1\ P_2\ P_3)_i\ (\overline{N}vN)$. Proton arms were at 20°, 32°, and the neutron arms at 23°, 26°, 29° and 38° on both sides of the beam. For each event several parameters are measured including the incident time-of-flight of the neutron, the pulse height recorded in P_3 which gives the proton energy, the time-of-flight of the final state neutron, and the proton time-of-flight between P_1 and P_2. This information, plus identification of the proton and neutron arm which fired, is read into a DDP-516 computer via a CAMAC interface and stored on magnetic tape for later analysis.

With this system data taking has been completed for the $np\gamma$ experiment and is presently being analysed. Initial setting up for this experiment included a precision measurement of the n-p elastic scattering cross-section for neutrons of 130 MeV. These data have now been analysed and the relative cross-section is compared with previous measurements in figure 59. The relative accuracy for our measurements is 3·5%.

With only slight modifications in the experimental set-up data has been taken for the elastic neutron scattering from deuterium and a kinematically complete experiment on the reaction d(n, np)n is in progress.

Fig. 58. Schematic diagram of the apparatus used in Experiment 34, to study $n+p \rightarrow n+p+\gamma$.

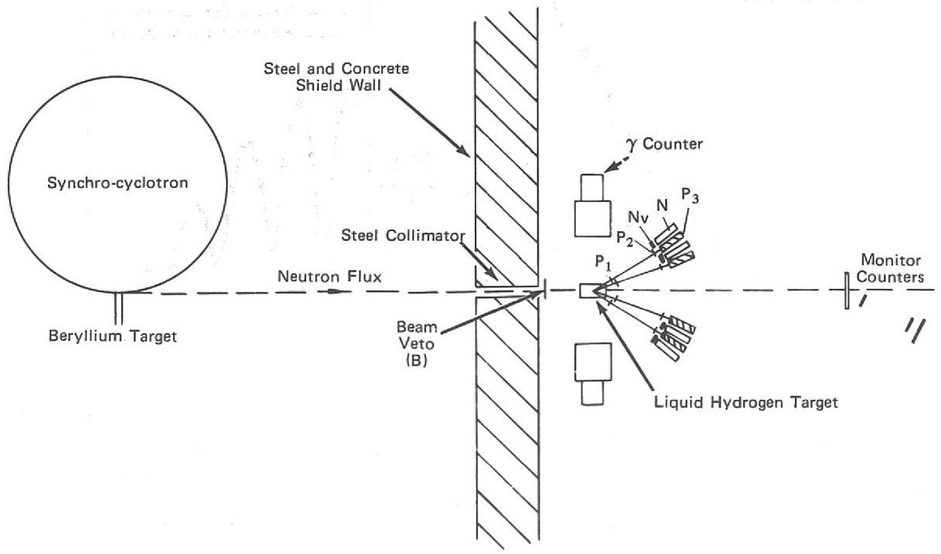

Experiment 35

KING'S COLLEGE, LONDON
WEST HAM COLLEGE OF TECHNOLOGY
UNIVERSITY OF BIRMINGHAM
UNIVERSITY OF KENT

Medium Energy Nuclear Reaction Studies

The backward angle data measured on the Proton Linear Accelerator (PLA), for the scattering of 50 MeV protons from Be, C, N and O nuclei have been analysed using the simple Optical Model. An improvement in the quality of the fits and better systematics in the parameters from nucleus to nucleus have been obtained by means of an unconventional absorption geometry, which has a dip in the radial distribution. The application of this geometry to other nuclei is being investigated, in particular to Mg, Al and Si.

Differential cross-sections and polarization measurements for 30 and 50 MeV protons scattered from $Cu^{63, 65}$ and of 50 MeV protons from Sm^{148} taken with the double focussing magnetic spectrometer on the PLA, have been analysed in terms of the standard and reformulated optical models. These data provide the first test of the latter at 50 MeV and typical fits to the Sm^{148} data are shown in figures 60 and 61.

Cross-section and asymmetry measurements have been made for the inelastic scattering of 30 MeV protons from the lowest 2^+ and 3^- states of $Zn^{64, 66, 68}$ and the first 2^+ states of $Mo^{92, 94, 96, 100}$. The analysis has been in terms of the Blair-Sherif model, in which the full grad term is used in the spin-orbit interaction (figure 62). The Mo elastic scattering data have been analysed with an optical model with a surface peaked real central term, and the results are being interpreted microscopically.

Angular distributions have been measured on the Variable Energy Cyclotron (VEC) for deuteron elastic scattering from $Sn^{112, 118, 124}$ at 20 MeV and $Sn^{112, 118, 119, 120}$ at 27 MeV, as little elastic scattering work has previously been done in this mass region with deuterons. More evidence has been found to favour a 100 MeV real well depth, mainly by comparing the resulting nuclear matter parameters with those obtained from proton scattering.

Fig. 59. The n-p elastic scattering cross-section for neutrons of 130 MeV measured in Experiment 34, compared with a previous measurement.

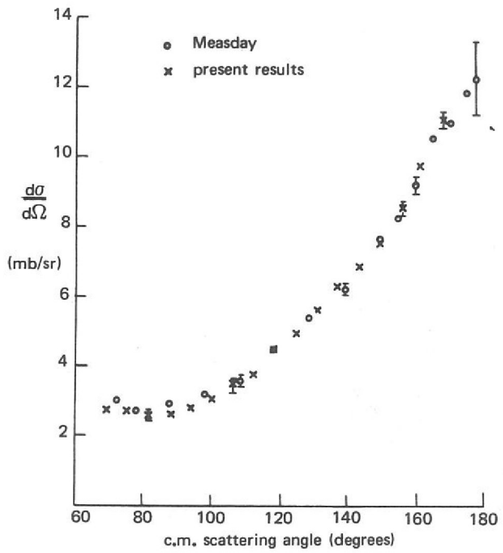

60. Fits to the differential cross-section data for the reaction Sm^{148}(p,p) Sm^{148} with standard and reformulated optical models. (Experiment 35).

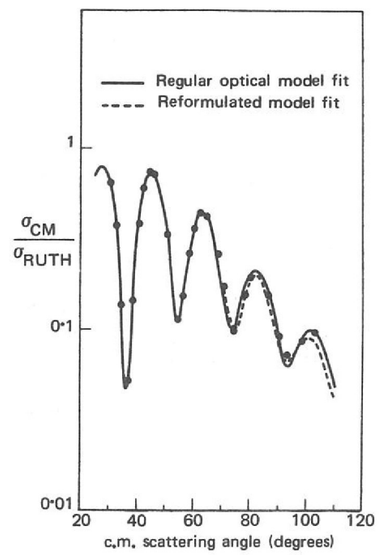

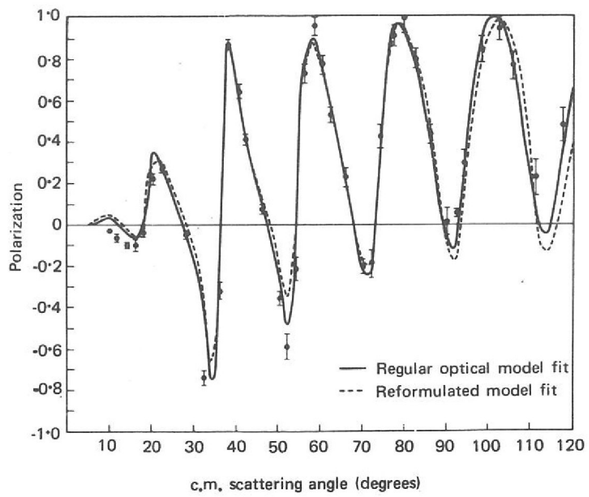

Figure 61. Fits to the polarization data for the reaction Sm^{148}(p,p) Sm^{148}. (Experiment 35).

Elastic and inelastic scattering of 53 MeV helions (He^3 ions) from Fe^{54} and Sm^{144} have been investigated on the VEC in order to provide more information on the interaction of complex particles with nuclei. This accurate data has helped to overcome some of the ambiguities usually present in complex particle scattering analysis.

The reaction Fe^{54} (h, d) Fe^{53} has been studied on the Harwell Tandem Generator using 18 MeV helions. The aim of this work is to investigate J dependence in these reactions and to obtain more information on the helion spin orbit interaction.

The group has participated in neutron scattering experiments on the 150 MeV Harwell Synchro-Cyclotron. These have consisted of p (n, pγ)n and n-d elastic scattering experiments. Preliminary information has been obtained on the d(n, 2n)p reaction and a feasibility study made for an n-d polarization experiment. (See Experiment 34).

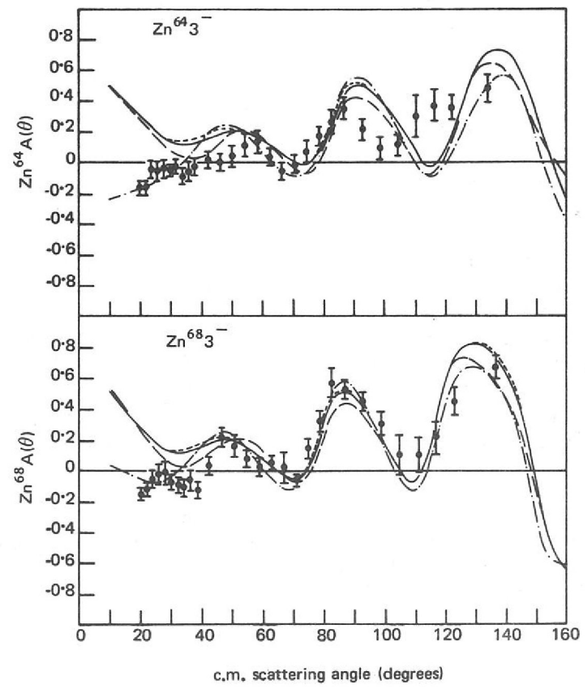

Fig. 62. Fits to $Zn^{64}3^-$ and $Zn^{68}3^-$ data. —.— Blair-Sherif model. ___ no spin orbit term. ____ simple radial term $\beta_{SO} = \beta_{real}$. ---- simple radial term $\beta_{SO} = 1{\cdot}25\beta_{real}$. (Experiment 35).

Theoretical High Energy Physics

The theory group works on a wide range of current problems, particularly in the realm of phenomenology – the confrontation of theory with experiment. This is thoroughly appropriate at the Rutherford Laboratory.

The interaction of theorists with experimenters was furthered by a series of informal two-day meetings at The Coseners House. The subjects were the Multi-particle Veneziano Model, Physics for the Omega Spectrometer, and Pion-Nucleon Resonances. About thirty participants from European centres were invited in each case. There was also the usual summer visitor programme.

The annual December conference this year was displaced into the first week of January, 1971. Over 200 physicists attended, mainly from British universities and laboratories.

The following brief accounts gives some idea of the interests of the group.

New Models for High-Energy Scattering. (ref. 6, 7.)

When the 70 GeV Serpukhov accelerator started working, more than doubling the highest available energy, surprising new results began to appear. The total cross-sections for $\pi^- p$ and $K^- p$ scattering, that had been steadily falling with increasing energy and were expected to go on falling, were found to level off at constant values above 30 GeV. This raised at least two questions:

(i) What new theoretical ingredient explains this levelling-off?

(ii) Since the $K^+ p$ cross-section is apparently constant up to the highest energies measured so far (20 GeV) and is considerably below the new constant $K^- p$ value, what has happened to the Pomeranchuk theorem that predicts asymptotic equality for these two cross-sections?

The Pomeranchuk theorem is not sacred. One of the assumptions on which it rests may be wrong, so failure of this theorem is an interesting possibility. But the Regge poles and Regge cuts that provide the usual language for discussing high energy scattering, happen to satisfy the Pomeranchuk theorem. So if the latter is to fail, some new ingredient must be added: Regge dipoles and singular cuts are among the suggestions made.

Alternatively, we may conjecture that whatever puts a kink in the $K^- p$ cross-section, changing its behaviour from a steady fall to a levelling-off, may also put a kink in the $K^+ p$ cross-section and cause it to start rising beyond 30 GeV, say – a region where it has not yet been measured. In this way the Pomeranchuk theorem could be preserved. We just have to find some ingredient to explain this kink. Here again there are many possibilities. Pole-cut cancellations, or an increasing component in the cross-section (behaving like ln E or ln $E)^2$ as energy $E \to \infty$) can all impart a kink. Complex Regge poles can give oscillations – repeated kinks, as it were.

Thus the Serpukhov data stimulate new thinking. The problem is to choose between the various new hypotheses. Fortunately, they lead to rather different predictions for other quantitites yet unmeasured, so that future experiments at Serpukhov and Batavia will help to distinguish between them.

$K_L \to K_S$ Regeneration Phase (ref. 5)

Simple Regge pole theory predicts that the phase of the amplitude for forward $K_L^0 p \to K_S^0 p$ regeneration should be near $-3\pi/4$, and experiments in the 2-8 GeV range confirm this value. However, preliminary results from Serpukhov suggest that the phase may change quite rapidly at higher energy, reaching perhaps $-\pi/4$ at 40 GeV. It is interesting to see if any of the new models being proposed to explain high energy cross-sections can also explain such a phase rotation. Several of them can. With violation of the Pomeranchuk theorem, the phase should go asymptotically to zero; whether it goes through $-\pi/4$ at 40 or 400 GeV is not determined – there is still a lot of freedom in such models. Models based on complex Regge poles also give a phase rotation, in the positive sense as observed.

The Line Reversal Puzzle

There are a set of line reversed reactions $ab \to cd$ and $\bar{c}b \to \bar{a}d$, of which the first is expected to have a real phase and the second a rotating phase, on the basis of dual Regge pole theory. Moreover, dual Regge poles predict the two cross-sections to be equal. Experimentally, however, the cross-section corresponding to the real phase seems always to be larger than the one corresponding to the rotating phase and this inequality is quantitatively significant for the hypercharge exchange processes. Modification of the Regge poles in terms of absorptive cuts generates an inequality, but in the wrong direction. If on the other hand the Regge poles are modified, in terms of colliding cuts, then the real amplitude gives the larger cross-section as observed. In fact a model based on pole-cut collision seems to fit the cross-section difference and polarization measurements quantiatively for hypercharge exchange processes.

Van Hove Plots (ref. 75)

The Van Hove Plot projects out the longitudinal components of phase-space which at high energy appear experimentally to contain most of the dynamical information while reducing the dimensionality of the problem. By this means several production processes were analysed in terms of a model which includes both Regge pole exchanges and their related phases at high subenergies and possible resonance formation at low energies. Besides Pomeron exchange, this analysis also stressed the importance of pion exchange in these reactions at the energies considered.

SU(3) Symmetry (ref. 85)

SU(3) has proved to be a very successful symmetry in classifying the observed particle spectrum and in relating three particle couplings. However the application of SU(3) predictions to scattering processes is difficult if the energies at which the comparisons are to be made are not specified. Prescriptions which involve superposing the thresholds in different reactions are only partially successful. For resonance decay, of course, the predictions are made at the resonance pole. Moreover the resonance masses can be prescribed by a simple formula, the Gell Mann-Okubo formula. It is natural therefore to try to extend this to a formula involving the energies at which comparison is to be made, this formula reducing to the Gell Mann-Okubo mass formula at the resonance poles. This prescription has been found to be successful in relating scattering processes.

Non-Linear SU(3) Symmetry

By treating SU(3) as a non-linear symmetry realised by the appearance of massless scalar mesons in the symmetry limit, and imposing Regge asymptotics on the scattering amplitudes of the theory, the usual algebraic consequences of SU(3) for vertices and masses are recovered. In addition there are new dynamical consequences for the couplings of a nonet of scalar mesons or perhaps instead for the tensor nonet of Regge trajectories at $\alpha = 0$.

Background to One-Pion Exchange, and Vector Dominance (ref. 58)

The notion of particle exchange goes back to the foundation of our subject; indeed, it is in this secondary role as 'virtual' quanta to mediate forces between other particles rather than in their primary role as free quanta, that a number of boson particles, notably pions, first impinged on our thinking (Yukawa, 1935). As is well known, the range of the force resulting from particle exchange is related to the exchanged mass by the 'Uncertainty Principle', i.e. Range = $\hbar$/(Mass x c), so that the lightest quanta correspond to the longest range. It is for this reason that the pion, the lightest strongly interacting particle, occupies a key place among exchanges. The 'Regge-picture' of high energy exchanges predicts a more sharply falling energy dependence for pion exchange than for rival mechanisms; none the less, pion exchange is conspicuous up to the highest observed energies.

Di-pion production and charged pion photo-production appear to be dominated by one pion exchange at small momentum transfer. In respect of di-pion production, this fact is exploited to infer $\pi\ \pi$ elastic scattering parameters upon which there exists very important and widely ramifying theoretical predictions from the notions of chirality and duality (di-pion production is essentially our only source of detailed $\pi\ \pi$ scattering information). In order for valid inferences to be made the background to one pion exchange has to be understood. As reported earlier, a simplified expression for the small t background has been developed involving rather few parameters. On fitting this parameterization to data at a number of beam momenta, a very simple behaviour for the transversely polarized rho background was noted. This was subsequently shown to conform to the predictions of the absorption model and the 'gauge invariant elastic Born' model and to be in agreement with 'Vector Dominance'.

Threshold Sum Rules from Unitarity (ref. 79)

The unitarity condition implies several constraints on the partial wave amplitudes, and these constraints may be converted into corresponding sum rules for the cross channel absorptive parts of scattering amplitudes. The super convergence and FESR relations (which are consequences of the absence of fixed poles in the angular momentum plane) and the unitary sum rules by Arbab and Slansky are typical examples. It has been shown that the unitarity condition may be explored further leading to sum rules for the crossed channel absorptive parts for fixed t at the respective two body threshold. It has been shown, using the t-channel unitarity condition, that the reduced partial wave $\pi\ \pi$ scattering amplitude evaluated at threshold for Re $\ell > -\frac{1}{2}$ vanishes and it has a known first derivative with respect to angular momentum ℓ at the point $\ell - \frac{1}{2}$. These properties imply sum rule constraints for the crossed channel absorptive part for t fixed at threshold. The sum rules have been analysed for $\pi\ \pi$ scattering. Their generalisation to other processes have also been investigated.

CP Non-Invariance in some Radiative K Decays

Work on possible CP-noninvariant effects in radiative $\tau^{\pm}$ decays has been extended to include effects of structure in the nonradiative amplitude and to consider also radiative $\tau'^{\pm}$ decays.

A systematic study of all possible tests for T- and CPT-invariances in the decays of individual neutral kaons in vacuum has been carried out. The importance of the various tests and their implications for the symmetry properties of interactions obeying different selection rules have been pointed out. These considerations, coupled with the known data on neutral kaon decays, lend support to the superweak theory of CP-nonconservation. Limits on possible CPT-(and T-) noninvariance of different interactions in neutral kaon decays are also being studied.

Sidewise Dispersion Relations (ref. 38)

Calculation of the anomalous magnetic moments of the nucleon from dispersion relations in the photon mass squared requires a knowledge of $\pi\ \pi \rightarrow N\bar{N}$ scattering below the physical threshold. On the other hand if we disperse in the nucleon mass squared, what is required is πN elastic scattering and πN photoproduction data in the physical region, so sidewise dispersion relations provide a better hope of calculating these quantities. Although the threshold region does not provide a satisfactory result, when the resonance region up to the limit of present scattering data is included, the experimental values of the magnetic moments are approximated.

Coulomb Corrections (ref. 52, 53)

Most scattering data refer to initial states of charged particles while in many cases the final states also involve charged particles. This means that a detailed study of these scattering processes entails treatment of both the strong and the electromagnetic interactions.

The inter-connection of the two interactions can be used to probe the electromagnetic structure of the scattered particles in simple cases such as $\pi^{\pm}N \rightarrow \pi^{\pm}N$. Alternatively, in the case of very accurate experiments this inter-connection must be taken into account when attempting to isolate information on the strong interaction.

The formulation for dealing with this situation has been developed for low energy πN scattering and it is being extended to cope with the low energy $K\bar{N}$ system.

Baryon Resonances (ref. 67)

Over the past few years the number of known particles and resonances has grown considerably, for example about ten years ago data compilations listed some seventeen states, now they list eighty with many more suspected to exist.

For the case of baryon resonances this increase has been largely due to the successful exploitation of the technique known as phase shift analysis. In this, one essentially analyses accurate two body scattering data in terms of amplitudes of known quantum numbers (spin, parity, isotopic spin etc.). By performing these anlyses at closely spaced mass intervals one is able to investigate structure which may be present and (hopefully!) isolate the resonant states. The major success to date with this technique has been in the field of pion-nucleon scattering below 2 GeV where the number of resonance states has grown from 4 in 1960 to 15 in 1970, with indications that there may still be more. The Rutherford Laboratory experimental teams have, since 1965, contributed of the order of half of the total world data used in these analyses, a very fine achievement. Currently Rutherford Laboratory teams (K13C, CERN SC23, K14A, π9, K15, K8) are engaged in measuring further pion nucleon two body scattering data to a far higher precision than obtained previously. Such data will go a long way to providing a complete picture of two body πN scattering below, say, 2 GeV, and when fully analysed should provide a wealth of new information.

At various times past members of the theory group have collaborated with experimental teams in phase shift analysing two body scattering data. In the last year these collaborators have been active in analysing both pion nucleon and kaon nucleon data.

'Exotic' Resonances (ref. 4, 80)

Currently much attention has been focused on K^+p scattering because here is a direct way of looking for strangeness + 1 resonances. A scheme which has been very successful in classifying known resonances is the quark model, where one invokes triplets of fractionally charged quarks to construct the baryon and their excited resonant states. The simplest of these models cannot easily accommodate low mass strangeness + 1 resonances, and so a strong test of such a model is whether such resonances exist. Recently, University College London have obtained

preliminary elastic K^+p scattering data between 1·4 and 2·3 GeV/c. Analysis of this data together with previous data has shown that a complete description of all currently available data can be obtained which does not require the existence of a strangeness + 1 resonance, at least with a mass less than 2·3 GeV.

A theoretical survey has also been made of the situation regarding the K^+p system and strangeness + 1 resonances, suggestions were made as to what might be the most valuable experiments to perform next. Further K^+p experimental work is being performed at the Rutherford Laboratory (K12, K15), the results of which are eagerly awaited.

Hyperon Resonances

Members of the theory group are also working on an analysis of strangeness - 1 kaon nucleon scattering. Systematic experimental data are now available over a wide range for the strangeness - 1 system for most two body final states. These various possible two body final states are related via unitarity (i.e. conservation of probability), but most analyses performed to date which take into account this relation have been restricted to the mass region below 1520 MeV. Work is now under way to extend such analyses into the mass range 1520 to 1720 MeV, where many resonant states are believed to exist. Values of the decay rates of the resonances into the various two body channels will be obtained the results being of relevance to the classification (e.g. in the quark models) of these states.

There is much work still to be done with the technique of phase shift analysis and, if the past progress is any guide, many exciting results should be forthcoming.

The A_2 Meson

One of the most exciting problems of the past year has been to understand the mass spectrum of the A_2 meson. Interest was aroused when the mass spectrum of the A_2^- meson, produced in the reaction $\pi^- p \rightarrow A_2^- p$, was found to have two closely spaced peaks with the separation between the peaks approximately equal to their width. The most widely accepted explanation of this phenomenon was that there exist two J = 2 mesons lying close in mass which interfere destructively to produce the dip. Of course the existence of a second spin two meson would pose many interesting questions as to its nature and the existence of its symmetry partners. In a subsequent experiment the A_2^+ was found to be unsplit, a fact that could be explained within the two meson hypothesis if the production of the A_2 meson included an isospin one component whose contribution would change sign between A_2^- and A_2^+ production. This would change the production phase to give no destructive interference for the A_2^+. This model would also explain the indications that A_2^o is split. However a recent experiment analysing the A_2^- at a much higher production energy has an unsplit mass plot and this is inconsistent with the simple picture presented above. It remains to be seen whether a plausible explanation of this new data is forthcoming or if indeed the two meson hypothesis is tenable at all.

The Y_0^* (1405)

The existing analyses of low energy $\bar{K}N$ scattering data parametrize the Y_0^* (1405), which lies between the $\Sigma\pi$ and $\bar{K}N$ thresholds, as a virtual bound state of these channels. However if the Y_0^* (1405) is interpretated as an isoscalar member of an SU(6) – L supermultiplet with orbital excitation $L = (1^-)$ it should be produced by the strong forces which give rise to the existence of the complete supermultiplet. Thus it should not be produced mainly by the $\bar{K}N$ and $\Sigma\pi$ channels. Re-analysis of the low energy $\bar{K}N$ data allowing different production mechanisms strongly suggest that the Y_0^* (1405) is indeed a virtual bound state of the $\bar{K}N$ and $\Sigma\pi$ channels and thus casts doubt on its supermultiplet interpretation.

Absorption from the Veneziano Model (ref. 31)

The infinite resonance spectrum given by the Veneziano model is perhaps suggestive that the model already includes the effect of numerous coupled channels. This hypothesis was used to determine the $\pi\pi$ and πK inelasticity parameters below 2 GeV from a partial wave dispersion relation. Approximating the integral over the left hand singularities by its Veneziano model equivalent, and assuming some plausible forms for the real parts of the phase-shifts, it was found there is considerable absorption above 1 GeV in the non-exotic channels.

Dual Model for πN Scattering (ref. 76)

Since the introduction of the Veneziano model for meson-meson scattering, several attempts have been made to construct a similar dual model for meson-baryon scattering. Among other difficulties, the apparent absence of parity doublets for leading baryon resonances is not easily reproduced. Recently, a prescription has been given for eliminating unwanted parity partners by introducing fixed J-plane cuts and constructing functions with poles in $S^{\frac{1}{2}}$ rather than in S. It is not clear, however that the resulting dual models can lead to a good description of πN scattering.

We have constructed explicitly a dual model which does not possess parity doublets along the leading trajectories. A feature of this model is that from one input trajectory it naturally produces two sets of degenerate baryon trajectories, half a unit apart. Mathematically it is simpler than previous models and we are able to analytically continue it to the physical region.

A Unitarised Veneziano Model (ref. 73)

An analysis has been carried out on a class of meson-baryon scattering processes using a form of unitarised Veneziano model. Unitarity is partly described by introducing all the coupled two-particle channels which are related to each other by the requirements of SU(3), duality, factorisation and absence of exotics. The Pomeron is interpreted as multi-particle absorptive corrections rather than as a t-channel exchange. The F/D ratio plays a particularly crucial role in understanding the behaviour of various reactions. To describe hypercharge exchange reactions, exchange-degeneracy breaking mechanisms are considered and evaluated.

Phenomenology based on the Veneziano Model (ref. 74)

Since its introduction two years ago much work has been done on the Veneziano model (this model was briefly discussed in the 1969 Annual Report). Despite its still rather serious drawbacks (e.g. it does not conserve probability, that is it does not obey unitarity) it is beginning to be used as a basis for phenomenological data fitting. One main area of application has been on 2 to 3 body reactions where early work showed (in one specific case) that a reasonable description of a lot of data could be obtained in a simple fashion (much to everyone's surprise!). A collaboration of theorists from CERN, Oxford and the Rutherford Laboratory have applied these ideas to all reactions involving the particles $K^+K^-\pi^-p\bar{n}$ and their charge conjugates. A qualitative description using a rather simple functional form has been obtained of a large body of data involving these particles. Also some interesting questions have been thrown up from this analysis concerning the dual nature of the pion Regge trajectory with low energy baryon resonances. By dual one means that in some sense a description of scattering data can either be in terms of the pion Regge trajectory or in terms of a sum of baryon resonances. It has been shown by the analysis that possibly the pion trajectory is not dual to known baryon resonances.

Antiproton Annihilation

The annihilation of antiprotons on nucleons are being investigated. A description of the 3-meson final state in terms of invariant amplitudes has been found, and is being used to inter-relate the various $\bar{p}p$ and $\bar{p}n$ final states.

The large single-gap sonic spark chambers mounted in K12A beam line. (Experiment 1).

INSTRUMENTATION FOR HIGH ENERGY PHYSICS

Instrumentation for High Energy Physics

The setting up of experiments requires considerable technical support. In this section of the Report, apparatus for particular experiments in the physics programme and general developments, including electronic instrumentation and targets for elementary particle scattering experiments are described. The Laboratory support groups are involved in the design, manufacture, installation and commissioning of apparatus not only for experiments at Nimrod, but also those carried out at CERN by research groups based on the Rutherford Laboratory.

APPARATUS FOR THE K12A EXPERIMENT

General Engineering Work

In experiment K12A (Experiment 9, Page 38) particle detectors were designed to define the incoming beam and detect the scattered particles within the spectrometer magnet and down stream of this magnet. The detectors (see figures 30 and 63) consists of:

(a) Magnetostrictive spark chambers and scintillation counters for beam definition in front of the magnet.

(b) Sonic spark chambers and scintillation counters within the spectrometer magnet aperture.

(c) Various scintillation counters within and around the target vessel.

(d) Sonic spark chambers and scintillation counter arrays behind the spectrometer magnet.

The new items in the beam line are the six magnetostrictive beam defining chambers. These chambers have an aperture of 16 cm diameter and the wire planes are mounted normal to the beam direction with relative wire directions rotated by 45° about the beam axis in consecutive chambers. The wire used is 0·1 mm diameter with 1 mm pitch between wires. As assembled in the beam line, the total length of the six chambers is approximately 60 cm. Downstream of the above chambers and close to the target are various veto scintillation counters; one of these is actually mounted within the target vacuum vessel. This counter is made from 6 mm thick by 60 cm wide sheet of plastic scintillator and is in the shape of a round-ended flask. It surrounds the target with its open end facing downstream towards the spectrometer magnet. Three light guide fish-tails transmit the light signals to the exterior of the vacuum vessel.

Placed within the spectrometer magnet poles is the first sonic spark chamber (C2, figure 30), this is a double gap unit 1·8 m long by 38 cm high, made completely from non-magnetic materials, and is of 'prestressed' design. Modules of PZT5H material (1969 Annual Report, page 85) are used for the sonic detectors.

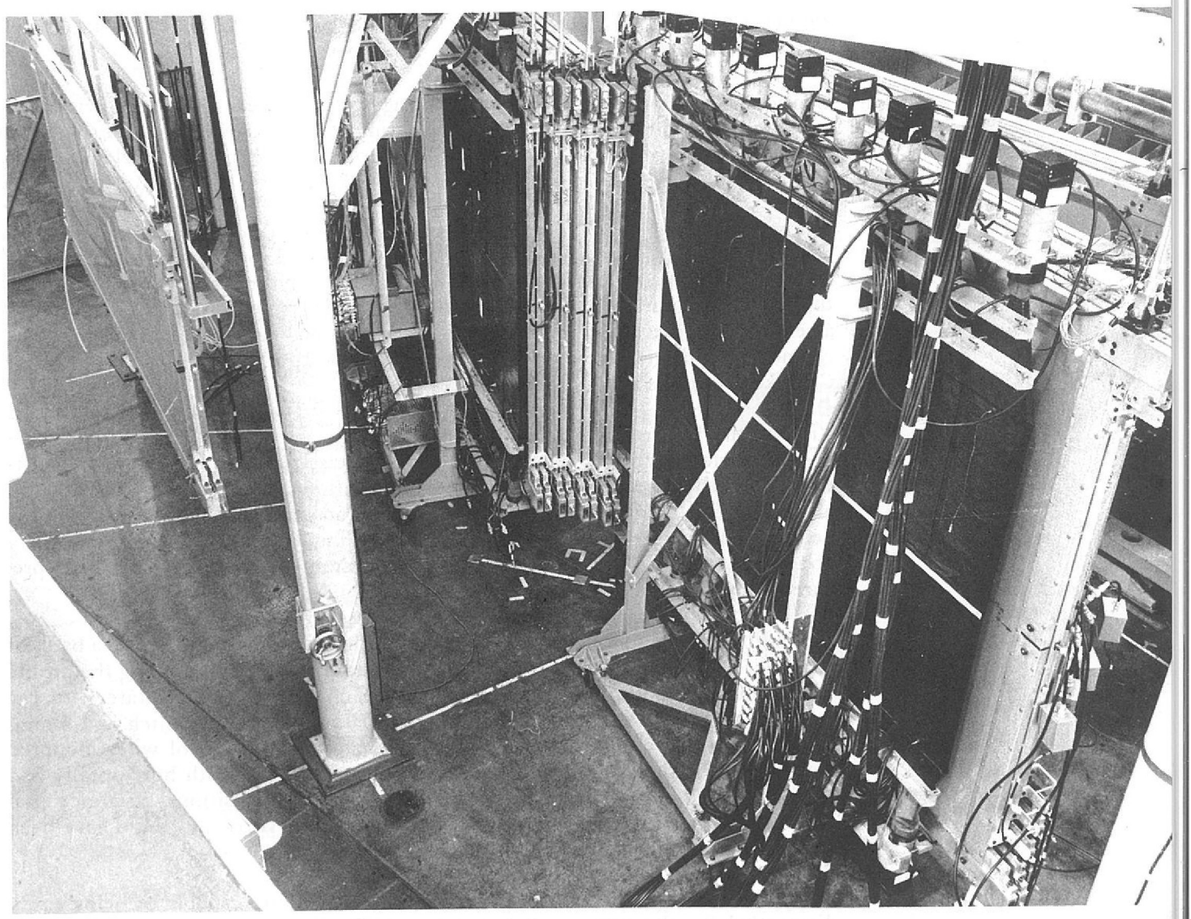

Figure 63. Large spark chambers and scintillator arrays for the K12A experiment.

Behind the spectrometer magnet are twelve very large single-gap sonic spark chambers in three groups of four. Four of these are 3·64 m long x 1·38 m high (C3, figure 30) and eight are 3·66 m long x 2·33 m high (C4). The latter are probably the largest spark chambers of their type in the world. The detector system for these spark chambers is a modification of PZT5H modules referred to above. It has been possible to achieve an accuracy of ± 0·5 mm in the relative positions of these large chambers.

Behind each group of C3 and C4 spark chambers is an array of scintillation counters totalling fifty units mounted on three mobile stands, the largest of which supports twenty-two assemblies covering an area of 5·9 m^2. The whole of the spark chamber system behind the spectrometer magnet is suspended from an open steel frame 3·9 m high x 7·2 m wide and 4·2 m long supported on six steel columns. This has been designed so that the chambers can be moved individually on rails to provide access for setting up and installation, and also permit mobility of other apparatus (e.g. the counter arrays above).

In addition a spark chamber test facility has been installed which moves these large chambers so that they can be scanned by a test beam with a positional accuracy of better than 1 mm, thus enabling the characteristics of each spark chamber to be precisely defined.

APPARATUS FOR THE ANTI-PROTON EXPERIMENT AT THE CERN PROTON SYNCHROTRON

General Engineering Work

Considerable effort has been spent during the past year on the provision of apparatus for the $\bar{p}$-p experiment (Experiment 10, page 39) currently being installed in the South Hall of the CERN Proton Synchrotron Accelerator (see figure 64).

The main component of the apparatus consists of a 130 ton magnet, mounted on clusters of spring loaded ball castors, which is required to rotate through an angle of 55° about a fixed pivot above which is mounted a hydrogen target. Surrounding the magnet are arrays of wire spark chambers. Banks of scintillator and light guide assemblies are accurately and selectively positioned around each of the spark chamber arrays and the hydrogen target. Also incorporated are Lucite and Water Cerenkov counters and a beam hodoscope.

An essential feature of the experiment is that the arrays of wire spark chambers and the various scintillator assemblies move precisely with the magnet during its rotation with the minimum of positional variation between items. In order to effect rotation of the castor mounted magnet and apparatus, and to maintain the height of the magnet with respect to the beam line within ±1·0 mm, an especially accurately constructed floor, surfaced with armoured steel plates has been prepared. Movement is effected by means of a hydraulic ram.

A total of 38 wire spark chambers are used in the experiment, including a bank of ten placed upstream of the experiment for the purpose of determining the profile of the beam. The majority of the remaining chambers, which rotate with the magnet and have a working area of 2·75 m x 0·75 m with a wire pitch of 1·5 mm, are of two basic configurations:— (a) single gap, with planes of wires mounted diagonally, (b) double gap, with planes of wires mounted both horizontally and vertically. Particular attention has been paid to the positional accuracy and catenary of the 0·125 mm diameter beryllium/copper wires and these have been kept to less than 0·5 mm total variation.

All the chambers which are required to be gas tight, are capable of being easily dismantled for the purpose of maintenance. They are mounted individually and any chamber may be removed on a special loading trolley. Their required positional accuracy with respect to the magnet is ±0·5 mm.

In order to economise in the amount of high purity neon/helium gas mixture required to continually circulate through the chambers and to keep the impurity level within the chambers to less than 0·1%, three gas purification systems, designed and developed at the Laboratory, are employed.

The techniques leading to the successful construction of all the spark chambers were established at the Laboratory, and subsequently all double gap spark chambers were manufactured by commercial firms using wire winding machines also designed and supplied by the Laboratory. The manufacture of the single gap spark chambers with diagonally mounted wires was undertaken in the Laboratory. All the spark chambers are being tested (see below) prior to shipment in specially designed crates.

After trial assembly at the Laboratory, installation of the apparatus, including three control and plant rooms, front and rear rotating platforms and spark chamber support structures, and a large overhead service gantry, commenced December 1970 at CERN. Further installation will continue between running periods with beam particles, when apparatus already installed will be tested. The main magnet will be available to complete the installation in May 1971.

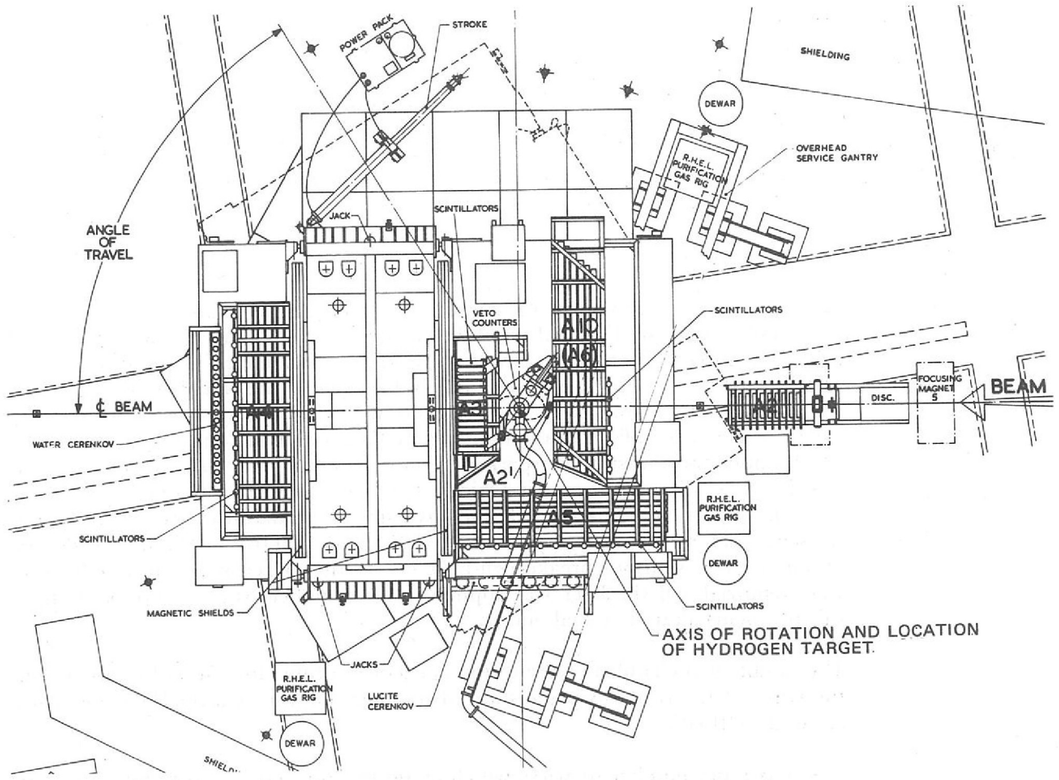

Figure 64. A plan view of the apparatus for the $\bar{p}$-p scattering experiment. A2, A3, A4, A5 and A6 are banks of wire spark chambers. A hydraulic ram rotates the magnet and secondary particle detectors through an angle of 55°.

As a result of close co-operation with the experimental team during the testing of the prototype spark chamber, a test specification and test facility were produced to ensure that all wire spark chambers manufactured for this experiment would be delivered to CERN fully tested and with known characteristics.

The chambers are designed for use with a core read-out system, wire spacings are 1·5 mm pitch and the active area dimensions are 2·75 m x 0·75 m and 1·17 m x 0·384 m.

The chambers are of two main types:—

1. **Three frame chambers**, each chamber having two gaps, one gap having both planes of wires wound on the frame in the 'x axis' and the other gap having both planes of wires wound on the 'y axis'. Of this type 13 are large chambers having an active area 2·75 m x 0·75 m and 4 are smaller chambers having an active area 1·17 m x 0·384 m.
2. **Two frame chambers**, these are single gap chambers, both planes of wires being wound diagonally on the frames. Of this type 6 are large chambers with an active area of 2·75 m x 0·75 m and 2 are smaller chambers with an active area of 1·17 m x 0·384 m.

Testing of the Wire Spark Chambers

The test specification was designed to ensure that all the chambers operated efficiently over the whole of the active area without having too great a spread on the spark efficiency-EHT curve. It was also necessary to check that each chamber reached maximum operating efficiency at an electric field strength well below that at which spurious breakdown in the chamber became a problem. Operating parameters such as gas mixture, gas flow and clearing field voltage were determined during testing of the prototype and the performance of the manufactured units was established using these criteria.

Test Procedure

Each chamber was flushed with helium gas for 12-24 hours, and during this time the chamber was tested for leaks and the value of the feed capacitor was measured. After the initial flushing the gas was changed to 30% helium, 70% neon with 10% of the gas flow being bubbled through N-butyl alcohol, the chamber being flushed for a further 12-24 hours. At the completion of the flushing period a source of electrons (see page 96) and a counter telescope were used to trigger the chamber EHT supply and measure the spark efficiency versus applied volts at each of three positions of each gap. The area in which a spark should occur due to the passage of an ionising particle was tightly defined by using a scintillator of area 1 cm^2 in the telescope system and a finely collimated beam of electrons. Then, in order to obtain a set of spurious breakdown-EHT curves the source and counter telescope were removed and the EHT was applied to the chamber using an external trigger; this test being a purely visual one.

The double gap chambers were tested one gap at a time, the gap not in use having the wires of the read-out plane shorted together and earthed, the HT plane being allowed to 'float'.

The maximum number of wires which could be connected to the test core read-out at any one time was 250; all remaining wires of the read-out plane were shorted together with copper foil and connected to earth.

Results of Tests

Figure 65 shows typical spark efficiency curves as a function of HT voltage for a small three frame chamber at each of three positions. To ensure that the value of the power supply HT was accurately known, the voltage was monitored using a potential divider and the value read out on a digital voltmeter. The voltage could be set to an accuracy of 5 V over the range 0-10 kV and a continuous monitor of this value was maintained throughout. Although the spark efficiency-EHT curves were not identical, all the chambers of each type had similar characteristics.

Figure 65. Spark efficiency—EHT curves at each of three positions for a small three frame wire spark chamber.

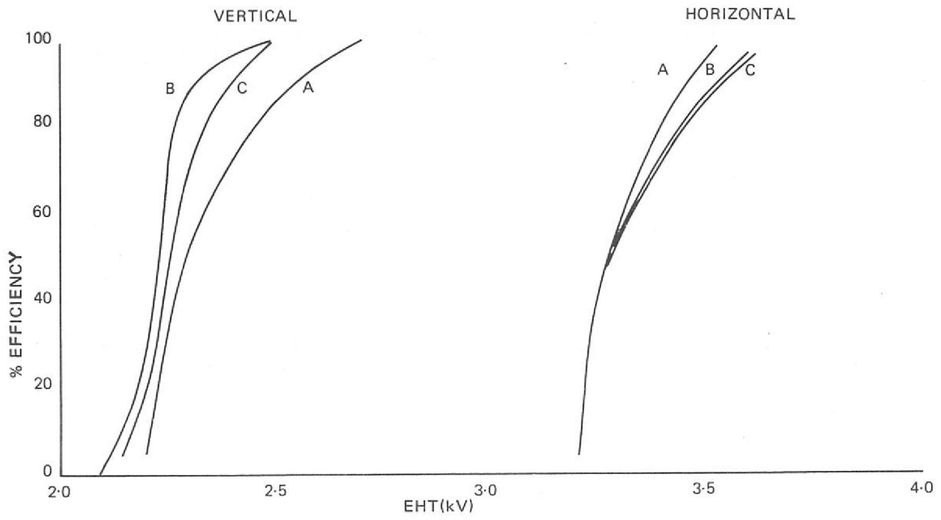

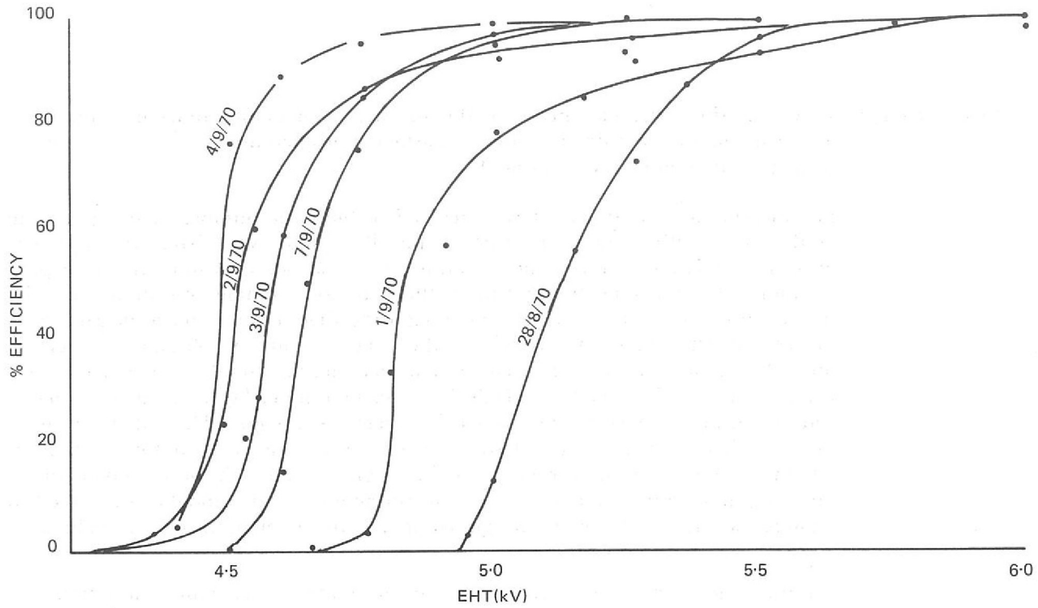

Figure 66. Spark efficiency—EHT curves, at a fixed point of a large wire spark chamber, showing variation with time.

Spurious breakdown for the small three frame chambers occurred only for values of HT above 5 kV. Although the other types of chamber were less impressive, tests showed that the spark efficiency-EHT curve plateaued well below the value of HT at which spurious breakdown became a problem. Preliminary analysis of the read-out data shows that a chamber operating at 100% efficiency was setting about 3 cores per spark. Whenever timescales allowed, additional tests were carried out and figure 66 shows typical results obtained in this case at one point of a large three frame chamber, where spark efficiency-EHT curves were plotted over a period of several days.

At the time of writing this report 20 out of the total of 25 chambers have been tested and shipped to CERN. It is anticipated that the remaining chambers will have been tested by mid-February 1971.

DESIGN AND CONSTRUCTION OF APPARATUS FOR THE MUON EXPERIMENT AT THE CERN INTERSECTING STORAGE RINGS

A new project during the past year was the design and construction of the apparatus for the muon experiment at CERN. (Experiment 18, page 51). The position in which the experiment is to be erected, Intersection II of the Intersecting Storage Rings, also houses two other experiments, and the requirements of all three have to be integrated into the overall lay-out. The major components of the muon detector, namely the absorber assembly, magnet assembly, thick plate spark chambers, scintillation counters, and optical system are in an advanced stage of design and construction.

The Absorber Assembly

The absorber consists of a lead mass approximately 80 in wide x 55 in high x 20 in thick weighing 12 tons contained in a steel casing supported centrally about the intersection region, and between the intersection region and the magnet. It is required to have an adjustment of 12 in under remote control and is mounted on trunnions slotted into bearings on a support frame, which is in turn supported on pivots bolted to the floor. The support frame is held upright by two supporting towers either side of the absorber assembly, and give reaction support for the adjustment. These towers are framed together to support other apparatus near the beam line, and are fitted with ladders to give access to this apparatus as the beam line is 13 ft from the floor.

Magnet Design

To enable the design parameters of the unusual magnet configuration required for use in the muon experiment to be established, a programme of work on a quarter-scale prototype model was initiated.

For measurement purposes it was decided to limit the number of plates on the model to give either side of the centre spine. Two plates were fitted with a pattern of search coils and these could be arranged in various positions in the magnet assembly. By reversing the current in the field coil winding and monitoring the signals from the search coils on an integrating digital voltmeter a measurement of flux density variation throughout the magnet could be obtained. To check the B/H characteristics of the magnet material, measurements of the H parameter were carried out by inserting a Hall Plate Magnetometer between adjacent plates and measuring as close to the iron-air boundary as possible. This information on the B/H characteristics of the material was used as data for a computer program set up to predict the performance of the magnet proper. From a comparison of the computed results and the survey measurements on the model it was hoped to establish accurately the major design parameters of the main magnet assembly.

An initial field survey was carried out on the model to determine the number of ampere turns required to produce a flux density distribution better than 15 kG ± 20% across the horizontal mid-plane in the magnet plates. Having established this value of ampere turns, measurements on the fringe fields around the magnet and the transverse fields existing between plates were made. These were found to be of the order of 10 G close to the magnet, dropping off to less than 1 G at a few feet from the magnet. As a result of these measurements it was decided to flatten the flux density distribution by increasing the ampere turns to approximately twice the previous value. Further survey measurements at this value of ampere turns were carried out and the flux density distribution across the horizontal mid-plane was found to be 15 kG within +10% and -5%. The fringe and transverse fields were also checked and in addition measurements on the vertical and horizontal fields existing along the circulating beam directions of the Intersecting Storage Rings were carried out. These were all found to be below the acceptable limit.

Data from both the model measurements and computer program have been incorporated in the design of the main magnet assembly.

The Magnet Assembly

The full-scale magnet consists of 26 steel plates 14 ft 6 in x 8 ft x 4 in thick arranged either side of a central spine at an angle of 15° (see figure 43, page 51) such that it forms a magnetised steel moderator. The energising coil is housed around the top half of the spine to produce an approximately circular flux pattern in the iron plates. It is important to the experimenter that the flux distribution is fairly constant across the plate, and also of the same value in each plate. As there are practically no air gaps, the main reluctance of the circuit is in the steel. To achieve the maximum uniformity of flux density across the plates, the steel has to be run at saturation (approximately 15 kG). It is also important that the stray field due to the magnet is low as the field tolerance at the intersection of the Intersecting Storage Rings is approximately equal to the earth's magnetic field and the magnet has to be sited very close to the intersection as shown in figure 43. These requirements have been checked in the quarter-scale model described above and the full-scale magnet is being assembled at the Rutherford Laboratory (see figure 45) for a final magnetic and dimensional check before being despatched to CERN.

Thick Plate Spark Chambers

The thick plate spark chambers are double gap optical chambers to be viewed from the side and the bottom. They will be located in the 4 in gaps between the magnet plates and have active areas which cover the majority of a 2 m x 4 m area.

To ensure that these chambers will record multiple events, the gap between the spark chamber planes must be held to 1 cm ± 0·05 cm. Several attempts were made to achieve this condition using various stiff materials such as 0·75 in thick aluminium plate, composite materials of aluminium and balsa and aluminium and plywood, but none of these were satisfactory, as they either presented extreme manufacturing difficulties or were not sufficiently flat. In these early attempts no spacers were used between the plates as these reduce the visible region.

As a compromise solution, aluminium sheet 0·1875 in thick, which meets the flatness specification, has been used. The plates are stiffened by a system of spacers which give a minimum of shadow. Twenty-four of these chambers are required, and they are being manufactured commercially using jigs and tools which have been designed at the Rutherford Laboratory.

Scintillation Counters

There are five banks of scintillation counters in the apparatus shown in figure 43. These scintillators are arranged in such a geometry that the spark chambers are only fired when a particle originates from the intersection region, thus reducing the number of triggers due to cosmic rays.

The B, C and D banks (see figure 43) are very large assemblies, the C bank being the largest and most complicated. It consists of 24 sheets of scintillation material, 20 mm thick x 1 m x 69 cm, with twelve sheets each side of the centre spine arranged 2 sheets wide x 6 sheets high to cover an area of 2 m x 4 m. The scintillators will be housed in light-tight aluminium casings together with acrylic light pipes. These assemblies are designed to hang in the 4 in gaps between the magnet plates in the same manner as the thick plate spark chambers.

The Optical System

Each of the 24 thick plate spark chambers and also 2 multi-gap foil chambers mounted between the absorber assembly and the magnet (see figure 43) are to be viewed directly from the side and the bottom and also at a 7·5° angled view from the bottom. To achieve this arrangement the side mirrors looking at both side and bottom views are required to be 21 ft long x 4 in wide. It is possible to split these into three 7 ft lengths, but even at this reduced length the only plant that is capable of producing front-aluminized glass with a protective coating is at the Rutherford Laboratory. The mirror system is arranged so that the spark chambers are viewed by a single camera which also records a considerable amount of other information by means of a data box. The camera is mounted at the rear of the apparatus.

Each spark chamber will be fitted with fiducial marks and calibration marks every 20 cm in both views, at the back and front of each chamber. These will be used to made spatial reconstruction of events and enable corrections to be made for any optical distortion due to spark chamber materials or mirror inaccuracies.

At the camera position will be a remote controlled indexing device, to enable 4 cameras, each loaded with 1,000 ft of film, to be used in turn. One position can also house a theodolite arranged such that it may be angled both horizontally and vertically to enable accurate checking of the optical system from the camera to the spark chambers.

The whole experiment will be covered with a light-tight igloo 37 ft long x 28 ft wide x 22 ft high. This structure will also be used to help support the mirror systems, provide support for the main cable runs and walk-ways and ladders to give access to the equipment.

APPARATUS FOR THE π 10 NUCLEAR STRUCTURE EXPERIMENT

Multi-wire Proportional Counter/Display Interface Unit

A portable beam-line investigation system, capable of displaying beam profiles and beam emittance data was required for the π 10 beam. (Experiment No. 32, page 68). This called for an interface between the particle detector, a multi-wire proportional counter with 36 wires, and the display device, a 'Laben' analyser.

A prototype interface has been developed which accepts the output pulses from the individual wire amplifiers of the counter. These signals are converted to BCD, then gated and modified so that the output pulses are compatible with the analyser address system in respect of pulse repetition frequency, amplitude and length. The 'Laben' analyser is an integral part of the beam diagnostic equipment for the experiment and is thus available for this additional function.

The Transmission Counter

The transmission counter is comprised of six light-tight cells mounted in a cylindrical vessel 42 in dia x 15·5 in long. Each cell is maintained concentric with the vessel's outer shell and contains an accurately positioned circular disk of scintillating material.

Figure 67. The Transmission Counter showing a typical scintillator cell.

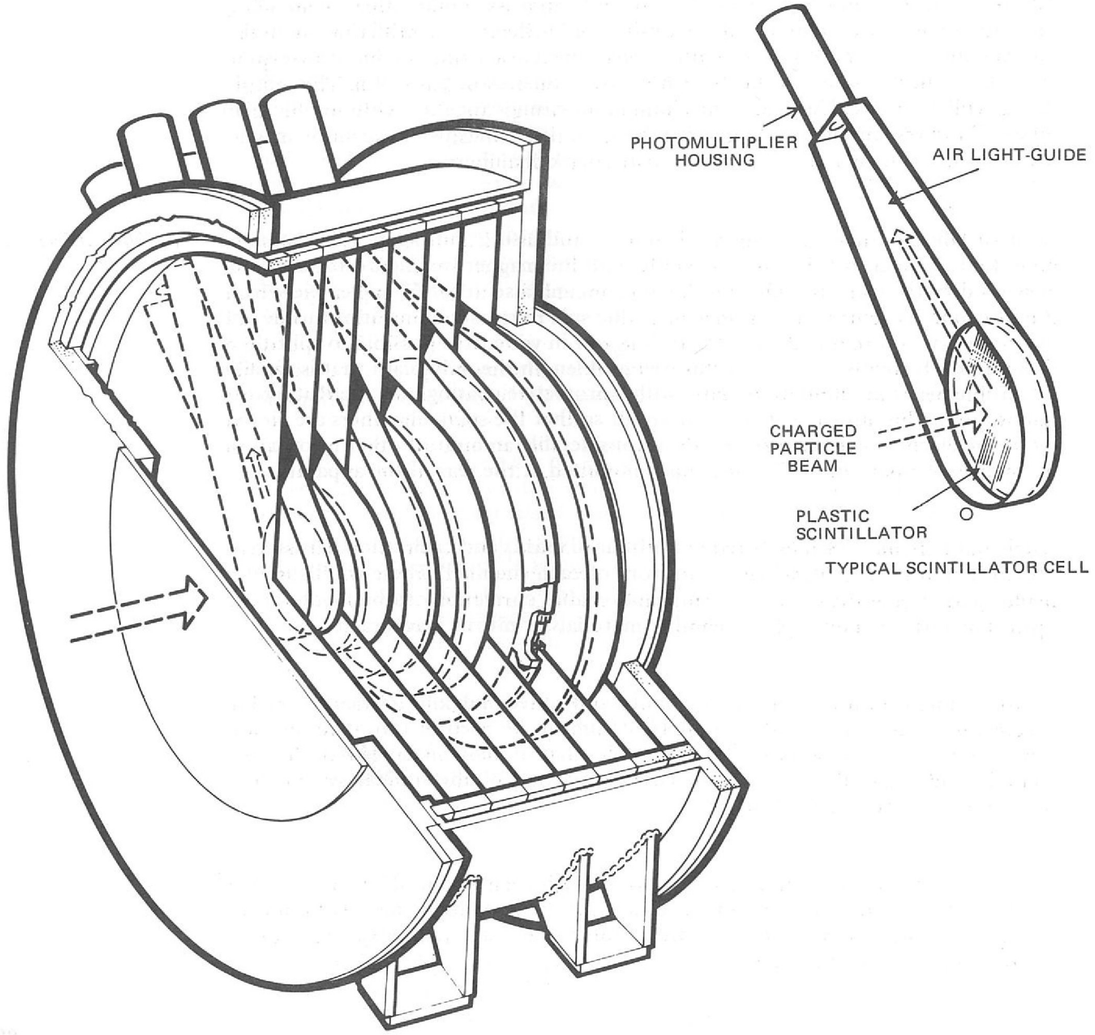

The light-tight cells are formed from a series of circular hoops of 41 in dia x 2 in wide x 0·5 in thick, each with an aluminised melinex sheet 0·002 in thick bonded 'drum-like' across one end so as to make a light-tight membrane between each cell. Six scintillator disks, ranging from 7 in dia x 0·375 in thick to 23·25 in dia x 0·5 in thick, are bonded one to each side of alternate cell membranes and are accurately located in relation to a datum face at the front of the transmission counter vessel. The advantages of this method of assembling a transmission counter is that a minimum of unwanted material is in the path of the beam, and by mounting the scintillators on both sides of a melinex sheet, the assembly is mechanically balanced. To make an efficient air light guide from scintillator to photomultiplier a strip of aluminised melinex, of width equal to that of the cell, is wrapped around the edge of the scintillator disk and tapered to the photomultiplier aperture where it is retained in position by small plate clamps. The counter is shown schematically in figure 67.

LARGE GAS CERENKOV COUNTER

K15 Cerenkov Counter

A 4 ft diameter by 6 ft long gas Cerenkov counter (figure 68) was installed in the K15 beam line. The vessel is constructed of carbon steel, having a 4 ft 6 in long cylindrical section with forged end domes. The vessel was designed to operate at a working pressure of 280 lb/in^2 gauge, initially using sulphur hexafluoride gas as the radiating medium.

A large aluminised perspex paraboloid mirror, mounted in the downstream end of the counter, focusses the Cerenkov radiation from charged particles passing through the counter on an array of seven photomultiplier tubes mounted in a branch on the top of the vessel.

The gas handling system has been designed to allow use of most radiating gases, either hazardous or non-hazardous. The equipment is built into a standard electronics console which contains and encloses the valves and pipework, also the electric heater and control systems. When used with a hazardous gas the console is ventilated and the containers for the electrical systems are purged with an inert gas. High pressure gas from storage cylinders is passed through a reducing valve after which the gas passes through a heater and a mass flow controlling nozzle. The heater is controlled by a sensing thermistor downstream of the nozzle to ensure that gas at the ambient temperature is fed into the Cerenkov counter.

A gas system has been set up specifically for the recovery of sulphur hexafluoride from the counter. Sulphur hexafluoride has a vapour pressure of about 310 lb/in^2 absolute at room temperature and is normally stored in liquid form. During the recovery process the gas is passed from the counter vessel through a 'Corblin' compressor into a water cooled vessel. There condensation of the high pressure gas takes place and the liquid gravitates into a bank of storage cylinders.

Figure 68. The large gas Cerenkov Counter (4 ft diam x 6 ft long) installed in the K15 beam line.

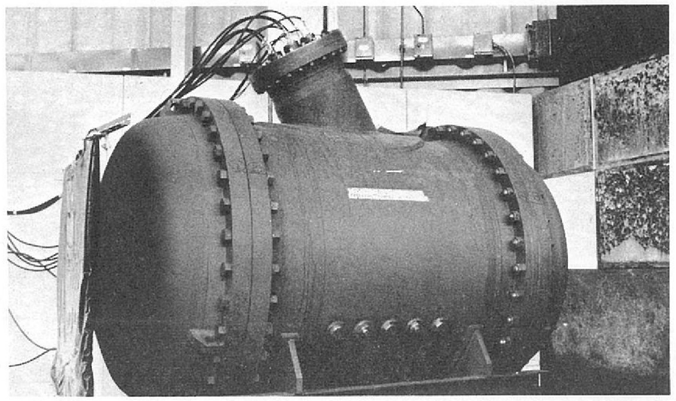

INSTRUMENTATION WITH GENERAL APPLICATIONS

Magnetostrictive Wands for Wire Spark Chambers

A programme of work on magnetostrictive wands is in progress to produce units suitable for use in the wire spark chamber arrays currently being manufactured for experiments at the CERN Intersecting Storage Rings. In all a total of approximately 100 units will be required in lengths ranging up to 2·5 m. In addition to the long spans covered by the wands, they will also be required to detect multi-spark events and to meet these requirements development work has been carried out to improve the acoustic damping and amplifier performance. Due to the restricted access of the spark chamber printed circuit board active areas, the cross sectional dimensions of the wands are severely limited and this together with the long spans involved has entailed special attention being given during design to ensure structural rigidity of the complete assembly. This has involved modifications to the wire clamping and the mounting arrangements for the coil and bias magnet. These now form an integral part of, or are mounted directly from, the wand spine. This minimises the effect of flexing between the spine and end cover assembly and simplifies the alignment procedure during assembly of the wands.

Improvements in acoustic damping have been achieved by providing a two stage damping system at the receive coil end. In this arrangement the acoustic pulse is channelled first through a soft damping pad consisting of a trough filled with wax and then through a graduated damping pad formed by a sandwich of synthetic rubber and tape. Modifications to the pre-amplifier include changes in the MA702 differential amplifier circuit and the provision of additional stages to increase the gain (approximately 500) and improve discrimination. Prototype testing of the wands is now completed.

Figure 69. Construction of a large thin foil spark chamber.

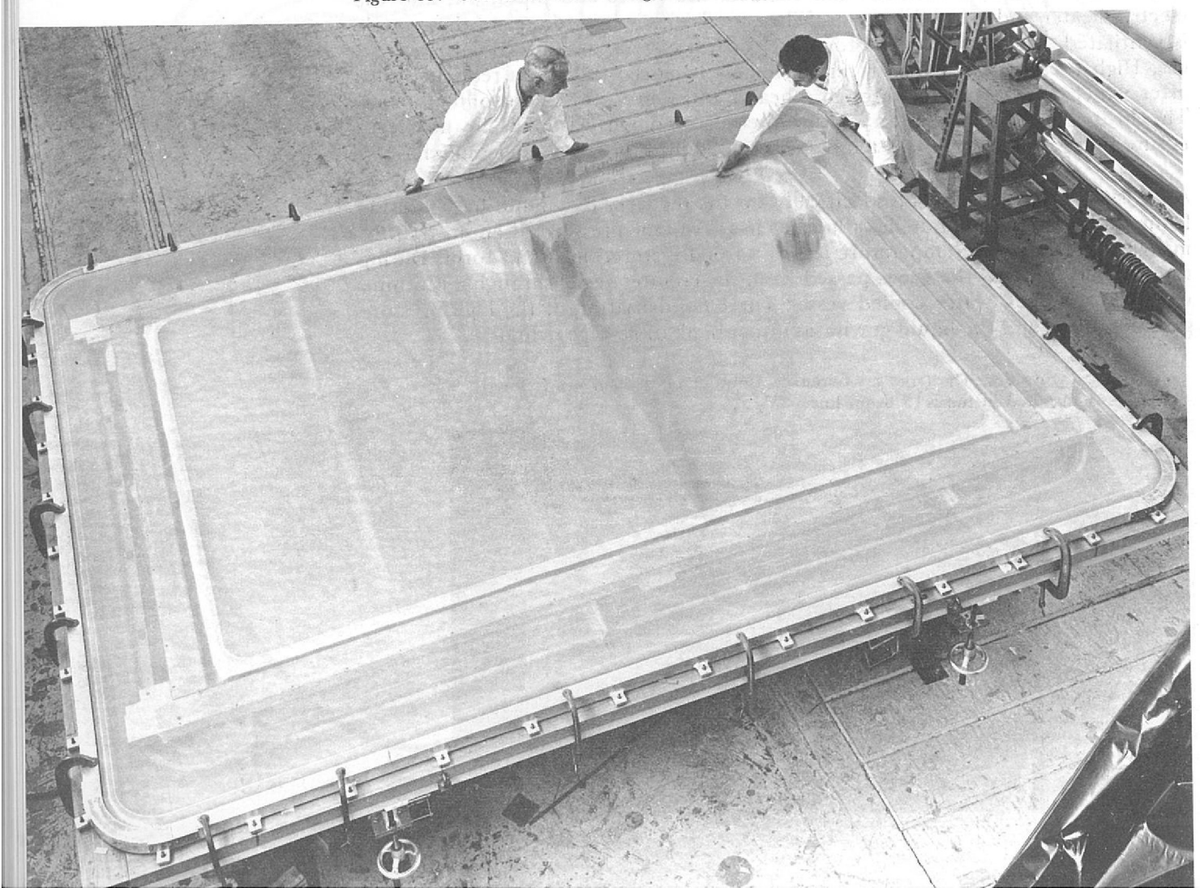

Development of Large Spark Chambers with Thin Foil Planes

The large spark chambers used in the K12A experiment required the development of special construction techniques because of their weight, 68 kg, and size, 3·64 m x 2·34 m. (See figure 69).

The spark chambers consist of pairs of matched frames, each frame supporting a single composite foil (an aluminium alloy membrane mounted in polyester film), and a polyester film pressure window. The large foil areas are prepared on a stretching frame; in the case of the largest chambers, two pieces of 0·025 mm thick aluminium foil 1·65 m wide x 4·2 m long, are placed side by side and bonded at a simple overlap joint of 15 mm. The frames are constructed from a specially developed aluminium extrusion with a high strength to weight ratio. The extrusion is hollow, thus allowing the horizontal members of one frame to be used for the helium gas distribution. The frames are pre-stressed so that the sides bow outwards. Prior to applying the foil, the sides are clamped so as to bow inwards. Then, after the foil has been bonded to the frame, the clamps are removed so that the frame tension compensates for 'adhesive creep' between bonding and final cure and maintains foil tension during dimension changes resulting from thermal cycling.

A Thyratron Pulser for Large Spark Chambers

A thyratron pulser has been designed to energise the large acoustic spark chambers used on the K12A experiment. The largest of these chambers measures approximately 3 m x 2 m, the active gap being 1 centimeter. These chambers operate on pulse voltages in the 10 to 15 kV range. At the high voltages and short pulse rise-times required to operate these chambers at high efficiency, heavy demands are made on the peak current capability of the pulsing device. Both the triggered spark-gap and the thyratron may be used to produce high voltage pulses of high peak current at a fast rate of rise. The thyratron, an English Electric CX1157, was chosen for this application because, unlike the spark-gap which suffers from spark erosion of its electrodes, it requires no servicing and will give trouble-free operation for long periods; up to 10,000 hours service has been claimed in some cases. In addition this valve has other advantages over the spark-gap. It will give extremely accurate and reliable firing at any voltage within its range without adjustment to the circuit being necessary and it requires a relatively low trigger voltage. Against these merits must be set the considerably greater cost of this type of thyratron compared to a spark-gap.

The circuit of the pulser has been designed using as few components as possible, consistent with efficient operation, in order to obtain maximum reliability. The firing circuit makes use of only two active components, an avalanche transister and a small special quality thyratron. It will operate from a 'type 2' standard pulse or any similar negative-going edge and produces an output pulse having a positive-going amplitude of 500 to 600 V, with a rise time of 12 to 15 ns. The delay time, input to output, varied from 35 to 50 ns over the 15 firing circuits tested. The delay time due to the thyratron pulser itself is variable, depending as it does on such factors as heater and reservoir voltages, but the measurements made suggest the overall delay through the pulser should not total more than 80 ns. The rise time of the output pulse is dependent to a large extent on the load circuit.

As supplied to K12A, the firing circuit was arranged for use with a standard power unit in the 2000 series and is contructed as a plug-in module, mounted close to the thyratron. The thyratron anode circuit is housed separately. This permits greater flexibility of use since the circuit can be designed to suit operating voltage, size or type of spark chamber, pulse repetition rate and so on. Operational experience with the pulser is limited thus far to a few hundred hours use of the prototypes on routine chamber testing, however the results suggest a high degree of reliability.

Electroluminescent Lamps for Spark Chamber Fiducials and Data Board Displays

Development work on the use of electroluminescent materials for reference marker and data display applications has continued during the year and has been directed mainly towards finding a more reliable material and to minimising the cost of power supply requirements.

Several British manufacturers can now supply material in standard sheet sizes and using a front masking technique the pattern can be defined to the accuracy required. However, although this approach solves the problem of material supply conveniently, it makes the cost of the power supplies prohibitive due to the additional area to be excited. Attempts to define the pattern required, by employing masking techniques during the manufacturing process thus limiting the excited area to a minimum, have met with only limited success. In the case of the inorganic ceramic type materials, the high temperature firing process involved during manufacture produces distortions in the finished product. Although it is quite feasible to obtain high definition patterns using screen printing techniques in the manufacture of the plastic and glass organic type of materials, the initial development costs are high, and for small quantities the cost is excessive. At present a compromise procedure is in use where high definition patterns are required. The material, in the form of a sheet, has a gross pattern printed during manufacture and the final definition is obtained by a front mask, produced either by machining a metal panel or by photographic techniques.

Equipment of this type is now being produced for the ISR and K10S experiments, and results obtained on prototype units are most encouraging. It is hoped that further developments in this field will enable extremely sophisticated data displays to be incorporated in future experiments.

Gas Recirculating Rig for use with Spark Chambers

Development work on gas recirculating systems has continued during the year and a modified version of the prototype unit reported previously has now been produced. This Mk II unit has been designed as a standard rack-mounted equipment which can be incorporated easily into the normal control room arrangements. The unit is self-contained, requiring only a mains electrical supply and a source of liquid nitrogen to replenish the purifier vacuum flasks. Special attention has been given in this design to providing a high level of protection both in respect of interlock circuits to ensure correct operating sequences being carried out and in the fault alarm circuits to allow continuous operation with minimal supervision.

The performance of this equipment has been most encouraging and at present two units are being used by experimental teams. The results obtained from this operational experience will be incorporated in the second stage of manufacture and it is hoped to have a total of six units completed and in service by mid-1971.

A Light Pulser for testing Photomultipliers

In order to fulfil the requirement for a standard light pulse for testing the performance of photomultiplier tubes, work was initiated to produce a unit comprising an alpha particle source in contact with a disk of plastic scintillator. Monoenergetic alpha particles of kinetic energy 5·5 MeV from an isotope of Americium, Am^{241}, are totally absorbed in the scintillator, thereby producing light pulses of constant intensity. The whole assembly is sealed in epoxy resin to provide for safe handling. Initially a unit employing a source of 18 μ-curies on a 0·125 in thick scintillator disk was tested. This produced good pulses but radiation damage in the scintillator was such as to reduce the output by 50% within a 2 to 3 week period. Work is continuing and it is hoped to produce a light pulser with a useful life of about one year.

Solid State Light Emitting Diodes for testing Scintillation Counters

Work on evaluating the performance of solid state light-emitting diodes has been carried out to decide upon a suitable diode for on site testing of scintillation counter arrays. The performance of several types has been evaluated in terms of light output and its variation with temperature, pulse rise time, price and reliability. Comparisons were made by pulsing the diodes using a Hewlett Packard 215A pulse generator and measuring the light output by means of an RCA 8575 photomultiplier tube. A green light emitter would be most suited to the spectral response of the photomultiplier (peak response at 4,500 Å), but the two types of green emitter tested were not found suitable. The most practical device so far tested is the Monsanto MV1 which emits light in the amber region.

In application, a hole is drilled in a scintillator at an appropriate point and filled with optical grease. The diode is inserted into this hole and is secured in position with epoxy resin. In event of failure the diode can be broken away and replaced.

Housing for the RCA 8575 Photomultiplier

This device has been developed in collaboration with the experimental physics groups currently working on the K12A and π 10 experiments. The outer housing is made from mild steel tube. Each end is flanged, one flange carrying the light guide clamping ring and the other supporting the base assembly. (See figure 70).

A primary consideration in the mechanical design is to provide good accessibility to the electrical components. This has been achieved by making the photomultiplier together with its associated electronics removable as a complete assembly separate from the outer shell. Electrical connections are made through sockets on a common base plate. The dynode resistor chain was chosen specifically for the RCA 8575 phototube. This chain operating at a tube current of 300 μA will produce a constant 2V output at up to $3{\cdot}5 \times 10^5$ counts/second. A further derivating using ancillary HT can maintain output at 107 counts/second. Units to this design are now being manufactured commercially.

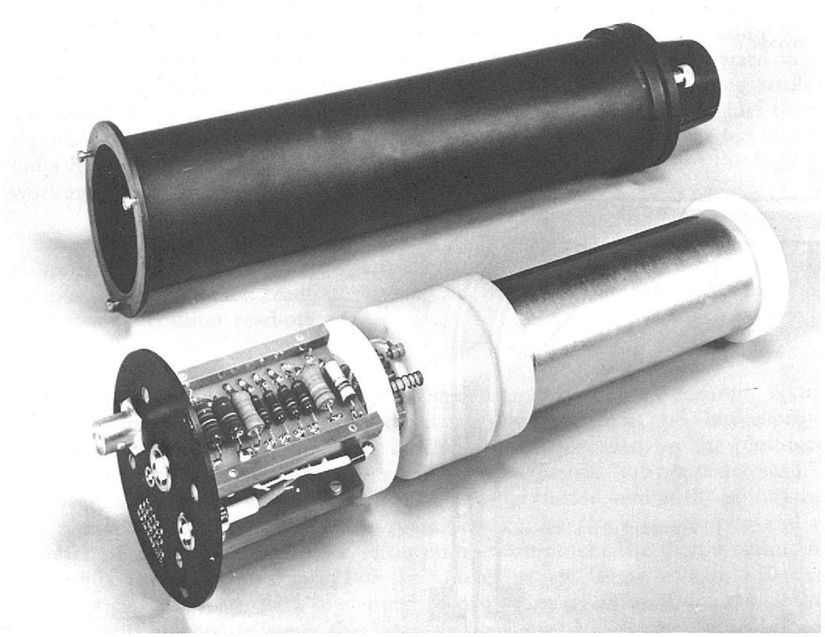

Figure 70. The RCA 8575 photomultiplier and housing.

A Mono-energetic Electron Source for testing Particle Detectors

Many of the tests and calibration measurements made on nuclear physics apparatus such as scintillation counters, spark chambers and proportional counters can best be carried out using energetic particles independent of an accelerator. An instrument has been developed to provide a convenient source of electrons in the form of a well defined beam having good energy resolution and a high count rate for use in such applications. The device is portable.

It has three main elements; a radio-active source of energetic electrons, an evacuated beam transport pipe and a double focussing spectrometer magnet. Electrons emitted by the source are collimated and transported through the magnet section in the evacuated beam pipe. In the spectrometer magnet section, electrons of the required energy are selected from the primary beam, by adjusting the field strength in the gap, and brought to a focus. (See figure 71).

In the unit constructed the radio-active source used is an isotope of Ruthenium, Ru^{106}. This decays with a relatively long half-life to an isotope of Rhodium, Rh^{106}, which subsequently decays rapidly, yielding electrons with a maximum energy of 3·5 MeV. The activity of the source is 0·8 milli-curies and this produces several hundred counts per second at electron energies near the peak of the spectrum. The spectrometer section is an electromagnet having a bending radius of 5 cm. For the high energy electrons this corresponds to a magnetic field requirement in the gap of 2·7 kG. The gap length is 15 mm and the field coil power required to produce this magnetic field is 5A at 10V which can be easily provided using a portable power unit. The magnet pole face is shaped to produce a double focussing effect on the beam and the image of a point source placed 10 cm from the entrance pole face is located 10 cm from the exit pole face. The beam transport pipe is a vacuum system with Melinex entrance and exit windows which can be evacuated and sealed thus maintaining the portable facility of the instrument.

Figure 71. Schematic diagram illustrating the use of the mono-energetic electron source for testing particle detectors.

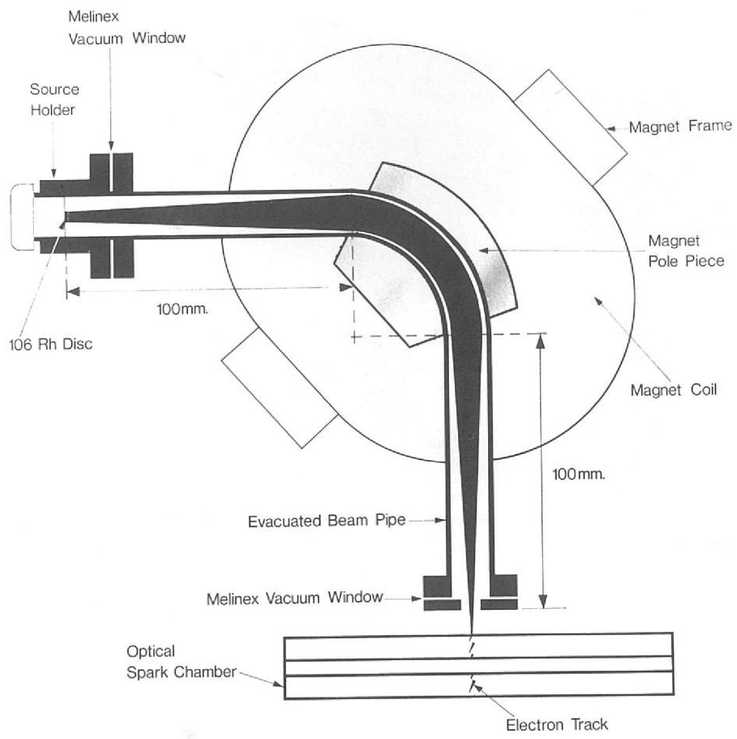

ELECTRONIC INSTRUMENTATION

The CAMAC System. (ref: 162)

During 1970 CAMAC has become firmly established as a world wide standard for modular electronics instrumentation associated with data acquisition. Much of this success is due to the thoroughness of the specifications issued by the ESONE working parties on which the HEP Electronics Group is represented. Specifications have been issued on the basic dataway (the crate) and on the branch highway (an assembly of up to 7 crates). Now consideration is being given to the possibility of standards at higher levels of CAMAC, the control of CAMAC systems and special purpose software.

More and more standard CAMAC,modules are becoming available on a commercial basis. However, it is evident that the 'data density' associated with high energy physics experiments is such that new modules still have to be designed for our applications. This is often done in collaboration with industrial firms, thus increasing their commercial potential. Though there is still work to be done at module level, it is at the higher level of system control where most effort is being expended.

Co-operation with CERN and Saclay has resulted in a common method of modular construction of controllers for CAMAC systems. It is expected that a controller containing a computer interface, an autonomous display and a link to the new terminal computer will become standard for most experimental teams at the Laboratory. It is proposed that the two Rutherford Laboratory collaborations at the Intersecting Storage Rings Project will link up with CERN equipment through such a system.

Counter Electronics

Development has been concentrated on a range of CAMAC modules for direct connection to counter hodoscopes and having direct output connection to the computer via the CAMAC highway. This marks a valuable step forward in the concentration of the various electronic operations – fast discriminating, strobing and coincidence logic, and the final gating of wanted events – into just two or three basic CAMAC units. By way of the CAMAC highway data can be fed into the units from the computer, to check that all parts of the system and the logic are working correctly.

Spark Chamber Read-out

Support has been given to several spark chamber groups in the construction of various spark chamber read-out systems including magnetostrictive, sonic and proportional counter read-out.

The Plumbicon System

A new effort which is being mounted is the construction of a TV scanning system, using plumbicon camera tubes, for the data taking system at the Omega project at CERN. In this system the images of sparks are recorded on the plumbicon photo-conductive surface, and are scanned out sequentially by a raster scan. At the beginning of each scan line a 90 mc/s clock is started, and at the point where the scanned electron beam hits a spark image, the clock is stopped and the number of counts is transferred to an on-line computer. The digital count then represents the spark position. For the Omega project there will be 110 spark chamber gaps to scan, with a scanned area of 3 m x 1·5 m. Two sets of three cameras will be used to cover this large area and give 17° stereo. Two additional cameras may be used in conjunction with a downstream chamber to improve momentum accuracy for high momentum particles. The principle of operation of the plumbicon system is shown in figure 72.

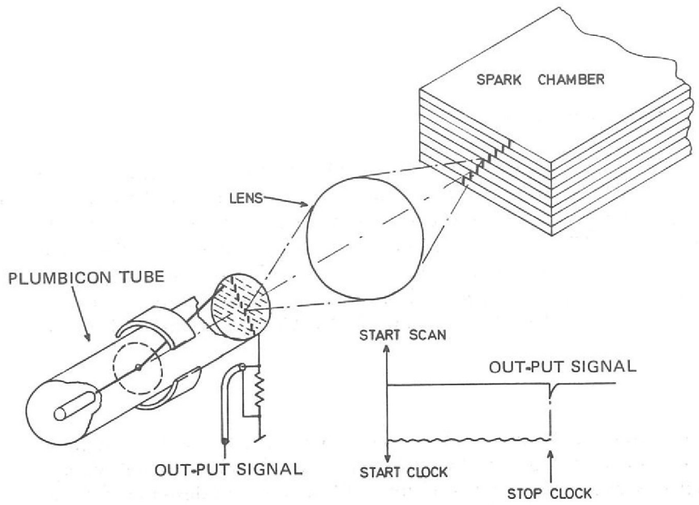

Figure 72. Principle of operation of the plumbicon system.

A careful study of the properties of plumbicon tubes has been completed and has shown that they should be very suitable for the proposed Omega scheme, having a fast recovery time and sufficiently good accuracy. A collaboration is being set up between HEP Electronics Group, Rutherford Laboratory Group A, Westfield College London, University of Birmingham, Ecole Polytechnique and CERN to build the fast data taking system for the Omega project.

Targets for High Energy Physics Experiments

POLARIZED PROTON TARGETS

A polarized proton target used on a π^+p scattering experiment (No. 4, see page 31) gave polarizations consistently greater than 65% in a Lanthanum Magnesium Nitrate crystal. The overall accuracy of the measurement was ±4% with a relative accuracy within ±1%. Very good agreement was obtained between polarization measurements made using nuclear scattering techniques and measurements made using a nuclear magnetic resonance spectrometer. An example is shown in figure 73 for a beam energy of 735 MeV, where a comparison is also made with results obtained by other workers. The experiment has been completed satisfactorily.

The New Polarizing Process. (ref: 50, 51, 63, 81, 93, 119, 128, 154, 156, 172, 174, 175)

Construction of a new type of polarized proton target for use in a charge exchange experiment $\pi^- + p \rightarrow n + 2\gamma$ is well advanced. The outstanding feature of this target is the large solid angle of free access to the target, exceeding 70% of the 4π steradian maximum. In this new system the hydrogen-rich target material is first polarized under optimum conditions for polarization at a temperature in the 0·8°K region and in a magnetic field of strength 50 kG. Under these conditions proton polarizations in excess of 60% have been achieved in organic target materials at the Rutherford Laboratory. The target is then cooled rapidly to about 0·3°K in order to reduce greatly the rate of depolarization from spin relaxation. In this frozen state the target is moved out of the uniform magnetic field used for establishing the polarization and into one of lower uniformity but providing the desired large angular access to the target.

To avoid excessive heating from eddy-currents during movement of the target from polarizing to holding positions the metal content of the cavity containing the target is made small. The resonant cavity, which contains the sample to be polarized is constructed from 12 micron thick foil supported by carbon fibre reinforced material. This construction has the added advantage of giving a target of low mean atomic number which is important in a charge exchange experiment.

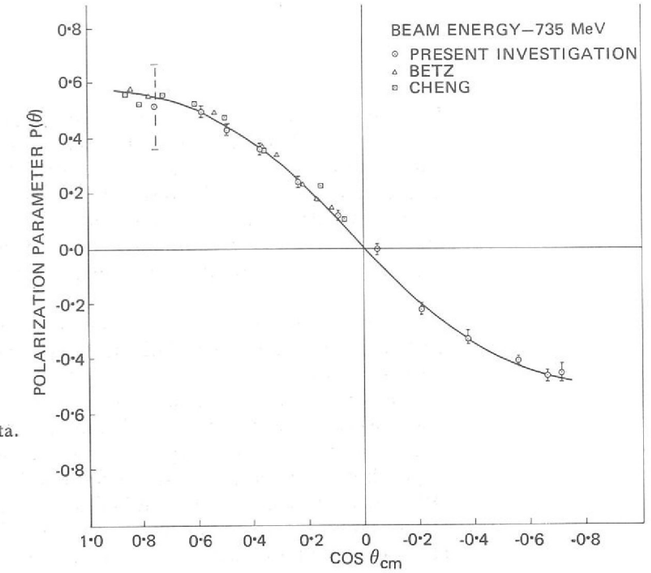

Figure 73. Comparison of polarization data.

The Refrigerator System

Experience gained in the use of a He^3 refrigerator operated during the last year in the temperature range of 0·9°K to 0·28°K has enabled simplification to be made in the design of the new frozen target. In particular, the target material now is to be cooled by direct contact with the He^3 refrigerant fluid. Using this refrigerator, extensive measurements of the main parameters of various possible target materials were carried out. These include polarization, proton relaxation rates, and polarization build-up times; the measurements were carried out over a range of temperatures and magnetic fields.

A continually operating absorption pump using activated charcoal is being developed for the frozen target. The principal advantage of such a pump is the extremely high pumping speed that can be achieved at low temperatures. In principal two absorption blocks, designed to have a rapid thermal repsonse time and small mass hold-up of the working fluid, are sequentially cycled thermally between about 4°K and a higher outgassing or release temperature. As one block is heated to release its gas content the other is absorbing gas at a low temperature. Figure 74 shows the frozen target being installed in the beam-line.

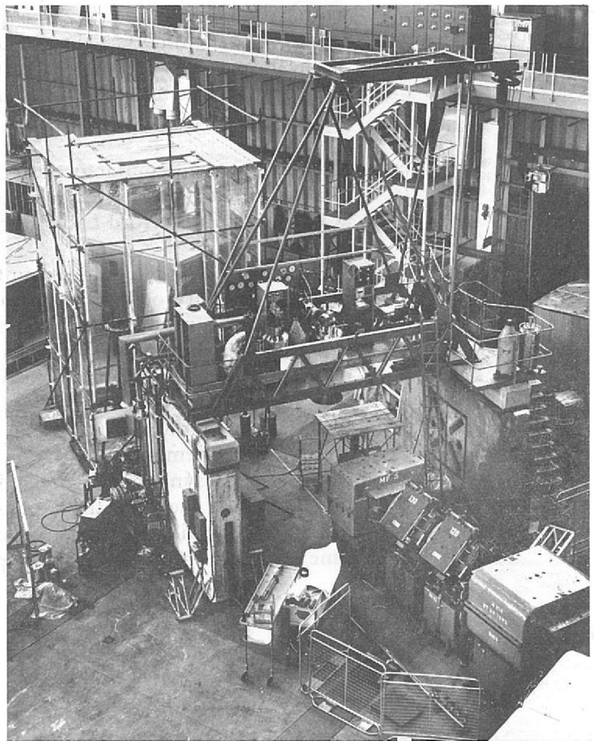

Figure 74. Installing the frozen polarized target in the π9 beam line.

For successful operation of the frozen target it is necessary for the target material to exhibit both high achievable polarization and low rate of depolarization. No known target material was satisfactory. Research was undertaken, therefore, to find a suitable material. Research was mainly carried out on porphyrexide dissolved in 95:5 butanol-water and in 50:50 glycerol-water. Particularly long relaxation times and good polarization were found in glycerol-water and in this material the values obtained are adequate for operation of the frozen target.

Extensive measurements were made down to 0·3°K and over the field range 20 to 50 kG. During the year polarization work was extended to 2 mm microwaves and 50 kG yielding polarization of $\sim$ 70% as against $\sim$ 40% with 4 mm microwaves. Preliminary work was carried out on other materials (at 25 kG and higher fields). These were solutions of Fremy's salt in glycerol-water and of Chromium-V ion in ammonia. One would expect these to be very good materials for polarized targets but so far the polarizations obtained have been less than with porphyrexide. Other materials have been studied at low magnetic fields (3 kG). High enhancements have been obtained in several alcohols containing Chromium-V ion complexes and further measurements have been made for pinacol, which looks promising for higher field work.

The electron relaxation mechanisms of the free radicals have been investigated by measurement of the relaxation time. Measurements at 1°K and 25 kG were started during the year, and concentration and temperature dependences gave evidence of relaxation through pairs and higher clusters.

LIQUID HYDROGEN TARGETS

Two further targets, using the Type II mechanically refrigerated condensing system, have been commissioned during 1970. The K15 target has a capacity of approximately one litre and has operated satisfactorily for 5,000 hours. The K12A target shown in figure 75 was installed and commissioned, using deuterium, during the December shut-down. This target has a capacity of 4 litres and a target mass of approximately 3 lb, the cool down and liquefaction time being 48 hours.

The beam entry end of the target flask incorporates a separate gas pocket within the liquid container. This pocket is connected to the liquid container at a point above the liquid level to ensure pressure equalisation. This allows the incoming beam particles to first encounter the liquid at a point well downstream of the metal support structure. The overall length of the flask is 70 cm and the liquid filled portion is 50 cm long.

The design and manufacture of the liquid hydrogen target components for the $\bar{p}$-p experiment was carried out during 1970. This experiment will be conducted at CERN by Rutherford Laboratory personnel.

One of the main problems encountered on the Type II system has been associated with the inability of the low power refrigerator to produce liquid at a reasonably high rate. This means that any excessive liquid evaporation taking place during an experimental data taking run involves the team in a period of lost time during which the evaporated liquid is recondensed to completely fill the flask.

Such an evaporation occurs when the target flask is emptied for protracted background measurement runs, and then refilled. The flask while in the empty conditions rises in temperature and therefore the refilling liquid has to remove the increased heat energy at the expense of some evaporative loss. Up to this time this restriction has dictated that the target empty runs are reduced to short periods of time such that the target flask temperature is not allowed to rise appreciably.

The Heat Pipe Device

For the K12A experiment, one of the requirements was that the flask should operate in the empty condition for many hours. For this requirement a 'heat pipe' was considered and a series of tests carried out using liquid nitrogen to investigate the possibility of using this device to provide an isothermal link between the refrigerator and target flask. The results of these tests showed the suitability of the heat pipe for this application.

Basically the device is a closed tube, lined with a wick material and containing a volatile fluid. Heat is removed from the external source by vaporisation of liquid within the tube of the evaporator end. This creates a slight pressure rise which assists the transport of vapour to the other end of the tube to which a refrigerated heat sink is attached. The heat sink removes heat which recondenses the vapour into the wick, the liquid being returned to the evaporator through the wick assisted by capillary action. The combination of vapour heat transfer and capillary action produce an extremely simple self-contained isothermal conduction device, having an effective thermal conductivity many hundreds of times greater than the best metallic conductors. The closed system was adapted to the K12A target (see figure 75). The condenser end of the pipe is opened into the heat exchanger vessel to allow the target liquid to soak the wick material as the target is emptied.

A test carried out during the K12A commissioning indicated a temperature rise of less than 2°K at the target flask over a 'target empty' period of 12 hours. The temperature increase took place during the first 10 minutes that the flask was empty and the flask temperature was completely stable for the remaining period. The satisfactory operation of this heat pipe has led to its inclusion in both the π8 and K15 target systems.

Figure 75. The K12A target system showing the target flask, heat pipe and liquid hydrogen reservoir.

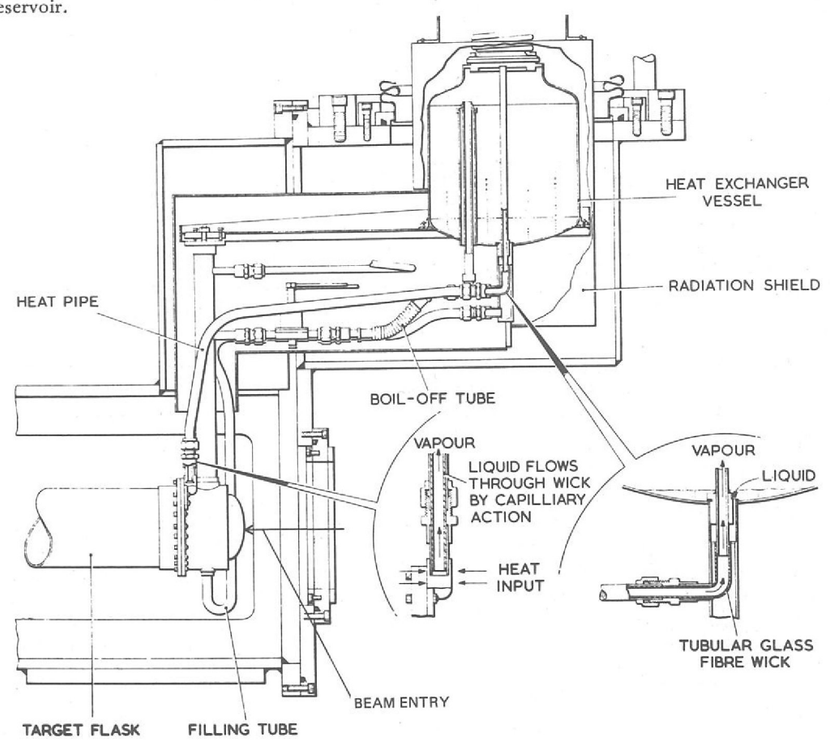

Vent System A vent system is provided to contain the large amount of gas which would be evolved from the escaping liquid hydrogen in the case of a burst target. The vacuum vessel in which the target is located is connected through a low pressure relief valve to an evacuated volume of sufficient capacity so that the maximum pressure reached in such a failure is less than one atmosphere absolute. Two simulated flask failures have been performed when the flask was mechanically punctured and the liquid hydrogen contents allowed to spill out into the vacuum vessel. Pressure transducers measuring the pressure rise at various points in the vent system indicated an acceptable pressure fluctuation, which at no position rose to greater than one atmosphere absolute. The results of these tests have proved the suitability and safety of this type of vent system.

Two new targets, for K13C and K16 experiments are being designed for operation with the Type II condensing system for installation on Nimrod in 1971. The proposed K13C target has a flask volume of 0·2 litres and the K16 target has a volume of 4 litres.

Cryogenic Valve A remotely operated valve for use with fluids in the temperature range 3°K to 500°K has been designed and is used on all current Type II Liquid Hydrogen Target systems. Made from stainless steel with a PTFE plug, it is actuated by helium gas at a low pressure acting on a sealed bellows assembly. The valve is very compact and can be operated in any orientation and may safely be used in a high vacuum or immersed in a cryogenic liquid. It has a fully open flow area of approximately 0·1 in^2 and functions as a combined stop and relief valve, (e.g. while positively closed against a pressure in one direction it will act as a relief valve in the opposite direction). Typically an operating helium gas pressure of 25 lb/in^2 absolute is used. At this pressure the leak rate across the seat is better than 5×10^{-2} lusecs at 15 lb/in^2 differential pressure. The standard valve has 0·375 in diameter ends and is suitable for 'in line' mounting. Alternatively it is possible to remove the actuator portion for use on any special body or manifold arrangement.

THE 1·5 METRE CRYOGENIC BUBBLE CHAMBER

Operations Summary During the year, 1·066 million pictures were taken in the 1·5 metre cryogenic Bubble Chamber. Of this total, 528 thousand pictures were obtained with a deuterium filling and for the remainder, the chamber was filled with liquid hydrogen. Four high energy physics experiments were completed.

Following the encouraging results obtained with the sensitive target technique during 1969, three months were devoted to work in this field. Unfortunately, no successful running was achieved and further development work is taking place to eliminate the problems that were encountered during the technical trials in collaboration with CERN.

Chamber Modifications Modifications to the chamber which are taking place over the winter shutdown are aimed at improving the pressures that could be obtained in the main insulating vacuum vessel. The existing chamber top plate and the lower portion of the expansion tubes and their heat exchanger loops are being replaced. The new top plate is of stainless steel and is welded directly to the new expansion tubes (see figure 76) which contain the inner heat exchangers and the lower cooling loop and blocks. The existing assembly will have the tubes cut through just below the upper cooling loop, these stubs being then entered into the new expansion tube assembly and welded. The seal between the top plate and the chamber body will be provided by an inflatable gasket pressurising indium seals.

Research and Development Two main areas of development have occupied this section during the year. The PDP8-I computer system has been brought into operation, logging data from the 1·5 metre chamber. Further developments are in hand which will be aimed at improving the usefulness of the system by implementing a more sophisticated OPERATOR/COMPUTER interface. The other main area of activity has been the new liquid phase expansion system. Most components are now delivered and the prototype assembly is being built up to allow proving trials to commence in early 1971.

Track Sensitive Bubble Chamber Target Research is continuing in the design of a flexible walled track sensitive target. Investigation of possible materials and model testing is in progress. The system will have sufficient flexibility to withstand malfunctions of operation which would normally burst the present type of perspex target. The aim of the design is such that it will be suitable for a variation of shapes and mounting dispositions, with the object of providing a basis for future targets.

Neon-Hydrogen Filling Technique Use of the sensitive target for particle physics research will require an homogeneous mixture of neon and hydrogen in known proportions in the chamber region surrounding the target. This condition has been checked experimentally by stopping protons in the chamber filled with various neon-hydrogen mixtures. See Experiment 31, page 67.

Figure 76. The new expansion tubes and stainless steel top plate for the 1·5 m Cryogenic Bubble Chamber.

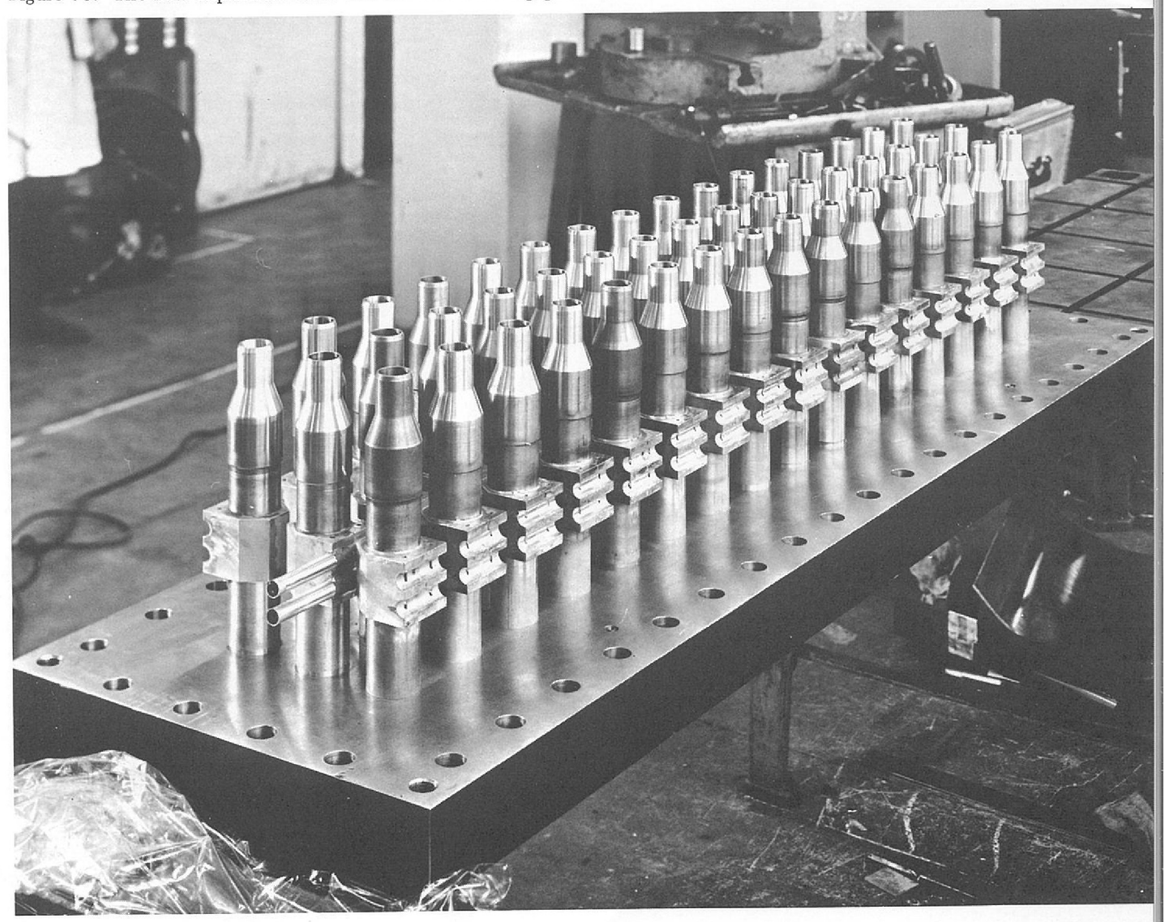

View of Nimrod Magnet Hall
showing the Inflector System used
to guide the protons from the
Linear Accelerator into the Synchrotron
Magnet Ring at the end of Octant 8.

Nimrod

OPERATION OF NIMROD 1970

During the period under review the beam intensity has been considerably increased, reaching a maximum of $3{\cdot}13 \times 10^{12}$ protons per pulse (average of 10 pulses), with an average beam intensity over the year of $2{\cdot}13 \times 10^{12}$ protons per pulse. This compares with an average beam intensity of $1{\cdot}66 \times 10^{12}$ protons per pulse in 1969. The total number of pulses with beam exceeded 6×10^{6}. Protons accelerated were $12{\cdot}88 \times 10^{18}$. This is another record and compares with $10{\cdot}45 \times 10^{18}$, in 1969.

Operation has continued in a three-week cycle, nominally 404 hours High Energy Physics research and 100 hours accelerator development and maintenance. The operating record is as follows:

Summary of Nimrod Operations for 1970 (Ref: 146, 147, 148, 149, 150)

HEP Research. Scheduled operating time 5297·64 hours. Good beam time 4708·01 hours. i.e. Beam on for 88·9% of HEP scheduled operating time. On the average there has been 4·4 experiments taking beam simultaneously during the year.

Accelerator Development. Scheduled operating time 1477·82 hours. Realised beam time 649·96 hours. Machine available time 996·59 hours. i.e. Machine availability 67·44% of scheduled operating time.

Nimrod is normally started up in the accelerator development period. This fact, together with the policy of switching repairs which can be postponed out of High Energy Physics research periods, is reflected in the somewhat lower availability of machine time in the scheduled accelerator development time compared with the High Energy Physics research figures. The operations record is detailed in the following table:

Table 14

Nimrod Operations January to December 1970.

Date From / Hours To		Clock Time	Shut-down	Shed. Maint.	High Energy Physics Research							Machine Physics and Development				
					Shed. Beam Time	Beam On Total	Beam On EPB	Set-Up	*Exp. Off	Nimrod Off	Nimrod Avail.	Shed. Beam Time	Beam On	*Exp. Off	Nimrod Off	Nimrod Avail.
Jan 1	Mar 31	2160·00	600·00	132·73	1013·37	847·67	847·67	20·08	0·40	145·22	848·07	413·90	188·79	73·63	151·48	262·42
Apr 1	Jun 30	2184·00	89·85	141·95	1342·42	1195·50	1195·50	2·68	1·00	143·24	1196·50	609·78	238·53	220·31	150·94	458·84
Jul 1	Sep 30	2208·00	108·00	79·63	1718·40	1536·32	1529·80	7·28	2·10	172·75	1538·42	301·97	117·28	28·25	156·44	145·53
Oct 1	Dec 31	2208·00	783·50	48·88	1223·45	1128·52	1128·02		2·40	92·53	1130·92	152·17	105·36	24·44	22·37	129·80
Totals		8760·00	1581·35	403·19	5297·64	4708·01	4700·99	29·99	5·90	553·74	4713·91	1477·82	649·96	346·63	481·23	996·59
Percent Clock Time		100·00	18·05	4·60	60·48	53·74						16·87				
Percent HEP Scheduled Time					100·00	88·87		0·57	0·11	10·45	88·98					
Percent MP Scheduled Time												100·00				67·44

*Beam off at Experimenter's request.

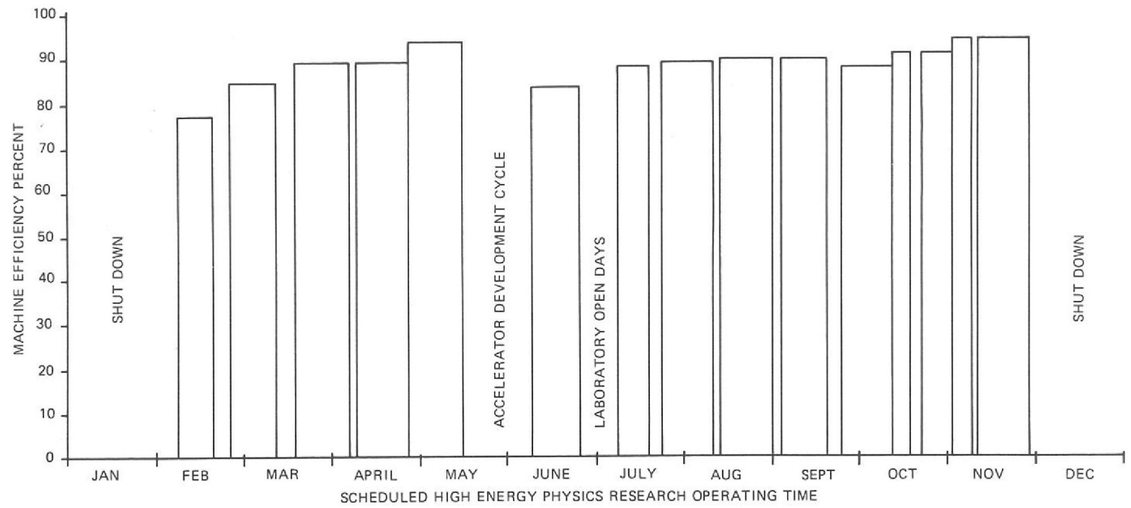

Figure 77. Nimrod operating efficiency during scheduled High Energy Physics research time. January to December 1970.

Out of a total scheduled beam time of 6,775 hours for Machine Physics plus HEP Research, beam was not available for 1,035 hours. The faults causing this loss have been categorised in Table 15. The machine efficiency during scheduled HEP research time has continued at a high level. This is summarised in figure 77.

Extracted proton beams were run throughout the year. Beam intensities measured at external targets have been a record with 10^{12} protons per pulse being measured in X2, which services secondary beams in Hall 1, and $1{\cdot}18 \times 10^{12}$ protons per pulse in X3 servicing secondary beams in Hall 3.

The general pattern of utilization is:–

1. X1/K9, the fast spill bubble chamber beam in Hall 1, has a share of every pulse.
2. Because X2 and X3 are mutually exclusive, one, (usually data-taking), has beam for four pulses out of five, with the other, (usually setting up), taking the remaining fifth pulse. In the main, this pattern is reversed on alternate cycles.
3. Scattered-out beams normally take beam every pulse, sharing being varied by the adjustment of target radii.

A new extraction system using a thin-septum magnet has been successfully tested for the X3 beam. This system gives an improved extraction efficiency of about 38% compared to 30% for the previous arrangement. Since early in June, the X3 beam has been extracted by this thin-septum energy-loss system during scheduled High Energy Physics research time, on a routine basis. It is planned to install a thin-septum magnet in the X1/X2 channel.

During the period January to August the pulse repetition rate was about 20 ppm. After the failure of No. 2 motor-alternator set of the Nimrod Magnet Power Plant in September, repetition rates varied between 9·6 ppm at 7 GeV to 22 ppm at 5 GeV using one half of the Nimrod Magnet Power Plant.

Table 15

The faults causing loss of beam time.

Fault Area	Lost Beam Time (hours)	% of Scheduled Op. Time	% of Nimrod Off Time
*Extraction Systems, Rotary Power Supplies	(88·48)	(1·31)	(8·55)
*Extraction Systems, excluding Rotary Power Supplies	(172·13)	(2·54)	(16·63)
*Extraction Systems, total	260·61	3·85	25·18
Nimrod Magnet Power Plant	166·30	2·45	16·07
*Vacuum Systems	91·89	1·36	8·88
Injector	90·86	1·34	8·78
Pole Face Winding Systems	63·47	0·94	6·13
Synchrotron r.f.	56·36	0·83	5·45
Coolant Systems	52·33	0·77	5·06
Targets and Target Mechanisms	39·43	0·58	3·81
Nimrod Magnet	8·19	0·12	0·79
Beam Control/Beam Spill Systems	5·51	0·08	0·53
Diagnostics	2·82	0·04	0·27
†Miscellaneous	46·41	0·69	4·48
Other Reasons			
Public Electricity Supply Mains Dips	22·65	0·33	2·19
Start-up	128·14	1·89	12·38
Totals	1034·97	15·27	100·00

* Includes routine inspection time.

† Miscellaneous includes such items as beam line elements, collimators and beam cut-offs inside the synchrotron hall, beam interlocks, wind and weather etc.

Shut-down December 1970-January 1971

A number of developments and installations are being undertaken in the scheduled annual shut-down, notably:

1. Replacement of the Mk 1 plunging mechanism with a Mk 2 system in Straight Section 2. This is associated with the X1/X2 extraction system.
2. Installation of a new shim magnet XHQ2/2 in the header vessel of Octant 3. This is in preparation for the change to a thin-septum energy-loss extraction system in the X1 beam line later in 1971. (Note that a corresponding magnet, XHQ2/3, is being manufactured for use with the X2 beam line).
3. Installation of a spare drive motor on the No. 1 motor-alternator set of the Nimrod Magnet Power Plant.
4. The re-installation of the repaired drive motor on the No. 2 motor-alternator set of the Nimrod Magnet Power Plant. (This motor failed on 1 September 1970).
5. Installation of a new solid pole motor and a new stator on the No. 2 motor-alternator set of the Nimrod Magnet Power Plant.

6. Installation of a spare Haefely EHT power supply for the pre-injector system. All components in the system with the exception of the rectifier stack will then be duplicated.
7. Commissioning of the No. 2 (stand-by) alternator system associated with the injector EHT platform.
8. Installation of a new debuncher ramper system.
9. The 250kW generator in the Magnet Hall has been re-positioned in order to allow installation of the new homopolar machine later in 1971.
10. A new target mechanism type 1c for the X1/X2 thin-septum extraction system has been installed in Octant 1.
11. Target mechanisms 5/14 and 4/21 have been removed.
12. The Mk 3 target mechanism in Octant 6, used for the $\pi 10$ beam, is being re-positioned.
13. Target mechanism 3/21 in Octant 3 has been re-positioned slightly.
14. The water cooled cables associated with the 300kW rotary power supply in the chalk pits are being extended so that this power supply may be used to power other thin-septum magnets. At present it only supplies RX3, a magnet associated with the experimental X3 resonant extraction system.
15. The power supply which feeds XHQ2/1 has been removed from Catacomb 6 and re-installed in the chalk pits.
16. Installation of new undercarriage rails in Straight Sections 4 and 7.
17. Installation of a stiffened support structure on XHQ2/1.

NIMROD MACHINE SYSTEM

Plunging Mechanism Improvements (Ref: 117)

The Mk II electronic control system was added to the existing Mk I plunging mechanism in December 1969. This has produced smoother control resulting in reduced stress on the mechanical parts. Since this time, swash pump failures have been greatly reduced and control faults virtually eliminated and the operational life has been increased from one to approximately five months i.e. from 1×10^6 to 3×10^6 cycles. The increased reliability has allowed a reduction in the frequency of inspection and hence improved the scheduled beam-time efficiency.

External Target Mechanisms

Modifications have been carried out on external target mechanisms resulting in a more reliable unit. The target arms of internal target mechanisms, which are subject to bearing failure, are now changed after 2×10^6 flips, or after receiving 10^{18} protons, whichever occurs first.

Magnet Pole-piece Bolt Failure

In February 1970 a Nimrod main magnet pole piece bolt failure, diagnosed as fatigue failure, caused concern. A special strain measuring device was developed by the workshop and a programme of measuring strain on the 1344 pole piece bolts was implemented. This bulk of this programme was completed by the end of the year. Some bolts have been removed and inspected, but to date no further evidence of fatigue has been found. Some 200 bolts are not readily accessible for measurement. It is intended to devise means to complete the measurements during 1971, without resorting to the dismantling of major components of the synchrotron.

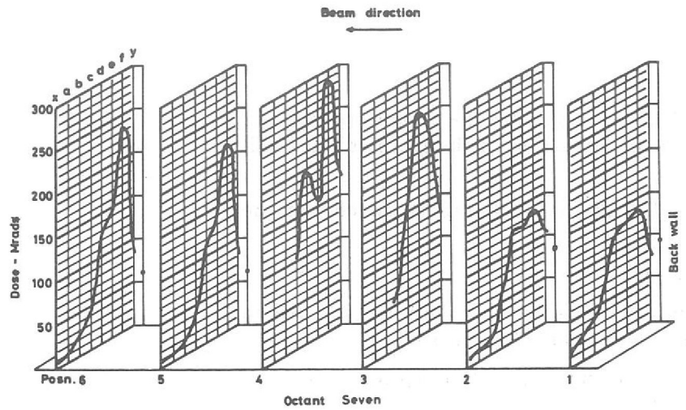

Figure 78. Radiation dose measurements for the inner vacuum vessel at Octant 7, A peak dosage of 290 Mrad was recorded.

Radiation Dosimetry Radiation Dosimetry of the Nimrod vacuum vessels, beam lines and pressure bags has continued throughout the year.

The dose distribution does not appear to have changed significantly during this period and the regions of highest accumulated dose continue to be in Octants 1, 7 and 8. Figure 78 shows the dose distribution pattern for the inner vacuum vessel at Octant 7, where the peak dosage of 290 Mrad was recorded.

Resonant Extraction Tests Resonant extraction tests, involving as they do much higher currents in the pole face windings, have highlighted radiation damage to the nylon tubes on pole face winding cooling pipes. Repair of these pipes was carried out at Straight Section 7 after modifications to the Straight Box support structure in order to allow access.

Nimrod Vacuum System During the annual maintenance period this year, the injector vacuum system has been singled out for attention and, in particular, the liquid air system which supplies the diffusion pump traps. The liquid air system has been in continuous operation since 1964 since when it has produced over half a million litres of liquid air.

An investigation has been carried out with a view to increasing the reliability of the Nimrod synchrotron vacuum system. This has resulted in the development of a novel, all-metal, vacuum seal for the booster pumps to work at a temperature of 200°C. Although some improvement has resulted from changing the booster pump fluid from Arachlor to Apiezon G, further tests showed that an improved performance would result from a change to Apiezon 201, a recently developed fluid, and this has been done. Tests have shown that it is possible to run the Roots roughing pumps without refrigerated traps thus removing a particularly troublesome component.

NIMROD MAIN RING MAGNET POWER SUPPLIES AND ANCILLARY PLANT

The magnet has been pulsed for the greater part of the year using both motor-alternator flywheel sets and the complete convertor plant. However, at the beginning of September a failure occurred on No. 2 Drive Motor rotor and from then until the planned shutdown at the end of November the magnet was pulsed using half the power supply plant. The mercury-arc convertor plant has continued to operate reliably, the arc-back rate remaining very low at about one in every 435 hours of operation. Further progress has been made in the change over to the re-designed grid control gear and the static ripple filter has achieved an acceptable standard of reliability although further work remains to be done. The operational statistics for the year are as follows:—

Machine running time	$6{\cdot}4 \times 10^3$	hours
Machine pulsing time	$6{\cdot}1 \times 10^3$	hours
Total number of pulses	$6{\cdot}8 \times 10^6$	

No. 2 Drive Motor Failure. The rotor of No. 2 Drive Motor failed at the beginning of September when an earth fault occurred immediately upon closing the stator circuit-breaker. Upon dismantling the machine it appeared that the origin of the fault was a breakdown of the insulation of a rotor bar in the region where the bar emerges from the core. This initial fault then seems to have involved a second rotor bar in a similar manner. A visual examination of the rotor showed a considerable amount of red dust, typical of the occurrence of fretting, in the region of one of the two composite keys which transmit the drive from the core to the shaft hub. That portion of the keyway which lies in the core laminations has been broached out to improve the profile and new oversize keys have been made. The rotor is being completely rewound and will also be fitted with the new design of slip-ring and brush gear assembly produced for the new drive motor. Delivery is expected by the end of 1970. The stator suffered limited superficial damage and this has been repaired. Subsequently a whole series of tests, including loss angle and dielectric loss analysis, was carried out by the manufacturer in order to predict the life expectancy of the stator winding. The final report has not been received but degradation has occurred to a significant extent and consideration is at present being given to the interchange of the line and star point connections on the stator. This will reduce the stress levels on the most affected parts of the windings.

Operational Experience with the First Solid Pole Rotor A solid pole rotor, acquired in 1969, is installed in No. 1 Alternator. During the 1969/70 shutdown, when the rotor was still within its guarantee period, a shorted turn was found to exist on No. 6 pole. The complete winding on this pole was removed and replaced by a spare, the faulty winding being repaired subsequently. During the dismantling of the bolted-on pole shoe assembly necessitated by this fault, it was found that virtually no slackening of the pole shoe retaining bolts had taken place and that the condition of the undersides of the pole caps and of the mating surface of the pole body was excellent. At this time the rotor had already performed about $4{\cdot}9 \times 10^6$ pulses. It has performed satisfactorily throughout the operational period this year.

Figure 79. The two Motor Alternator sets which provide power for the Nimrod Magnet.

Spares for Magnet Power Supplies Rotating Plant

The new alternator stator, solid pole rotor and drive motor mentioned in the report for 1969 have been received. The two new flywheel assemblies are expected early in 1971. The new stator and rotor are being installed on No. 2 set and the new drive motor is to be fitted on No. 1 set. Tests will then be conducted to investigate the load sharing between the two alternators, each now with a solid pole rotor, when operating electrically paralleled but mechanically separate.

Electronic Analogue Wattmeters

Electronic Analogue Wattmeters will play an essential part in the tests referred to above. The wattmeter specification is now fully patented in the United Kingdom and provisionally so in the USA. The equipment was demonstrated at the 1970 Physics Exhibition, and several other organisations have also shown great interest.

Alternator Rotor Vee Coil Support Bolt Design

Fretting was found to exist between the bolt shank and its fibre-glass insulating sleeve as mentioned in the Report for 1969. It has now been confirmed by a series of investigations in a special test rig that the coating of the bolt shank with a 0·010 in layer of adiprene prior to the application of the fibre-glass appears to prevent damage from this cause. During early 1971 the opportunity will be taken to examine a limited number of Vee coil support bolts treated with adiprene which have seen one year's service in a rotor.

Drive Motor Rotor Resistors

A flashover occurred early in February on one phase of No. 1 Drive Motor fixed rotor resistor. This is believed to have been caused by contamination by airborn debris drawn in by the cooling fans. A spare unit for this phase was installed. The remaining units were cleaned, but only to a very limited extent owing to the very poor accessibility. It was decided that a complete new assembly of six units should be ordered and these are being installed during the 1970-71 shutdown. The units removed from service will be overhauled and kept as spares.

Mercury-Arc Rectifier Control System

Fifteen out of the sixteen operational grid control systems have been modified to permit access when the convertor plant is working.

Static Ripple Filter

A compressed air operated contactor has been developed and installed to replace the vacuum contactors which could not be made to operate consistently or reliably. Together with modifications to the protection circuitry, this has resulted in regular operation of the filter under normal pulsing conditions. Further development is proposed to improve the overall ripple reduction factor and the reliability of the installation.

Primary Ripple Filter

A prototype pre-amplifier of a new design has been operational on the A2 amplifier during the year and has been found to be much more trouble-free and consistent in performance than the originals. Two new pre-amplifiers have been constructed to this new design and are at present being installed.

Ancillary Plant

De-mineralised/Raw Water Heat Exchangers. The four heat exchangers for the No. 2 Magnet Circuit and the Experimental Area have been dismantled for examination and overhaul. The shells have been grit blasted to remove the old neoprene coating and then treated with epoxy resin paint. The tubes were in a generally satisfactory condition and after re-assembly and pressure testing the units were returned to service. A similar programme is to be carried out on the two Bubble Chamber heat exchangers during the 1970/71 shutdown.

Hall 3 Cooling Water System. The installation has been taken over from the contractors and is now in service. The loading so far has not been sufficient to test heat dissipating capabilities of the whole system and a load test, carried out under adverse ambient conditions, proved inconclusive. It is proposed that a further load test be carried out before the expiry of the guarantee period in June 1971 although the performance to date gives no cause for concern.

Instrumentation. A multi-channel alarm and annunciation system has been installed on the R4/R10 ancillary plant and it is planned to include the Hall 3 system at a later date. Indication is given in the alternator control room. A considerable amount of existing instrumentation has been overhauled and repaired.

ACCELERATOR DEVELOPMENT

Proposal for a 2nd Harmonic R.F. Accelerating System

The present maximum working beam intensity in Nimrod is about 3×10^{12} protons per machine pulse. It has been confirmed that the limitation at this intensity is due to the space charge forces on the particles at the outside of the beam bunches. These forces are defocussing forces which counteract the focussing forces due to the magnet field gradient and, in the limit, lead to beam loss through radial and vertical betatron resonances. If the bunches could be lengthened and their maximum height reduced, more particles could be accommodated in them for the same space charge limit.

To examine this possibility, a design study was carried out assessing and costing the feasibility of installing an additional accelerating stage in Nimrod. Its function would be the addition of a 2nd harmonic r.f. field at eight times the orbital frequency. With such a field in the correct phase and amplitude the acceleration field is modified from its normal sinusoidal form to that shown in figure 80. The accelerated particles receive the same synchronous energy gain per turn but there are now two stable phase angles ϕ_A and ϕ_B and two unstable phase angles, ϕ'_C and ϕ_S, compared with the normal case where the synchronous energy gain occurs at ϕ_S (stable) and ϕ_C (unstable). The effect is to lengthen the phase stable area, and reduce its maximum height in the desired manner. An increase of 40% in beam intensity is possible.

Figure 80. Effect of 2nd harmonic r.f. accelerating field on beam bunches.

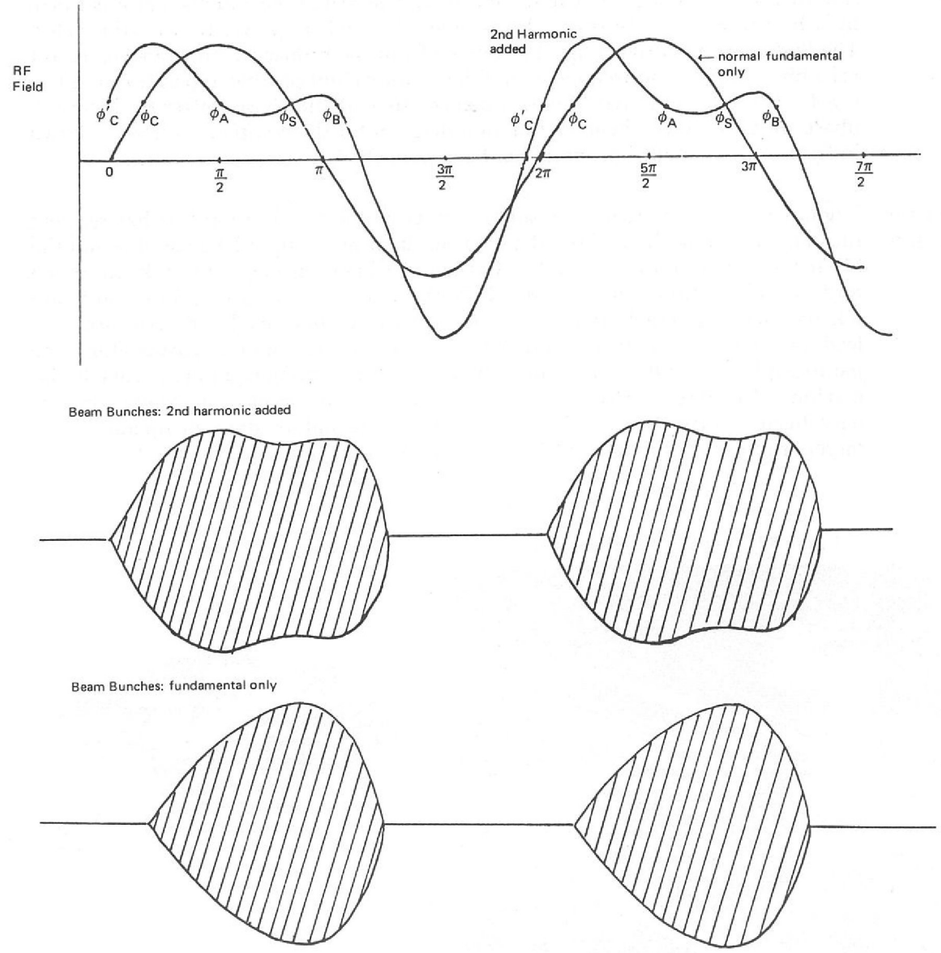

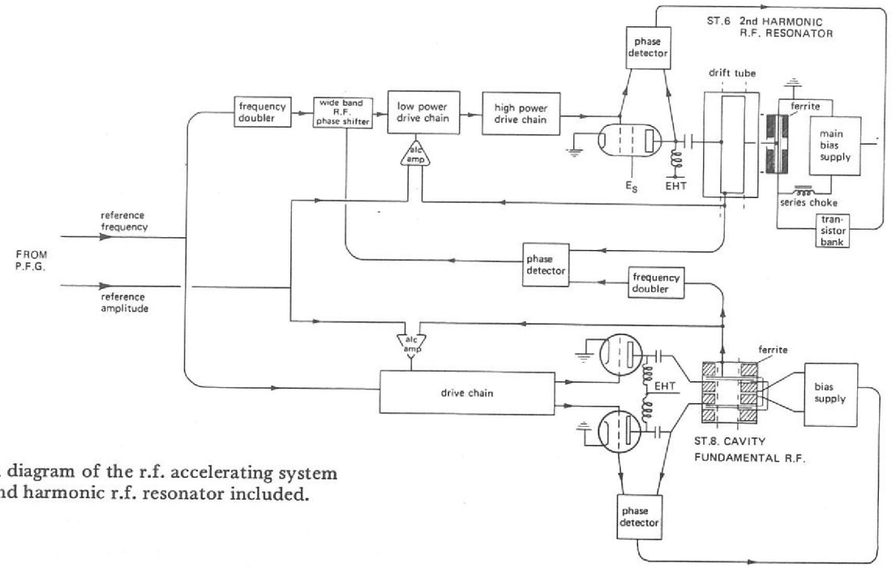

Figure 81. Function diagram of the r.f. accelerating system with the proposed 2nd harmonic r.f. resonator included.

Of the possibilities examined the most promising comprises a drift tube installed in Straight Section 6 tuned by a pair of ferrite-loaded resonators mounted on each side of the containing straight section box. The drift tube and resonator is tuned by a bias field in the ferrite and driven at r.f. by a high power transmitting valve. The 2nd harmonic driving signal is derived from the Primary Frequency Generator via a phase shifter and frequency doubler, a wide band phase comparator monitoring the drift tube and cavity fields and correcting via the phase shifter for incorrect phase shifts between them. A function diagram for the complete system is shown in figure 81. A detailed proposal has been published.

Target Mechanisms for Insulated Targets

Engineering development on insulating internal targets continues. It has reached the stage where both the Mk III target mechanism for the $\pi 10$ beam line and the Mk Ic target mechanism for the X1/X2 beam line has been adapted to take insulated targets. This is shown in figure 82. In both these cases the target, shown in figure 83, has been insulated from its supports with ceramic insulators. An electrical lead taken from the target through rotating sprung contacts passes along the pantograph arms and mechanism framework to measuring equipment outside the machine. This does not restrict the movement of the target. The sprung contacts have been incorporated to eliminate wire fatigue failure since in operation the target arm rotates through a 90° arc once every 3 seconds.

Figure 82. Insulated target mechanism.

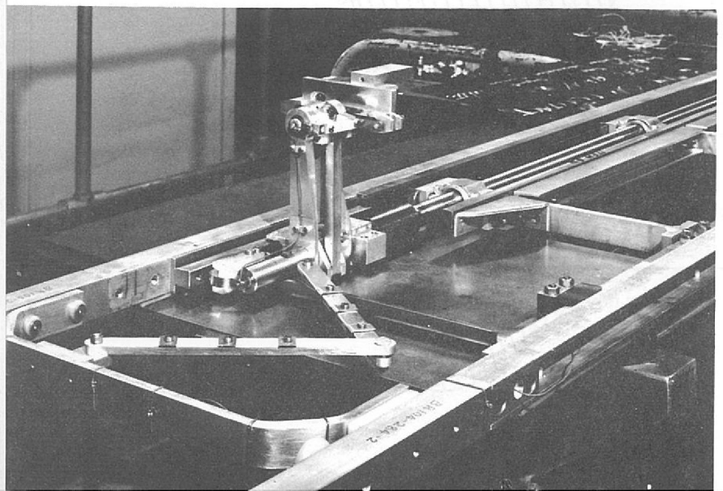

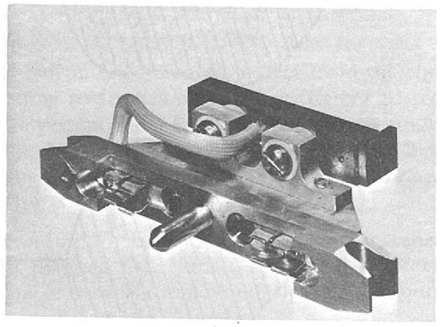

Figure 83. Insulated target

The circulating beam on hitting the insulated target induces a current which is measured and calibrated to indicate the proportion of proton beam taken by the target. The insulated target can also be used as a beam monitor. This design of insulated target with monitoring will be fitted to all internal target installations in Nimrod as time permits.

Time Structure Analyser of Synchrotron Beams

The measurement of time intervals in the sub-microsecond region is often necessary in nuclear physics experiments. In a typical measurement the first event detected triggers a time to amplitude converter, TAC, with a second event stopping the converter. The output of the converter, a pulse or d.c. level, proportional to the time interval measured is stored in a pulse height analyser.

This same technique is used in beam diagnostics when studying the time interval distribution or "structure" of a beam of particles. Beam intensity may be measured by means of counting secondary events, e.g. scintillations produced by secondary particles on a target monitor, with a TAC being used as above. This method is necessarily slow as after each measurement the TAC must be reset and the analogue placed in store before the next measurement can commence. Even in the fastest systems several microseconds may be lost between measurements.

This disadvantage is overcome in the instrument described below in which time measurement is a continuous process and the necessary time lapses for storage and resetting are catered for by employing a trio of binary counters, only one of which is in the read mode at any one instant. The arrangement is shown in figure 84. It is based on a three stage shift register or ring counter, ABC, and a 100 MHz oscillator. The pulses derived from the scintillation counter are fed to the clock line of the shift register, moving a previously loaded logic 1 from stage to stage as each pulse arrives. Each stage controls an AND gate steering the 100 MHz oscillator into one of the binary counters. When counter A is operating, counter C is being read and counter B is being reset. In this way no time is lost between pulses and all consecutive time intervals are measured and stored in the analyser. An integrating store is employed in the counter read-out circuits. Each binary number is then decoded and stored as a unit of charge in one of 256 capacitors. Each capacitor, termed a 'bin', stores the number of time intervals occurring within its range; each bin width is 10 nanoseconds.

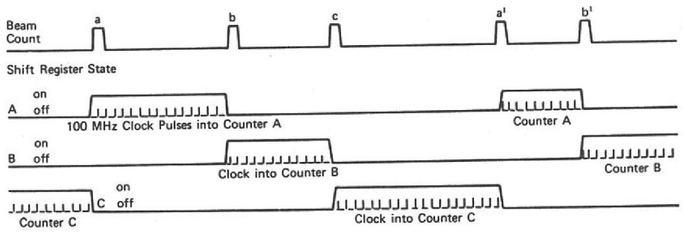

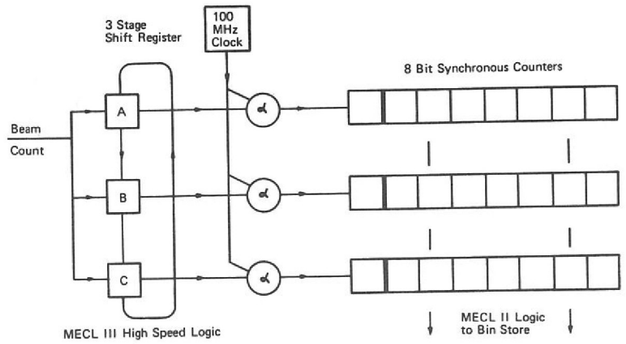

Figure 84. Fast digitizer for the time structure display.

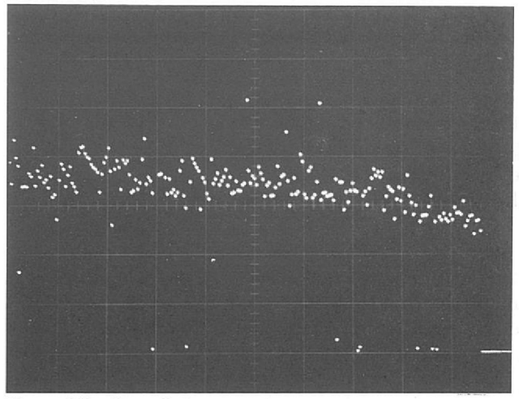

Figure 85. Use of the Time Structure Analyser Instrument showing beam structure minimised during ejection by detuning the accelerating cavities. Counting conditions: 44,000 Counts per burst length of 400 ms. Oscilloscope sweep rate 250 n sec/large division.

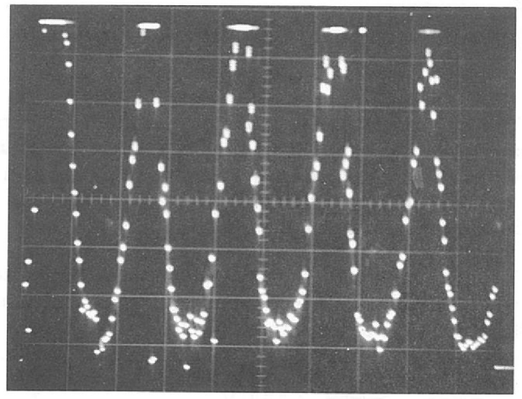

Figure 86. Beam structure during ejection with cavity detuning 'off'. Conditions otherwise as in figure 85 with same oscilloscope gain setting.

The full range of the instrument is thus 2·56 microseconds. A multiplex switch couples the complete bin store to a CRT for visual display. The complete instrument, apart from its power supplies, is housed in a single CAMAC crate. A prototype instrument has been built and is currently in use on the CERN PS, with a further model presently being constructed for use on Nimrod.

The instrument is capable of monitoring and displaying the high frequency components of beam structure encountered on the CERN PS and because of its capacity for acquiring and storing data can be used to observe pulse to pulse structure variations.

The analyser may be used when setting up the PS on slow-ejection. To keep beam structure to the minimum value it is necessary to detune the accelerating cavities, which, although not energized during ejection, can have a profound effect on the beam through resonating interaction. Figure 85 shows the display when beam "structure" has been minimised. This may be compared with figure 86, which clearly exhibits pronounced structure of about 2.5 MHz period, occurring with the r.f. accelerating cavities "detuning" off. The first 2.5 microseconds of the time interval spectrum is displayed.

EXTRACTION TECHNIQUES AT NIMROD

Extracted Proton Beams (Ref: 118)

Nimrod has three extracted proton beams (figure 87). Two of these (X1 and X2) derive from a single extractor magnet, whose current may be switched during flat-top to provide a fast spill for X1 and slow spill for X2. The third line (X3) serves the Experimental Hall 3 and is fed from a magnet which is situated 90° round the ring from X1.

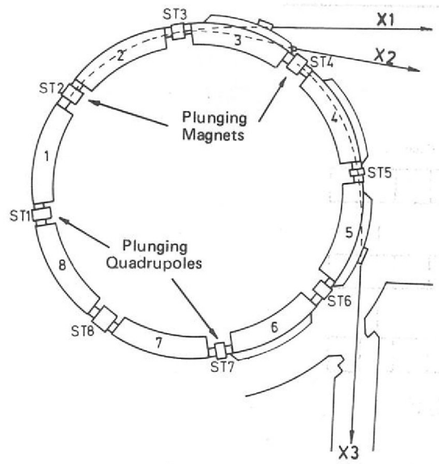

Figure 87. Extracted proton beams at Nimrod, X1, X2 and X3. The magnet octants are labelled 1 to 8, and straight sections ST1 to ST8. The proton beam is injected into the magnet ring at ST1.

Until June 1970 the achromatic energy-loss extraction method was used for both channels, the extraction efficiency being typically around 30%. Each channel required a plunging quadrupole in addition to its 6 cm septum extractor magnet. Since over 80% of the circulating beam is used for extraction purposes, plans were made to test two further methods of extraction with the aim of increasing this efficiency.

The first of these methods, called Thin-Septum Piccioni, was commissioned in January 1970 and has been in use with the X3 beamline since June 1970. The second, Resonant Extraction, has also been tested but further studies are required before it can become an operational system.

Thin-Septum Piccioni Extraction System

As its name implies, this method requires the use of a plunged extractor magnet having a thin-septum, which in practice is 11 mm thick (figure 88). The beam is steered on to a beryllium energy-loss target 1·85 cm in length, in which the most probable energy loss is 5·1 MeV. Because of the sudden change in closed orbit, most of the beam enters the extractor magnet just over one turn later and is deflected towards XHQ2, a pulsed half-quadrupole situated in Nimrod's fringe field (figure 89). In this quadrupole the large radial divergence introduced by the fringe field is partially overcome, after which the protons enter the first elements of the standard beamline. An important operational feature is that there is no need for a plunged quadrupole.

The thin-septum scheme was successfully commissioned in X3, using the computer control system introduced 6 months earlier. At this time, the extractor magnet, XM9, was in use, having a vertically laminated septum which behaved very well magnetically, but which, by virtue of its construction, was not sufficiently reliable for operational service. This was later replaced by a modified extraction magnet XM10.

From the outset it proved possible to accelerate normal beams with XHQ2 energised in a d.c. mode at the current required for 7 GeV. However, because the magnetic forces on XHQ2 caused it to move excessively each time Nimrod was pulsed, it was not possible to make full use of the range of adjustment provided, until additional strengthening was added to its support structure. The beam was viewed by means of scintillators placed upstream and downstream of XHQ2, enabling immediate diagnosis of beam misalignments as they arose.

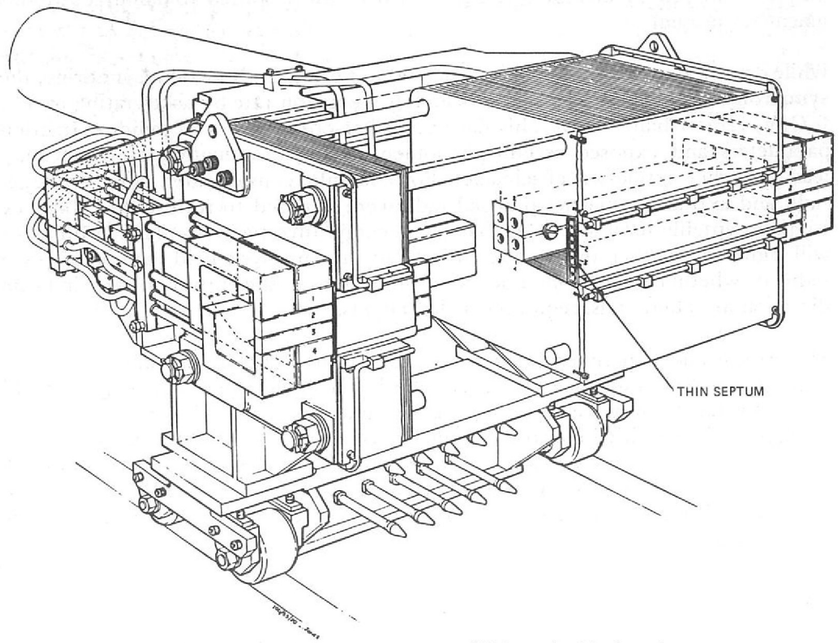

Figure 88. Thin-septum extractor magnet (XM type) with 4 stack septum.

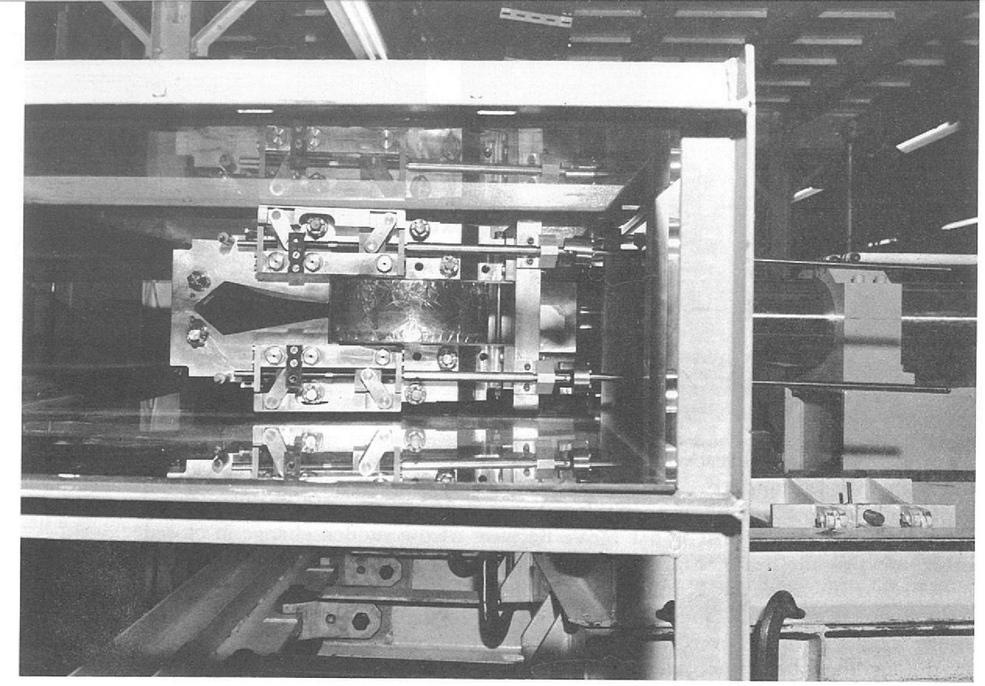

Figure 89. The half-quadrupole shim XHQ2. This is now installed in Octant 5 Header Tank as part of the thin-septum extraction system.

Extraction Efficiency of the Thin-Septum Energy-Loss System

After optimising the energy-loss target length, 10^{12} protons per pulse were extracted from Nimrod for the first time, representing an efficiency of about 45%. A foil exposed at the entrance to XHQ2 showed the beam to be of the expected shape and to contain 66% of the circulating beam. The transmission factor of the beamline, including XHQ2, was therefore 76%.

It is known that XHQ2 introduces a bend of $\sim$ 3 m-radians which another quadrupole, XHQ3, was to have counteracted in addition to providing further focusing. Since XHQ2 appeared to offer adequate focusing alone, a small bending magnet has been installed in the X3 beamline to deal with the excess bend at XHQ2, and to avoid the disruption of installing the extra quadrupole in the machine header vessel. More recent calculations show that an increase in efficiency of about 10% may be achieved by including XHQ3, but it is not proposed to manufacture this magnet at present.

While one alternator only has been available to power the Nimrod magnet ring, the synchrotron has been operated at near full repetition rate by accelerating to 5 or 6 GeV, rather than 7 GeV. This has entailed re-optimisation of major extraction parameters and exposed certain phenomena, a full examination of which may lead to higher extraction efficiencies. For example, considerably increased target radii and extraction magnet plunged radii were required to restore the efficiency to an acceptable level after the change in energy. Investigations planned for 1971 will indicate whether this is due entirely to the improved field regions at larger radii, or whether it is a consequence of alterations in the abrupt changes in beam direction at octant ends, requiring angled targets.

Resonant Extraction

Theoretical and experimental studies have shown that it is possible to use the radial $Q_r = 2/3$ resonance to extract the beam down the existing X1 and X3 lines: this has been made easier by the introduction of the thin-septum extractor magnet for the modified Piccioni scheme. A vertically plunged 2 kG magnet (RX3) is situated one octant upstream of XM10, having a septum which is 2·5 mm thick (figure 90). Once the resonance has been created those protons which pass across the RX3 septum are diverted into the mouth of XM10 and then ejected in the normal manner.

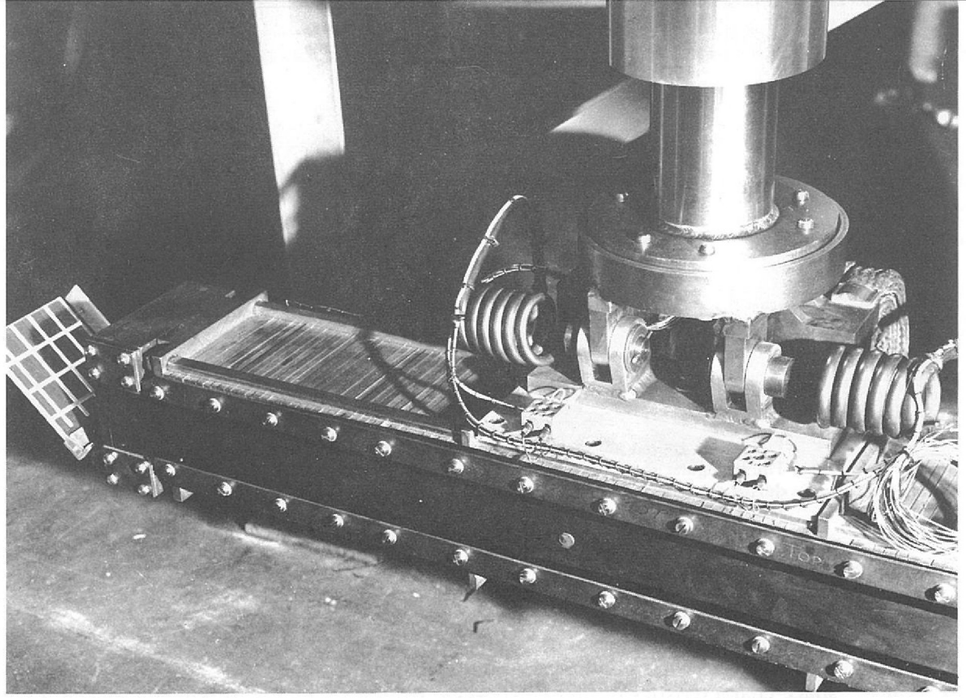

Figure 90. The vertically plunged kicker magnet, RX3, looking towards the face of the 2·5 mm septum. This magnet is used for resonant extraction. An adjustable scintillator can be seen on the left of the photograph.

The Nimrod pole-face windings are used to adjust the field gradient and to produce the necessary second harmonic sextupole component. Nimrod's field gradient across the aperture at 14 kG is shown in figure 91. On R_o the field index n is equal to 0·7, considerably higher than the resonant n-value, $n_{2/3} = 0{\cdot}647$. If the resonance were approached from the higher n-value the amplitude growth would become limited by a large octupole field component: for this reason n has to be moved to about 0·6 before extraction begins (see broken curve on figure 91). Approaching the resonance from this lower n-value, the protons see an average field gradient which gets closer to $n_{2/3}$. Their amplitude begins to grow, as shown on figure 92. The gradient is further depressed towards the outside radii using another pole-face winding, with the intention of providing a small net sextupole component: this allows the beam to be steered into the unstable region as one possible method of spill. The other principal method of spill envisaged is to hold the beam at a constant radius and to increase the n-value to $n_{2/3}$ in a controlled manner throughout the flat-top period.

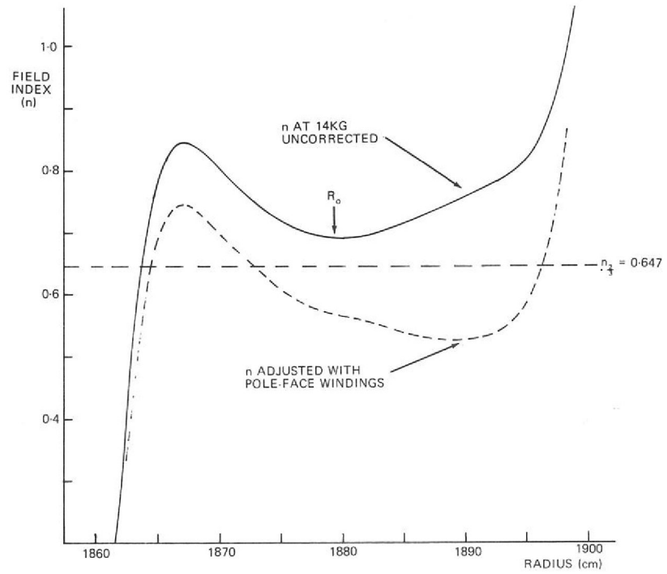

Figure 91. Nimrod magnet field gradient index, n, at 14 kG (corresponding to 7 GeV). n is defined by $\frac{dB}{B} = -n\frac{dR}{R}$ where B is the magnet field strength and R the radius.

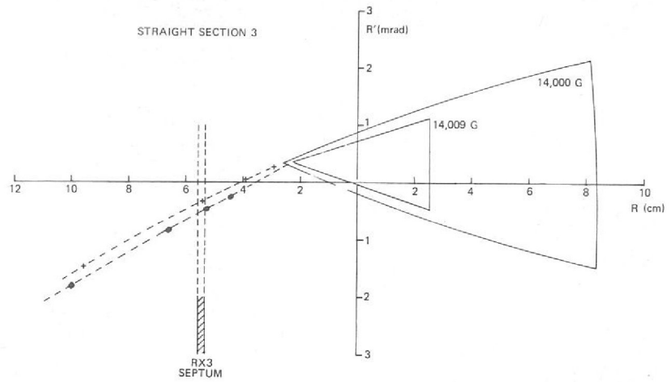

Figure 92. Radial phase diagram at Straight Section 3 during resonant extraction. The triangular shape indicates the stable particle region. This shrinks as indicated during extraction due to the small 'flat-top' magnetic field variation and particles are "peeled-off" from the periphery. Successive particle positions after every three orbits of the magnet ring are indicated.

The width of the circulating beam is between 12 cm and 15 cm, and because the good field region measures only 20 cm at most, there is little room for manoeuvre. Furthermore, protons cannot be allowed to penetrate too far into the first magnet (RX3) because the non-linear guide field at these small radii will distort the phase space characteristics during the passage from RX3 to XM10. For this reason RX3 is placed close to the inside edge of the beam; as a result the jump per three turns at the septum radius varies widely throughout the spill as the stable region shrinks in size (figure 92). A further disadvantage is that there is a large change in divergence of the emergent beam during the spill (figure 93).

The first trials of this scheme have been moderately encouraging. The method of spill was to hold the beam at constant radius and to increase n through $n_{2/3}$. The spill time was about 100 msec. As anticipated, it was difficult to steer the beam on to flat-top without premature loss, but between 50% and 60% of the circulating beam was transported to the external target, where the spot was of good quality and measured only a few mm in both dimensions. A foil which was irradiated at the entrance to XHQ2 registered 70%. At this stage commissioning studies were halted by failures of the pole-face windings, due to the unusually high currents demanded in them and to radiation damage which has occurred at their end connections. These mechanical faults will take some time to overcome. Moreover, compared with the thin-septum energy-loss scheme, resonant extraction requires an additional plunging mechanism, involves difficulties in beam sharing with internal targets, and has the known disadvantage of spill modulation due to field ripple. Further theoretical and experimental assessment is under way to determine the future course of the resonant extraction work: the current philosophy is that, unless the system can be shown to give about 80% efficiency, Nimrod will continue to operate with thin-septum energy-loss extraction.

Figure 93. Radial phase diagram at Straight Section 4 during resonant extraction. (See figure 92).

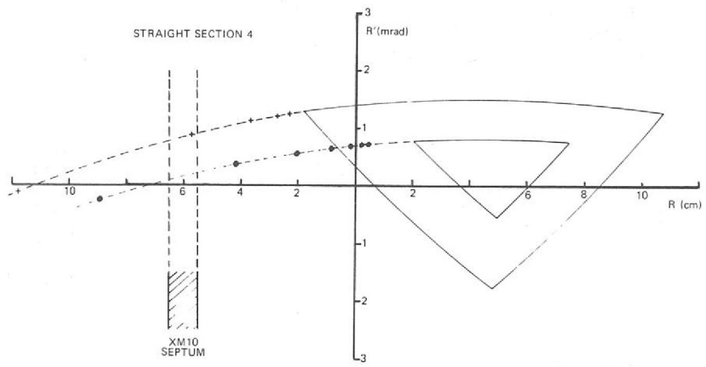

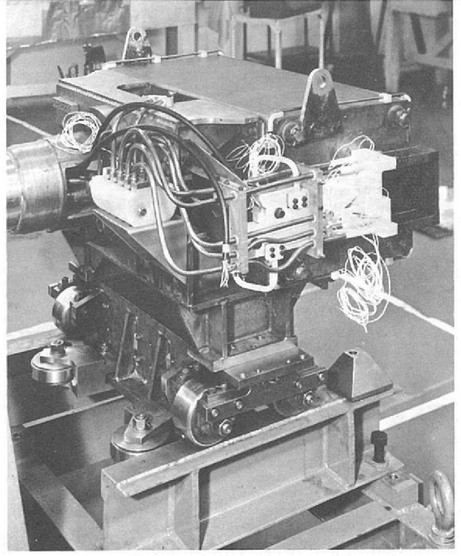

Figure 94. Extractor magnet, with 4-stack septum, and undercarriage.

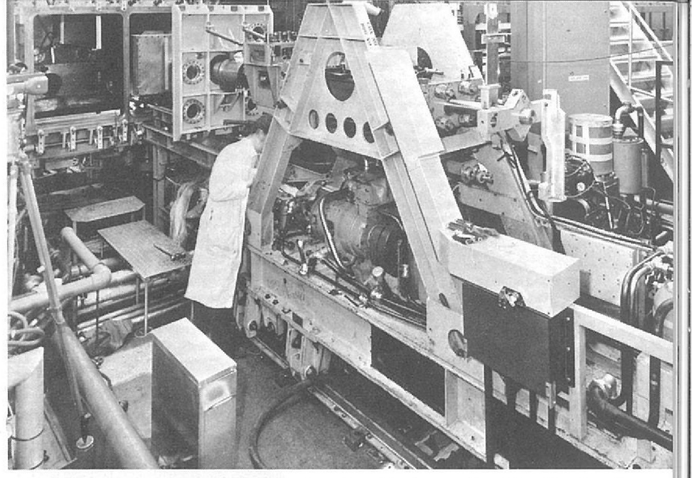

Figure 95. Mk II plunging mechanism installation at Straight Section 2.

EXTRACTED PROTON BEAM COMPONENTS

Septum Magnets

The XM type magnet with 4-stack septum, figure 94, has been running in Nimrod Straight Section 4 during the past year. A similar magnet is fitted in Straight Section 2 attached to the newly installed Mk II plunging mechanism, (figure 95), which provides the power to move the magnet (weight about 1500 lbs) about 20 inches in and out of the beam each Nimrod magnet pulse.

The 4-turn 4-stack septum, about 1 cm thick (figure 88), was designed to improve reliability and to reduce the manufacturing time of the vertical type septum. The 4-stack septum can be manufactured from readily available flat copper bars and plates suitably drilled and brazed together. Each turn is wrapped in 0·0035 in thick glass tape impregnated with epoxy resin, with the 4-turn assembly encased on three sides with a 0·03 in thick stainless steel channel. The rear conductors are coated with 0·01 in thick nylon to provide the necessary insulation. The final brazed joints connecting the nylon coated rear turns to the resin bonded glass fibre front turns was made possible by using special jigs, water cooling baths and high conductivity, low temperature, relatively high tensile strength silver braze.

The magnet is powered through flexible water cooled cables up to the plunging mechanism over the arch, through the junction box and ram tube to the septum, (figure 96). The estimated total resistance, power, water flow and temperature rise is shown in the following summary:

XM10 4-turn 4-stack septum, (Peak current 14,000 amps, Average current 7,000 amps)

	Resistance $\mu\Omega$		Peak Power	Average Power	Water Flow gpm	Peak Temp. Rise	Average Temp. Rise
Cables	250						
Arch	420	790	154·8 kW	38·7 kW	12·0	74·0° F	18·5° F
Services	120						
Magnet Septum	390		76·4 kW	19·1 kW	3·6	120·4° F	30·1° F

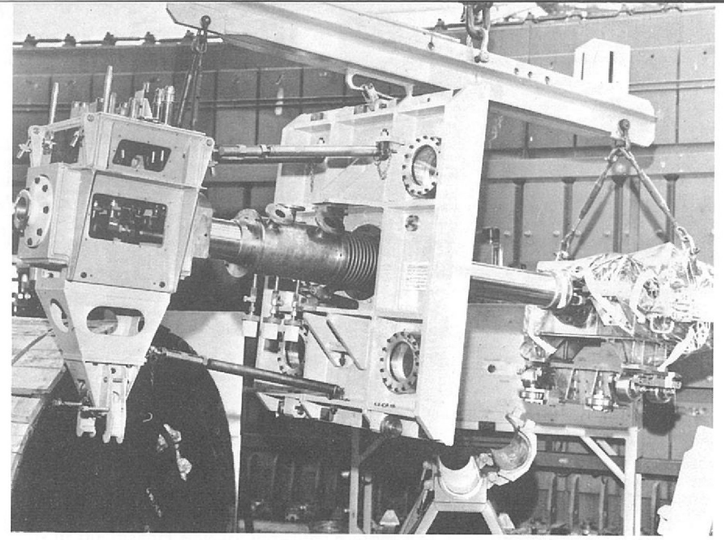

Figure 96. Assembly of junction box, ram tube services, labyrinth seal, cover plate and extractor magnet being lifted into position.

The magnet undercarriage operates in high vacuum and in high levels of radiation which presents serious problems of lubrication and wear. A reasonably satisfactory life has been achieved by mounting each wheel between two torsion bars, which permit independent twist and lift of each wheel thus ensuring that full contact is achieved between each wheel and rail throughout every stroke. The rails are made from EN24 steel, burnished with dry molydenium powder and bolted into an accurately positioned cradle.

Mk I Plunging Mechanism

A strengthened swash plate and modified control rods have been tested for $2{\cdot}5 \times 10^6$ cycles. Further investigation into the location of the slipper plate is in hand.

Mk II Plunging Mechanism

The Mk II mechanism with the V6S type swash pump was tested for 2×10^6 cycles and the control system optimised to give smooth running with accelerations of less than 4 g. Throughout the year there has been a reasonably trouble free period of running of these mechanisms.

The buffer arrangement of spikes and metal membranes, used to absorb the energy in stopping the magnet assembly if it overruns its specified distance, was tested. The finalised number of plates and spikes stopped the overrun magnet assembly in about 2 inches.

Further development continues on swash plate lubrication and bearings. A Mk IA mechanism which consists of a Mk I mechanism main frame fitted with the Mk II control system, components, hydraulic circuit and flexible pipes has been designed and will be built in 1971.

8-Stack 8-Turn Septum

This septum, shown in figure 97, is manufactured from copper tube 0·375 in square with a 0·15 in square hole. In this system improved mechanical reliability is possible since there are no joints in the vacuum system. The water pressure drop across this septum is much higher than the 4-stack septum. The eight turns are arranged to form a curved septum, bonded together with 0·003 in thick glass tape and epoxy resin and are encased on three sides with 0·03 in thick stainless steel.

Development of Thin Septum Magnets

Beam extraction efficiency can be improved by using an extraction magnet with a thinner septum and a higher magnetic field.

Basically, these conditions require a higher rate of heat transfer between the septum and its cooling water, and this has been effected by increasing the ratio of surface area to volume of the cooling channels and by using a high water velocity.

However, the improvement is limited by the increase in the ratio of length to diameter of these channels and boundary layer effects at the cooling water - copper septum surfaces. Tests have shown that the Darcy equation for calculating the pressure drop in pipes is valid when applied to extremely small bore capillary tubing.

Investigations are in progress to optimise the septum size, water pressure drop and current density. In addition transversely cooled septums are being considered and testing of possible septum profiles is in progress.

Inorganic Insulation

As a corollary to the work on thin-septum magnets some research is necessary on inorganic insulation. This is because the thin-septum will run at a temperature above that permitted for the type of epoxy resin now used for coil insulation. This type of insulation will give far greater radiation resistance than epoxy resins, and will also allow a greater margin of safety in the time taken to turn off power in the event of a water flow failure.

The forces involved on the coils of the septum magnets are considerable and techniques have to be evolved to make the septum construction sound both mechanically and electrically. A number of alternative materials have been considered, but work will be restricted to aluminium oxide, with which experience exists on other applications.

Following the construction of the first concrete insulated magnet, a second improved design has been constructed and demonstrated at the 1970 Physics Exhibition. This magnet has a resistance to earth of over 20 MΩ and withstood a 5 kV flash test.

Undercarriage Development

A rig designed for testing rails and various combinations of undercarriage wheels (loaded from 1 to 500 lbs) in a high vacuum has been in use throughout the year.

The results to date show that:

(a) EN 24T tyred wheel running on a EN 24T rail burnished with dry molydenium powder – satisfactory after $2{\cdot}13 \times 10^6$ cycles with only slight markings on burnished rail.

(b) Tyre coated with 0·05 in polyurethane – unsatisfactory. Polyurethane coat stripped off after 10 hours running.

(c) Solid polyurethane wheel – satisfactory after $2{\cdot}08 \times 10^6$ cycles, no measurable wear on the wheel diameter. Irradiation tests not complete.

Further tests are continuing using other materials.

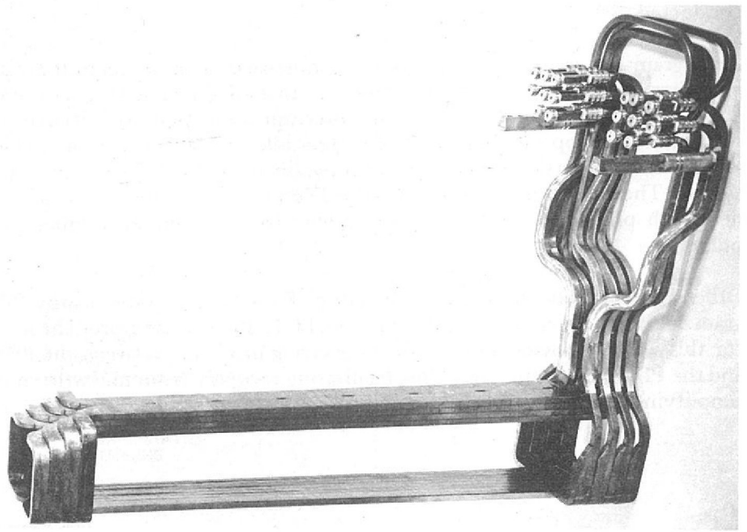

Figure 97. 8-stack, 8-turn septum.

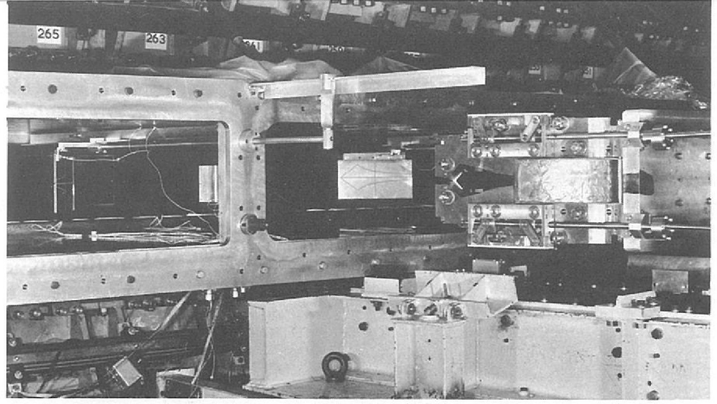

Figure 98. XHQ2/2 half-quadrupole magnet with upstream and downstream diagnostic scintillators.

Powered Shim XHQ2/2

During the December 1970 shutdown the second header vessel quadrupole magnet was fitted in Octant 3 for use with X1 beam. Figure 98 shows XHQ2/2 with its upstream and downstream diagnostic scintallators. Future scintallators will be attached direct to the magnet apertures.

Powered Shim XHQ2/3

The XHQ2/3 magnet and support structure has been designed for the X2 beam. Since it is in very close proximity to the X1 beam the whole support structure has been designed as an integral unit with the beam line quadrupole magnet and stand. This will limit movement of XHQ2/3 to ± 2 in radially and to ± 1 in azimuthally. Access is limited and removal of XHQ2/3 will necessitate removal of the X1 quadrupole magnet.

COMPUTER CONTROL OF BEAMS

Computer Control of X3 Extracted Beam Line (Ref: 139)

Commissioning of X3, the extracted proton beam for Hall 3, was made easier by the computer control system for beam line elements. The system has control over magnet current settings and collimator jaw positions.

Experience with this system early in 1970 quickly revealed two limitations. The first was that the maximum of 63 disk-stored files allowable in the PDP-8 Monitor System was rapidly being reached and this rather than the capacity of the disks (2 x 32K words) would limit the storage available.

The second limitation arose when it was realised that certain of the user programs would be better run as a time-shared activity, thus being executed each Nimrod pulse as well as, rather than instead of, one of the main programs. Notable in this category were programs dealing with presenting data, such as digital displays (nixie tubes), and target monitoring programs.

Extra disk and core storage has recently been incorporated in the computer to overcome these limitations and the first trials of the time-sharing system have been conducted.

A program for controlling the linking of time-shared programs to the system program has been tested successfully, and the first of the time-sharing programs has also been tested. They are run in the interrupt mode and are initiated soon after the end of flat-top on Nimrod. The system allows 7 such programs to be run and also permits 7 versions of the same program to be loaded sequentially into the system. The linking program controls the deletion of programs and can successfully deal with programs which have self-ended after a specified number of Nimrod pulses.

Other activities have been the engineering of a data link to the nearby PDP-5 program development computer, which has a DECTAPE backing store. The main reason for this was to provide a means of transferring programs between the PDP-8 disks and the PDP-5 magnetic tape, thus facilitating recovery from mis-written disks and simplifying updates of the disk-stored files.

The scope of the data acquisition and control equipment has been extended to include some of the X1 and X2 extracted beam instrumentation, and various quantities concerned with the operation of Nimrod, such as beam radius, data from insulated internal targets, and pole-face winding currents involved in resonant extraction.

Preparations have been made for enlarging the system to accommodate the extension to X3, which is being installed during the Winter shut-down.

Computer Control of K9 Bubble Chamber Beam Line

The basic details of the control system to be installed in K9 Local Control Room are as shown in figure 99. It was decided to interface the K9 devices with CAMAC, and the initial system will be contained in two crates of CAMAC modules, probably enlarging later to three. The computer is a PDP-8 with 12K words of core store, one disk of 32K words capacity, a single drive unit for magnetic tape and a fast reader, but no fast punch. Programmed transfer of single or double precision data between the CAMAC system and the computer is possible. The system has control over magnets and collimator jaws in a way similar to X3, and data is acquired concerning magnet currents, separator voltages, collimator jaw positions, beam counters and detailed status of the beam line. The system differs in many details from that of X3; one worthy of note is the multiplexing of the collimators, which will allow simultaneous control of any number of stations. This system will ultimately be applied in X3 and its extension.

There are also some differences in the philosophy of the control system. Much more emphasis is being placed on the day-to-day running mode of K9 beam, as opposed to the tuning of it, and there are two distinct ways in which the software will operate, the RUN and TUNE modes. 'TUNE' resembles the initial form of the X3 system, with, for instance, scanning and setting programs. 'RUN' consists largely of data collection, fault reporting and analysis, and gathering of statistics.

Figure 99. Block diagram of computer control system for the K9 beam-line.

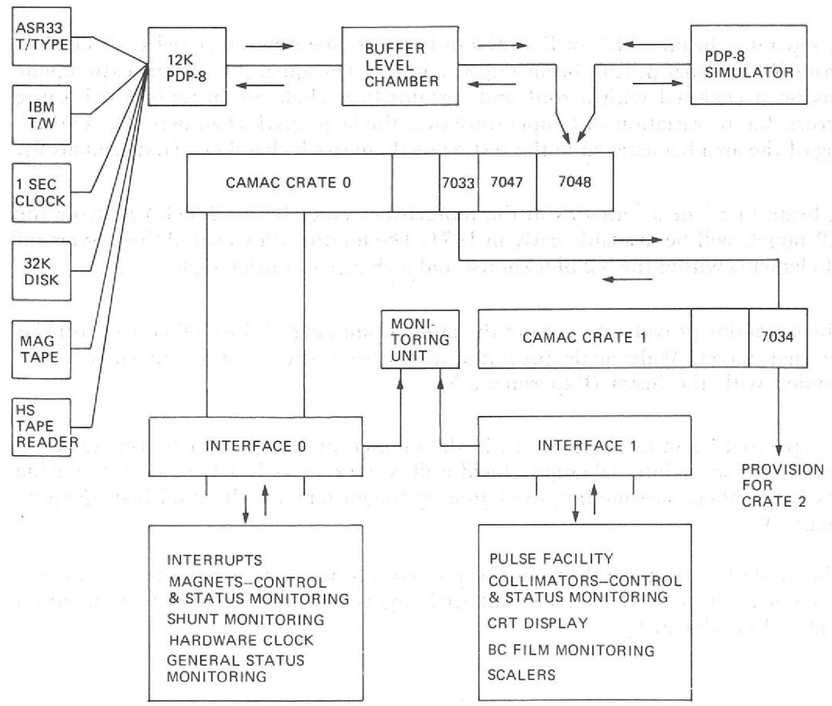

BEAM LINES AND ASSOCIATED EQUIPMENT

The year commenced with the major effort being concentrated in Hall 1: two beam-lines ($\pi 7\gamma$ and K14) were removed completely and four beam-lines were modified (K12A, K13B, K10S, K9).

During the summer the beam-line in the northern section of Hall 2 (K8) was re-arranged and re-named $\pi 10$.

For the remainder of the year, with the exception of a quick change round, during November, of components of K9 for a neutron experiment, the main effort was concentrated on planned maintenance and activities in Hall 3.

The arrangement of beam-lines at the end of 1970 is shown in the two pull-outs at the end of this Report.

X2 Blockhouse (Hall 1) With the dismantling of K14A, the last of the three beam lines were taken away from the end of X2. The blockhouse roof has been removed to allow extraction of all redundant elements. With the removal of these elements a beam stop has been specially built to allow the Radiation Protection Group to take measurements at various depths of shielding. The opportunity has been taken to add a second personnel access point and modify the front end of K13. Additional shielding has been placed around the blockhouse and a more homogeneous roof is envisaged.

K9 (Hall 1) This beam-line is the continuation of the X1 external proton beam and transports beams of π mesons, K mesons or protons to the 1·5 m Bubble Chamber. A 20 ton lifting beam with electric hoists has been installed over the tilting platform section of the beam. For safety reasons this section is inaccessible to the Experimental Hall overhead crane unless the Bubble Chamber is emptied. The beam-line was temporarily modified for a neutron experiment and magnets and collimators have been prepared for the introduction of computer control of the beam-line components.

K12A (Hall 1) A separated beam of K^+ or K^- mesons in the momentum range 0·4 to 1·0 GeV/c from X2 external proton beam target is in use. The apparatus for the experiment has been enclosed with a roof and curtains to exclude air currents which cause errors due to variation of temperature over the large spark chambers. The darkening of the area has assisted in the testing of these spark chambers. (Experiment 9).

K13C (Hall 1) A beam of π^+ or π^- mesons in the momentum range 0·5 to 2·0 GeV/c, from the X2 target, will be available early in 1971. The modifications entail the movement of elements within the X2 blockhouse and a change of outlet angle.

P71 (Hall 1) The beam-line provides protons in the momentum range 1·3 to 3·6 GeV/c from an internal target. Wide angle proton-proton elastic scattering is currently being studied with the beam (Experiment 5).

K10S (Hall 1) A separated beam of K^- mesons, in the momentum range 0·65 to 1·2 GeV/c, is provided from an internal target; shield walls were removed early in 1970 to enable spark chambers surrounding the liquid hydrogen target to be modified. (Experiment 3).

$\pi 7$ (Hall 2) This beam-line is currently in use to provide a beam of π^- mesons in the momentum range 1·0 to 4·0 GeV/c. Two internal targets are used to cover the momentum range. (Experiment 6).

$\pi 10$ (Hall 2) In the latter half of the year, $\pi 10$ beam-line was set up to provide π^+ or π^- mesons in the momentum range 0·7 to 2·0 GeV/c for a nuclear structure experiment. This beam-line is a modification of K8. (Experiment 32).

Extension of the X3 Beam-Line (Hall 3 Phase II) The X3 beam line has now been extended to a second target station. This extension has been designated X3X and the new station will serve the new beam line $\pi 9$. It also has the facility to be extended to a third target station, or provide a 0° beam.

The installation was carried out in two stages. Stage 1 from the existing target station to the beam cut-off unit (approximately half way to the second target station), and the remainder in stage 2. In this way it was possible for X3 to run and provide beam for $\pi 8$ and K15 with minimal interruption.

It also provided the opportunity for radiation experiments to be carried out in the vicinity of the beam cut-off unit as a result of which two design modifications were carried out. (i) Due to the increased efficiency of the extraction system a second beam cut-off had to be installed. (ii) With the new radiation knowledge the design of the beam stop for the second target blockhouse was modified thereby saving approximately 380 tons of steel. The whole installation used 4,263 tons of steel and 2,571 tons of concrete.

$\pi 8$ (Hall 3) The beam-line is set up to provide π^+ or π^- mesons, in the momentum range 0·5 to 1·7 GeV/c, from X3 target. (Experiment 16). Under normal operating conditions it has been found necessary to provide temperature control of all environments housing the videcon cameras. Further development work has now achieved the high accuracy demanded for the successful operation of these units. A new beam-line safety barrier and interlock system was commissioned.

$\pi 9$ (Hall 3) A π^- meson beam in the momentum range 0·4 to 4·1 GeV/c is being set up. This beam-line, one of the beam-lines from the X3X target station was first laid out early in 1970. Throughout the year the design has continued embodying all the modifications and alterations associated with a new beam-line. Components are being assembled ready for operation in February 1971. To accommodate the large number of Local Control Rooms in the space available a high level unit has been installed.

The experiment will use the new frozen target (see page 98) which requires a large elevated mounting platform 12 ft above floor level with an associated gantry reaching 32 ft high. Special concrete blocks and cork mountings were designed to eliminate the transmission of vibration from the structure to enable the target to function correctly.

$\pi 11$ (Hall 3) On the completion of the Shielding Tunnel experiment mounted at 90° from the X3 target station for the Radiation Protection Group, approval was given for a radiobiological and dosimetry facility at this position. The beam-line takes particles from the target at 15° above the horizontal plane and then bends particles of the selected momentum parallel to the floor at a height of 8 ft. This is the first beam-line to differ from the standard height of 6 ft 3 in and assists the radiation shielding by blocking straight paths of particles from the target. Beams of π^+ or π^- mesons in the momentum range 0 to 0·2 GeV/c are available.

The beam-line is now operational and AERE Health Physics will be the initial users followed by teams from either St. Bartholomew's or Churchill Hospitals. (See Radio-biological Pion Irradiation Facility page 179).

K15 (Hall 3) This beam originates from X3 target. Separated beams of $\pi^{\pm}$ and $K^{\pm}$ mesons in the momentum range 1·0 to 2·0 GeV/c are available. A light tight igloo for testing large spark chambers has been added to the beam-line (Experiment 8).

Collimators Development of collimators has continued. Modifications include a new centre position indicator, a digitizer unit required for computer control of the collimator and a new drive system incorporating an electric clutch and torque limiter.

Work is in hand to facilitate easy and expeditious removal of collimator jaws from collimators installed in a beam line. This is desirable so that irradiated jaws can be removed before handling becomes difficult due to high induced radioactivity.

Consideration is being given to adapting the early Mk I collimator so that it can, when necessary, be used as a beam spoiler.

Beam Cut-off Unit A 'type VI' version of beam cut-off unit, figure 100, has been developed and two of these units have been installed in X3X, the extension of Hall 3 external proton beam.

The unit consists of two thick steel disks mounted on a shaft parallel to the beam direction. Each disk has an 8 in dia beam hole off-set from the axis of rotation and by rotating the disks the holes can be aligned to transmit the beam. The system is pneumatically operated and, in the event of a failure of either air supply or electric power, will fail safe. The disks rotate under influence of gravity and are linked so that the holes are displaced relative to each other, thus making maximum use of shielding material.

The disks are enclosed in a vacuum vessel so as to form a continuation of the evacuated beam pipe and the external dimensions of the vessel match the shielding block module size.

Figure 100. Type VI beam cut-off unit.

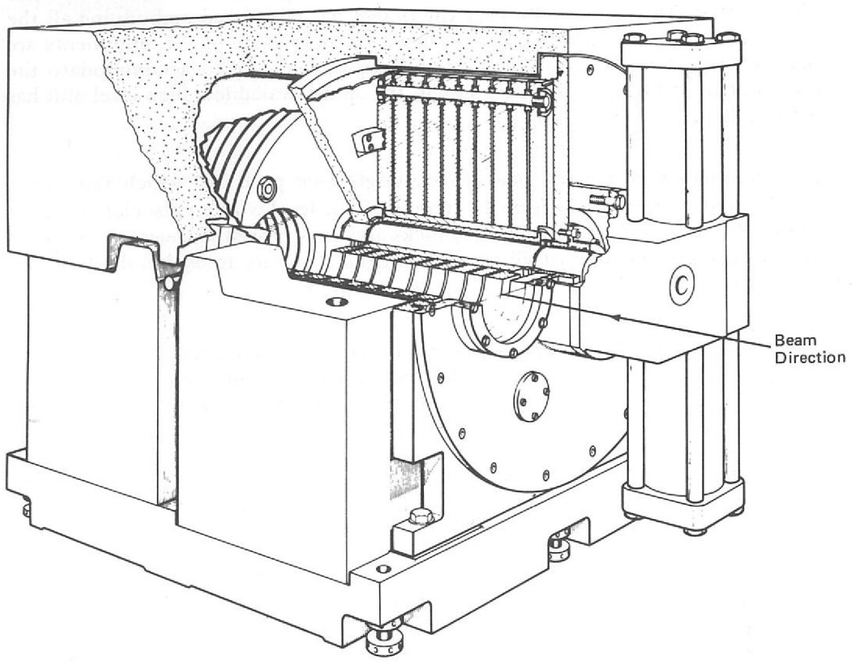

Electrostatic Air Filters Filter systems have been installed in K13 and π8 light tight igloos to protect the surfaces of the spark chamber mirrors from the very small dust particles which are normally present in the atmosphere.

Air-Conditioning of Experiment Control Rooms Alterations and additions to control and diagnostic equipment in LCR's during the winter months has resulted in an increase in control room ambient air temperatures. This increase has had no immediate detrimental effect but it is calculated that if no action is taken beam line computers in particular will be in trouble, because of excessively high temperatures, during the summer. Additional air conditioning plant has therefore been installed in π8, K12A, K13B, and K14A, LCR's.

Beam-Line Magnets and Power Supplies During the year, in addition to beam-line installation work, 40 magnets have been overhauled. Six 5 kW d.c. power supplies stabilized to ± 0·5% have been ordered. The first of these units has been delivered and tests indicate that stability is well within the specified figure of ± 0·5% over the range 15 to 150A. They will be used to power the M3 and Q7 range of beam-line magnets, where only low field levels are required.

NIMROD BEAMS—DESIGN STUDIES

Low-Momentum K-beam for 1·5 m Chamber, (K9)* Using the track-sensitive hydrogen target in the 1·5 m bubble chamber, there is considerable interest in the interactions of K-mesons below 1 GeV/c momentum.

A preliminary design for a 600-800 MeV/c kaon beam has now been completed, and is illustrated in figure 101. Outside this momentum range, muon contamination presents severe problems.

An alternative design, based on 2-stage separation, is being studied at present: greater beam purity over a wider momentum range would be achieved at some cost in kaon flux.

Superconducting RF Separated Beam Design of this beam, referred to in the 1969 Annual Report, was completed during 1970. However, in the K^- momentum range 2·0-3·5 GeV/c, the final flux estimates are below the requirements for the proposed experiment: only by going to zero-degree production, implying sole use of an EPB target, could the required fluxes be obtained.

Figure 101. Preliminary design layout of the low momentum K beam for the 1·5 m bubble chamber.

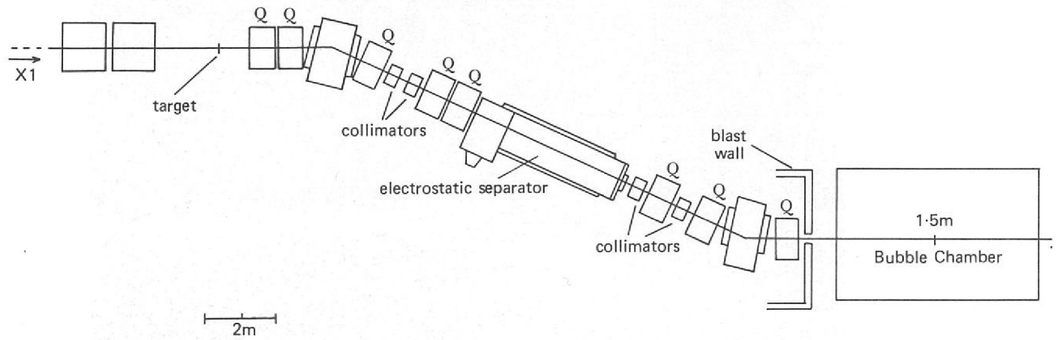

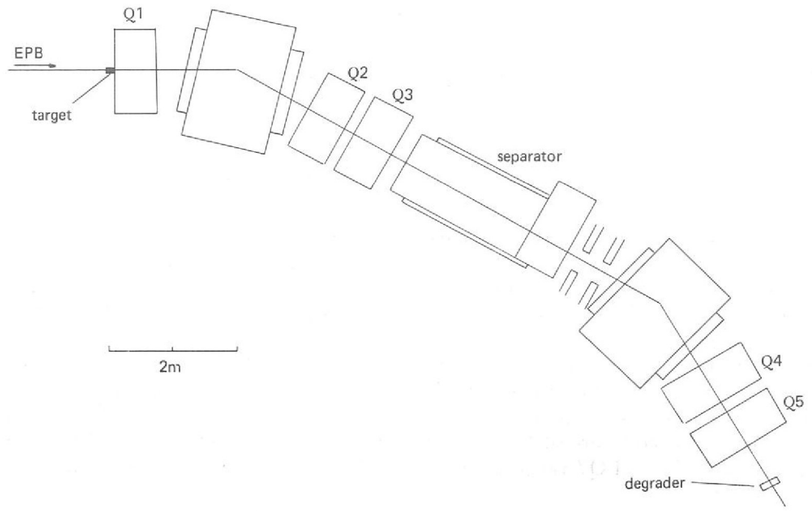

Figure 102. Design layout for a Stopping-Kaon beam.

Stopping K-Beam

Layout design for a "Stopping-Kaon" beam is shown in figure 102, and its optics is illustrated in figure 103.

About 18,800 K^- per pulse of 10^{12} protons, transported and separated at 600 MeV/c should be focused on to a "degrader" at the final focus; (i.e. a block of material which would bring them to rest in the detector). The contamination by μ^- and π^- would be about 30:1, and the efficiency of the degrader would be about 10%.

The beam requires 5 large aperture (30 cm) quadrupoles, and would be the sole user of an external beam target—for example, a third target in X3.

Beam Design Programs

Beam designs and beam-tuning procedures are being developed with the aid of interactive visual display computer techniques. (See page 172).

Figure 103. Optics of Stopping-Kaon beam. An example of computer produced graphic output.

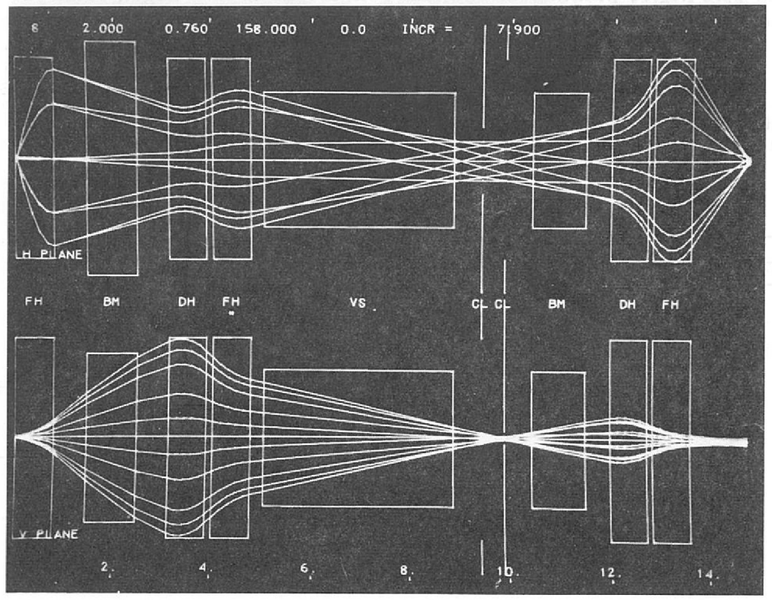

ELECTROSTATIC SEPARATOR OPERATIONS AND DEVELOPMENT

There has been a total of seven separators in operation in Nimrod beam-lines during 1970. The year has seen the final elimination of oil diffusion pumps from separators and their replacement by turbo-molecular pumps. The decision last year to complete the change over as quickly as possible has already been justified by the superior performance and increased reliability of the turbo-molecular pumps.

Wire Mesh Electrodes (Ref: 95)

Following the discovery at the end of 1969 of the outstanding performance of a wire mesh electrode used as the anode of an electrostatic separator, effort has been devoted in 1970 to the design of a version suitable for use in an actual beam line.

Mechanical Design

The problem is to construct an electrode of an open screen of wires with a screening ratio (the ratio of the open area to the entire area) of about 0·8 and yet still retain sufficient mechanical stiffness to maintain the required degree of geometrical accuracy under the action of the electrostatic attractive forces, which are in the region of 160 Nm^{-2}. A prototype was produced, based on preformed wires, in order to test the electrical performance of the arrangement. This turned out to be even better than that of the early, rather crude, mesh electrode, giving a performance equal to that of the glass electrodes used hitherto, namely a peak performance of 7·2 MVm^{-1} and a working performance of at least 6·0 MVm^{-1}. These figures are for a 100 mm gap.

A more rigid mesh has now been constructed. The electrode is an array of flattened stainless steel tubes mounted so that their edges are presented to the electric field. Electrically this is equivalent to an array of round wires of diameter equal to the length of the minor axis of the flattened tubes, but mechanically it is much stiffer. Each electrode, which is 150 in long, requires 368 tubes. In the construction and alignment procedure groups of 12 to 14 tubes are assembled into jig drilled retaining blocks, set level on a bench and securely locked in position. This group of tubes is then mounted onto a rigid box beam and aligned as a group to adjacent assemblies. This method allows easy replacement of tubes in the event of electrical or mechanical damage. Figure 104 shows the arrangement of the wire mesh electrodes and figure 105 shows an actual assembly.

Figure 104. General arrangement of the wire mesh electrodes showing modular method of construction.

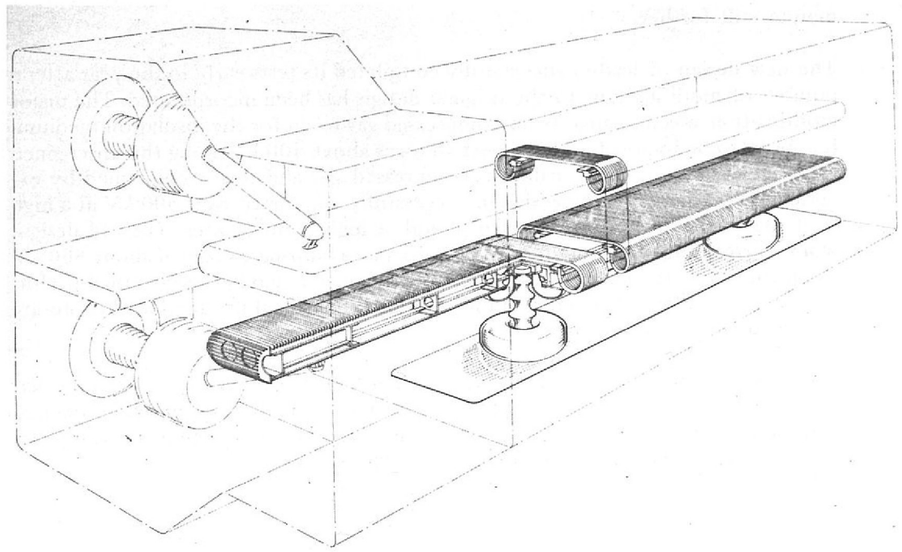

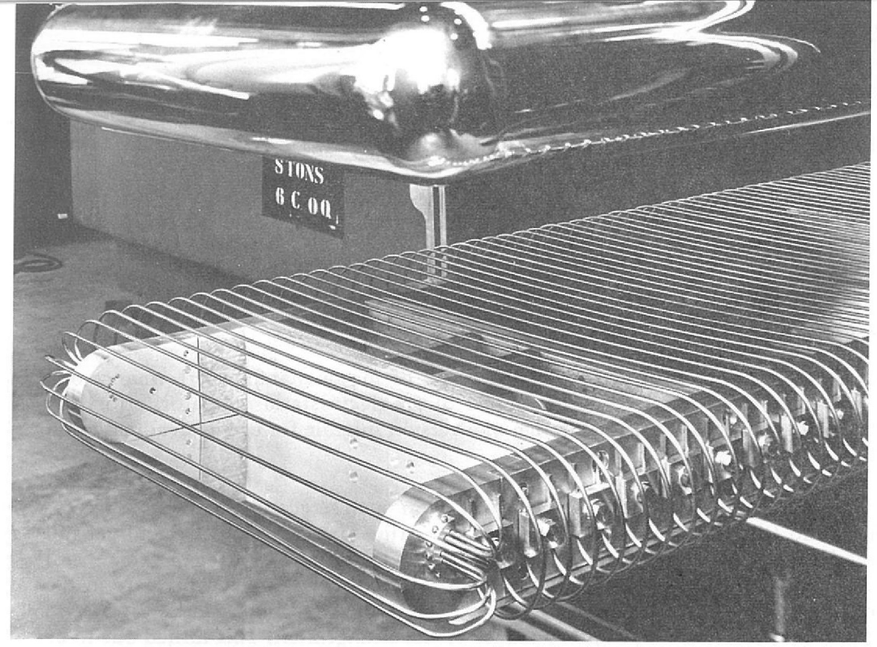

Figure 105. An assembled wire mesh electrode.

Advantages of Wire Mesh Electrodes

The advantages of wire mesh electrodes over heated glass electrodes are:—

1. The conditioning time is reduced from over a week to about 24 hours.
2. They do not require to be heated, thus saving the complication of heater controls and giving a further saving of start-up time of about 4 days.
3. They are insensitive to contamination of the vacuum system, which means that the expensive to run liquid nitrogen trap is no longer required and also that there is far greater immunity against vacuum failures, and services interuptions. Delivery of the final prototype is awaited for testing before ordering enough wire mesh electrodes to equip all separators in current use.

Electrode Support Insulators

The new insulators, described in the 1969 Annual Report, which withstood accelerated life tests so successfully, did not perform so well in service due to certain mechanical problems. These problems have recently been overcome and a further accelerated life test is currently in progress. The opportunity has been taken to introduce some electrical modifications with a view to increasing the security margin still further.

High Voltage Lead-in Insulators

The new design of lead-in successfully completed its tests early in the year after a number of modifications to the original design has been incorporated. The major modification was a change from compressed gas to oil for the insulation medium. It appears to be impossible to support voltages above 400 kV along the unscreened termination region of the cable in compressed gas and this is confirmed by experience elsewhere. The new design successfully supported over 500 kV at a high load sparking rate for an extended period at high temperatures. The old design, whilst performing very well for short periods, had a limiting voltage of about 360 kV when run for extended periods. As well as having a much better electrical performance the new design is much simpler to assemble. Final production versions are now undergoing tests.

Basic Vacuum Breakdown Research (Ref: 96)

Only a limited amount of time has been available this year for this work and it has been spent on consolidating the previous rarher hurriedly acquired experimental data, improving the accuracy, extending the range of the parameters investigated and investigating certain anomalies in the previous results.

A cryostat assembly used for testing superconducting magnet coil systems.

APPLIED RESEARCH

Applied Research

A large part of the applied research in the Rutherford Laboratory is directed towards applications of superconductivity. During the coming decade superconducting magnets are expected to come into widespread use in high energy physics, providing more powerful magnetic fields and/or lower capital and running costs for bubble chamber magnets, beam transport, proton synchrotron magnets, and synchrotron power supplies. These can make possible definite advances in the experimental studies of fundamental particle physics.

Long term studies of possible accelerators to supersede Nimrod are under way, and, in line with the Laboratory's interests in superconducting technology, accelerators based on pulsed superconducting magnets have great attraction in this context. The design study of a 25 GeV Superconducting Synchrotron, which could replace Nimrod (a 7 GeV Synchrotron) in the existing Magnet Hall, is described.

Such a machine would give an extended return from our large capital investment in the whole Laboratory support complex, by providing a basis for home-based high energy physics in the 1980's. It could also constitute an extremely valuable pilot project for a future very high energy superconducting accelerator in Europe. In addition, it would open the way to further accelerator development by acting as an injector for a larger superconducting ring, should the scientific and financial climate become favourable for such a project.

In connection with new accelerator developments, the design status of the new CERN 300 GeV accelerator is summarised.

Development work on superconducting r.f. separators is presented. These will provide separation of secondary particle beams into their constituent types, with high resolution and with low r.f. power requirements.

Some special purpose magnets which have been designed to control particle beams and for future experiments are described. Other sections include the status of the High Flux Beam Reactor design study and descriptions of apparatus designed and constructed at the Rutherford Laboratory as engineering models or actual flight models for satellite mounted experiments.

A Department of Engineering Science has been established within the Engineering Division with the specific responsibility of providing direct support for applied research and with the general objective of applying technological advances in science and engineering as speedily as possible to the work of the Laboratory.

SUPERCONDUCTING MAGNET STUDIES

Following the successful development of composite filamentary conductors suitable for these applications, the emphasis is now on the solution of the remaining hardware problems, and the development of reliable and economic engineering techniques. In particular, considerable priority is now being given to the evolution of prototype pulsed magnets suitable for use in proton synchrotrons, which would enable the energy of the proposed European accelerator (initially 200-300 GeV) to be subsequently increased to over 1000 GeV.

Figure 106. Compacted multi-strand cable.

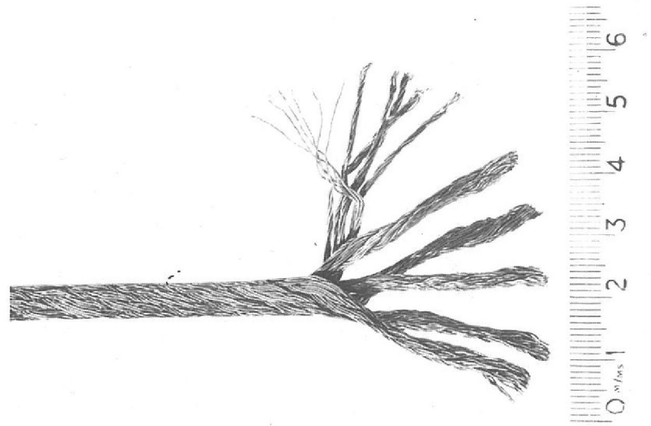

Because of the importance and difficulty of the latter possibility, the scope of the programme has been widened during 1970 to include practical and theoretical studies of all of the problems associated with the development of pulsed superconducting magnets with the necessary degree of precision and reliability.

Conductor Development (Ref. 155)

Work has continued on the development of NbTi conductors in collaboration with Imperial Metals Industries, and composites containing larger numbers of filaments and with better filling factors have been produced. Magnetisation measurements on composites containing both copper and cupro-nickel in the matrix, have given results in accord with theory. A new test rig is under construction which will allow future larger cross-section conductors (up to 10,000A) to be tested for critical current, stability, magnetisation, and a.c. loss, at rates of change of field up to 60 kG/sec.

An important problem tackled during 1970 has been the fabrication of the basic composites into compacted, fully transposed, multi-strand cables, capable of carrying currents in the 2000-8000A range. A cabling machine has been purchased and techniques developed for the manufacture of fully transposed systems containing up to 216 strands, with subsequent shaping into rectangular or square section to improve the packing and facilitate coil winding (figure 106). Further work is still necessary to completely eliminate wire breakage during the final compaction stage.

Coil Performance

The study of fully impregnated magnets initiated in 1969 was continued throughout 1970, the object being to determine how good a performance can be achieved and which impregnants are most suitable. The programme consists principally of tests on a series of separate quadrupole coils using a variety of impregnants, including filled and unfilled epoxy resins, waxes, and frozen liquids (figure 107). About 16 separate poles have now been tested. The principal conclusion is that at least 90-95% of the critical current can usually be achieved, but that the impregnant does have a considerable effect on the amount of initial 'training' necessary. The latter has been shown to be correlated with the mechanical strain energy created during fabrication and/or cooldown; materials incapable of storing appreciable strain energy (e.g. wax) or with low thermal contraction (filled resins) show least training, while coils incorporating crack resistant unfilled resins may sometimes require dozens of quenches and many cooldowns before the maximum current can be achieved.

Figure 107. A quadrupole coil with connecting rings.

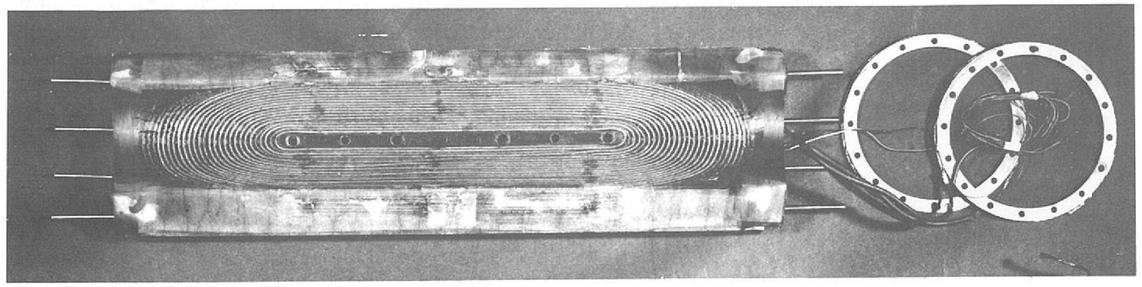

Four of these coils were assembled to form a complete quadrupole, which reliably reached over 95% of critical current, giving a peak field of 40 kG in a 12 cm bore diameter, the coil current density being 27,000 A/cm^2. This is the first full-scale demonstration that simple fully-impregnated coil systems will be suitable for the construction of d.c. superconducting beam elements.

Cryogenics

The preceding tests were carried out with the coils immersed directly in liquid helium, whereas in practice indirect cooling techniques may be preferred (e.g. circulation of the coolant through adjacent tubes). To verify that the performance is equally good under these conditions the tests will be repeated in a horizontal cryostat cooled by supercritical or two-phase helium. Manufacture and assembly of the cryostat, together with auxiliary dewar, heat exchanger, and reciprocating pump, is now complete and the first magnet tests will be carried out early in 1971.

Comparative theoretical studies have been made of the various methods of employing liquid helium as a coolant: (i) two-phase, 1 atmosphere, (ii) single phase, supercritical pressures (iii) single phase, 1 atmosphere (sub-cooled), (iv) free boiling, with, in each case, the option of assisted or natural convection as an alternative to pumped circulation. In addition some small-scale experiments have been carried out to check the conditions under which oscillations in two-phase helium may occur.

Pulsed Magnets

Extensive tests on small solenoids during 1969 had already confirmed the basic suitability of filamentary conductors for pulsed magnets, and during 1970 the construction of prototype pulsed synchrotron magnets was initiated. A small dipole (35 kG, 30 cm long, 4 cm x 2 cm aperture) was constructed and operated satisfactorily with continuous triangular current waveforms at frequencies up to 0·5 c/s. In parallel with this, work began on a larger and more realistic dipole, length 40 cm, aperture 10 cm, designed to give 45 kG at 7,000A and 1 sec rise time. By the end of 1970 all magnet components and associated equipment had been manufactured and a trial section of the superconducting coil had been wound and tested. Some delay has arisen from the above-mentioned strand breakage problem in the compacted cable, but the complete magnet is still expected to be operational during the first half of 1971.

This magnet is fully impregnated but incorporates laminated copper mats to conduct the heat from the interior of the winding to the coolant. This technique is being compared with the alternative of internal cooling channels, in preliminary design studies for a proposed fully-realistic synchrotron magnet prototype.

Synchrotron Magnet Design (Ref: 60)

In parallel with the studies of magnet performance, theoretical and experimental work has been in progress on the problems of designing and fabricating coils which will have, and maintain, the degree of precision (typically 1 in 10^3) needed in a synchrotron. Analytical and computer studies have yielded suitable designs for the coil cross-section and for the coil ends, and have indicated the magnitude of the various winding tolerances which must be met. As a convenient, and inexpensive, way of studying these problems practically, a programme of field measurements has been initiated using low-field copper models at room temperature and also in liquid nitrogen to check thermal distortion effects. The manufacture of formerless coils to a very high accuracy has required the development of novel production techniques in the Laboratory workshops. Patent action has been taken on the processes involved. The first precision-wound dipole (90 cm long, 10 cm bore) has been completed (figure 108), and preliminary measurements indicate quadrupole (asymmetry) errors certainly no greater than 1 in 10^3 – an extremely encouraging result, since it is already within the typical tolerance requirements of a synchrotron. Development is now in hand to further the techniques to give greater accuracy and reduce manufacturing time. The coils so far produced have been hand-built, but a higher degree of mechanisation is envisaged in the form of improved jigs and fixtures.

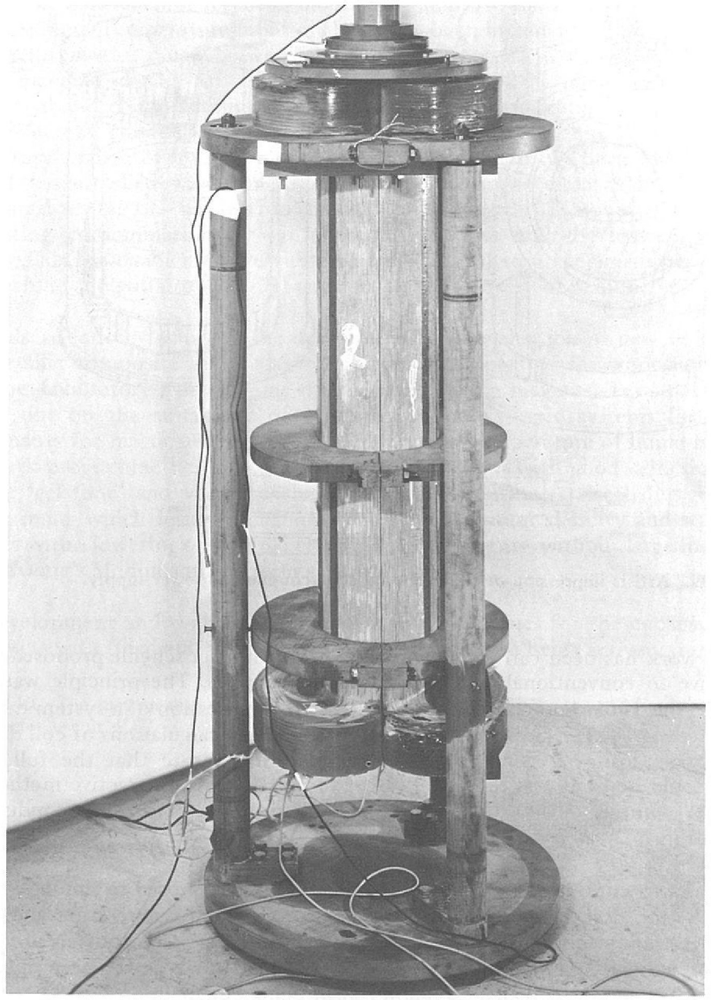

Figure 108. The precision-wound dipole magnet.

Forward assessment of a number of synchrotron design problems has continued, both to assist the course of the technology programme and as a guide to future possibilities. A major item in this part of the programme has been a detailed study of a specific scheme for the construction of a 25 GeV superconducting synchrotron in the existing Nimrod Hall. This has clarified many of the injection, ejection, and lattice design problems, as well as indicating typical aperture, field, and rise time requirements. (See Superconducting Synchrotron Design Study page 146).

Other problems studied include estimation of tolerable field errors during resonant ejection, calculations of the degree of lamination required in iron shielding, studies of the feasibility of self-powered superconducting correction windings, and first assessments of the effects on magnet design of any requirements for rapid Q-shift (e.g. during transition). Subsequent studies will be oriented in particular towards problems associated with the possible conversion of a large European accelerator.

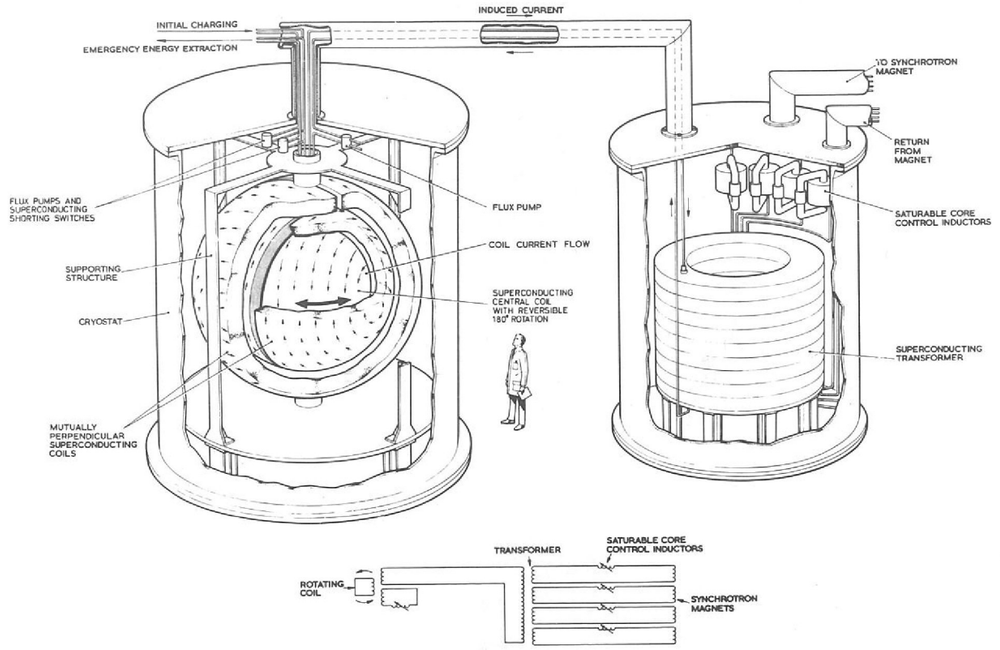

Figure 109. Artists impression of the proposed superconducting power supply.

Energy Transfer (Ref: 61, 168.)

Further work has been carried out on the energy transfer scheme proposed as an alternative to conventional synchrotron power supplies. The principle was described in the 1969 Annual Report, and an artist's impression of a system capable of transferring 10^8 J is shown in figure 109. Preliminary calculations of coil design, stresses, a.c. losses, dynamic behaviour, and cost indicate that the full scale system could be both feasible and economic, and offers an attractive method of powering a future 1,000 GeV ($\sim$ 1,000 MJ stored energy) superconducting synchrotron.

In addition to continued theoretical assessments, it is proposed to simulate many aspects of the design and behaviour by means of a room temperature analogue, using electronic techniques to imitate superconducting behaviour in a copper model of the coil system. A preliminary analogue of this type has been operated successfully and a more realistic version is now being designed.

As a first step towards superconducting prototypes, a small low-field superconducting model has been designed (overall diameter 30 cm, peak field 5 kG, transferred energy $\sim 10^3$ J) and this will be constructed during 1971.

INSULATING MATERIALS FOR SUPERCONDUCTING MAGNETS

(Ref: 152, 160, 161.)

Research on insulating materials for superconducting magnets has a two-fold objective:

(i) The study of the behaviour of materials when cooled to very low temperatures.

(ii) The provision of insulating systems whose manufacture is technically feasible.

Most constructional materials undergo marked changes in their physical properties when cooled to temperatures in the cryogenic range. For this reason a continuous programme of physical testing of materials is being pursued and the equipment described in the 1969 Annual Report has been updated and improved.

The 450 kg test machine has been modified to improve the sensitivity of extensometer readings. Temperature monitors have also been included so that tests can be carried out in the range between room temperatures and 4°K. In addition, a testing machine capable of applying a force of 10,000 kg has been made fully operational and commissioning tests are in progress on apparatus used for measuring the thermal conductivity of materials at 4°K. A further improvement to the Laboratory's range of low temperature testing equipment has been the construction of a controlled environment cabinet, permitting specimens intended for mechanical testing on the 'Instron' machine (see figure 110) to be changed whilst eliminating contamination by air and water vapour and the loss of gaseous helium. This has enabled the test rate to be increased to 5 specimens per day on this machine and still provide full facilities for the recovery of helium.

Materials selection, including the development and evaluation of new resins and non-metallic composite materials, is an important aspect of the work associated with the Laboratory's programme on superconducting magnets. Tests have been carried out on the suitability of a number of epoxy resin systems for use as impregnants for magnets designed to operate at the temperature of liquid helium. The work programme has aimed at producing a system with good adhesion and suitable 'gel time' and viscosity characteristics. Attention is also being given to filler systems which lead to an improvement in radiation stability and strength, together with a lowering of thermal expansion co-efficients, without large increases in the Young's Modulus of the resin system.

The development and evaluation of application techniques for the encapsulation of magnets with filled and unfilled plastic materials is also being actively pursued.

Figure 110. The Instron test machine for use at 4°K.

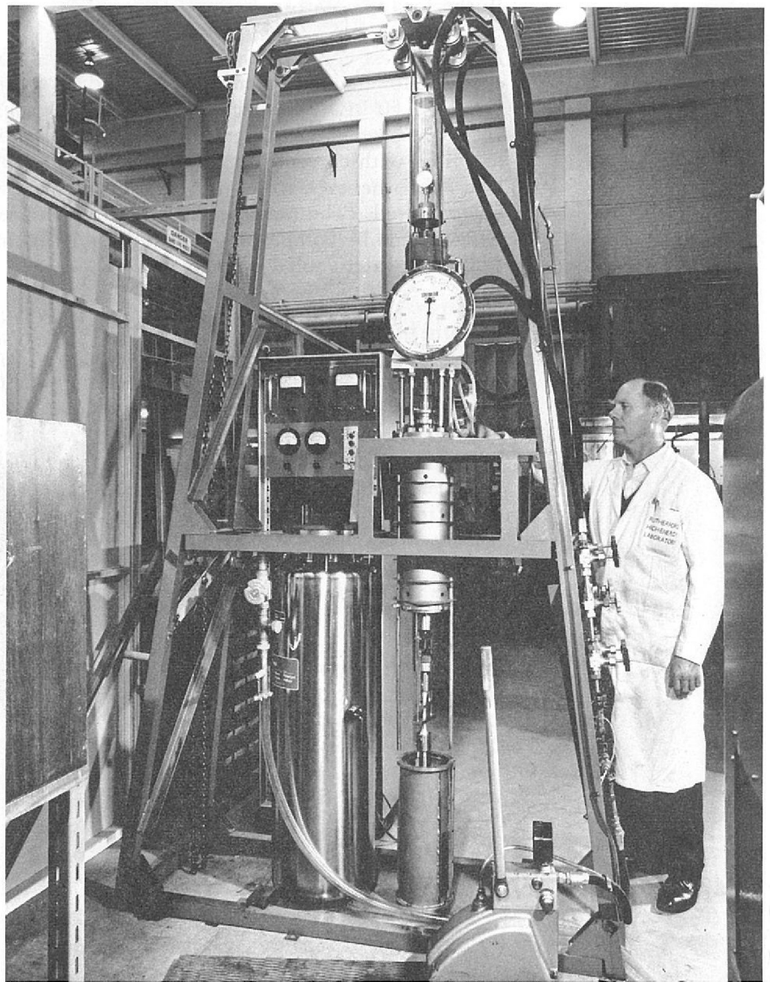

THE PROPOSED HIGH FIELD BUBBLE CHAMBER

With capital approval for the proposed High Field Bubble Chamber (HFBC) expected during the first half of the year much effort was devoted to finalising the design. Studies on the design of the refrigeration and expansion system made in conjunction with industrial organisation were completed satisfactorily.

The research and development programme continued with the emphasis placed, as before, on the superconducting magnet, glass reinforced plastic bellows for the expansion system and the optical system. Short reports on this work are given below.

Although approval by Council for the project was obtained, the financial implications of possible British participation in the proposed 300 GeV Accelerator project at CERN led to capital approval being deferred. As a result the design work has been discontinued and the research and development programme reduced.

Superconducting Magnet

Following the successful operation in 1969 of the RACOON I magnet designed to test the performance of the conductor first selected for the HFBC magnet, further conductor development has taken place. A final conductor configuration has been chosen which consists of 361 individual niobium-titanium alloy filaments embedded in a matrix of pure copper of cross-section 25 mm by 6 mm (see figure 111). The filaments are twisted about the longitudinal axis of the conductor with a pitch of 50 cm, to eliminate almost persistent magnetisation currents which would otherwise produce significant time dependent distortions of the magnetic field in the bore of the magnet. The conductor was developed and manufactured by Imperial Metal Industries (Kynoch) Ltd, working under contract to the Rutherford Laboratory.

A further test coil RACOON II has been built from this conductor to provide the evidence for final acceptance of the conductor for use in the 70 kG magnet of the proposed HFBC. The magnet has recently completed the first stage of its two-stage test programme. Operating fully immersed in liquid helium RACOON II was energised with currents up to 14,800 A and reached a peak magnetic field of 66 kG. This is believed to be the highest current at which a superconducting coil has yet operated. (The peak current density achieved in the conductor, almost 100 A/mm^2, can be compared with the 5 to 10 A/mm^2 at which copper conductors of typical water-cooled magnets run.)

Figure 111. The conductor of the RACOON II coil consisting of 361 niobium-titanium alloy filaments of about 0·3mm diameter in a copper matrix of cross-section 25mm x 6mm. The filaments are twisted about the longitudinal axis of the conductor with a pitch of 50cm to eliminate magnetisation currents.

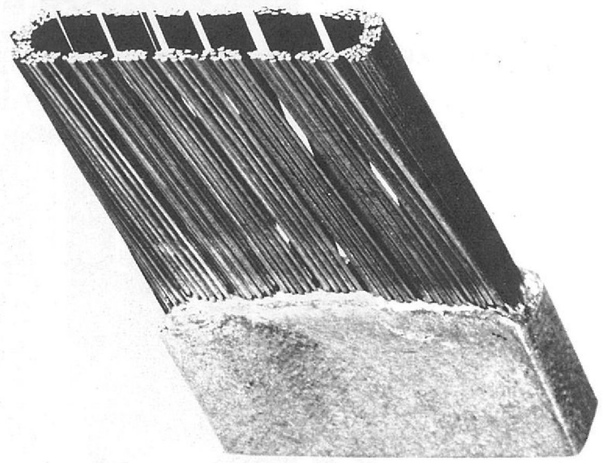

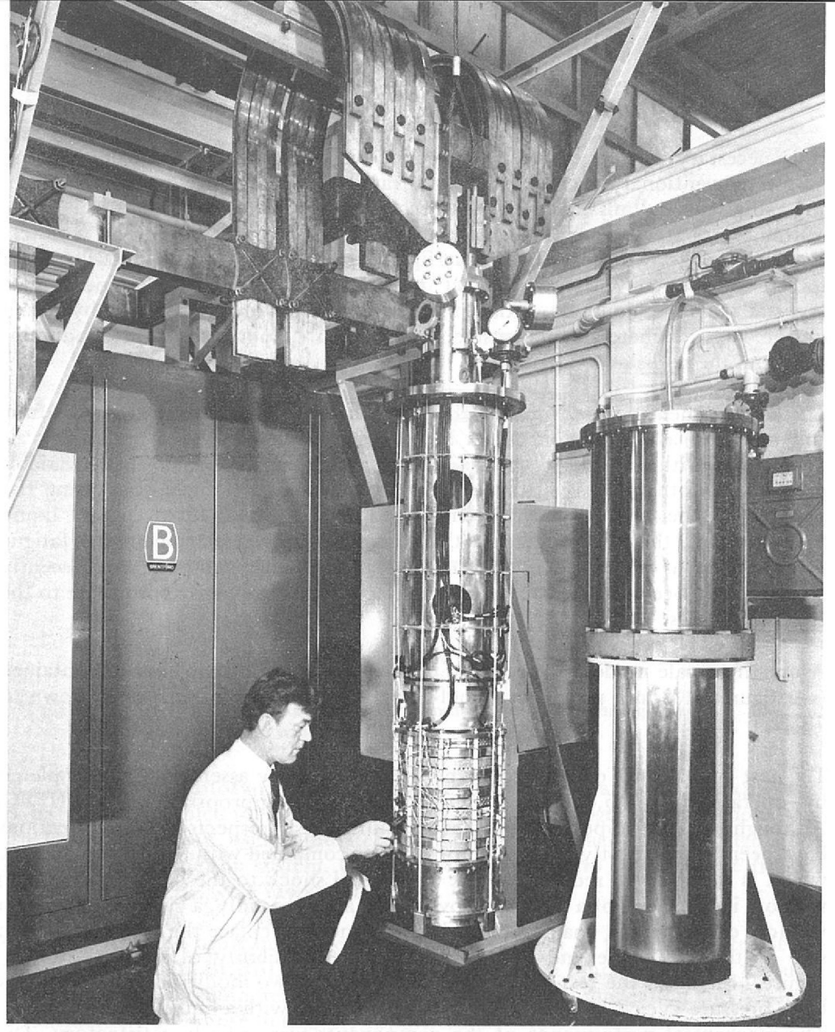

Figure 112. The RACOON II superconducting coil built to test the conductor for the magnet of the proposed High Field Bubble Chamber is shown connected to its 15,000A power supply.

RACOON II uses about 100 m of stabilised superconducting strip wound into six double pancake coils each of 25 turns. (See figure 112). In the HFBC magnet the conductor will operate at 7,500 A. The stable performance observed at currents of almost 15,000 A in the recent tests confirms that the conductor will have an entirely adequate margin of stability when operating at its design current. The twisted filament conductor ensures that magnetisation current loops set up within the conductor of a coil which is being energised will decay fairly rapidly. Measurements of the decay of such currents in RACOON II yielded a time constant of 40 minutes. In the HFBC application similar time constants are predicted. This means that the magnetic field distortions produced by these currents (which would persist almost indefinitely if twisted filaments were not used) will indeed disappear within the first hour after each energisation of the magnet.

The second stage of the RACOON II test programme is aimed at proving that the selected superconducting strip will also carry its design current of 7,500 A in a magnetic field of 84 kG, this being the peak field of the HFBC coils. For this test RACOON II in its own cryostat will be mounted within the bore of a conventional 50 kG water-cooled magnet at the Royal Radar Establishment, Malvern. When both coils are energised simultaneously it is expected that peak fields in excess of 84 kG will be generated.

It is necessary to support the superconducting magnet directly from the coil of the conventional magnet. Forces generated between the two magnets due to any radial or axial misalignment between the respective magnetic centres must be restrained to prevent any movement of the superconducting coil. The remotely operated wedges which can be seen in figure 112 transmit the radial misalignment forces to the conventional magnet by means of the specially constructed cryostat standing alongside. Axial misalignment forces are transmitted by means of the large diameter stainless steel tube which supports the superconducting coil from the cryostat top plate.

Expansion System

The development of glass-reinforced plastic bellows has continued successfully and as many as 20 million cycles have been completed with a one-fifth scale prototype, without failure. These tests have been performed with variable pressure at both room temperature and 78°K. Flexural fatigue tests using flat samples of the material have been carried out in liquid nitrogen and liquid hydrogen and the results indicate that there is no deterioration in the fatigue properties as a consequence of operating at the lower temperature. Recently attention has been directed towards manufacturing techniques appropriate to the full-size bellows.

A one-fifth scale model of the piston in glass-reinforced plastic has been obtained (see figure 113) and provisional cool-down tests have been performed down to 78°K.

Optics

The test programme of the prototype fish-eye window assembly was completed by operation for 15,000 cycles under conditions appropriate to the HFBC. Although the prototype performed satisfactorily in all respects two modifications have been tested. Firstly, a fused silica window combined with an invar 'spinning', which is designed to reduce the risk of thermal shock to the central heat shield window in the event of a main window failure and, secondly, a glued seal between window cartridge and chamber, which is designed to replace the standard indium seal of the prototype and thereby reduce the possibility of spurious boiling. Figure 114 shows the test piece incorporating these two modifications, which has been pressure cycled in the 10 inch bubble chamber with a liquid nitrogen filling. The mechanical performance of the components was entirely satisfactory. The nucleation properties of the glued seal will be tested in the fast-cycling bellows test rig now being designed.

Figure 113. One-fifth scale glass-reinforced plastic piston.

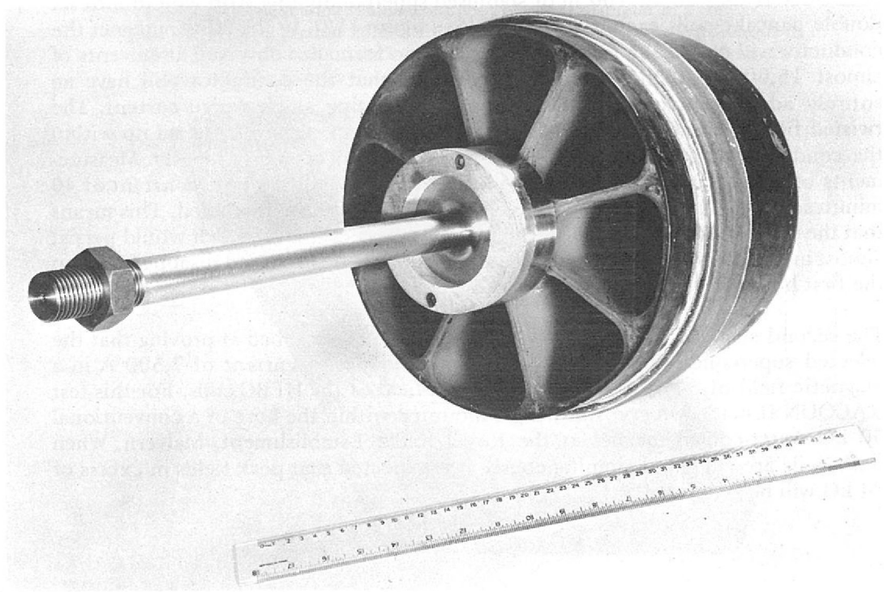

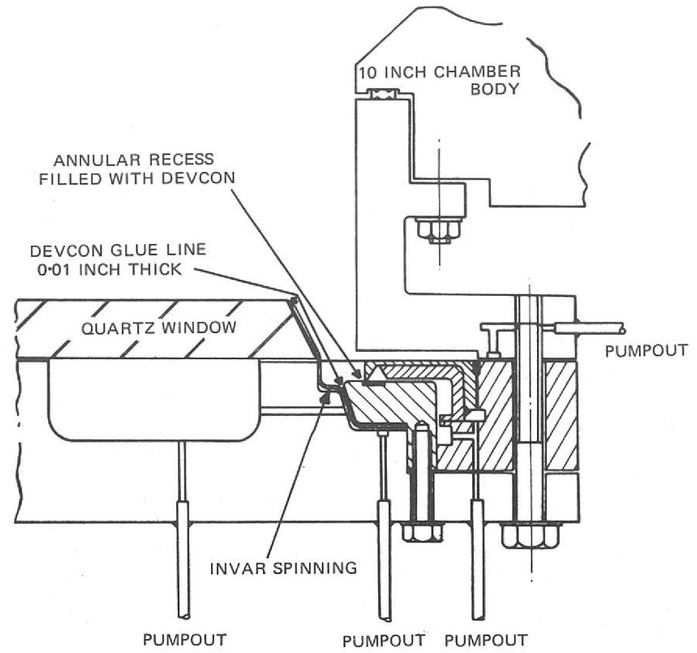

Figure 114. Window assembly incorporating an invar spinning and glued seal between window cartridge and chamber.

An experimental prototype camera designed for operation at up to 10 exposures/sec has been assembled for testing. Extensive tests of photographic emulsions have also been carried out using simulated bubble chamber tracks with a bright field (Scotchlite) illumination system. Conditions appropriate to the complete fiducial volume of the HFBC were investigated.

Computing

A number of new programs have been developed, two of particular interest are BUBBLE and NIFE. BUBBLE calculates bubble size as a function of time throughout the expansion-recompression cycle from the time of nucleation and has been of considerable use in predicting the conditions associated with fast cycling, where the time for bubble recompression is very significant. Figure 115 shows the variation of bubble size in the HFBC when operating at 10 expansions/sec. NIFE has been developed to calculate the dynamic stresses in the bellows and is based on a finite element method.

Figure 115. Bubble growth and recompression curve for 10 expansions per second operation of the HFBC, with a chamber expansion period of 40 milliseconds.

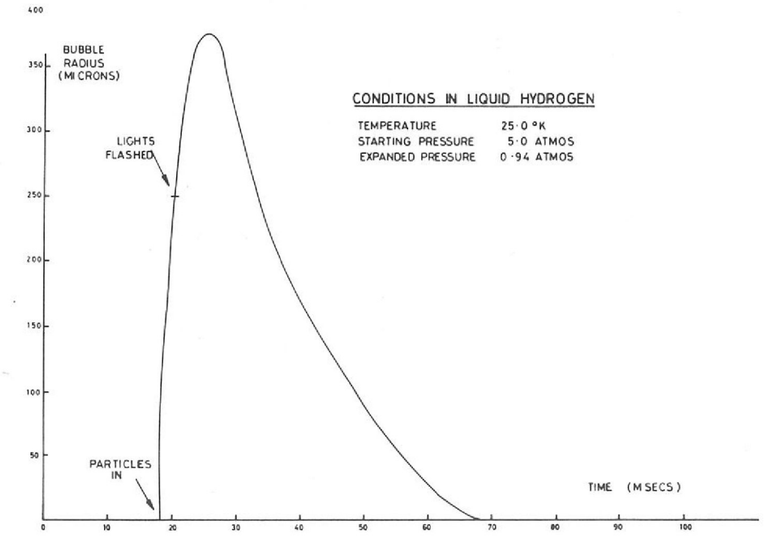

SUPERCONDUCTING SYNCHROTRON DESIGN STUDY

During 1970, a detailed theoretical design has been carried out for a superconducting synchrotron (SCS) which would fit in the Nimrod magnet hall, and which would use the existing Experimental Halls 1 and 3: see figure 116. Proton energies of about 25 GeV could be achieved.

The design incorporates a separated-function doublet lattice, with 20 focusing periods, divided into 4 super-periods: one period within each super-period contains a long straight section of 6·05 m, created by omitting bending magnets from an otherwise normal focusing period. The two quadrupoles in each period are 0·5 m long, and the bending magnets are in units of 0·95 m. From the existing 15 MeV linac, protons would be accelerated to 400 MeV in a small booster synchrotron, one quarter the radius of the SCS. This would be a combined-function machine using conventional iron-cored magnets. With the booster cycling at 20 cycles/second, 12 booster bunches would be transferred into 6 r.f. "buckets" in the SCS. Injection would take place in the vertical phase plane. The resulting SCS flux would be $1{\cdot}5 \times 10^{13}$ protons accelerated to full energy every 6·75 s. With a 0·75 s injection platform, 2 s rise time, and 2 s flat-top, the mean proton flux would be $2{\cdot}2 \times 10^{12}$ protons/second. Taking a conservative estimate for the effective spill time, 75% of flat-top, the effective duty cycle would be 22%.

With 60 kG peak field in the SCS bending magnets, the proton momentum would be 21·84 GeV/c: the corresponding gradient in the quadrupoles is 6·32 kG/cm.

The mean radius of the machine would be 27·85 m, and the bending radius 12·09 m. The diameter of the beam aperture (good field region) would be 11·6 cm, achieved with the aid of closed orbit control. The machine would be particularly well equipped with diagnostic, control, and monitoring devices. Figures 117 and 118 illustrate the processes of injection and ejection respectively. Injection requires the use of 2 fast kickers of 50 ns rise time. At ejection, the $Q = 4\frac{2}{3}$ resonance is induced to send protons across a thin magnetic or electrostatic septum upstream of the ejection long straight: in the long straight section itself, they cross a series of magnetic septa of increasing thickness, to emerge at an angle of about 95 mrad. The efficiency of the process should be over 95%. Tables 16 and 17 list the major booster and main ring parameters.

Figure 116. Layout of a superconducting synchrotron which would fit in the Nimrod Magnet Hall and which would use existing Experimental Halls 1 and 3. The filled-in blocks are quadrupole magnets.

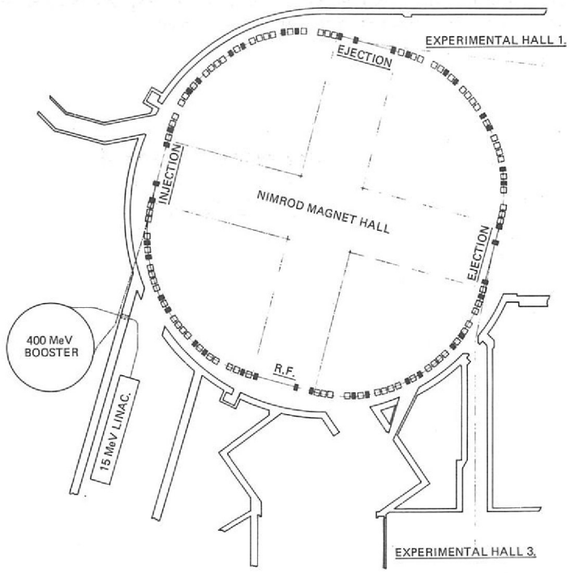

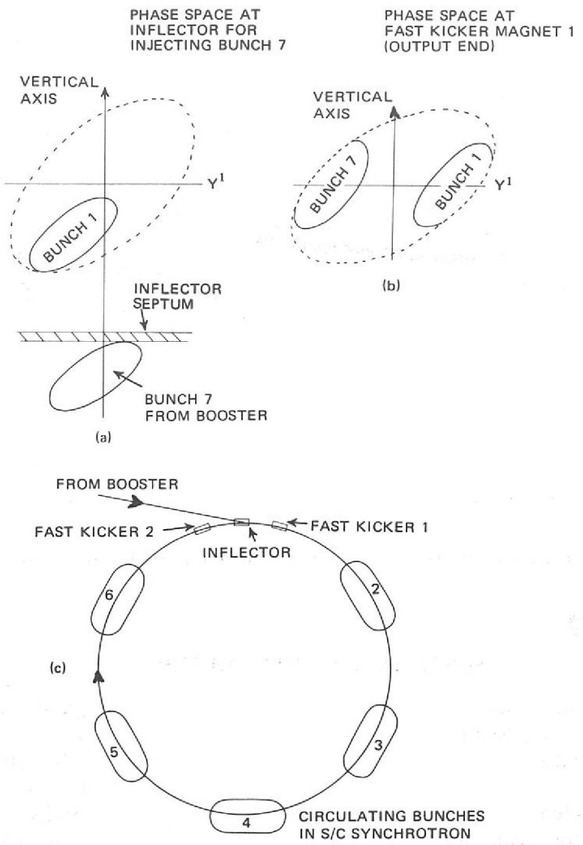

Figure 117. A 2-turn vertical injection system for a superconducting synchrotron. (a) The phase space diagram shows the relative vertical positions of particle bunches 1 and 7 at the thinseptum inflector magnet as bunch 7 from the booster is about to be injected. Fast kicker magnet 2 is used to adjust bunch 1 prior to this. (b) shows the phase space diagram for bunches 1 and 7 as they leave the fast kicker magnet 1. Successive pairs of bunches i.e. 2 and 8, 3 and 9 etc. are treated similarly. (c) The relative position of the first six bunches in the synchrotron magnet ring as bunch 7 is about to be injected.

Table 16

400 MeV BOOSTER PARAMETERS

Injection kinetic energy	15 or 50 MeV
Booster beam intensity (protons per pulse)	$1{\cdot}5$ or 3×10^{12}
Ejection kinetic energy	400 MeV
Transition kinetic energy	680 MeV
Magnet repetition rate	20 Hz
Booster circumference	43·747 m
Booster orbit radius	3·361 m
SCS/Booster circum. ratio	4
AG Structure (CF)	8 (FO_1DO_2)
Radial Q, Vertical W	1·81, 1·77
Length of straights	1·33 m, 1·50 m
Length of magnets	1·32 m
Magnet profile parameters	1·30 m^{-1} (D), 1·00 m^{-1} (F)
Magnet apertures (vert., rad)	8·89 cm, 17·0 cm
Ejection kicker rise time	127 ns
Bucket phase space area	0·1 eV second
RF frequency range	1·21 to 4·89 MHz

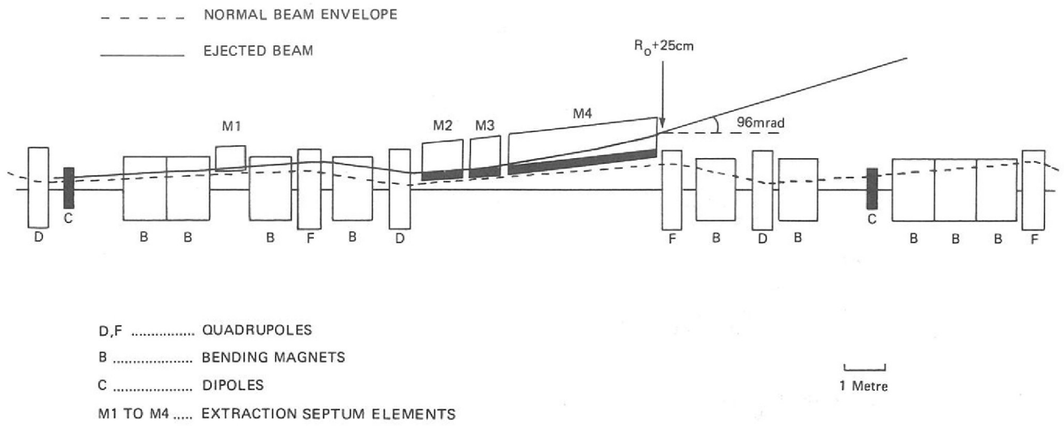

Figure 118. A beam ejection system for a superconducting synchrotron (theoretical extraction efficiency $\geqslant$ 95%).

Table 17

SCS MAIN RING PARAMETERS

Maximum Momentum	25·38 GeV/c
Maximum Bending Field	7 T
Protons per Pulse	$1{\cdot}5 \times 10^{13}$
Cycle Time	6·75 s
Ejection Efficiency	>95%
Injection Energy (Kinetic)	400 MeV
Field at Injection	0·267 T
Transition Energy	3·82 GeV
Aperture Diameter	0·12 m
Stored Energy	51 MJ
Circumference	175 m
Circumference Ratio	2·3
Mean Radius	27·85 m
Bending Radius	12·09 m
Maximum Quadrupole Gradient	63·2 T/m
Number of Focusing Periods	20
Number of Superperiods	4
Number of Betatron Oscillations per Revolution: Q_H, Q_V	4·8, 4·85
Resonant Q Value	4·66
Phase Advance per Period	86·4°
Maximum β Value	13·7 m
Effective Length of Bending Magnets	0·95 m
Effective Length of Quadrupoles	0·5 m
Length of one Period	8·75 m
Length of Long Straights	6·05 m
RF Frequency : Injection	7·32 MHz
: Ejection	10·26 MHz
RF Harmonic Number	6
Number of Pulses Injected	12
Injection Platform	0·75 s
Peak r.f. Volts	54 kV
Average Power in Beam	30·5 kW
Length of r.f. Cavity	2 x 2·0 m

EUROPEAN 300 GeV ACCELERATOR

Design work on the proposed European 300 GeV has culminated in the Project B* proposal. The essence of the proposal is to build the 300 GeV proton synchrotron and its laboratory adjacent to the present CERN site at Meyrin, Geneva. This enables major capital facilities of the existing laboratory to be used as an integral part of the 300 GeV programme. For instance, the CERN 25 GeV accelerator will be used as the injector for the 300 GeV machine and the West Hall of CERN as its first experimental area. This reduces the cost of the 300 GeV programme and allows research to start several years earlier than would be expected otherwise.

A design study has been carried out by the '300 GeV Machine Committee', under the direction of Dr. J. B. Adams, and 14 Working Groups with Machine Committee members as convenors. Only 3 people were employed full-time on the design, the rest of the work being done by staff from CERN and national accelerator laboratories on a part-time basis. The Rutherford Laboratory has taken a full part in the study, having 3 members on the Machine Committee and 15 people contributing in a major way to the work of 8 of the Working Groups, viz. magnet system, magnet power supplies, vacuum system, control system, radiation protection system, ejection, experimental areas and general equipment and buildings. Each Working Group has produced a chapter of a design report published by CERN for the 300 GeV Machine Committee.* The first chapter, a separate volume, is a summary of the design.

* Report MC/60. A Design of the European 300 GeV Research Facilities. CERN, December 1970.

SPECIAL PURPOSE MAGNETS

High Field Pulsed Magnets

Approval has been granted, in principle, for the mounting of a Λ hyperon experiment at CERN during 1971, using the equipment developed at this Laboratory during the last few years.

Two complete magnet assemblies, each with one spare coil, are available and tested. The coils are of the type shown in figure 119, with a bore of 40 cm. The coil illustrated has been tested for more than 120,000 pulses at 70 kG. Improvements have been made to the water-cooling and containment systems as a result of experience gained in tests during the year.

Figure 119. 40 cm aperture pulsed-magnet coil.

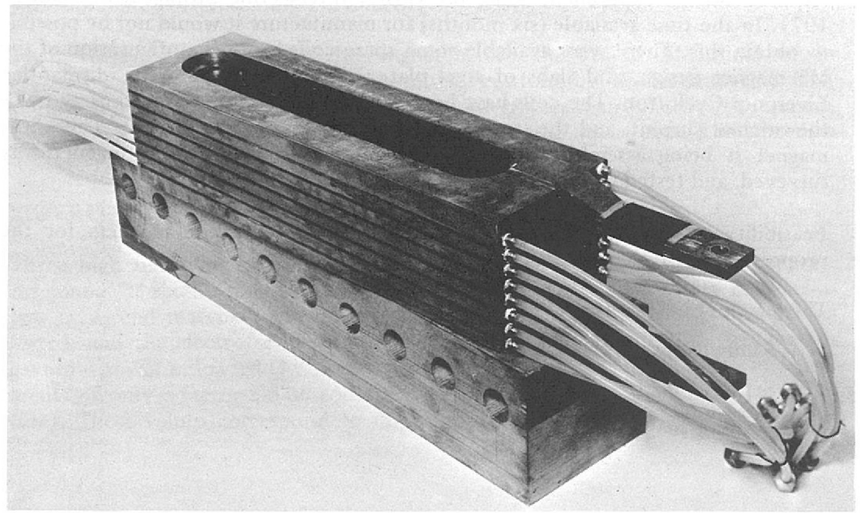

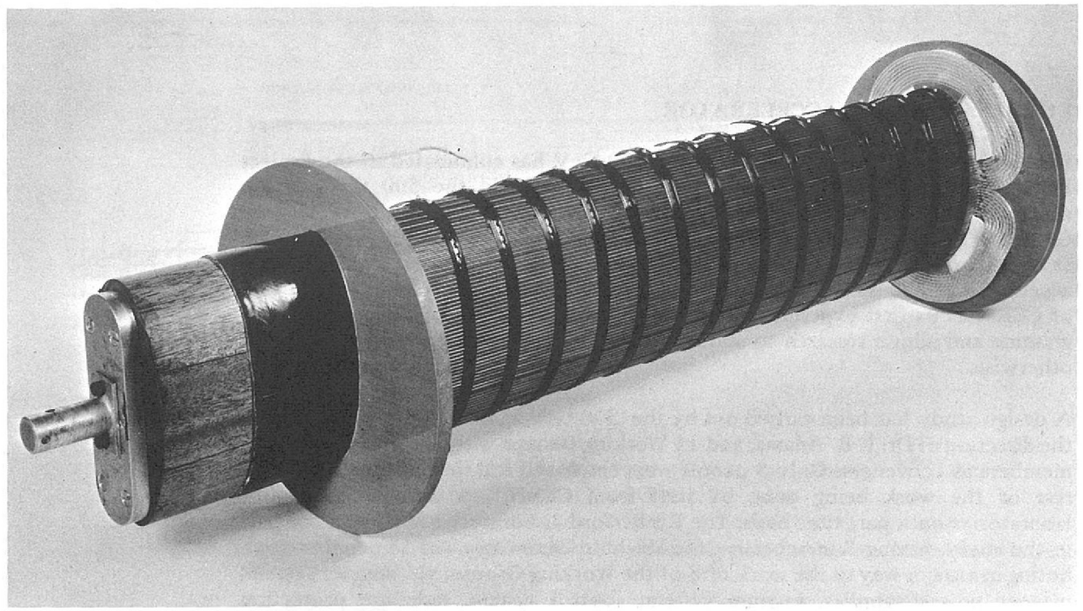

Figure 120. 30-turn flat-top field pulsed magnet during construction.

Beam Switching Magnets

The fast-rise, flat-top field pulsed magnet developed for beam switching, consists of a remote pulse-forming network feeding a magnet coil constructed within the walls of a 1 cm thick vacuum flight tube. With 20 kV anode drive voltage, a large triode drives 300 A in the 1 mH 30-turn coil, within 25 μs of command, and for up to 1 ms, depending on requirements; the pulse may be terminated earlier by a signal derived from the beam.

By linking the two sets of coil conductors in parallel, the rise-time may be halved at the expense of deflecting field. Figure 120 shows such a coil during assembly around an elliptical mandrel.

Magnet Trigger Systems

Development of the fast switchgear for a variable 20-70 kV pulse-forming network for stepmagnets and similar switches has continued, using avalanche transistors, thyratrons and sparkgaps. The emphasis is on reduction of total delays between a command signal and the establishing of a precise current of up to 20,000 A in an iron- or ferrite-cored magnet.

M5D Sepctrometer Magnet

A magnet, corresponding to our standard M5 spectrometer magnet design, is required for an experiment using the CERN Intersecting Storage Rings during 1971. In the time available (six months) for manufacture it would not be possible to obtain this. There were available some spare coils for one configuration of the M5 magnet design, and slabs of steel plate 7·75 in thick from the dismantled Liverpool Cyclotron. The coils have been modified to up-rate them to carry twice the original current, and the steel plate utilised to form a 50 ton yoke. The whole magnet is being assembled in Experimental Hall 2, and will be magnetically surveyed, and tested ready for dispatch to CERN by mid-March, 1971.

CERN 300 GeV Special Purpose Magnets Study

Feasibility studies have been carried out of special purpose magnets for the proposed new European accelerator.

Three types of magnets were considered:—

(i) Sandwich magnets

(ii) Septum magnets

(iii) Dividing magnets

The design of some of these calls for current densities in excess of 100 A/mm^2, and consequently very high heat transfer rates. The proposed construction allows for the use of inorganic insulation by known techniques. (Some of the septum magnets in use in Nimrod beam lines have current densities of 150 A/mm^2).

M11 Spark Chamber Magnet

The heavy liquid bubble chamber magnet has been dismantled and is now being rebuilt in Experimental Hall 3 as a spark chamber magnet. Modifications will make this magnet as versatile as possible for future use as a general experimental facility. In the present assembly three coil pancakes have been removed to give an aperture of 31 in with a field of 10 kG. This magnet yoke has been modified to enable the original hydraulic jacking system to be used in conjunction with the existing magnet transporter, to enable the 200 ton magnet to be moved for positional and alignment reasons. A turn-table is under construction to give small angular movements (±5°) of the magnet during experiments. The rotating part will slide on PTFE pads and accurate position will be obtained by a hydraulic ram system. Trails were done with PTFE pads suitably loaded, to ascertain the static and dynamic friction of this system. The static friction was found to be almost identical to the dynamic friction, thus accurate angular positioning should be possible.

Handling gear has been built to enable the magnet to be dismantled expeditiously to change the size of the gap and to introduce experimental apparatus.

Magnet Field Survey Equipment

The semi-automated magnetic field survey unit mentioned on Page 91 of the 1969 Report is being modified in line with user recommendations when it is hoped that the overall errors in surveys due to the unit will not exceed ± 0·2%. The modified unit will be used in surveying the M5 magnet for use at the CERN Intersecting Storage Rings and the M11 spectrometer magnet.

SUPERCONDUCTING QUADRUPOLE LENS

Superconducting magnets offer particular advantages in their compactness and high magnetic field for use in beam-lines. Such applications will be investigated by studying the performance of a commercially manufactured quadrupole magnet initially under test conditions and then in an actual beam-line.

An order for a prototype superconducting quadrupole was placed with British Oxygen Company Ltd in June 1970, and is due for delivery in June 1971. The magnet will have a room temperature bore 12 cm diameter, gradient 6·5kG/cm, and an effective length 33 cm. By paying attention to the elimination of end effects, the magnetic length of the quadrupole is expected to be constant to a higher degree than previously achieved over most of the bore, and unwanted harmonics are correspondingly reduced.

To increase the flexibility of the magnet in use, the overall dimensions of the cryostat have been kept to a minimum, (62 cm long by 49 cm diameter). Consumption of liquid helium is expected to be not greater than 1.7 litres/hr in operation. Provision for adding magnetic shielding is being made, should this become necessary under certain operating conditions.

SUPERCONDUCTING R.F. SEPARATORS

High Field Test Cavities.

Three high field test cavities have been made during the year: two of separate machined 'T' sections, and one of electroformed copper. Each cavity consists of two cells, end matching sections and short beam pipes. The first two have been tested, and the electroformed model is being tested at present. The first models gave low power unloaded Q-values of the order of 3×10^7 at 4·2°K, with improvements of only a factor 2-3 on cooldown to 1.85°K (the design operating temperature). These values correspond to improvement factors within a factor 5 of the

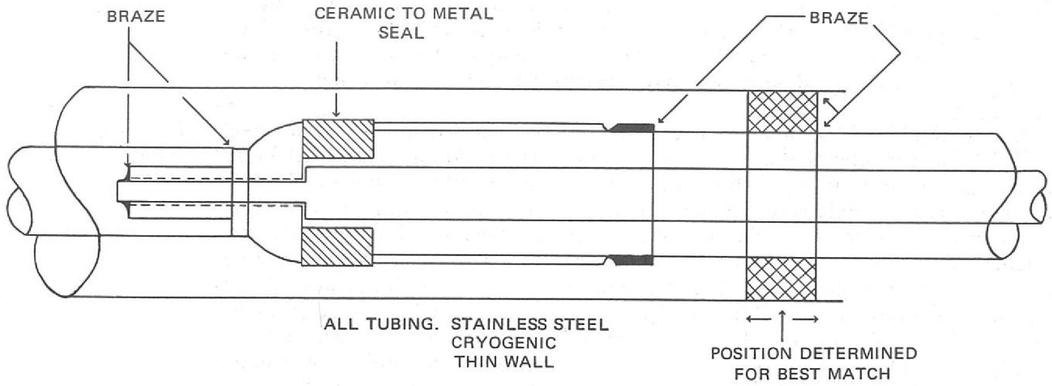

Figure 121. Details of a microwave window for operation at cryogenic temperatures.

theoretical value at 4.2°K, but worse by a factor 100 at 1.85°K. Possible causes for the relatively low Q-values are poor vacuum, quality of plating (which is particularly important under high electric field conditions), and imperfect joints. The lead-plating procedure has been improved in detail during the year, and was further checked by tests on an S-band TE011 Mode cavity. Over a wide range of plating currents, Q-values of the order of 10^{10} were obtained. The quality of the vacuum has generally been rather poor, but baking and the use of a new double sealed vacuum manifold should improve this for the electroformed model. The most likely reason for the low Q-values is the joint used on the model (each has 5 joints). The joint is a simple spigot type with a bolted flange, with which one cannot guarantee good lead-to-lead contact over the whole temperature range. This problem is avoided with the one-piece electroformed model. Tests are now being concentrated on this model.

New Plating Shop The new plating shop was brought into use at the end of 1970. This incorporates many improvements over the old one, in particular conditions are cleaner, and handling is improved. The actual plating will be done with the cavity revolving round collapsible anodes. Glove boxes have been modified so that the plated parts are handled either under vacuum, or in an inert gas.

RF Components Difficulties have been experienced with solid state strip line amplifiers at 1300 MHz. R.f. power for the separator system will now be provided by a conventional beam tube. Development of other strip line components has continued. A new microwave window for operation at cryogenic temperatures has been designed, and is shown in figure 121. The window proper is a standard feedthrough cylindrical insulator, which can withstand thermal shock (unlike the conventional planar window in coaxial line). The diameters of the conductors to and from the window are chosen to give the usual 50 Ω impedance, and the location of the terminating plane is chosen to give a match (typically voltage standing wave ratios better than 1.1:1 are obtained).

A new joint for the disc-loaded structure has been designed, which separates the function of providing a tight vacuum seal and making good lead-to-lead contact, as in figure 122. The indium is maintained under pressure by the cantilevered arm, to provide the seal, and the lead contact is maintained at the spigot. The joint has been immersed in liquid helium to temperatures below 2°K several times, with no sign of leak. An E010-E011 mode cavity is being made to test the r.f. properties of the joint.

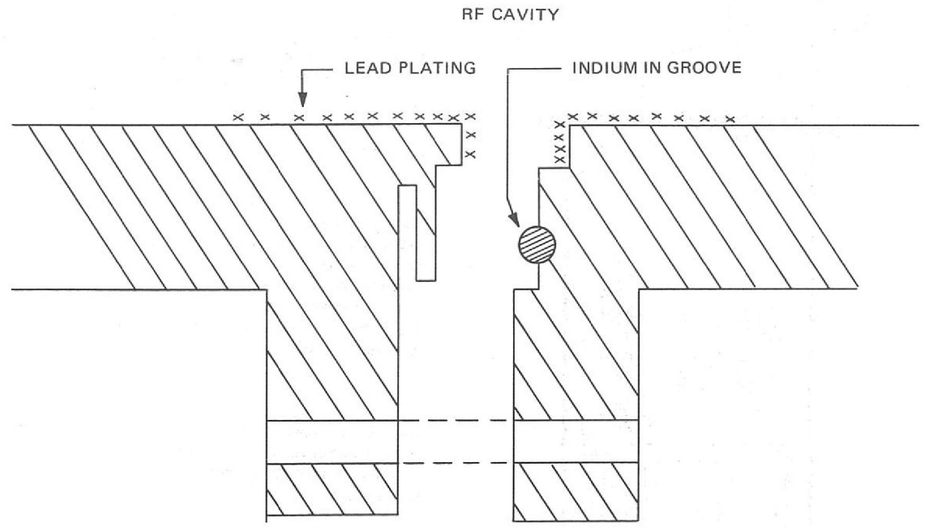

Figure 122. R.F. joint for operation at cryogenic temperatures.

Refrigerator Design

Operation of the proposed superconducting r.f. separators will require large scale production of super-fluid helium to fill the two cryostats (400 litre capacity) and maintain a refrigeration load of about 40 watts at 1·85°K. A secondary refrigerator to function in series with an existing 4·7°K refrigerator system has been designed.

The design is based on a modified 'Hempson process' utilising three counterflow and two pre-cooling heat exchangers along with two Joule-Thomson expansion stages balanced to give the best efficiency. The existing 4·7°K refrigerator will be adapted to supply liquid at 4·7°K and gas at 66°K for the five heat exchangers and further gas at 66°K to cool the heat shield along with the transfer pipe and cryostat heat shields. A 'Roots' pump will be added to the existing two stage vacuum pump and used to maintain the 1·85°K liquid vapour pressure and return this vapour back to the main system for recirculation.

Figure 123 shows the proposed design, features include

(a) a novel counterflow heat exchanger for the low pressure vapour cold return giving high efficiency and very low pressure loss. (Note:—a 1 Torr. increase in pressure loss would necessitate a 10% larger 'Roots' pump).

(b) tandem purifiers to allow continuous operation i.e. no 'down-time' required for regeneration of purifiers

(c) a method for the 1·85°K liquid extraction from, and the cold vapour return to, the bottom end of the refrigerator.

The latter feature creates many advantages over the normal top entry coupling schemes in respect to heat transport from the refrigerator to the cryostat vessels. For this a common 1·85°K liquid supply cold vapour return culvert type transfer pipe is proposed. This gives a common liquid level from the refrigerator to the cryostat vessels; one level control is therefore adequate. The extra liquid surface area in the culvert gives improved control stability. The high heat transfer rate of the superfluid liquid in the culvert reduces the temperature differential between the two cryostats. The heat losses of this composite transfer pipe including its coupling heat losses will be considerably reduced.

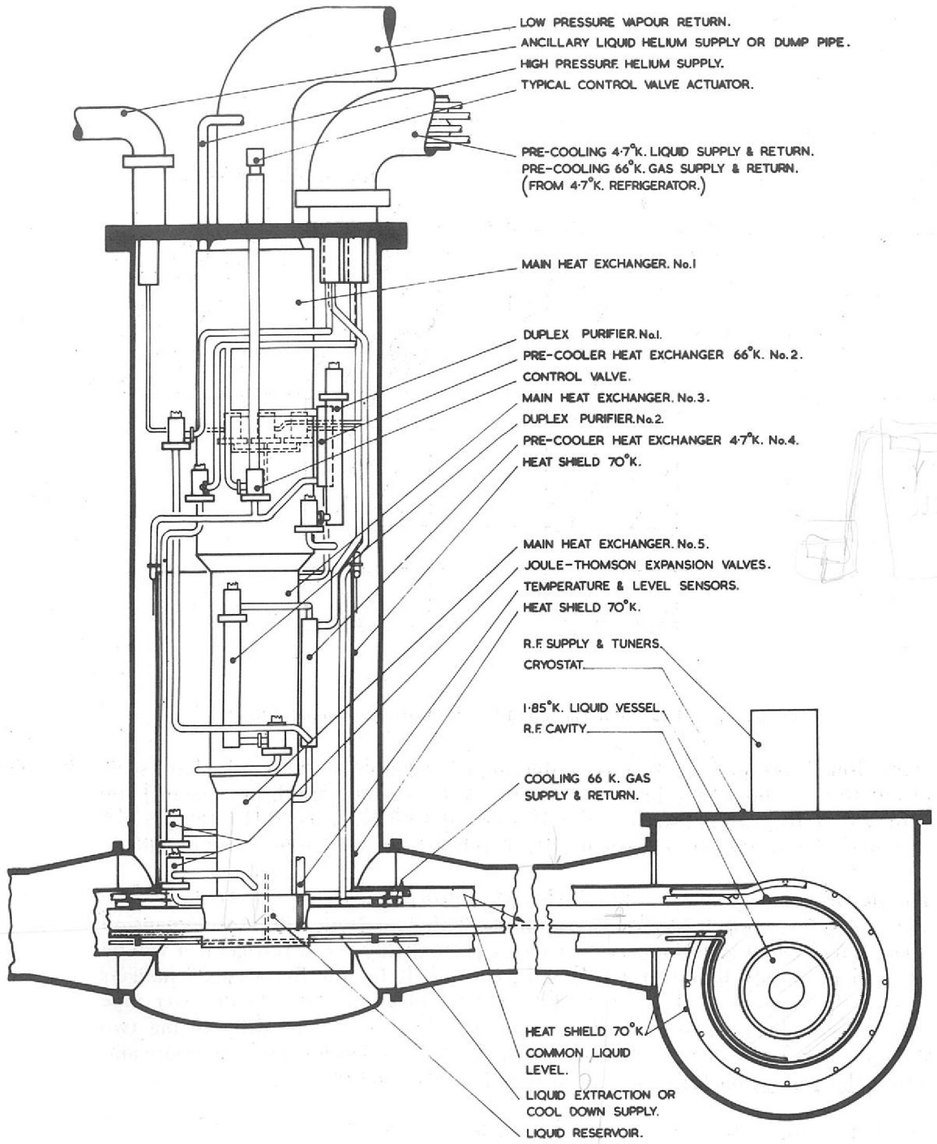

Figure 123. The 1·85°K refrigerator for the superconducting r.f. separators.

Work is now proceeding to embody this proposed culvert type transfer system into the cryostat design, (see figure 123). Problems in design of control valves, level sensors, and sealing methods, all compatible with superfluid helium are being studied and various seals for superfluid helium are to be tested.

From a preliminary study of cryogenic control methods it is considered that the close tolerances of liquid level, temperature and pressure demanded for operation of the r.f. cavities, although difficult, can be achieved.

It is envisaged that the 1·85°K refrigerator when once set will give continuous operation without attention. Further study is being undertaken with the aim of reducing the operational attention necessary for the existing 4·7°K refrigerator plant. Figure 124 shows a typical layout of the r.f. separator in a beam line.

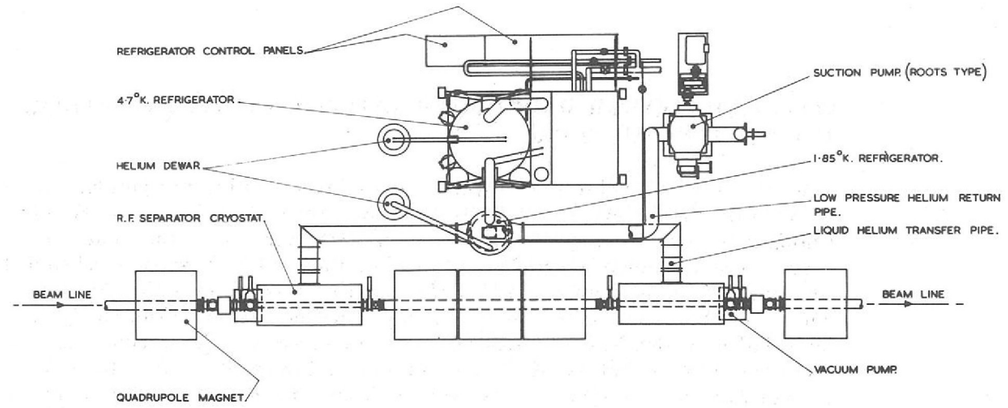

Figure 124. Proposed layout of the refrigeration equipment and the superconducting r.f. separators in a beam-line.

Cryostat Design

A design is completed of a cryostat to house the r.f. cavity. The cavity will be supported by the more rigid encompassing helium reservoir which in turn is supported by thin stainless steel wires to the outer vacuum vessel. The design of this support system, the attachment to the beam-line vacuum pipe and other connections such as r.f. tuners, r.f. power feed and helium vent line have been optimized to give adequate mechanical strength, minimum thermal distortion and minimum conductive heat influx.

A method of assembly of the cryostat has been planned so that the cavity is at all times kept under vacuum or purged with an inert gas to prevent contamination of the lead with which the cavity is plated.

In operation the cryostat will be mounted on a table that can be adjusted in all planes. This will be attached to a base of large mass and the assembly mounted on vibration isolators. Work is now in hand detecting and recording the frequency and amplitude of vibrations encountered in the Experimental Halls to provide information for the selection of these isolators. Operation of the r.f. cavity is susceptible to this type of disturbance.

When the r.f. separator is not operational, or when the helium refrigerator is not working, the cavity is kept below 70°K by cooling with liquid nitrogen fed through a standby cooling loop.

The separator has been designed so as to be suitable for transportation. In such circumstances the cavity and helium reservoir will be locked to the outer vacuum casing and the whole system will be transported either under vacuum or purged with an inert gas.

A design of vacuum system for both the cryostats and the beam line has been completed. Work is under way assessing the strength and permeability of certain coated melinex films to ensure the minimum ingress of contaminants into the cavity through beam-line windows.

Fast Shut-off Valve

In the beam pipe to the proposed superconducting r.f. separator, a rapid closing high vacuum valve will be required to prevent accidental contamination of the separator surfaces. In order to give the necessary protection the valve must close in a time of about 5 ms. The design of this 5 in valve incorporates some of the existing techniques which were developed for the 8 in and 4 in fast shut off valves, but also includes an electrostatic clutch in place of an electromagnetic device to operate the trigger system. A design study for this valve is proceeding.

SELECTIVE CHOPPER RADIOMETER EXPERIMENT FOR ATMOSPHERIC TEMPERATURE SOUNDING.

Since May 1969 a small team of engineers, draughtsmen and technicians have been working on the design, development and environmental testing of the Selective Chopper Radiometer engineering model. A flight version of the model to be manufactured commercially will be mounted on the Nimbus 'E' satellite scheduled for launching in the Spring of 1972. This experiment is a joint project by Oxford and Heriot-Watt Universities and is the only experiment from outside the USA to be included on this NASA meterological research satellite. The satellite will have a circular orbit of 600 nautical miles altitude and inclined at 80° retrograde to the equator in a sun-synchronous orbit with an orbit period of 107·4 minutes. This orbit permits viewing of all parts of the earth twice a day, once near local noon and once near local midnight.

The primary objective of the experiment is to observe the global temperature structure of the atmosphere at altitudes up to 50 km over an extended period of time. It will also make supporting observations of water vapour distribution and cloud cover and it should also be possible under appropriate conditions to infer the size and number density of ice particles in cirrus clouds. This information is obtained by selective measurements of infra-red radiation and the equipment is calibrated by views to deep space (3°K) and to a measured 'black body' radiator in the apparatus.

The apparatus, shown in figure 125, is mounted on the under-side of the satellite with one aperture facing earth. Two other apertures on the side of the housing view space. Radiation from the atmosphere is reflected by the calibration mirror and the off-axis paraboloid mirror on to the rotating chopper mirror. Radiation from space reaches the chopper mirror direct, but at right angles to the radiation from the atmosphere. The incident radiation is divided into four channels; the rotating chopper mirror, which is a circular disk with alternate quadrants removed, splits the radiation into two channels. Dichroic filters (beam splitters), which transmit one wavelength band but reflect other wavelengths, effect the final beam splitting. Due to the action of the chopper mirror the radiation in each channel consists alternately of atmospheric and space radiation.

Observations are made in sixteen spectral intervals utilizing only four detectors (A, B, C, D) by mounting four different filters on each of four disks. Each filter remains in position in front of a detector for 1 second, after which all four disks are rotated by 90° to bring the next filters into position, so that observations in all sixteen spectral intervals are made every 4 seconds. The four filters associated with detector A will give radiance information from 0 to 20 km altitude. The CO_2 cells associated with detector B will give radiance information from 20 to 45 km altitude. Some of the other channels have functions of measuring water vapour content of the atmosphere, determination of ice particle size and density in cirrus clouds and measuring reflected sunlight.

The calibration mirror is to be rotated about every 8 minutes to receive radiation from the 'black body' and in the opposite direction to receive space radiation for calibration purposes. This mirror also moves during the 4 second observation cycle to compensate for the motion of the satellite relative to the region of atmosphere under observation.

The technical problems which have been studied in the engineering model have included the use of dry lubricants for bearings and gears in ultra-high vacuum. The lifetime requirement of over 10,000 hours makes friction and wear the limiting factors for operation in outer space. To test the model under simulated space conditions a large vacuum test tank with nitrogen cooled targets has been designed and constructed. Other equipment simulates all the satellite commands and services and provides the logic and power circuits to operate the mechanisms of the apparatus.

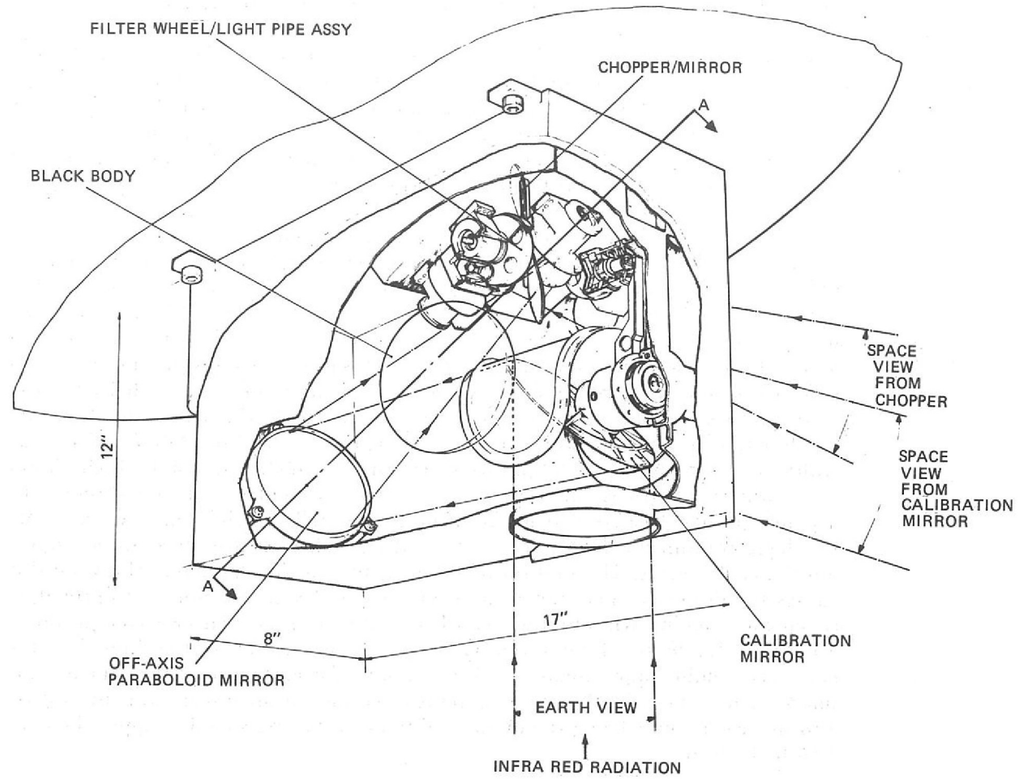

Figure 125. The selective chopper radiometer showing:
(i) the general arrangement, (ii) view on A-A.

MEASUREMENT OF THE ULTRA VIOLET FLUXES OF STARS

The S2/68 Experiment for the ESRO TD1 Project was initiated jointly by the Royal Observatory, Edinburgh (ROE) and the Institute of Astrophysics, Liege. It is the largest of seven experiments on board the TD1 satellite, the latter being the largest and most complex scientific satellite so far produced by ESRO and is to be launched in February 1972. (The name TD1 is taken from the American launch vehicle used which is a Thor-Delta).

S2/68 is an ultra violet reflecting telescope with four photomultiplier detector channels, as shown in figure 126. Ultra violet light from stars is reflected from the off-axis Cervit primary mirror into the spectrometer box. The field of view is defined by slots in the focal plane of the primary mirror. The telescope is fixed inside TD1, the latter having a near polar, sun synchronous orbit and rolling about the sun pointing axis once per orbit. This motion causes the star images to scan across the focal plane slots. A narrow slot allows ultra violet light to pass through to the photometer channel, the passband of which is defined by the combination of photocathode and glass filter; it is centred on 2800Å with a half width of 400Å. Next to the photometer slot is a much wider slot which allows ultra violet light to pass through to an ellipsoidal secondary mirror and thence to a plane grating. Dispersed light from the grating falls on three narrow exit slots the light transmitted by these is reflected by Fabry mirrors into three photomultiplier detectors. The motion of the primary star images across the wide slot causes the dispersed spectrum to move across the fixed exit slots, thus providing spectrum scanning without the use of any moving parts. The wavelength range 1330Å to 2600Å is fully covered by the spectrometer, each of the three detector channels yielding approximately 20 data points for each scan of the primary star image. The data is in the form of photon counts in an integration interval of 148 ms, each count being the number of photons in a passband of approximately 35Å half width.

Figure 126. The S2/68 ultra violet reflecting telescope showing the four photomultiplier detectors.

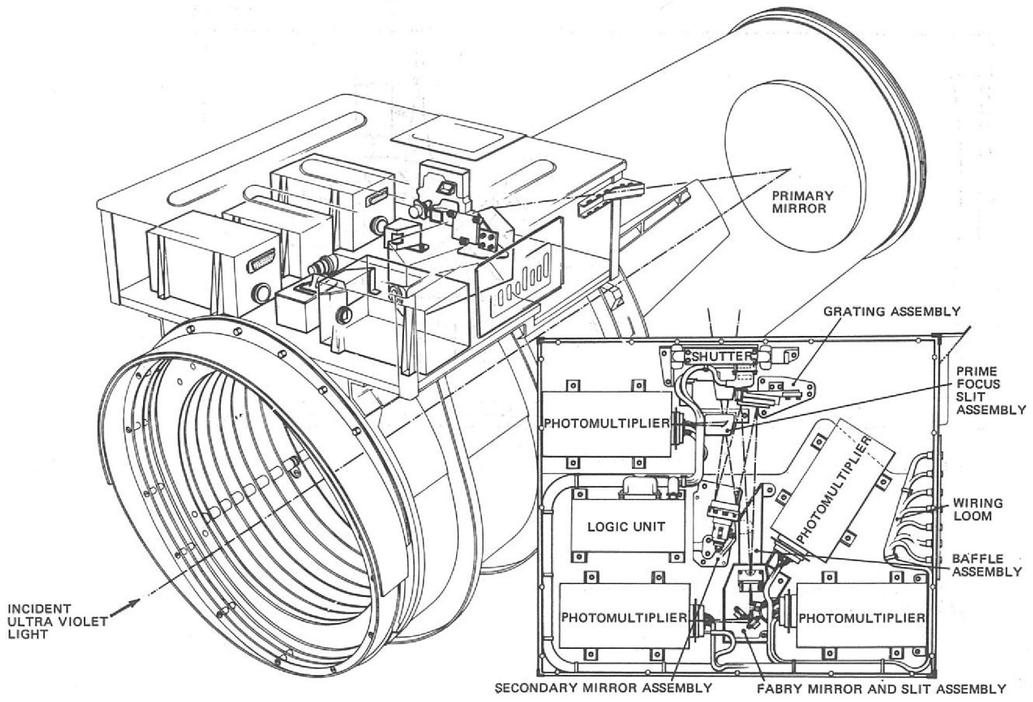

During the six month lifetime of TD1, S2/68 will produce a complete scan of the sky, measuring photon fluxes of stars down to the 9th magnitude. It will be the first complete sky scan with one instrument and will yield a valuable consistent set of stellar fluxes. The data will be particularly suitable for studies of inter stellar ultra violet absorption and its distribution over the sky.

The SRC is responsible for the structure and optics of the instrument (S68) and the Institute of Astrophysics, Liege is responsible for the detectors and filters and associated electronics (S2).

The SRC project team is based at the Rutherford Laboratory, overall control being exercised by a Management Committee. The activities of the project team include the following:

1. General Project management involving such aspects as:
   (a) supervision of the industrial contract, with Hawker Siddeley Dynamics Limited,
   (b) liaison with Liege, European Space Research and Technology Centre (ESTEC) and Goddard Space Flight Centre, USA.

2. Production of detailed specifications for the telescope, optics etc. This is a very important aspect of the project management and requires considerable manpower.

3. Design of the stray light baffle system in conjunction with consultants at University College, London. This is particularly important because TD1 is always in full sunlight and the baffle system must attenuate the solar flux by a factor of at least 10^{14} to enable 9th magnitude stars to be observed. Initial design, based mainly on geometrical considerations, has been subjected to analytical treatment involving multiple ray tracing by computer to derive an estimate of overall system attenuation. By this means the attenuation due to the combination of spacecraft and telescope baffling has been calculated as better than 10^{16}.

4. Design and construction of devices for checking the alignment of the optical system of a development model of the telescope before and after vibration tests and during thermal vacuum tests. Thermal vacuum tests have been successfully completed and have shown that the alignment of the flight model will be within specification in the orbital thermal environment.

5. Design and construction of a portable monochromator-collimator unit for checking the optical performance of the finished telescope. This device is now nearing completion.

6. Laboratory calibration of the flight model. This will be done at ROE where a complex equipment is almost completed. A major component of this apparatus is a secondary standard photomultiplier used to scan the ultra violet beam used for calibration and measure its absolute intensity. This photomultiplier is itself calibrated absolutely against a thermopile in an apparatus constructed at the Rutherford Laboratory.

7. The implementation of a contamination monitoring scheme. The mirror coatings are specially made for use in the ultra violet and are susceptible to very thin contaminating films. A running check is being kept on the state of the mirrors during the 12 months between coating and launch by measuring the ultra violet reflectance of small sample mirrors which accompany the flight mirrors at all times and which were coated at the same time. A precision, vacuum reflectometer, at ROE, is used for reflectance measurements.

THE HIGH FLUX BEAM REACTOR

Prior to 1965 the National Institute for Research in Nuclear Science (NIRNS) supported the use of UKAEA reactors by University scientists for research into the properties of condensed matter. This arrangement was maintained by the Science Research Council (SRC) when it took over NIRNS and currently the SRC supports the work of some 100 scientists and research students in this field. Neutrons of around thermal energies have long been used in solid state physics and their use has been steadily extended in both solid and liquid state studies in chemistry and more recently in biology. For much of this work the special properties of the neutron — its zero charge, its mass, its magnetic moment — give it characteristics of scattering and penetration which lead to information which cannot be obtained in any other way.

It has been recognized for some time that to provide adequate support in future years for this important field, new facilities would be needed which would raise significantly the available beam intensities and provide more experimental space and more advanced research instruments. One possibility would be to build a 100 MW reactor giving a thermal neutron flux of $1{\cdot}5 \times 10^{15}$ n cm^{-2} sec^{-1} (maximum intensity available now in the UK is 10^{14} n cm^{-2} sec^{-1}). The Atomic Energy Authority (AEA) have already prepared a basic design for such a reactor, known as the High Flux Beam Reactor (HFBR), which it was hoped could be constructed as a joint AEA/SRC project. When it became clear that this joint approach was no longer possible, the Council decided to consider adopting the project as a purely SRC one. In May 1970 the Rutherford Laboratory was asked to prepare a proposal for a costed programme of detailed design and project planning which could be undertaken as the next stage of proceeding with the project. This proposal has been prepared with the assistance of the AEA which would be asked to carry out much of the detailed work of the project. It was submitted to Council in December 1970, but no decision has yet been taken concerning the adoption of the proposed project design programme.

As envisaged now, the reactor would be heavy water cooled and moderated using a core of highly enriched uranium 235 aluminium alloy fuel tubes. Twenty seven neutron beam tubes pierce the reflector to the high-flux zone around the core. In order to reduce the unwanted fast-neutron and gamma-ray components in the beams most of these tubes are placed tangentially to the core. Hot and cold neutrons are provided by beam tubes arranged to look at special sections of moderator maintained at the appropriate temperatures. A radial hole pointing directly towards the core provides a high intensity neutron beam having a high epithermal component. This beam hole can be aligned to a 300 m flight path for time-of-flight measurements. The twelve highest-flux holes are horizontal; eight high-angled and six low-angled holes and a sloping "through" hole give a somewhat lower flux. There are 17 irradiation holes in the reflector, and one in the core.

Figure 127 illustrates the present design of the reactor and some of the beam tubes. It would be located at the centre of a large containment building some 150 ft dia and 110 ft high with the main experimental floor extending from the biological shield to the wall of the building.

The whole facility could be constructed over a five year period at a total cost of about £20M. It would eventually require a staff of about 500 and would support some 150 university research scientists.

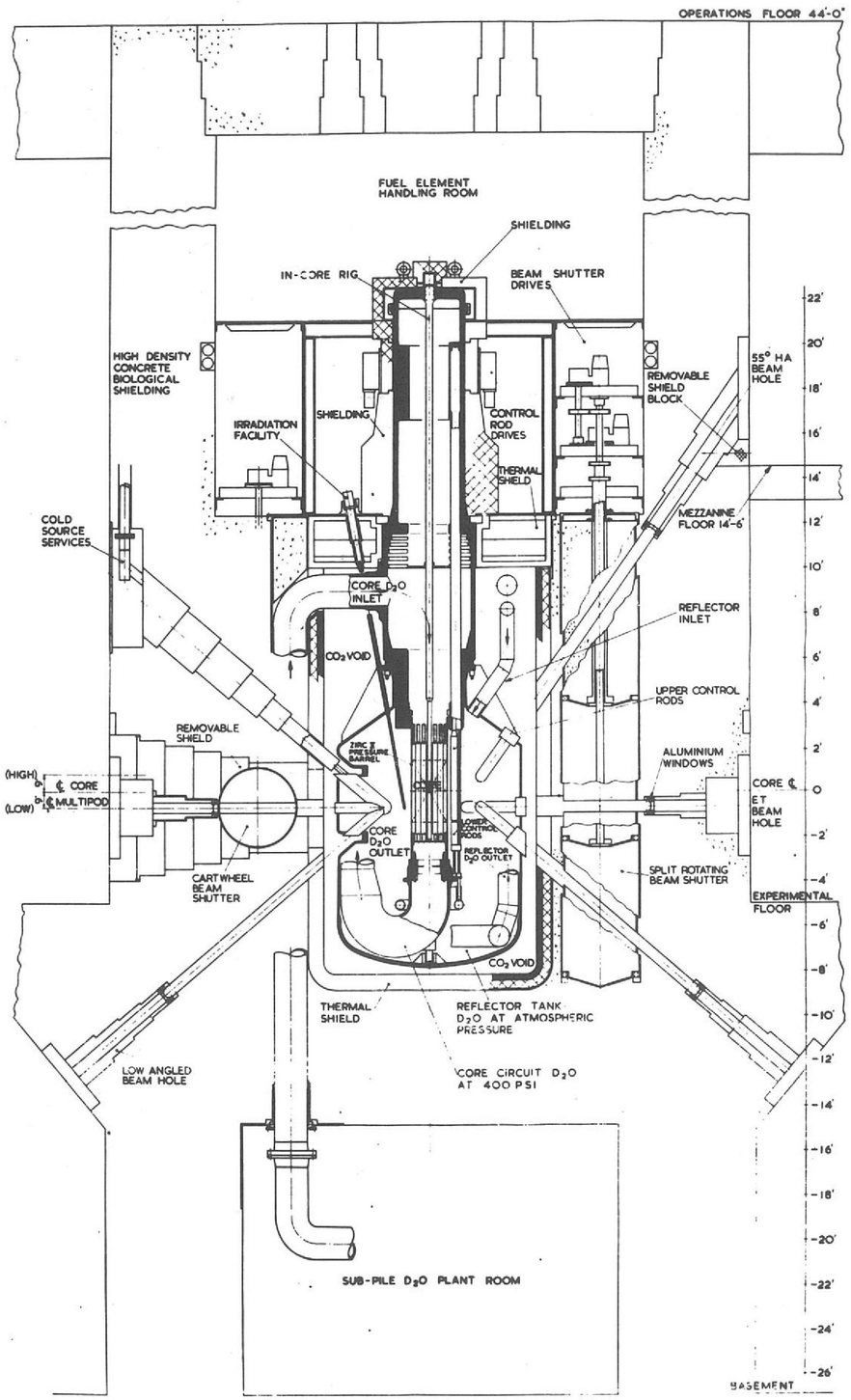

Figure 127. Sectional elevation of the proposed High Flux Beam Reactor. (Reproduced by courtesy of AERE Harwell).

Part of the automatic film measuring machine (HPD II) showing the laser beam used as a light source for the flying spot.

COMPUTER SYSTEMS AND APPLICATIONS

Computer Systems And Applications

(*Ref: 178*) **THE NEW CENTRAL COMPUTER–IBM 360/195**

Approval was received on 10th November 1970 for the purchase of an IBM 360/195 computer, with peripheral equipment, at a total cost of £3·6M. This sum includes the cost of the building extension estimated at £122K.

An Advisory Committee has been formed to advise the Director of the Rutherford Laboratory on Computer Policy. Membership of the Committee represents the respective interests of the Rutherford, Daresbury and Atlas Laboratories. The computer will be available not only to the Rutherford Laboratory but will also be used for off-loading work from the Daresbury Laboratory and computers used at universities for bubble chamber film analysis. Computing facilities for nuclear structure groups and Elementary Particle Theorists will be authorized through the Rutherford or Daresbury Laboratories. A small proportion of time (10 to 20%) will be authorized through the Atlas Laboratory for its own users.

At its first meeting on 18th January 1971, the Advisory Committee approved the following configuration for the computer:

IBM 360/195 CPU + 2 Mega-byte Store
4 Line Printers
Card Reader/Punch
Block Multiplexor
Fixed Head File
2314 Disk Store
3330 Disk Store
8 x 1600 bpi Magnetic Tapes
2 x Dual Density Magnetic Tapes
2 x 7-Track Magnetic Tapes

All of the peripherals (except the Line Printers and Card Reader) are of IBM 370-type.

The Central Computer (CPU, Store, Multiplexors) is scheduled for delivery on 1st November, 1971. This part will be installed and tested without interruption of the 360/75 operation during November and early December. When commissioning is complete the existing 360/75 peripherals will be switched over. The down-time is estimated to be 5 days during the latter part of December.

The 370-type peripherals will not be available until February 1972. A phased programme of installation has been prepared causing as little inconvenience to users as possible during the period February to April 1972.

Work has started on the new southern extension to the computer wing. The new computer area should be available for occupation by mid-August, 1971.

THE IBM 360/75 CENTRAL COMPUTER

Hardware Changes

The small 2311 disks have been replaced by two 8-drive 2314 disk sets. This change has eased maintenance and development, and given better throughput and better facilities for user data. A second console (1052 plus 2150) has been added, primarily to facilitate tape and disk mounting. Additional parallel data adaptors have been put in the two 2701 data control units, for attachment of the terminal IBM 1130 and DDP 516 computers as extra satellites. An IBM 2702 Multiplexor to be commissioned shortly will provide another 12 access points to the 360/75. Six of these will go through the Rowstock Telephone Exchange. The IBM 1130 has been delivered and accepted, and communication between the 360/75 central computer and all its satellites is now reliable. Two visual display units (Tektronix storage tubes) have been attached to the DDP 224 satellite. The data-link to the London Institute of Computer Science has been made bi-synchronous.

Operations

Four-shift working is now normal and 4,000 jobs per week were being done by the end of the year. During the last quarter the overall machine efficiency was about 98%, with CPU utilisation of 88%; 9-track magnetic tapes were mounted 33,000 times. Performance during 1970 is shown in figures 128(a) and (b).

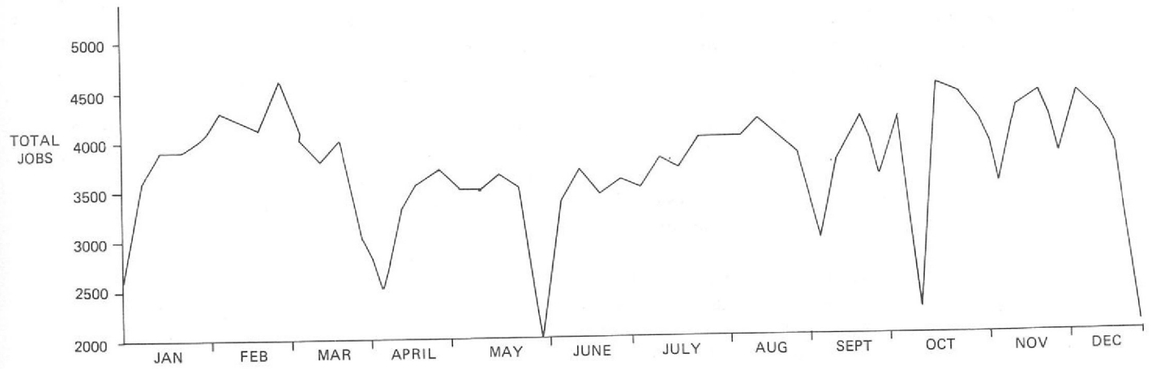

Figure 128(a). Total number of Jobs on Central Computer during 1970.

Figure 128(b). Central Computer machine statistics during 1970.

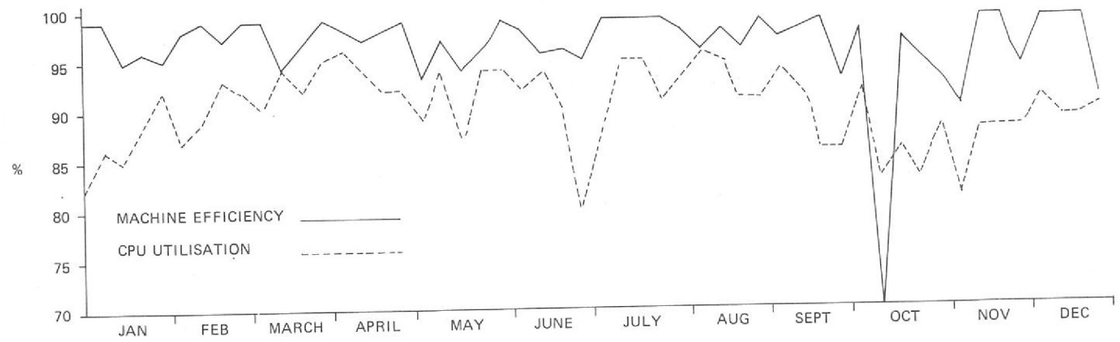

System Software

Release 18·6 of the IBM Operating System was installed in September. After some initial troubles and insertion of PTF's (Program Temporary Fixes), it was decided to obtain in advance some modules of release 19 and retain some of 17, and the resulting system is very reliable. The main reason for introducing 18·6 was software support for the second control console. The sub-system HASP-2 was introduced in December, mainly because of its facility for remote job submission from the interactive terminals controlled by the ELECTRIC program.

Studies on changing the operating system from multi-programming with a fixed number of tasks (MFT) to multi-programming with a variable number of tasks (MVT) are well advanced, and methods of avoiding memory fragmentation (aggravated by very long jobs such as on-line automatic measuring machines) have been developed.

Program Libraries

The CERN and AERE libraries of programs and subprograms have been made available, and facilities developed whereby users can incorporate items from these libraries in their programs. Hitherto subprograms of general use written at the Rutherford Laboratory had been incorporated in the Fortran automatic-call library and the IBM Scientific Subroutine Package. These latter have now been left as they are issued and the Rutherford-written routines form a new library on their own.

The Multi-Satellite Control Program MAST-DAEDALUS

The MAST program, for controlling several satellite computers by the DAEDALUS method, was written during the year and installed in December. It now runs whenever the computer is on, at present handling 3 satellites (DDP 224, IBM 1130, DDP 516. The control program that runs in the DDP 224 satellite is now stored in relocatable form in the 360 disk store, whence it is fetched by a small loader as required. The programs which control the various devices attached to the DDP 224 are also stored in this way, and the space occupied by them in the DDP 224 is freed when the user goes off-line. Data buffer-space is also acquired and released dynamically. Messages destined for fast or slow devices are now handled differently and output data can be buffered if requested.

The present version of MAST is designed to be secure against misuse, and to give the various concurrent users complete protection from each other. DAEDALUS code in the DDP 224 and IBM 1130 is virtually complete for the present level of design, and is being written for the DDP 516.

On-Line Computer Applications

AUTOMATIC FILM MEASURING

HPD I

During 1970 HPD I measured 210,000 events on film from four experiments undertaken by the Bubble Chamber Research Group. The film was exposed at CERN 2 metre chamber (some as long ago as 1966, but originally intended for a different experiment). The total is made up as follows:—

Experiment	Events
$\bar{p}$ p (Momentum range 1·23 to 1·43 GeV/c)	26,000
K^-p (14 GeV/c)	92,000
K^-p (Momentum range 0·96 to 1·36 GeV/c)	90,000
π^+d (4 GeV/c)	2,000
Total	210,000

Over 90,000 antiproton events had already been measured at the start of the year, and the remaining 26,000 were added by the summer to complete this experiment.

A few high energy K^-p events, from film exposed in February to April 1969, were measured last year; and this year saw the remainder done. Early in 1971, however, a further large exposure for this experiment will be made at CERN.

The low energy K^-p experiment over a range of incident momenta is an extension with much better statistics of the first experiment put on HPD I (in 1968) from the Saclay 82 cm chamber in operation at Nimrod. With 90,000 events measured this experiment is well under way.

Film of pion interactions in deuterium was taken in the summer of this year and measurement has barely started. University Groups at Birmingham and Durham are collaborating in this experiment, and the HPD will be used to measure film scanned at Durham.

With some fluctuations the measuring rate has improved during the year to reach 68,000 events in the final quarter, with a peak of over 10,000 events in one week. The average weekly totals of measurements are shown for each month in figure 129 To achieve these figures a regular maintenance schedule has been formulated and carried out. In addition, improvements have been made in the hardware, particularly to the measuring stage hydraulic control and the film transport, which is now more dependable and easier to operate. There has been some development of the on-line control program in the IBM 360/75, mainly for ease of operation but also to reduce the core space occupied (from 160k-bytes to 130k-bytes).

All events measured were first scanned and pre-digitised and the yield from the scanning laboratory has corresponded closely with this progress.

Short test runs have been made with the Minimum Guidance pre-digitising system, though the cost in extra computing time prohibits its regular use on the IBM 360/75 for our present rate of measuring. The normal Road Guidance system from pre-digitising through to HAZE filtering, but excluding KINEMATICS and SUMX, etc. takes some 10 seconds CPU time for four-pronged events, and the Minimum Guidance system nearly twice as much.

Figure 129. Average weekly totals of events measured on HPD I during 1970.

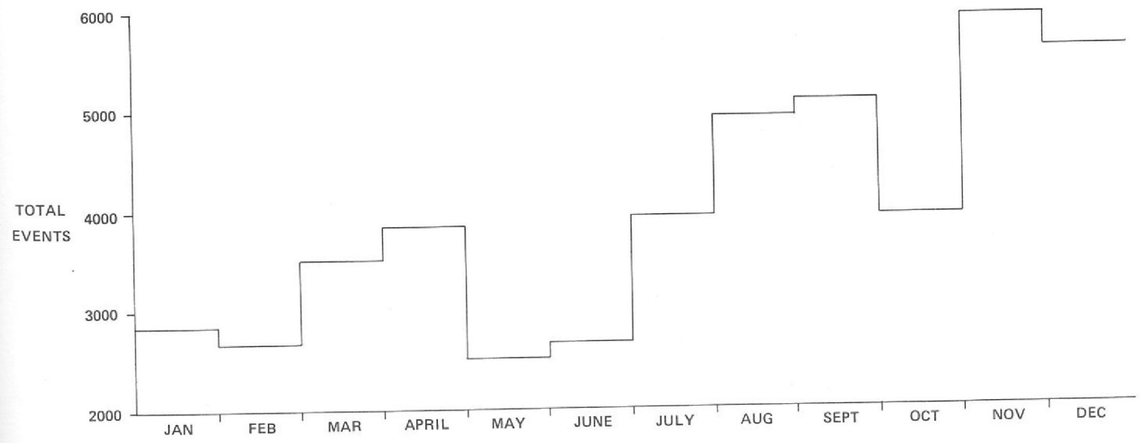

CYCLOPS Film from two spark chamber experiments was measured on CYCLOPS during 1970. During the first half, 120,000 more events were measured from the Cambridge /Rutherford Laboratory experiment begun last year (Experiment 13). In the last quarter, half of the 500,000 events exposed at the Daresbury Laboratory for a π° photo-production study by a Glasgow/Sheffield University group were measured. The rates achieved were about 300 events per hour in the first case, and 600 in the second (due to the small format, with two events on every frame measured).

The combined total of 245,000 frames is well below the capacity of CYCLOPS. The measuring time was less than 720 hours in the year and was due to lack of film. The machine is, however, expected to be fully occupied next year.

A side-line, taking a few hours of CYCLOPS time, was the measurement of film showing action potentials in nerve cells. This arose from an investigation being carried out in the University Pathology Department at Oxford.

HPD II While sharing most of its operating principles with HPD I, the new machine incorporates many improvements made possible by advances in technology. Taken together, these are expected to facilitate measurement of low-contrast film from the new generation of large bubble chambers (using fish-eye optics and Scotchlite illumination) on films up to 70 mm wide, and to improve the measuring rate by up to a factor of two.

The new light source is a 200 milli-watt Argon laser (blue-green) which provides a spot at the film 300 times as bright as in HPD I, with a width of only 3 μm and excellent signal/noise ratio. This was developed in collaboration with Imperial College London and is expected to be the model for other laboratories, both within the UK and outside.

The disk speed in HPD II is 6,000 rev/min and the possibility of operating at 9,000 rev/min is under investigation. This compares with the 3,000 rev/min speed of HPD I, and is faster than any other in Europe. The film transport system will handle the new standard 300-metre spools, and position individual frames with respect to Brenner marks or perforations.

A dedicated DDP 516 satellite computer, linked to the central IBM 360/75 and running under the MAST-DAEDALUS system, has been fully exploited in designing the HPD II circuits. Data checking, formatting and some data reduction is carried out by the DDP 516, which also supports a graphics unit comprising two Tektronix 611 storage cathode ray tubes, a keyboard, and interactive tracker-ball. This is a very flexible system, with much scope for development.

HPD II digitised its first frame of bubble chamber film in December. The first production measurements of spark chamber film from an experiment on the CERN Intersecting Storage Rings are expected in Autumn 1971.

VISUAL DISPLAY SYSTEMS–'COMPUTER GRAPHICS'

IDI Display and Light Pen (Ref: 157) Operation of the IDI display and light pen system continued throughout the year. Apart from a little tidying-up, there was no change to the patch-up process for bubble chamber events measured, with pre-digitised Road Guidance, on HPD I.

Two new programs were developed, the first for patching-up failed spark chamber events from CYCLOPS, and the second (not yet complete) for bubble chamber events measured with Minimum Guidance.

The main users were the Bubble Chamber Group. Tracks from over 40,000 events, measured on HPD I, which had failed the criteria set in the subsequent HAZE/

GEOMETRY processing were patched-up. Up to 50 hours per week were used, and usually about 60% of the faulty events were rescued.

The IDI system was also used to rescue 2,000 failed events from spark chamber film measured on CYCLOPS, and to display events from a non-visual spark chamber experiment for viewing and labelling tracks. Both of these applications were subsequently transferred to the DDP 516 graphics terminal.

Computek Display The Computek display system has been developed to provide easy and immediate visual access, initially on a Computek 400 storage display, to data generated in the IBM 360/75 computer. Files of pictures (which may be line drawings, scatter plots, text or a mixture of all three) are created by batch programs, incorporating standard graphics routines, running in the 360/75.

The files are stored on disk and can be displayed at any linked graphics terminal by a standard program, now part of the ELECTRIC system and permanently loaded and available.

The system has already been widely used: some examples by High Energy Physics groups are the display of SUMX output while Applied Physics groups have utilised the facilities as an aid to design of bubble chambers and superconducting magnets. The Beams Theory group is using the display in developing an interactive beam-design program based on TRAMP. Figure 130 shows some applications.

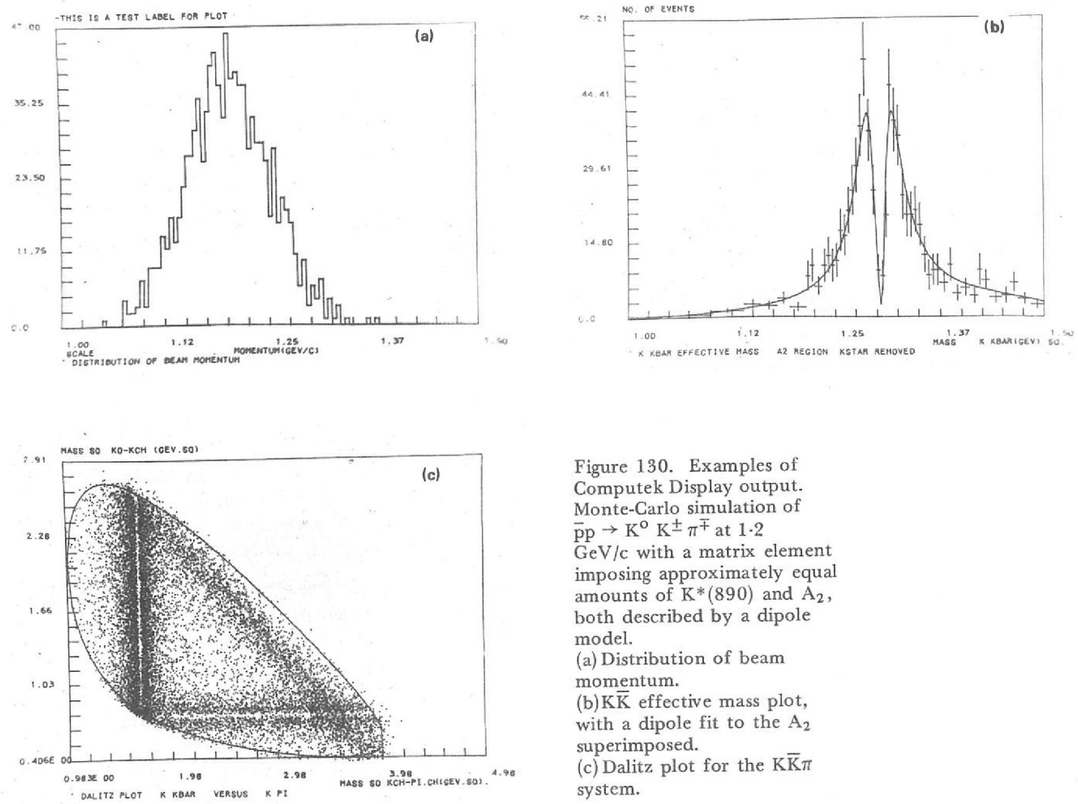

Figure 130. Examples of Computek Display output. Monte-Carlo simulation of $\bar{p}p \to K^\circ K^\pm \pi^\mp$ at 1·2 GeV/c with a matrix element imposing approximately equal amounts of K*(890) and A_2, both described by a dipole model.
(a) Distribution of beam momentum.
(b) $K\bar{K}$ effective mass plot, with a dipole fit to the A_2 superimposed.
(c) Dalitz plot for the $K\bar{K}\pi$ system.

Other developments include the 'interception' of data intended for the Atlas Laboratory's Stromberg-Carlson plotter, or for the line-printer on the IBM 1130 terminal computer, with the object of providing immediately a 'first look' at data.

SUMX–Graphics Package

The statistics program SUMX has been modified for use with the graphics display facilities. Histograms and scatter plots produced by SUMX can now be viewed at the graphics terminal, and examples are shown in figures 130a, b and c.

A routine to minimise functions of several variables has been added to this SUMX-Graphics package, so that analytic functions can be fitted to histograms of experimental date at the end of the SUMX run. The fitted function is displayed superimposed on the data, and figure 130b, shows an application.

DDP 516 Graphics Terminal (Ref: 142)

A stand-alone interactive graphics system has been developed. It consists of an 8k DDP 516 computer, a tape drive, a disk unit and two consoles each comprising a Tektronix 611 storage tube, a keyboard and an interactive tracker-ball. An operating system has been written which permits simultaneous operation of all the peripherals.

At present, the facility is used for Experiments 1 (page 26), 13 (page 44) and 14 (page 45). An example of the interactive feature is shown in figure 131, where the CYCLOPS digitisings of an event from Experiment 13 are displayed. The crosses indicate the patch-up points supplied by the operator (using the tracker-ball). The event reconstruction program in the 360/75 uses these points for guidance. About 30 events may be patched-up per hour.

Possible developments of the system include expansion of the computer memory, a data link to the IBM 360/75, and acquisition of additional graphics consoles.

COMPUTER GRAPHICS AS AN AID TO DESIGN

Design of Bubble Chambers and Superconducting Magnets

A wide variety of computer programs have been written to aid the research and design of bubble chambers and superconducting magnets. A substantial reduction in the amount of work involved in studying computer output and in improved understanding of results can be achieved by use of graphical output. The Computek display system has been applied to several applied physics problems, some examples of these applications are now given. In figure 132 is shown the predicted growth and recondensation of a bubble compared with experimental measurements from the DESY bubble chamber operating under the same conditions. The prediction incorporates vapour expansion and compression and heat transfer by conduction and convection.

Figure 133 shows the geometry and field prediction of a superconducting magnet for a polarized target experiment. In this design the coil shape had to be optimised to give maximum magnetic field at the centre whilst maintaining a wide angle aperture for experiments. Because of the dependence of superconductor current density on magnetic field, the performance of the magnet is limited by the maximum field at the coil windings. It is a feature of this program to search for the peak field and display the results on the screen immediately below the geometry. Further shapes can be tried by resubmitting the program remotely from the terminal.

Finally in figure 134 is shown a picture of a beam entry optimisation. The results of a trajectory plotting program called TOPIC are shown, this program will draw the geometry of a magnetic device and compute and plot the path of charged particles in a non uniform magnetic field. The user stipulates the initial conditions and submits the job remotely. After processing by the 360 batch the pictures can be retrieved, studied and new initial conditions decided in order to improve the beam entry. Special features include loss of energy by ionisation whereby the position along the track at which the beam reaches a prescribed momentum is flagged.

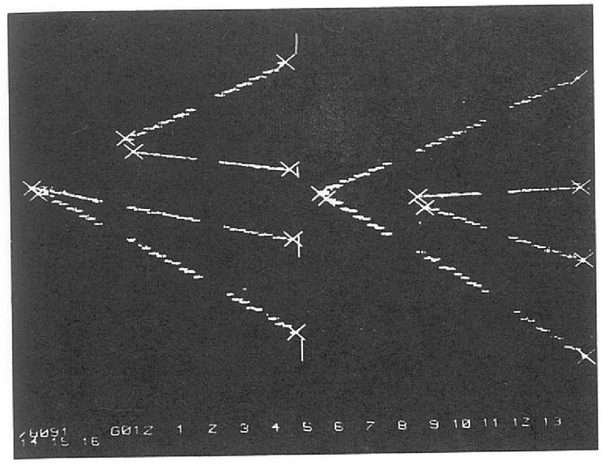

Figure 131. An example of the interactive graphics display showing the CYCLOPS digitisings of an event from Experiment 13.

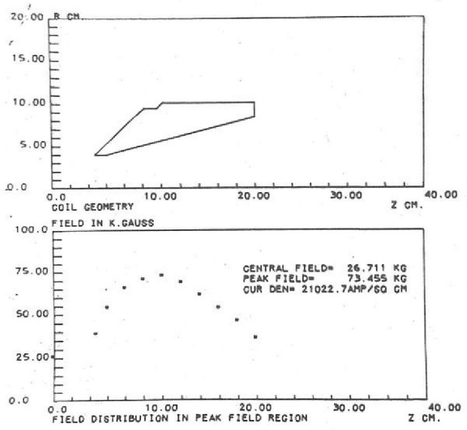

Figure 133. Optimisation of superconducting coil geometry.

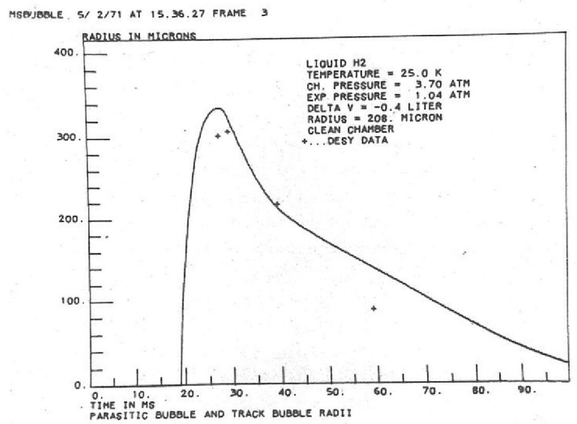

Figure 132. Predicted growth and recondensation of a bubble compared with experimental measurements.

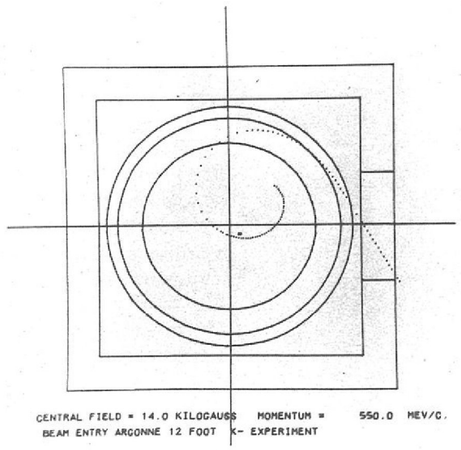

Figure 134. Tracking program for optimising beam entry.

Beam Design Programs

An interactive visual-display (graphics) program is being developed to complement the existing and widely used beam optics programs, TRAMP and IPSO FACTO. Initial definition of the beam is based on TRAMP, but thereafter the flow of the program has been completely changed to simplify the task of adding extra facilities as their need becomes apparent.

Output is routed via the DDP224 satellite computer either to the Computek display for graphical output, or to an adjacent typewriter. Communication with the program is via the typewriter keyboard. Modifications to the beam-line or automatic numerical matching can be performed and the resultant effect on stored particle trajectories can be displayed rapidly. This interactive aspect of the program is its key feature and should greatly facilitate the task of beam design, and the development of tuning procedures for existing beam-lines. An example of graphic output from the program is shown in figures 101 and 102 referring to the stopping K beam described on page 130.

EXTENSION OF ON-LINE SYSTEMS

New Satellite Computers

In addition to the DDP 224, through which all on-line users have communicated with the central computer so far, two new satellites will soon be in full operation. They are a DDP 516 dedicated to HPD II, and an IBM 1130, which will be situated in the Nimrod Experimental Area, and function as a remote terminal. In due course the IBM 1130 used for gathering data from the scanning and pre-digitising machines will also be linked to the central computer.

A new multiplexor is being built for the DDP 224, to allow simultaneous operation of the existing typewriter consoles and connection of up to a total of 16 similar devices.

The terminal IBM 1130 is at present connected to the 360/75 by a short distance link, and the magnetic tape unit, line printer and card reader are being commissioned using an operating system similar to that on the DDP 224. A unit has been added to the terminal computer to allow connection of a further eight devices. One is a multiplexor, connecting users in the Experimental Area via their CAMAC systems. Another is an 880 kilo-bit per second 'serial' link, capable of operating over distances exceeding half a mile, which will be used when the terminal computer reaches its site in the Experimental Area (500 yards from the central computer).

Once established there, the terminal will allow users to submit jobs or data (cards or 7-track magnetic tape) to the 360/75 and receive back output on an 80 lines per minute printer. It will also be possible to connect various user terminals (teletypewriters, small computers, or visual displays).

A direct link between the DDP 516 computer (controlling HPD II) and the central computer has been established and is operating satisfactorily. Current hardware, including a newly-built multiplexor for the direct control feature of the IBM 360/75, allows the connection of up to six satellite computers.

The ELECTRIC Program

A program named ELECTRIC has been developed to provide remote job entry to the central computer from typewriter consoles which will be distributed around the Laboratory. It operates under the DAEDALUS message switching system and gives a general service. A user may create and edit files containing the text of programs, job control statements or data, and may submit a file as a job for batch execution. The program also allows monitoring of the subsequent progress of the job.

In addition to these normal facilities for conversational remote job submission, the program allows the user to hold files in the form of text with associated editing instructions. The files can then be used in their original text form or as updated by their associated edit instructions (or sub-sets of these instructions). A comprehensive set of manipulations of both text and edit instructions is available.

ELECTRIC is also intended to help in the following problem situations which often arise in computing:

(i) Keeping several slightly different versions of the same big basic program.

(ii) Supplying new versions of programs to outside users who have themselves modified the previous version.

(iii) Difficulties when more than one person is working on a program.

The system has been in use with a limited number of typewriter consoles since mid-1970.

DATA ANALYSIS SOFTWARE

Bubble Chamber Programs

Maintenance and modifications of the existing Road Guidance system, and development of the Minimum Guidance system, have been the main activities this year.

Automatic Track Matching was introduced early in 1970, and has been used in processing all of the three experiments measured since. No other changes of principle have been made to the production version of the date processing program, though there have been numerous small changes.

Data safety has been considerably improved by an automatic file protection program now in regular use. Tapes containing data accumulate at several stages of HPD production measurement, e.g. digitisings prior to week-end HAZE runs, and geometry input prior to merging with output from the patch-up system, which may not be available for a week or two. To prevent tapes being accidentally overwritten a record is held (on disk) of the current use of each HPD tape, and programs which output data to tape have been modified to check that the tape is available for use, and to update the record. A list of free tapes can be generated at any time.

In the Minimum Guidance system, two major problems are the number of digitisings produced (two to six times as many as in Road Guidance) and the CPU time taken by the filter program (about three times Road Guidance). A method under test would reduce the digitisings by defining, at the measuring stage, a cone containing all tracks of an event, and gating-out other digitisings.

A sample of events from the low-energy K^-p experiment is being used for Minimum Guidance tests. The main problems arising in matching tracks found in the three views have been due to non-interacting beam tracks close to the production vertex, and (in multi-vertex events) tracks being picked up by the filter program at more than one vertex. For example, the track from a Σ decay may well be picked up at the production vertex and at the decay vertex.

A patch-up system using the IDI display and light pen has been developed, and has been successfully applied to 'rescue' more than half of the failed events in a test batch. The region of the picture close to the vertex is displayed, but without digitisings of tracks already successfully matched. The operator marks three points on tracks chosen (as in Road Guidance), and filtering then proceeds as in Road Guidance.

Spark Chamber Programs

The general filtering program, which finds tracks from CYCLOPS digitisings, has been modified to search for curved tracks by performing a parabolic fit for each track. A version of the program is being used to find tracks and fiducial centres from digitisings of film taken at the Daresbury Laboratory for a Glasgow/Sheffield University photoproduction experiment. The program is now in a production state for this experiment and runs will start soon. Tape output will go to the Daresbury Laboratory for final processing and analysis.

Production runs on automatically measured events in Experiment 13 (page 44) ended in June 1970, and all remaining runs use information from events patched-up, either on the DDP 516 Graphics terminal, or on digitising tables. In future experiments, it appears desirable to reconstruct sparks from CYCLOPS digitisings, and then link sparks together to form tracks.

A program used in an earlier experiment has been developed, and tests with K13 data have shown the method is faster (by a factor of two) than the direct linking of digitisings to form tracks. It also facilitates correlation of tracks between different views. However, the direct method is more successful in finding tracks, and further work is being done on the two-stage program to improve its success rate.

Many spark chamber experiments require momentum determination from particle trajectories through regions of non-uniform magnetic field. To minimise computing time for such analysis, it has proved valuable to express the momentum as a function of entry and exit parameters. A program has been written to find appropriate functions for Experiment No. 16 (page 48) and tests on data generated by a Monte Carlo program have been satisfactory. A program for expressing inhomogeneous magnetic fields in terms of Chebyshev polynomials is under development, and should be widely applicable.

USE OF SMALL COMPUTERS

Small computers are in extensive use in the Laboratory. Their application ranges from routine data-logging for complex apparatus to control of sophisticated devices such as the 'flying spot' film measuring machines. Some of these computers have been referred to in various chapters of this Report and those in use as on-line satellites to the central 360 computer are described in the immediately preceding sections of this chapter. The use of other computers are briefly described below and a complete summary is presented in Table 18.

High Energy Physics Experiments using electronic techniques

The most common application is in the recording of raw data and continuous monitoring of the performance of counters and spark chambers. These functions are carried out in parallel. Without such a service most modern experiments requiring large statistics and high data collecting rates, and using large numbers of detectors, would be impossible. Some experiments are able to analyse, at least partially, their raw data in between each beam pulse from Nimrod, e.g. reconstruct the topology of an event to see if it is of the required category. This speeds up the data analysis time considerably.

The advent of the CAMAC electronic system will enable control and data-logging of beam line magnet currents to be included in the computer duties. This will further increase the data-collection efficiency.

Beam line Control

The extracted proton beam X3 was set up using a computer to perform magnet scans to optimise the beam. This proved to be a very efficient operation and plans are in progress to enable a similar procedure to be used for the K9 beam.

Bubble Chamber Control

A computer system is being developed for data-logging and to control the chamber operation.

Film Analysis

Scanning and road-making of bubble chamber events is carried out on-line to a small computer which checks and records the data. A future development may be the direct connection of this computer to the central computer so as to perform a more detailed quality-control of the data.

Table 18

SUMMARY OF THE USE OF SMALL COMPUTERS

Computer	Application
DDP 224 (360 satellite)	HPD I; CYCLOPS; IDI light pen and visual display; COMPUTEK display; typewriter consoles, etc.
DDP 516 (360 satellite)	HPD II system.
IBM 1130 (360 satellite)	Terminal computer to be located in experimental area. Typewriter consoles; direct data-links between central computer and experiments.
IBM 1130	Bubble chamber film scanning and pre-digitising machines.
DDP 516	Graphics device for spark chamber film analysis.
PDP 8LA	Control of conventional bubble chamber film-plane measuring machines (not yet operational).
PDP 5	Development in Nimrod area.
PDP 8	Control of X3 beam (also linked to PDP 5).
PDP 8	Control of K9 beam.
PDP 8–I	Data-logging and control of 1·5 m hydrogen bubble chamber.
DDP 516	K12A (experiment 9, page 38).
DDP 516	K13 (experiment 13, page 44)
DDP 516	π9 (setting up).
DDP 516	Intermediate Boson Experiment, to be run at the ISR, CERN (experiment 18, page 51).
Ferranti Argus 400	K15 (experiment 8, page 36).
PDP 8	π10 (experiment 32, page 68).
IBM 1130	π8 (experiment 16 and 17, pages 48 to 50).
PDP 9L	$\bar{p}p$, at CERN (experiment 10, page 39).
Modular 1	Electronics: testing of CAMAC modules and CAMAC systems used in experiments.

View of the Laboratory from the main entrance.

TECHNICAL AND ADMINISTRATIVE SERVICES

Technical and Administrative Services

RADIATION PROTECTION

Personal Dosimetry

The six-monthly issue of thermo-luminescent dosimeters (TLD) to lightly exposed persons continues as a successful routine service, and has been extended to include those exposed to fast neutron radiation as well as beta gamma radiation. A new holder, designed and supplied by AEE Winfrith, is gradually replacing the 'home-made' holder originally used. The dose response of Li^7 F/Teflon discs (the standard whole body beta gamma sensitive TLD used at the Laboratory) to Co^{60} gamma radiation has been measured over the whole of the usable dose range i.e. up to a mega-rad.

The two element dosimeter (neutron track film plus slow neutron sensitive TLD), designed to overcome the neutron spectrum dependent response of the track film alone, is now issued to all personnel exposed to the prompt leakage radiation of Nimrod – the use of the track film alone being discontinued.

At November 1970 regular dosimeter issues were as follows:

Beta gamma films (monthly issue)	460
Beta gamma TLD (6 monthly issue)	160
Fast neutron films plus slow neutron TLD (monthly issue)	310
Beta gamma TLD plus slow neutron TLD (6 monthly issue)	180

As in previous years the personnel engaged in the maintenance and repair of Nimrod continue to be the most heavily exposed group at the Laboratory but none, however, is expected to exceed the permitted dose for the year.

Environmental Health Physics

There have been no new problems associated with the operation of Nimrod: the X2 extracted beam blockhouse has continued to be the main cause of significant prompt leakage radiation particularly when operating at lower than normal proton energies. There has been no significant change in the pattern of induced activity either in or near the machine or the extracted proton beams.

There have been no requirements during the year to handle work involving significant amounts of loose contamination in the Radioactive Workshop (R52) but there has been an increase in the unsealed source usage of the Radiochemistry Wing of R34.

Radiation Studies

During the year the angular distribution of the lower energy secondary particles emitted from targets in extracted beams was examined in detail. Measurements with activation detectors and film, thermo-luminescent and pressure dosimeters were made around targets of Cu, 'Heavy alloy' (mainly W) and Al bombarded by 7 GeV protons (Nimrod X3 beam) and also around a Cu target with 24 GeV/c protons (CERN PS e7 beam). The dose and secondary particle production data obtained show excellent agreement, for angles up to about 3°, with both the predictions of the Ranft-Trilling empirical extrapolation formula and Ranft's calculations from the thermodynamic model. Differences at larger angles arise from using models of proton-proton interactions to predict yields from proton-nucleus interactions.

A high-resolution gamma spectrometry facility has been developed, using a 25 cm^3 Ge(Li) crystal and a Victoreen-SCIPP 1600-channel analyser. The system is to be used for studies of radio-nuclide production in well-developed hadron cascades and to assist the work of isotope identification in operational health physics. Computer programmes have had to be developed to simplify handling the spectral data. Analysis of these data is carried out using the SAMPO routine of Routti (LRL Berkeley), which has been modified for use on the RHEL IBM 360/75.

These fields of study have both increased the understanding of problems of shielding design, residual activity patterns and radiation damage around Nimrod, and have formed part of the RHEL contribution to the Radiation Problems Group of the CERN 300 GeV Design Study.

Correlation and interpretation of the results of activation detector measurements in the stray radiation field outside the shielding of Nimrod have continued, and methods of dose estimation from such measurements have been critically assessed.

Radio-biological Pion Irradiation Facility

A low momentum beam line, which is intended primarily for radio-biological and dosimetric studies using stopping negative pions, was built during the summer. This beam line (π 11) lies at 94° to the Nimrod X3 extracted proton beam and shares a target with the π 8 and K15 beam lines. π 11 was designed by the Radiation Protection Group who have set it up and measured the beam parameters, which have largely reached the required values. Preliminary tests showed that the beam can provide dose rates in the stopping pion peak of 20 rad per hour, of which less than 15% is due to beam contamination. Preparations for the first biological experiment are now well advanced.

SAFETY

As in previous years the surveillance and inspection of potentially hazardous situations and apparatus has been the main accident prevention activity of the Safety Group. Tours by parties of safety professionals augumented by a member of the Safety Committee have continued. Publicity displays and "Safety News" sheets have emphasised new and existing sources of hazard. A completely new edition of the Safety Handbook was prepared during the year for distribution to all staff and visitors.

During the year reported injuries involving Laboratory staff totalled 126 (1969 total 126) of which 11 (15) resulted in lost time, the average absence of the latter being 18·8 (20·1) days. The causes of the accidents were:—

Handling goods	25
Stepping on or striking objects	28
Falls of persons	22
Use of hand tools	21
Machinery	4
Falls of objects	9
Electric shock	1
Miscellaneous	16

A nationally used method of representing injury incidence is to compute the Injury Frequency Rate which is defined as (number of injuries x 100,000)/(number of man hours worked). The figure of 100,000 is the number of working hours in an average man's career. The Rutherford Laboratory figures are 4·57 (4·61) for all injuries and 0·4 (0·55) for lost time injuries.

The number of items registered with the Safety Group and requiring periodic inspection increased once again, the total being 4,407, a 13% increase on 1969. The figure was made up as follows: lifting tackle 2,341, lifting machines 392, pressure vessels 975, high voltage equipment 408, breathing apparatus and safety equipment 139, fire prevention 49 and safety valves 103. The latter were included in a new service introduced during the year to test, set and register all safety valves used at the Laboratory. The total number of inspections of registered items was 7,780 (1969 total 6,498).

ENGINEERING SUPPORT SERVICES

A large fraction of the Laboratory's engineering and technical staff are integrated into the project teams that execute the Research and Development programme described in the foregoing sections of this Report, and their contributions to these projects are, whenever possible, included there. In addition, there are several units which provide support services to the Laboratory at large; the year's work in this field is reviewed below.

Experimental Equipment – Manufacture and Installation

Development of winding techniques for superconducting magnets continued and 26 coils were made for d.c. superconducting quadrupoles. Methods suitable for a.c. dipole magnets have also been examined, as have constructional techniques for superconducting energy storage systems. Fabrication methods for cementitious insulated magnets have been carried to the stage where a magnet has been successfully constructed by a commercial firm.

Power supplies for the XM9 and RX3 magnets of the Nimrod X3 extraction system, consisting of a 21 kA and a 10 kA regulator with the associated generators, switchgear etc., were installed in the magnet room area; supplies have also been provided for the homopolar generator which will be the permanent current source for XM9. Experimental Hall 3, as described elsewhere in this Report, is now entering phase II of its development and 75 additional magnet power supply rectifiers, of ratings up to 200 kW, have been installed.

Electronic Services

170 different printed circuit boards were designed. Many of these were special termination boards for wire spark chambers. The precision required cannot be achieved using conventional methods (e.g. etching) and it was necessary to use optical line generation and chemical milling techniques. Manufacture of electronic units to a total value of over £300,000 was undertaken. About two-thirds of this was done outside, the remainder in the Laboratory's prototype and small production shops. The largest single job done internally was the bench check-out unit for the Nimbus E satellite experiment.

The new film measuring machine HPDII, incorporating a laser light source, has been commissioned. New input and digitising electronics were developed for this machine. Other support has been provided for maintenance of the operational film measuring devices and data aquisition equipment used in experiments on Nimrod.

Figure 135. Experimental Halls 1 and 3.

Figure 136. Building R1. Main office and laboratory block.

Buildings – Construction and Provision of Services

The major building schemes initiated during the year have been associated with Building R1. Additional plant rooms and storage spaces for track analysis and data processing activities have been provided by extensions to the east wing. A large ground floor extension on the south-east corner will house the IBM 360/195 central computer which will replace the present 360/75 late in 1971.

Improvements to services have been carried out in several areas. Air-conditioning plant has been installed or upgraded in the scanning laboratories, parts of the bubble chamber area and the Nimrod magnet hall. Heating and water supplies in the R18 and R56 extensions and at The Cosener's House have received attention, as have cooling supplies to R8, R9 and the Atlas Laboratory. Electrical installation work has also been called for in these and other areas.

Mechanical Manufacturing Services

Mechanical manufacture ran at a rather higher level than last year; 850 jobs were undertaken in the Laboratory's workshops and 1,350 externally, the value of the latter being in excess of £350,000.

Helium Recovery

Large quantities of helium are used in the Laboratory – in liquid form for superconductivity studies and in gaseous form in spark chambers. Recovery of 'waste' helium continues to be an important activity. Some 75,000 litres of liquid helium were issued during 1970, an increase of about 50%. Nearly three quarters of this was recovered for re-liquefaction.

ADMINISTRATION

Housing

The demand for furnished accommodation has continued to be high, both at the Laboratory and at CERN. The local demand has substantially exceeded the capacity of the Laboratory-owned houses and flats. Numbers of staff at CERN have increased (following a drop last year) as a result of preparations for the Laboratory's experiment on the ISR. 24 flats (half of which are privately owned) are now occupied.

Office Services

The acquisition of new equipment (suitable for A3 size printing) and alterations to the Reproduction area have made it possible to execute internally a higher fraction of the jobs undertaken, as well as a higher number of jobs in absolute terms. Among the documents printed internally were 31 Preprints, 14 Memoranda, 15 Stores Catalogues and 4 Theses.

Finance In the financial year 1970/71, the total Laboratory expenditure was £8·05 million, of which £1·1M was for capital items and £6·95M was recurrent. Corresponding figures for 1969/70 were £7·3M, £1·1M and £6·2M. The total expenditure is conventionally subdivided in the table below, the figures in brackets being for last year.

	£ million
Staff Expenditure (salaries and wages, SET, insurance, travel etc.)	2·91 (2·51)
Research and Development (see below)	4·40 (3·72)
Plant and Equipment (chiefly major components such as beam-line magnets)	0·71 (0·86)
Building Works	0·03 (0·21)
	8·05 (7·30)

The £4·4 million R and D expenditure can be further subdivided to show the cost attributable to each Division and to certain other items. This breakdown is shown in the pie chart (figure 137).

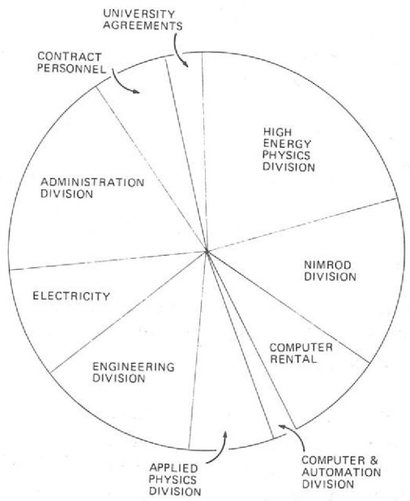

Figure 137. Breakdown of the £4·4 million R & D expenditure.

Administrative Computing The year under review has seen a further expansion of the use of the Laboratory's computer for administrative calculations and record-keeping. Salaries of monthly paid staff are now calculated by computer, and crediting of individual bank accounts is done by writing a magnetic tape to be read by the clearing Bank's computer in London.

Extensive revisions of programs have been necessary to cater for the introduction of decimal currency, and the opportunity was taken to incorporate several improvements which had become desirable in the light of operational experience. Training of administrative staff in computing techniques by attaching individuals to the computer section has continued. The intention is to enable the staff who will be using programs to modify and update them themselves, thus leaving the computer section free to develop new programs. The Laboratory is also playing a full part in the SRC Administrative Computer Committee at which the main topics discussed have been personnel records and the use of terminals.

Table 19

Staff Numbers 1970

The staff position at the beginning and end of the year.

	Opening Strength 1.1.70	Changes during 1970		Closing Strength 31.12.70
		Gains	Losses	
PROFESSIONAL				
Senior and Banded Staff	23	2	1	24
SO class	65	14	5	74
Research Associates	48	29	28	49
Exp. O. class	116	13	11	118
Engineers I, II, III	99	13	5	107
ADE	5	0	1	4
Total Professional	356	71	51	376
ANCILLARY				
SA and SSA	51·5	13	18	46·5
Draughtsmen	41	4	2	43
Technical class	200	7	14	193
Non-Techs. and Stores	44	0	2	42
Executive	30	6	6	30
Librarian	1	0	0	1
Clerical	47·5	11	9·5	49
Secretarial and Typing	29	12	8·5	32·5
Photographers	4	0	0	4
Photoprinters	5	1	1	5
Machine Operators	67·5	16	14·5	69
Asst. Hostel Manageress	1	0	0	1
Telephone Operators	2	0	0	2
Total Ancillary	523·5	70	75·5	518
INDUSTRIAL				
Craft	178·5	31	21	188·5
Non-craft	134	31	25·5	139·5
Apprentices	34	8	12	30
Total Industrial	346·5	70	58·5	358
GRAND TOTALS	1,226	211	185	1,252

The figures listed under "changes" include new entrants, resignations and promotions. Staff on sandwich courses, and those working part-time are counted as half.

Staff Relations The most important item of business has been the finalisation of the Productivity agreements at both National and Local level. The negotiations between Management and Unions were both long and difficult, but well worthwhile. There is now a Joint Consultative Productivity Committee. Participation of shop stewards in Laboratory affairs has grown as a result of new arrangements whereby every shop steward serves on at least one of the many committees with Trades Union representation. This development is most welcome as it brings more of the shop stewards closer to the everyday problems encountered in a research laboratory.

The Safety Committee has been reconstituted to include both Trades Union and Staff Association members. Another area in which representatives of both the industrial and the non-industrial staff were involved was the setting up of the Death Benefit Scheme. This is financed by voluntary deductions from salaries or wages, and its purpose is to provide an immediate cash payment to next-of-kin.

Joint discussions and negotiations, both formal and informal, take place under the umbrella of the Local Joint Committees, the Consultative Committee for industrial employees and the Whitley Committee for non-industrials. Both bodies have met several times during the year, including Annual Meetings, chaired by the Director, at which the previous year's work of the Laboratory and its future prospects are surveyed. The Annual Meeting was the first of its kind for the Consultative Committee, the members of which considered it to have been a most successful innovation.

There has been a substantial increase in Trades Union membership within the Laboratory, a trend welcomed by both sides as leading to more representative discussions. Several Unions now have schemes whereby subscriptions can be deducted from wages; a similar system for Staff Associations has existed for some time.

Training

The number of Rutherford Laboratory Staff who received day release and evening training concessions during the academic year 1969/70 showed yet another fall compared with the previous year, from 185 to 159, but this figure still represents 13% of the whole staff of the Laboratory. The continuing fall in numbers is almost certainly a consequence of the much reduced recruitment of junior staff in the last year or two. The 138 students who sat examinations achieved an overall pass-rate of 79%, which is well above the national average for part-time courses and higher than any previous figure for the Laboratory.

One full-time student from the Laboratory completed his studies this year; he was awarded the Diploma of the Oxford Polytechnic in Mechanical Engineering and earned exemption from the Part II examination of the CEI. Six other members of the staff attended full-time courses; three attended Honours Degree courses in Applied Physics, one an Honours Degree course in Electrical Engineering and two HND courses in Mechanical Engineering. One of these students held a Laboratory Award and the others received unpaid leave, although they returned to the Laboratory for industrial training where appropriate.

The majority of short courses on technical and management topics attended by Rutherford Laboratory Staff were run by the AERE Education and Training Department, in fact 231 out of a total of 292. Staff also attended courses run by Universities, Polytechnics and Technical Colleges, the Cranfield School of Management Studies, PERA, the Industrial Society, the Welding Institute, ASLIB and a number of commercial firms, as well as courses run centrally by SRC.

Three members of the staff of the Laboratory were registered as Research Students with Universities or the CNAA and will be allowed to submit theses based on work done in the Laboratory.

In addition to training concessions awarded to permanent staff, 32 Craft and Student Apprentices received training in the Apprentice Training Scheme run jointly with AERE. All 9 apprentices who completed their training during the year joined the staff of the Laboratory, 6 as Craftsmen, 2 as E III's and one as a Draughtsman – the first Draughtsman to qualify within the scheme. Two Student Apprentices not yet out of their "time" were awarded Honours degrees in Mechanical Engineering by the University of Cambridge, one with First Class Honours.

The Rutherford Laboratory acted as host establishment for an SRC Central Induction Course held in January 1970. This is likely to become an annual event during December or January, since this enables the visitors from other SRC establishments to visit Nimrod during the annual shut-down.

During the academic year the Laboratory provided industrial training for five members of its own staff attending sandwich courses and for 41 college-based students in Applied Physics, Applied Chemistry, Applied Mathematics, Computer Science and Electronics. This brings the total of college-based students who have received industrial training in the Laboratory since 1961 to 266.

Liaison with Schools (Ref: 44, 47)

Two years ago 9 science masters spent a month at the Rutherford Laboratory, working with individual groups on a variety of projects. They were encouraged during their visit to look around and see whether any of our activities could be transplanted to the schools as school projects. The objective was to provide a continuing contact between the schools and the Laboratory, and also to make the boys from the schools aware of the fact that any big project is made up from a large number of component activities, in one of which they were themselves participating.

The idea is interesting, but it has its difficulties. The project must on the one hand not be so sophisticated that it is beyond the ability of a sixth-former: on the other hand, it must not be dull, so that the project becomes boring. The other problem is that of time: the amount of time that masters and boys can devote to a project is limited, and in general small compared with a full time laboratory worker.

Some seven projects have been undertaken by schools. These include:

High Energy Particle Flux Measurement (Chipping Norton School).

The objective is to measure, for radiation protection purposes, the high energy component in a high intensity background of neutrons and gamma rays. The method uses fissionable elements in contact with thin foils (mica, mylar); tracks of fission products are counted in the foil following an etching procedure. The school have undertaken to investigate a variety of techniques for developing and counting the tracks.

Studies of Bearings in Vacuum (Burford School).

Equipment has been lent to the school for a study of bearing performance in vacuum—a useful introduction, of course, to vacuum physics as well as to bearing problems. This project is drawing to a close, and may be replaced by the construction of heat pipes or of vortex pumps. This collaboration is of interest because it has involved the interaction of several individuals within a group at the Rutherford Laboratory with several masters at the school: the master responsible for technical drawing has taken interest in design studies current here, the craft master is studying various technical aspects of current practice, and in several ways a community interest is growing.

Thermal Expansion and Thermal Conductivity of Resins at Room and Liquid Nitrogen Temperatures (Abingdon School).

The superconductivity programme at the Laboratory requires the development of suitable resins for coil encapsulation and collaboration has recently been initiated between ourselves and Abingdon School. The boys have been invited to devise their own method of measurement of thermal expansion at room temperature, and have shown considerable ingenuity in developing their own techniques. They will in due course develop methods suitable for measurements at liquid nitrogen temperatures. This collaboration shows considerable promise.

Figure 138. Visitors during the Open Days.

Exhibitions On account of the large amount of preparatory effort needed for the Open Days, the Laboratory contributed to only one exhibition during 1970 – the Physics Exhibition held in London during March. Four items were shown:– Superconducting magnet technology in high energy physics, including bubble chamber and proton synchrotron applications; a high speed electronic analogue wattmeter developed originally for monitoring the performance of the Nimrod magnet power supply; cementitious insulation techniques for electromagnets, offering the promise of improved resistance to irradiation damage; a flat-top field pulsed magnet for fast beam switching, involving current changes of several hundred amperes in times of less than a millisecond.

Open Days On Thursday and Friday, July 2nd and 3rd, the Laboratory was open to invited guests. These were the first Open Days for four years, and about 300 people came each day. Nimrod was closed down for the occasion, and there were 22 exhibits. Eight of these were located in Hall 3 and there was a linking introductory exhibition in the reception marquee. A press preview was held on July 1st and on July 4th, a Saturday, staff and their families were able to tour the Laboratory during the afternoon; the attendance was estimated as 1,500.

Figure 139. One of the many exhibits during the Open Days.

Figure 140. Visit of the Minister of State.

Visits

Mr. G. T. Fowler MP, Minister of State, Department of Education and Science, visited the Rutherford and Atlas Laboratories on January 28th. He was accompanied by Sir Brian Flowers. During his visit, the Minister saw Nimrod, the $\pi 8$ experiment in Hall 3, the 1·5 m Bubble Chamber, the Film Analysis equipment and a selection of items from the fields of applied physics, instrumentation and engineering. Mr. Fowler met representatives of the Staff Associations and Trades Unions, and also local press reporters.

In October, the Laboratory was visited by four members of the Russian Delegation on Plasma and Fusion Research, who had been spending several days at the Culham Laboratory. In figure 141, the Director is seen shaking hands with Dr. L. I. Artemenkov, leader of the delegation, at the conclusion of their visit.

Conducted tours were arranged for groups of students, members of professional and learned societies, and others with an interest in the Laboratory's work. These groups totalled 1,086 individuals, significantly fewer than last years record figure of 1,652 on account of Open Days.

A series of internal conducted tours was arranged for junior and intermediate grades of staff. The various Divisions of the Laboratory took it in turns to present their work in non-technical terms, each tour lasting about 1½ hours. A total of 430 staff attended.

Figure 141. Visit by members of the Russian Delegation on Plasma and Fusion Research.

The Library.

PUBLICATIONS AND LECTURES

List of Publications

JOURNAL ARTICLES

1 AHMED M., LOW J., ROLFE P. M., KARMAN O.
Differential cross-sections, polarizations and proton-gamma angular correlations for Fe^{54}, Ni^{60} (p,p) and (p,p'γ) at 10 MeV.
Nucl. Phys., **A147** (2) 273 (May 1970).

2 BAKER C. H., BATTY C. J., BONNER B. E., FORD P., FRIEDMAN E., TSCHALAR C., WILLIAMS L. E., CLOUGH A. S., HUNT J. B.
Medium energy neutron time-of-flight spectrometer, I. Instrumentation.
Nucl. Instrum. Meth., **85** (2) 259 (August 1970), preprinted as RPP/P27.

3 BAKER S. L., DORNAN P. J., GOPAL G. P., WEBSTER G. J., BULL V. A., MARCH P. V., TAYLER V., TOWNSEND D. W.
Positive pion-proton elastic scattering at 895, 945, 995 and 1040 MeV/c.
Nucl. Phys., **B18** (1) 29 (April 1970), preprinted as RPP/H64.

4 BARBER P. C., BROOME T. A., DUFF B. G., HEYMANN F. F., IMRIE D. C., LUSH G. J., MARTIN B. R., POTTER K. M., RITSON D. M., ROBBINS L. A., ROSNER R. A., SHARROCK S. J., SMITH A. D., HANNA R. C., LEA A. T., SACHARIDES E. J.
K^+p elastic differential cross-section measurements between 1·4 and 2·3 GeV/c and a phase shift analysis.
Phys. Lett., **32B** (3) 214 (June 1970).

5 BARGER V., PHILLIPS R. J. N.
$K_L \rightarrow K_S$ regeneration phase in Regge models.
Phys. Lett., **33B** (6) 425 (November 1970), preprinted as RPP/C3.

6 BARGER V., PHILLIPS R. J. N.
New Regge models of asymptotic behaviour.
Phys. Rev., **D2** (9) 1871 (November 1970).

7 BARGER V., PHILLIPS R. J. N.
Regge cuts, Pomeranchuk theorem and the Serpukhov total cross-section data.
Phys. Rev., Lett., **24** (6) 291 (February 1970).

8 BARGER V., PHILLIPS R. J. N.
Unconventional asymptotics.
Phys., Lett., **31B** (10) 643 (May 1970).

9 BATTY C. J.
Single particle potentials and nucleon density distributions for Pb^{208}.
Phys. Lett., **31B** (3) 496 (April 1970).

10 BERTHON A., VRANA J., BUTTERWORTH I., LITCHFIELD P. J., SMITH J. R., MEYER J., PAULI E., TALLINI B.
The reactions $K^-p \rightarrow \Sigma^{\pm}\pi^{\mp}$ in the c.m. energy range 1915 to 2168 MeV.
Nucl. Phys., **B24** (2) 417 (December 1970).

11 BERTHON A., RANGAN L. K., VRANA J., BUTTERWORTH I., LITCHFIELD P. J., SEGAR A. M., SMITH J. R., MEYER J., PAULI E., TALLINI B.
The reaction $K^-p \rightarrow \Lambda\pi^\circ$ in the c.m. energy range 1915 to 2168 MeV.
Nucl. Phys., **B20** (3) 476 (July 1970), preprinted as RPP/H60.

12 BOTTERILL D. R., BROWN R. M., CLEGG A. B., CORBETT I. F., CULLIGAN G., EMMERSON J. McL., FIELD R. C., GARVEY J., JONES P. B., MIDDLEMAS N., NEWTON D., QUIRK T. W., SALMON G. L., STEINBERG P. H., WILLIAMS W. S. C.
Form factors in the decay $K^+ \rightarrow \pi^\circ + \ell^+ + \nu$.
Phys. Lett., **31B** (5) 325 (March 1970), preprinted as RPP/H62.

13 BUGG D. V., BUSSEY P. J., DANCE D. R., SMITH A. R., CARTER A. A., WILLIAMS J. R.
$\pi^- p \rightarrow \pi^\circ n$ charge exchange cross-sections between 90 MeV and 290 MeV.
Nucl. Phys., **B** (in the press).

14 CAMPBELL J. R., MORTON W. T., NEGUS P. J., GOYAL D. P., MILLER D. B.
The elasticity of the $\Sigma(2030)$.
Nucl. Phys., **B25** (1) 75 (January 1971).

15 CARNE A.
Low and medium energies Alvarez structures. Linear Accelerators (P. M. Lapostolle and A. L. Septier eds)
C.I.1b p. 587.

16 CARNE A., SCHNIZER B., LAPOSTOLLE P., PROMÉ M.
Numerical methods. Acceleration by a gap.
Linear Accelerators (P. M. Lapostolle and A. L. Septier eds)
C.I. 2b p.747.

17 CARTER A. A., WILLIAMS J. R., BUGG D. V., BUSSEY P. J., DANCE D. R.
The total cross-sections for pion-proton scattering between 70 MeV and 290 MeV.
Nucl. Phys., **B** (in the press).

18 COX C. F., ISLAM G. S., COLLEY D. C., EASTWOOD D., FRY J. R., HEATHCOTE F. R., CANDLIN D. J., COLVINE J. G., COPLEY G., FANCEY N. E., MUIR J., ANGUS W., CAMPBELL J. R., MORTON W. T., NEGUS P. J., ALI S. S., BUTTERWORTH I., FUCHS F., GOYAL D. P., MILLER D. B., PEARCE D., SCHWARZSCHILD B.
A partial wave analysis of the reaction $\bar{K}n \rightarrow \pi^-\Lambda$ in the c.m. energy region from 1900 MeV to 2100 MeV.
Nucl. Phys., **B19** (1) 61 (May 1970) preprinted as RPP/H63.

19 DASS G. V., FROGGATT C. D.
Comments on the Regge-pole model for the reaction KN → K*(890) N.
Nucl. Phys., **B19** (2) 611 (June 1970), preprinted as RPP/T7.

20 DASS G. V., JACOB M., PAPAGEORGIOU S.
Duality and unnatural-parity trajectories.
Nuovo Cim., **67A** (3) 429 (June 1970).

21 DASS G. V., KAMAL A. N.
Magnetic radiation in $K^\pm \rightarrow \pi^\pm\pi^\circ\gamma$ decays.
Phys., Rev., **D1** (5) 1373 (March 1970).

22 DICKSON J. M.
Proton linacs for nuclear physics studies.
Linear Accelerators (P. M. Lapostolle and A. L. Septier eds)
C.3.2 p.987.

23 DRAGO F., LOVE A., PHILLIPS R. J. N., RINGLAND G. A.
Lack of dip systematics in strong cut models.
Phys. Lett., **31B** (10) 647 (May 1970).

24 DRAGO F.
Regge cuts, Schmid loops and resonance bumps.
Phys., Rev., Lett., 24 (11) 622 (March 1970).

25 EBEL G., JULIUS D., MULLENSIEFEN A., PILKUHN H., SCHMIDT W., STEINER F., KRAMER G., SCHIERHOLZ., MARTIN B. R., PISUT J., OADES G., DE SWART J. J.
Compilation of coupling constants and low-energy parameters.
Springer Tracts in Modern Physics 55, p.239.

26 FAISSNER H., REITHLER H., THOMÉ W., GAILLARD J. M., GALBRAITH W., JANE M. R., LIPMAN N. H., MANNING G.
Measurement of the branching ratio $K_L^\circ \to 2\pi^\circ$ to $K_L^\circ \to 3\pi^\circ$.
Nuovo Cim., 70A (1) 57 (November 1970).

27 FIELD J. H.
General tests of the $\Delta I = \frac{1}{2}$ and $\Delta S = \Delta Q$ rules in $K_{\ell 3}$ decays.
Nuovo Cim., 1A (1) 89 (January 1971), preprinted as RPP/H69.

28 GREENLEES G. W., HNIZDO V., KARBAN O., LOWE J., MAKOFSKE W.
Elastic scattering of 30·3 MeV polarized protons from Ni^{58}, Sn^{120} and Pb^{208}.
Phys. Rev., C2 (3) 1063 (September 1970).

29 HARBISON S. A., GRIFFITHS R. J., STEWART N. M., JOHNSTON A. R., SQUIER G. T. A.
An analysis of polarization and cross-section data for the p–He^3 system at 30 and 50 MeV.
Nucl. Phys., A150 (3) 570 (July 1970).

30 HARBISON S. A., GRIFFITHS R. J., STEWART N. M., JOHNSTON A. R., SQUIER G. T. A.
An analysis of the angular distributions of the reactions $He^4(p,d)He^3$, $He^4(p,t)2p$, $He^4(p, He^3)pn$ and $He^3(p,d)2p$.
Nucl. Phys., A152 (3) 503 (September 1970).

31 HUMBLE S.
Unitarity effects in the Veneziano model.
Phys. Rev., D2 (7) 1308 (October 1970).

32 HUNT J. B., BAKER C. A., BATTY C. J., FORD P., FRIEDMAN E., WILLIAMS L. E.
Medium energy neutron time-of-flight spectrometer, II. Neutron detection efficiency of organic scintillators.
Nucl. Instrum. Meth., 85 (2) 269 (August 1970), preprinted as RPP/P28.

33 KABIR P. K.
What is not invariant under time reversal?
Phys. Rev. D2 (3) 540 (August 1970).

34 KARBAN O., GREAVES P. D., HNIZDO V., LOWE J., GREENLEES G. W.
Inelastic scattering of polarized protons at 30·3 MeV by $Fe^{54, 56}$, Ni^{58}, Sn^{120} and Pb^{208}.
Nucl. Phys., A147 (3) 461 (June 1970).

35 KEMP M. A. R., WARD D. L.
π^-p elastic scattering from 1225 to 2070 MeV/c compared with phase shift analysis.
Phys. Lett., 31B (9) 613 (April 1970).

36 KENNY B. G., KABIR P. K.
Unitarity and the phase of the mixing parameter in superweak theories.
Phys. Rev., D2 (1) 257 (July 1970).

37 LITCHFIELD P. J.
Partial wave analysis of $K^-N \to \Lambda\pi$ between 1·0 and 1·85 GeV/c.
Nucl. Phys., B22 (1) 269 (September 1970), preprinted as RPP/H66.

38 LOVE A., RANKIN W. H.
Sidewise dispersion relations and the nucleon anomalous magnetic moment.
Nucl. Phys., B21 (1) 261 (August 1970).

39 LOWE J.
Analysis of inelastic scattering of polarized protons by B^{11}.
Nucl. Phys. (in the press).

40 MANI G. S.
Inelastic scattering of 50 MeV protons by Fe^{54}.
Nucl. Phys., A157 (2) 471 (November 1970).

41 MAYEUR C., BINST P. Van., WILQUET G., FLIAGINE V. B., GUY J. G., KNIGHT W. L., TOVEY S. N., DOWD R. M., GOVAN M., SANDERS A. J., SCHNEPS J., WOLSKY G.
A search for the radiative decay $Y_0^*(1327) \to \Lambda\gamma$.
Phys. Lett., 33B (6) 441 (November 1970).

42 MORGAN D., PISUT J.
Low energy pion-pion scattering.
Springer Tracts in Modern Physics 55.

43 MORGAN D., SHAW G.
Pion-pion scattering below 850 MeV. A unique solution.
Phys. Rev., D2 (3) 520 (August 1970).

44 MORTIMER A. R.
An unusual experiment.
Project (12) 34 (Spring 1970).

45 MORTIMER A. R.
The Engineer's new place in society.
Project (13) 28 (Summer 1970).

46 MORTIMER A. R.
High energy physics. Collaboration effort between physicists and engineers.
Project (15) 8 (Spring 1971).

47 MORTIMER A. R.
Technology in schools.
Secondary Education 1 (1) 1970.

48 NELSON J. M., CHANT N. S., FISHER P. S.
A comparison of polarization analysing powers of two-nucleon transfer reactions leading to mirror final states.
Phys., Lett., 31B (7) 445 (March 1970).

49 NELSON J. M., CHANT N. S., FISHER P. S.
A study of some (p,H^3) and (p,He^3) reactions induced by 49·5 MeV polarized protons.
Nucl. Phys., A156 (2) 406 (November 1970).

50 NICHOLAS D. J., BANKS P. H. T., CRAGG D. A.
Proton relaxation rates and polarization measurements in butanol/water samples at 25 kG.
Nucl. Instrum. Meth., 88 (1) 69 (November 1970), preprinted as RPP/A75.

51 NICHOLAS D. J., WILLIAMS W. G., BANKS P. H. T., CRAGG D. A.
Proton polarization measurements at high magnetic fields and low temperatures.
Nucl. Instrum. Meth., 87 (2) 301 (October 1970), preprinted as RPP/A80.

52 OADES G. C.
Coulomb corrections in the analysis of πN experimental scattering data.
Springer Tracts in Modern Physics 55.

53 OADES G. C., RASCHE G.
Electromagnetic structure and coulomb corrections to strong interactions.
Nucl. Phys., **B20** (2) 333 (July 1970), preprinted as RPP/T1.

54 PHILLIPS R. J. N.
Lectures on Regge phenomenology.
Acta Physica Austriaca, Suppl. VII, 1970.
(developments in High Energy Physics, Urban P. ed) p.214.

55 PHILLIPS R. J. N., RINGLAND G. A.
Resonance recognition in a Veneziano model.
Proc. Roy. Soc. **A318** (1534) 299 (September 1970).

56 PHILLIPS R. J. N., RINGLAND G. A.
Review: Regge phenomenology.
High Energy Physics Vol. V (E. H. S. Burhop, ed).

57 SAXON D. H., MULVEY J. H., CHINOWSKY W.
π^-p reactions at 456, 505 and 552 MeV/c.
Phys. Rev., **D2** (9) 1970 (November 1970).

58 SCHARENGUIVEL J. H., GUTAY L. J., MILLER D. H., McILLWAIN R. L., MEIERE F. T., MORGAN D., JACOBS L. D., MARATECK S., FROGGATT C. D., HUWE D., MARQUIT E.
Forward structure of the single pion-production amplitude.
Phys. Rev., Lett., 24 (7) 332 (February 1970).

59 SINHA B. C.
Isospin dependence of optical model potentials using a realistic effective interaction.
Phys. Lett., **33B** (4) 279 (October 1970).

60 SMITH P. F.
The Rutherford Laboratory superconducting synchrotron program: Notes on work in progress.
Particle Acc. 1 (3) 151 (July 1970).

61 SMITH P. F., LEWIN J. D.
Superconducting energy transfer systems.
Particle Acc. 1 (3) 155 (July 1970).

62 VENTURI G.
Infinitely rising Regge trajectories and unitarity.
Phys. Rev., **D1** (6) 1717 (March 1970), preprinted as RPP/T6.

63 WILLIAMS W. G., NICHOLAS D. J., BANKS P. H. T., CRAGG D. A.
Proton polarization and relaxation times below 1°K for glycerol water doped with porphyrexide.
Nucl. Instrum. Meth., **88** (1) 73 (November 1970), preprinted as RPP/A77.

64 WOOLLAM P. B., GRIFFITHS R. J., GRACE J. F., LEWIS V. E.
Optical-model analysis of elastic scattering and polarization of 49·5 MeV protons on Sm^{148}.
Nucl. Phys., A154 (3) 513 (October 1970).

UNPUBLISHED PREPRINTS

65 ANSORGE R. E., ATHERTON A. R., NEALE W. W., RUSHBROOKE J. G., STREET G. S. B.
Anomalies in electromagnetic processes. I.
Electron-pair production.
Cambridge preprint HEP 70–1.

66 ANSORGE R. E., ATHERTON A. R., NEALE W. W., RUSHBROOKE J. G., STREET G. S. B.
Anomalies in electromagnetic processes. II. Bremsstrahlung.
Cambridge preprint HEP 70–2.

67 APLIN P. S., COWAN I. M., GIBSON W. M., GILMORE R. S., GREEN K., MALOS J., SMITH V. J., WARD D. L., KEMP M. A. R., LEA A. T., McKENZIE R., OADES G. C.
DC-S for π^-p elastic scattering from 1·2 to 3·0 GeV/c and phase shift analysis.
RPP/H67.

68 BENNETT J. R. J.
A biased source for a cyclotron.
RPP/A74.

69 CALUCCI G., DRAGO F., JENGO R.
A jet model for e^+e^- annihilation into pions.
RPP/C1.

70 CARTER A. A., WILLIAMS J. R., BUGG D. V., BUSSEY P. J., DANCE D. R.
The total and charge-exchange cross-sections for pion-proton scattering between 70 MeV and 290 MeV.
RPP/H70.

71 DEEN S. M.
Generalised partial wave analysis.
RPP/H68.

72 FROGGATT C. D., MORGAN D.
Non evasive contributions to forward rho-production and vector dominance.
RPP/C4.

73 GUNION J. F., ROBERTS R. G.
Analysis of meson-baryon scattering processes related by SU(3) in a unitarized Veneziano Model.
Stanford preprint SLAC-PUB-818.

74 HOYER P., PETERSSON B., LEA A. T., PATON J. E., THOMAS G. H.
Crossing symmetric description of the complex $K^+K^-\pi^-\bar{p}n$.
CERN preprint CERN/TH. 1262.

75 HUMBLE S.
High energy single particle production on the Van Hove plot.
RUL-R 3583.

76 HUMBLE S., VAUGHN M. H., ZIA R. K. P.
A dual model for πN scattering without parity doublets.
RUL-R 3454.

77 KABIR P. K.
Superweak interactions and TCP – invariance.
RUL-R 3280.

78 KABIR P. K., KAMAL A. N.
Muon flux deep underground and the question of strong W-interactions.
RPP/C6.

79 KWIECINKSI J.
Possible new threshold sum rules implied by unitarity.
RPP/C5.

80 LEA A. T., MARTIN B. R., THOMPSON G. D.
K^+p partial-wave amplitudes below 2 GeV/c.
RPP/C2.

81 MADDEN D. R.
Broad-band NMR spectrometer for dynamic proton-polarization measurements.
RPP/A78.

82 MARINOV A., BATTY C. J., KILVINGTON A. I., NEWTON G. W. A., ROBINSON V. J., HEMINGWAY J. D.
Evidence for the possible existence of a super-heavy element with atomic number 112.
RPP/NS1.

83 MORGAN J. T., SHELDON R., STAPLETON G. B.
Stress relaxation of butyl rubber during irradiation.
RPP/E15.

84 OTT R. J., PRITCHARD T. W.
A precise measurement of the K^+ life-time.
RPP/H65.

85 ROSS G. G.
Mass differences and symmetry predictions.
RUL-R 3585.

CONFERENCE PAPERS

86 COLLEGE DE FRANCE, RUTHERFORD LABORATORY, SACLAY COLLABORATION.
Resonance formation in the reaction $K^-p \to \Sigma\pi$ in the mass region between 1915 and 2168 MeV.
American Physical Society. Spring Meeting, Washington USA, 27-30 April 1970. Abstracts in Bull. Amer. Phys. Soc., 15 (4) (April 1970).

87 COLLEGE DE FRANCE, RUTHERFORD LABORATORY, SACLAY, STRASBOURG COLLABORATION.
Elastic and charge exchange K^-p scattering between 1·26 and 1·84 GeV/c.
Ibid.

88 COLLEGE DE FRANCE, RUTHERFORD LABORATORY, SACLAY COLLABORATION.
Reactions $K^-p \to \Sigma^{\pm}\pi^{\mp}$ in the E* range 1915 to 2168 MeV.
Ibid.

89 COLLEGE DE FRANCE, RUTHERFORD LABORATORY, SACLAY COLLABORATION.
Reaction $K^-p \to \Lambda\pi^\circ$ in the E* range 1915 to 2168 MeV.
Ibid.

90 DONALD R. A., EDWARDS D. N., HOWARD D., MOORE R. S., BACON T. C., BUTTERWORTH I., MILLER R. J., PHELAN J. J.
A formation study of $\bar{p}p$ interactions through the T-meson region.
Ibid.

91 LOWE J., AHMED M., ROLPH P. M., HNIZDO V.
C^{12} $(p,p'\gamma)$ with polarized incident beam.
Ibid.

92 SMITH K. M., BOOTH P. S. L., RENSHALL H. R., JONES P. B., SALMON G. L., WILLIAMS W. S. C., DUKE P. J., HILL R. E., HOLLEY W. R., JONES D. P., THRESHER J. J.
Study of the decay modes $K^\pm \to \pi^\pm\pi^\circ\pi^\circ$ and $K^\pm \to \pi^\pm\pi^\circ\gamma$.
Ibid.

93 READ S. F. J., DUNCAN G. W. L., MADDEN D. R., NICHOLAS D. J., WILLIAMS W. G.
Measurement of dynamic nuclear polarization and relaxation rates for a range of concentration, temperature and magnetic field in porphyrexide doped N-butanol and water.
16th Colloque Ampere, Bucharest, Romania, September 1970, preprinted as RPP/A82.

94 FISHER C. M.
The optimisation of bubble chamber design parameters for strong interaction experiments.
International Conference on Bubble Chamber Technology, Argonne, USA June 1970.

95 SMITH W. A.
Wire electrodes in electrostatic separators.
IV International Symposium on Discharges and Electrical Insulation in Vacuum, University of Waterloo, Canada. September 1-4, 1970. Proceedings, p.185.

96 SMITH W. A., INNESS M. J., FIELDING K. A., PRADHAN R.
Impulse breakdown of large gaps in vacuum.
Ibid., p. 96.

97 PHILLIPS R. J. N.
Unconventional asymptotics.
Fifth Moriond Meeting on Electromagnetic Interactions, Meribel-les-Allues, France. Proceedings, p. III. 74.

98 RINGLAND G. A.
$\pi^-p \to \Lambda K^\circ$.
Ibid., p. III. 167.

99 COLLEGE DE FRANCE, RUTHERFORD LABORATORY, SACLAY, STRASBOURG UNIVERSITY COLLABORATION.
K^-p elastic and charge exchange scattering in the c.m. range 1915 to 2168 MeV.
Fifteenth International Conference on High Energy Physics, Kiev, August 1970, USSR.

100 RUTHERFORD LABORATORY, ECOLE POLYTECHNIQUE COLLABORATION.
K^-p elastic scattering at 14·25 GeV/c.
Ibid.

101 RUTHERFORD LABORATORY, OXFORD UNIVERSITY COLLABORATION.
Asymmetries in π^+p elastic scattering in the momentum range 622 to 2500 MeV/c.
Ibid.

102 SMITH K. M., BOOTH P. S. L., RENSHALL H. R., JONES P. B., SALMON G. L., WILLIAMS W. S. C., DUKE P. J., HILL R. E., HOLLEY W. R., JONES D. P., THRESHER J. J.
Study of the decay modes $K^{\pm} \to \pi^{\pm}\pi^{\circ}\pi^{\circ}$ and $K^{\pm} \to \pi^{\pm}\pi^{\circ}\gamma$.
Ibid.

103 BARBER P. C., BROOME T. A., DUFF B. G., HEYMANN F. F., IMRIE D. C., LUSH G. J., MARTIN B. R., POTTER K. M., RITSON D. M., ROBBINS L. A., ROSNER R. A., SHARROCK S. J., SMITH A. D., HANNA R. C., LEA A. T., SACHARIDES E. J.
$K^{+}p$ elastic scattering between 1·4 and 2·3 GeV/c.
Hyperon Conference, Duke University, USA, 24-25 April 1970. Proceedings ("Hyperon Resonances – 70", Fowler E. C. ed.) p. 453.

104 BARBER P. C., BROOME T. A., BUSZA W., DUFF B. G., GARBUTT D. A., HEYMANN F. F., IMRIE D. C., LUSH G. J., MGBENU E. N., POTTER K. M., RITSON D. M., ROBBINS L. A., SHARROCK S. J., SMITH A. D., HANNA R. C., ROSNER R. A., SACHARIDES E. J.
$K^{-}p$ elastic differential cross-section measurements between 1·7 and 2·5 GeV/c.
Ibid, p. 223.

105 COLLEGE DE FRANCE, RUTHERFORD LABORATORY, SACLAY COLLABORATION.
Reaction $K^{-}p \to \Lambda\pi^{\circ}$ in the E* range 1915 to 2168 MeV.
Ibid, p. 205.

106 COLLEGE DE FRANCE, RUTHERFORD LABORATORY, SACLAY COLLABORATION.
Reactions $K^{-}p \to \Sigma^{\pm}\pi^{\mp}$ in the E* range 1915 to 2168 MeV.
Ibid, p. 211.

107 LITCHFIELD P. J.
Partial wave analysis of $K^{-}N \to \Lambda\pi$ between 1·0 and 1·85 GeV/c.
Ibid, p. 215.

108 BATTY C. J.
Neutron density distributions.
Summer School on Intermediate Energy Physics, Banff, Canada.

109 BATTY C. J.
Single particle potentials and nucleon density distributions for Pb^{208}.
IPPS Conference on Nuclear Physics, University of Surrey, 7-9 April 1970.

110 COLEMAN C. F., CAVANAGH P. E.
Levels of the even isotopes of tin excited by the (p,t) reaction.
Ibid.

111 MANI G. S., JACQUES D.
Inelastic scattering of 50 MeV protons by Ca^{42} and Ca^{44}.
Ibid.

112 MANI G. S., JACQUES D., DIX A.
Inelastic scattering of 50 MeV protons by Li^{6}, Li^{7}, and Be^{9}.
Ibid.

113 MANI G. S., JONES D.
Inelastic scattering of 50 MeV protons by Zr isotopes.
Ibid.

114 MANI G. S., JACQUES D., DIX A.
Optical model for elastic scattering of 50 MeV protons by Li^{6}, Li^{7} and Be^{9}.
Ibid.

115 MANI G. S., JONES D., JACQUES D.
Optical model for 50 MeV proton scattering by various nuclei.
Ibid.

116 SINHA B. C.
Nucleonic point density and the central part of the optical potential.
Ibid.

117 CLOKE V. C.
Electronically controlled hydraulic systems for extractor magnets.
2nd USSR National Conference on Particle Accelerators, Moscow, 16-23 September 1970, preprinted as RPP/N21.

118 GRAY D. A., HAROLD M. R., MORGAN R. H. C., KING N. M., O'CONNELL M. J.
Extraction techniques at Nimrod.
Ibid., preprinted as RPP/N22.

119 BANKS P. H. T., CRAGG D. A., MADDEN D. R., NICHOLAS D. J., PICKLES D. C., READ S. F. J., RUSSELL F. M., WARNER G. P., WILLIAMS W. G.
A frozen polarized target.
Third International Symposium on Polarization Phenomena in Nuclear Reactions. Madison, USA, 1970, preprinted as RPP/A81.

120 GREAVES P. D., HNIZDO V., KARBAN O., LOWE J.
Microscopic analysis of 30·3 MeV inelastic proton scattering by light nuclei.
Ibid.

121 HNIZDO V., GREAVES P. D., KARBAN O., LOWE J.
Collective-model analysis of inelastic proton scattering using potentials derived from nuclear matter distributions.
Ibid.

122 DONALD R. A., EDWARDS D. N., HOWARD D., MOORE R. S., BACON T. C., BUTTERWORTH I., MILLER R. J., PHELAN J. J.
A formation study of $\bar{p}p$ interactions through the T-meson region.
Fourth Topical Conference on Resonant Particles, Athens, Ohio, USA, June 15-17, 1970, Proceedings: Particles and Nuclei, 1 (2) 105 (November 1970).

123 RINGLAND G. A.
Regge cut phenomenology.
Xth Krakow School of Theoretical Physics.

124 DASS G. V.
Relative phase of ρ and ω production amplitudes in Regge phenomenology.
Meeting on Vector Meson Production and Omega-Rho Interference, Daresbury, 12-14 June 1970. Proceedings (DNPL/R7, Donnachie A. and Gabathuler E. eds.) p. 207.

DOCTORAL THESES

125 ANSORGE R. E. (University of Cambridge).
A study of electromagnetic processes in a hydrogen bubble chamber.

126 BARBER P. C. (University College, University of London).
The elastic scattering of K mesons on protons and the capture of K mesons in heavy nuclei.
Reprinted as HEP/T11.

127 DANCE D. R. (University of Cambridge).
The scattering of pions by protons.

128 DUNCAN G. W. L. (University of Oxford).
Nuclear and electron interactions in condensed media with particular references to the production of polarized targets.

129 ELCOMBE P. A. (University of Cambridge).
Production of strange particles in neutron-proton collisions.

130 ELLIS R. J., (University of Oxford).
A study of the sigma hyperon decay.
Reprinted as HEP/T8.

131 GOPAL G. P. (Imperial College, University of London).
A study of the excitation of nucleon resonances in positive pion-proton interactions.
Reprinted as HEP/T9.

132 HNIZDO V. (University of Birmingham).
Elastic and inelastic scattering of 30 MeV polarized protons.

133 MADEN D. (University of Cambridge).
The reaction $np \rightarrow pp\pi^-$ below 7·5 GeV/c.
Reprinted as HEP/T7.

134 PEARCE D. (Imperial College, University of London).
A Study of Kaon-deuteron interactions at low energy.
Reprinted as HEP/T12.

135 SINHA B. C. (Kings College, University of London).
The real central part of the nucleon-nuclear optical model potential.

136 SMITH A. D. (University College, University of London).
A magnetostrictive read-out system for wire spark chambers and the elastic scattering of positive kaons on protons.
Reprinted as HEP/T10.

137 STOKES W. P. C. (University of Cambridge).
High multiplicity neutron-proton interactions.

138 WILSON J. G. (Imperial College, University of London).
A search for the A2 meson near threshold.

REPORTS

139 ADAMS P.
A real-time interpreter for computer control.
RHEL/R 207.

140 BANFORD A. P., TELLING F. M. (eds.).
The work of the Rutherford Laboratory in 1969.
RHEL/R 191.

141 BATTY C. J. (ed.).
Final PLA progress report 1969.
RHEL/R 187.

142 BELL S. B. M. Mrs.
Computer graphics patching of failed CYCLOPS events for spark chamber experiments.
RHEL/R 205.

143 COLYER B.
Heat transfer and pressure drop for forced flow of pressurized liquid helium and two-phase helium in tubes.
RHEL/R 193.

144 COUPLAND J. H.
Equations and formulae for magnets with air cored windings of 'saddle coil' type.
RHEL/R 203.

145 EVANS D., MORGAN J. T., SHELDON R., STAPLETON G. B.
Post irradiation mechanical properties of epoxy-resin glass composities.
RHEL/R 200.

146 GRAY D. E. (ed.).
Nimrod operation and development. Quarterly Report, July 1 to September 30, 1969.
RHEL/R 194.

147 GRAY D. E. (ed.).
Nimrod operation and development. Quarterly Report, October 1 to December 31, 1969.
RHEL/R 195.

148 GRAY D. E. (ed.).
Nimrod operation and development. Quarterly Report, January 1 to March 31, 1970.
RHEL/R 198.

149 GRAY D. E. (ed.).
Nimrod operation and development. Quarterly Report, April 1 to June 30, 1970.
RHEL/R 206.

150 GRAY D. E. (ed.).
Nimrod operation and development. Quarterly Report, July 1 to September 30, 1970.
RHEL/R 210.

151 MACE P. R., WELCH E.
Temperature stabilised magnets – Resistor for 0·1% magnetic field measurements.
RHEL/R 192.

152 MIDDLETON A. J.
A low temperature materials test rig and some typical data.
RHEL/R 202.

153 MORGAN J. T., SCOTT G., SHELDON R., STAPLETON G. B.
Gas evolution from epoxy-resins by high energy radiation.
RHEL/R 196.

154 NICHOLAS D. J., BANKS P. H. T., CRAGG D. A.
The present status of polarized targets at the Rutherford Laboratory.
RHEL/R 201.

155 RANDLE T. C.
Estimates for the field errors from coil winding irregularities in superconducting magnets.
RHEL/R 197.

156 RUSSELL F. M.
A new target material for the Rutherford Laboratory frozen target.
RHEL/R 199.

157 SCOTT D. B.
Computer graphics patching of HPD failed events.
RHEL/R 190.

MEMORANDA

158 BRANDSTETTER A.
Polynomial evaluation of the CERN 2m HBC field measurements for use in the Rutherford Laboratory geometry program (subr HMAG).
RHEL/M/H3.

159 BRANDSTETTER A.
The "SLIJES" (SLICE to JESTER) translating routine.
RHEL/M/H2.

160 EVANS D., STAPLETON G. B.
The influence of structure and strain rate on the cryogenic mechanical properties of some metals.
RHEL/M/E2.

161 EVANS D., MORGAN J. T., STAPLETON G. B.
Microscopic examination of super-conductive coils.
RHEL/M/E3.

162 GIBBINGS D.
The hardware/software interface between a CAMAC branch highway and a 16 bit digital computer for program controlled CAMAC operations.
RHEL/M/H1.

163 GILL P., KNIGHT K. M.
The multiplexor for the direct control feature of the IBM 360/75.
RHEL/M/C3.

164 HACK R. C.
Personal fast neutron dosimetry around Nimrod. A second note.
RHEL/M/R1.

165 HACK R. C.
Radiation protection group (operations) progress report for 1969.
RHEL/M/R2.

166 HOLMES M. J.
A special purpose hinge for use with 19 inch panel and racking systems.
RHEL/M/C1.

167 JOHNSON C. D., SHELDON R., STAPLETON G. B.
Measurement of radiation dose distribution generated by targetting in the CERN Proton Synchrotron.
RHEL/M/175.

168 LEWIN J. D.
Some calculations relating to the design of magnets for superconducting energy transfer systems.
RHEL/M/A2.

169 MARSH E. Mrs. (Compiled by).
Reports issued by the Rutherford High Energy Laboratory 1960-1969.
RHEL/M/118 (Revised 1970).

170 MARSH E. Mrs. (Compiled by).
Reports issued by the Rutherford High Energy Laboratory 1960-1970.
RHEL/M/118 (Revised 1971).

171 MITCHELL M. J.
Seven track automatic compressor for keeping experimental results.
RHEL/M/C2.

172 NICHOLAS D. J.
The design of the magnet system for the Rutherford Laboratory separated function polarized target.
RHEL/M/A1.

173 PHILLIPS R. J. N., WALKER T. G. (eds.).
Physics with the Omega spectrometer:
Notes from a meeting held at the Cosener's House, 19/20 June 1970.

174 RUSSELL F. M.
Refrigeration for the frozen target.
RHEL/M/180

175 RUSSELL F. M.
Some thoughts on polarized targets: Segmented advanced polarized targets (SHPT).
RHEL/M/169

176 STAPLETON G. B., THOMAS R. H.
Experimental studies of the Sorption of Be^7 on chalk.
RHEL/M/E1.

177 STEVENSON G. R., WALLACE C. M.
Optimization of flux density to dose rate conversion factors for activation detector sets in broad neutron fields using the KALCHAS routine.
RHEL/M/R4.

178 WALKINSHAW W., LEA A. T. (eds.).
Computing and Automation Division, Quarterly report, October 1 to December 31 1970.
RHEL/M/C4.

179 WALLACE C. M.
Derivation of practical values of dose equivalent in broad neutron spectra using two detector systems.
RHEL/M/R3.

180 WALSH T. R.
AG focusing quantities derived from the profile equation with application to linacs.
RHEL/M/NIM 2.

181 WALSH T. R.
Notes on closed orbit control.
RHEL/M/NIM 4.

182 WALSH T. R.
Notes on the probability theory of retrieval systems.
RHEL/M/NIM 5.

183 WALSH T. R.
The SDI programmes SELENSA and ATLASEL.
RHEL/M/NIM 1.

Lectures

NIMROD LECTURES

A weekly series in which physicists active in high energy physics talk about their current or proposed research programmes, or on topics related to particle physics.

PHILLIPS R. J. N. (Rutherford Laboratory) (5 January): Serpukhov surprises and/or the asymptotic myth.

BRANDSTETTER A. (Tel Aviv and Rutherford Laboratory) (12 January): Phenomenology of neutral vector meson photoproduction.

DOWELL J. (Birmingham) (19 January): Possible evidence for a Z* resonance.

EDEN R. J. (Cambridge) (26 January): Pomeranchuk Theorem and the Serpukhov data on total cross-sections.

HUGHES I. S. (Glasgow) (2 February): K^+p interactions in the range 0·9-1·5 GeV/c and evidence for a K* (2200) in K^+p interactions at 10 GeV/c.

BOWLER M. (Oxford) (9 February): Recent studies of the "Q" bump.

NEALE W., and RUSHBROOKE J. (Cambridge) (16 February): Anomalies in electromagnetic processes.

MOORHOUSE R. G. (Glasgow) (23 February): High energy photoproduction.

FOX G. C. (Cambridge) (2 March): B5 God's gift to the bubble chamber.

CHARPAK G. (CERN) (3 March): Project of experiments with multi-wave proportional chambers.

HOMER R. J. (Rutherford Laboratory) (9 March): Report on the Chicago APS meeting and news from the Laboratories.

STENGER V. (Heidelberg) (16 March): Dominant processes in the reaction $\pi^-p \to \pi^-\pi^-\pi^+p$ at 3·9 GeV/c.

KEMP A. (DNPL) (23 March): Phase shift analysis of πp and structure in differential cross-sections.

BOTTERILL D. (CERN) (13 April): Recent results of the CERN boson spectrometer.

COHEN-TAUNOUDJI G. (Saclay) (20 April): Duality and unitarity.

BELLETINI G. (CERN and Pisa) (27 April): Polarization in high energy hadron scattering: also discussion of ISR experiment.

WINTER K. (CERN) (4 May): Experiments to test the validity of the $\Delta S = \Delta Q$ rule.

WERBROUK A. (Turin) (11 May): Analysis of multi-body meson resonance decays.

BUTTERWORTH I. (Rutherford Laboratory) (18 May): Report on the APS and Philadelphia Meson Meeting.

KANE G. (Michigan and Rutherford Laboratory) (1 June): The structure of high energy scattering – experimental and theoretical.

ASTBURY A. (Rutherford Laboratory) (8 June): Σ Beta decay.

HEYMANN F. (UCL) and LEA A. T. (Rutherford Laboratory) (15 June): Elastic K^+p scattering from 1·4-2·4 GeV/c.

SCHMID C. (CERN) (22 June): Phenomenology of meson baryon scattering and the elimination of parity doublets.

WOLFENDALE A. W. (Durham) (29 June): The search for Quarks.

KUGLER M. (Weizmann Inst.) (30 June): Do we need exotics?

LUBELSMEYER K. (Bonn) (6 July): Recent results on pseudoscalar photoproduction.

BIALAS A. (Krakow and Rutherford Laboratory) (13 July): Some recent results in the Quark Model of high energy scattering.

BROWN R. M. (Rutherford Laboratory) (20 July): β-decay of polarized Λ.

WIPF S. L. (Atomics International, California) (28 July): Electromagnetic levitation and guidance of high speed vehicles.

DUKE P. J. (Rutherford Laboratory) (7 September): Review of the Kiev conference.

BURKHARDT H. (Birmingham) (14 September): The perils of phase shifting.

BUGG D. V. (QMC) (21 September): πp Scattering below 300 MeV.

STEINBERGER J. (CERN) (28 September): K° Detector using multiwave proportional chambers.

WEYERS J. (CERN) (12 October): Duality and the particle spectrum.

NEWTON D. (Lancaster) (19 October): A Berkeley experiment on $K^+ \to e^+ + \nu_e$

PHILLIPS R. J. N. (Rutherford Laboratory) (26 October): The Serpukhov $K_L \to K_S$ regeneration mystery.

KALMUS G. (LRL and CERN) (2 November): Strange particle production in π^+p interactions between 1 and 2 GeV/c.

LUNDBY A. (CERN) (9 November): $\pi^\pm p$, $K^\pm p$, and $\bar{p}p$ elastic and inelastic scattering at 5 GeV/c.

WHITE D. H. (Cornell and UCL) (16 November): Pion charge exchange in the backward direction at high energies at BNL.

GABATHULER E. (DNPL) (23 November): Present and future physics with Electron Storage Rings.

FIELDS T. (Birmingham) (30 November): Two-body states in $\bar{p}p$ annihilation.

MORIARTY K. (Imp. Coll.) (7 December): The inclusion of spin in a phenomenological Veneziano model with applications to three particle production.

MURPHY P. (Manchester) (14 December): $K^\circ_L \to \pi^+\pi^-\pi^\circ$.

RUTHERFORD LABORATORY LECTURES

A series of lectures in which eminent people are invited to the Laboratory to address the staff on subjects of general scientific importance.

MOLE R. H. (MRC Harwell) (12 February): The work of the Radiobiology Unit.

MARSHALL W. (AERE Harwell) (9 April): The Harwell Research Programme.

SCHUMACHER E. F. (NCB) (13 May): Intermediate technology – the missing factor in overseas aid.

BOYD R. L. F. (UCL) (16 July): X-ray astronomy.

HARRISON E. R. (Amherst, USA) (3 September): The big bang cosmologies.

MASSEY Sir Harrie (UCL) (1 October): The present position in space science.

HIDE R. (Met. Office, GFDL) (29 October): Motions in planetary atmospheres.

STREET W. B. (US Military Academy) (17 November): The structures and motions of Jupiter's great red spot.

YOUNG J. Z. (UCL) (3 December): Memory.

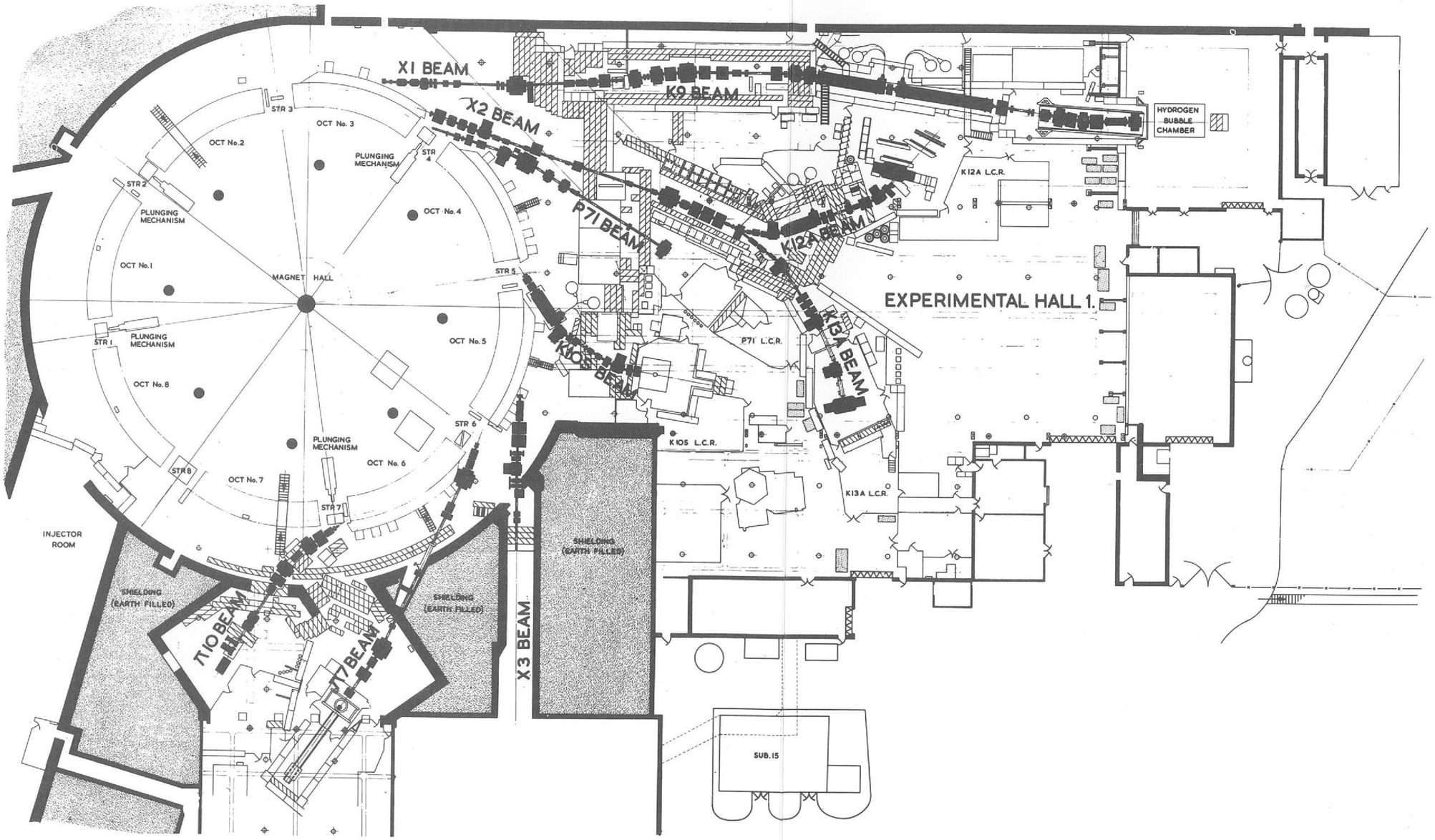

Nimrod Experimental Halls 1 and 2, Layout at 31st December 1970.

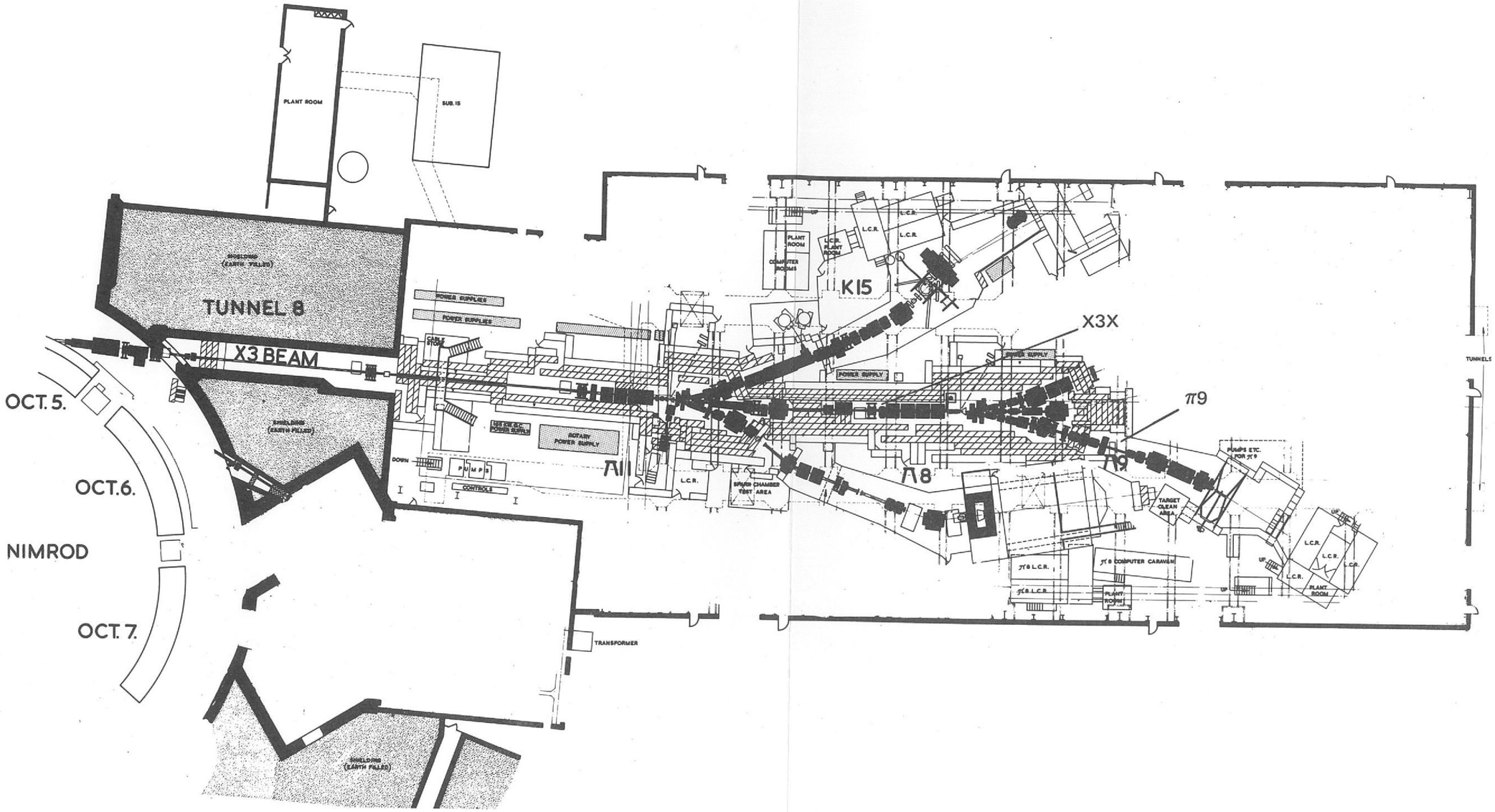

Nimrod Experimental Hall 3. Layout at 31st December 1970.